UNIVERSITÀ
DEGLI STUDI
DI PADOVA

Head Office: Università degli Studi di Padova

Department of Geosciences

Ph.D. COURSE IN:

(IF ANY) CURRICULUM:

SERIES XXXIV

ANALYZING GEOMORPHOLOGICAL AND ECOLOGICAL CHANGES IN VENICE LAGOON SALT MARSHES THROUGH REMOTE SENSING AND FIELD OBSERVATIONS

(financed by Fondazione Cariparo)

Coordinator: Prof. CLAUDIA AGNINI & Prof. ANDREA D'ALPAOS

Supervisor: Prof. ANDREA D'ALPAOS

Co-Supervisor: Prof. MARCO MARANI

Prof. SONIA SILVESTRI

Ph.D. student: ZHICHENG YANG

ANALYZING GEOMORPHOLOGICAL AND ECOLOGICAL CHANGES IN VENICE LAGOON SALT MARSHES THROUGH REMOTE SENSING AND FIELD OBSERVATIONS

ZHICHENNG YANG
Supervisors: **ANDREA D'ALPAOS, MARCO MARANI, SONIA SILVESTRI**

January 12, 2022

Abstract:

Salt marshes are important ecosystems, providing vital ecosystem services, but at the same time they are among the most fragile landscapes in the world. Halophytic vegetation is of critical importance in supporting marsh survival through complex eco-morphodynamic feedbacks. Analyzing the role of halophytic vegetation in biogeomorphic processes on salt marshes is a key step to understand and predict their morphodynamic evolution. Towards this goal, using both field data and remote sensing observations, we have analyzed changes in marsh vegetation distribution both in the vertical and horizontal frames, between 2000 and 2019, for the San Felice salt marsh (in the Venice Lagoon, Italy). Our main results suggest that: i) the previously reported vegetation-elevation relationship (e.g., halophytic vegetation species encroach specific elevation ranges, i. e., ecological niches, displaying a species sequence with increasing elevations) is found to be reliable and consistent at the whole marsh scale and, most importantly, over a period of 20 years. This is suggested to be a signature of vegetation resilience to changes in the forcings. ii) Although all marsh sites increased their absolute elevations with site-specific rates, marsh elevations relative to the current relative mean sea level (RMSL) decreased in time, indicating the possible drowning of the marsh. This indicates the need to consider local marsh elevations referenced to RMSL when monitoring marsh surface evolution and response to changes in the environmental forcings. iii) Halophytic vegetation species modified the elevation at which they populate the marsh platform with site- and species-specific trends in response to the increase in RMSL. iv) The proposed Random Forest Soft Classification algorithm developed for vegetation classification is accurate and allows one to analyze vegetation dynamics in space and time. We note that *Spartina* and *Salicornia* are more likely to be replaced by bare soil, whereas *Limonium* and *Sarcocornia* tend to encroach unvegetated areas, and the transitions among different species or between vegetated and unvegetated spots are widely observed over the marsh, indicating that eco-geomorphic patterns are highly dynamic and site-specific. v) The newly developed Random Forest Regression algorithm for the analysis of Lidar data is reliable to construct lidar-derived DEMs over the marsh with high accuracy. This represents an important tool to monitor marsh eco-geomorphic patterns, furthermore providing means to inform and test eco-geomorphic models. vi) The coupling of the corrected lidar-derived DEM and remotely sensed vegetation maps suggests that the vegetation-elevation relationship is also consistent at the whole marsh scale. vii) Finally, we also realized that marsh vegetation can quickly balance the loss in the above-ground biomass (AGB) caused by a dieback event of *Spartina* through the eco-morphodynamic feedbacks.

Our results are of critical importance for further eco-morphodynamic analyses, especially in the case of marshes encroached by multiple halophytic vegetation species. In addition, we also suggest that the application of different types of remote sensing data is a useful tool to analyze eco-morphodynamic processes over the marsh.

Sommario:

Le barene sono ecosistemi di grande importanza che forniscono servizi ecosistemici vitali, ma allo stesso tempo sono tra gli ambienti più fragili al mondo. La vegetazione alofila svolge un ruolo fondamentale nel sostenere la sopravvivenza delle barene attraverso complessi feedback eco-morfodinamici. L'analisi del ruolo della vegetazione nei processi bio-geomorfologici sulle barene è un passaggio fondamentale per comprendere e prevedere la loro evoluzione morfodinamica.

A tal fine, utilizzando sia dati di campo che dati telerilevati, abbiamo analizzato i cambiamenti nella distribuzione della vegetazione alofila sia nel piano verticale che orizzontale, tra il 2000 e il 2019, per la barena di San Felice (nella Laguna di Venezia, Italia).

I risultati principali dello studio suggeriscono che: i) la relazione tra vegetazione e quota, precedentemente riportata da altri autori (ad es., specie alofite diverse popolano specifici intervalli di quota, cioè nicchie ecologiche, che mostrano una sequenza di specie a quote crescenti) è risultata affidabile e coerente a scala di barena e, soprattutto, per un periodo di 20 anni. Si suggerisce che questo sia un segno della resilienza della vegetazione ai cambiamenti delle forzanti; ii) sebbene diversi siti sulla superficie di barena abbiano aumentato la loro quota assoluta con tassi diversi, le quote delle barene rispetto all'attuale livello medio relativo del mare (LMRM) sono diminuite nel tempo, indicando la possibile sommersione della barena. Ciò suggerisce la necessità di considerare le quote locali delle barene riferite al LMRM per monitorare l'evoluzione della superficie di barena e la risposta ai cambiamenti delle forzanti ambientale; iii) le specie alofile hanno modificato la quota alla quale popolano la barena con andamenti *sito* e *specie* specifici in risposta all'aumento del LMRM; iv) l'algoritmo di Random Forest Soft Classification sviluppato per la classificazione della vegetazione, si è dimostrato accurato, consentendo di analizzare la dinamica della vegetazione nello spazio e nel tempo. *Spartina* e *Salicornia* hanno maggiori probabilità di essere sostituite da suolo nudo, mentre *Limonium* e *Sarcocornia* tendono a invadere le aree prive di vegetazione, e le transizioni tra specie diverse o tra zone vegetate e non vegetate sono ampiamente osservate sulla barena, indicando che i modelli eco-geomorfici sono altamente dinamici e sito specifici; v) il nuovo algoritmo Random Forest Regression per l'analisi dei dati Lidar è affidabile per costruire DEM derivati dal lidar sulle barene con elevata precisione, rappresentando uno strumento importante per monitorare i processi eco-geomorfologici di barena, fornendo inoltre mezzi per informare e testare modelli eco-geomorfologici; vi) L'accoppiamento tra il DEM derivato dal lidar e le mappe della vegetazione telerilevate suggerisce che la relazione vegetazione-elevazione è coerente anche a scala di barena. vii) Infine, le analisi evidenziano che la vegetazione di barena può bilanciare rapidamente la perdita di biomassa superficiale causata die back della Spartina attraverso i feedback eco-morfodinamici.

Tutti questi risultati sono di grande importanza per ulteriori analisi eco-morfodinamiche, soprattutto nel caso di barene popolate da molteplici specie di vegetazione alofila. Inoltre, suggeriamo anche

che l'applicazione di diversi tipi di dati telerilevati sia uno strumento utile per analizzare i processi eco-morfodinamici sulle barene.

CONTENT

List of figures

List of tables

Chapter 1: INTRODUCTION

1.1 OVERVIEW

This study mainly explores marsh eco-morphodynamic processes through the analysis of salt-marsh vegetation elevation and vertical and spatial distribution patterns. Salt-marsh eco-morphodynamic processes and feedbacks are agreed to be a key factor controlling marsh development, survival, and resilience to climate changes and human pressures. These processes are crucially controlled by the presence of vegetation, whose dynamics is strongly intertwined with the dynamics of marsh topography. Indeed, halophytic vegetation influences marsh erosional and depositional patterns, thus controlling the marsh surface evolution and survival (Bouma et al., 2005; Fagherazzi et al., 2020; Kirwan et al., 2016; Kirwan and Murray, 2007; Langston et al., 2020; Marani et al., 2013; Morris et al., 2002; Mudd et al., 2010, 2009; Roner et al., 2016; Silvestri et al., 2005; Temmerman et al., 2003; Yousefi Lalimi et al., 2020, 2017). Therefore, improving our current knowledge of halophytic vegetation distribution and temporal dynamics, coupled with the dynamics of marsh platform elevations, is of critical importance to understand marsh eco-morphodynamic feedbacks. Towards the goal of better understanding marsh vegetation eco-morphodynamic processes, vegetation distribution and changes are analyzed through remote sensing observations and field campaigns. The vertical distribution of halophytic vegetation, represented by the known vegetation-elevation relationship (i.e., each species tends to encroach specific elevation ranges, resulting in the observation of a species sequence with increasing elevations), was first analyzed at both the local and whole marsh scales. Temporal changes in this relationship were explored through the analysis of a unique dataset including accurate vegetation-elevation *in-situ* measurements in different years. The vegetation-elevation relationship was then analyzed at the whole marsh scale by coupling the lidar and multi-spectral remote sensing data. Finally, the marsh eco-morphodynamic processes were explored through the analysis of vegetation spatial changes by the application of a newly developed species-classification method to a series of multi-spectral data. This work was mainly carried out in the San Felice marsh (in the Venice lagoon, Italy) as a study case. Although we have tailored our analyses to the case of the Venice Lagoon, as a mirror of what climate change and human interferences have in store for coastal landforms of the future, the results and conclusions from this study would be of great value to improve our current knowledge of the ecological and geomorphological processes over marsh platforms in different contexts.

Keywords: eco-morphodynamics; salt marshes; halophytic vegetation; remote sensing

1.2 STATE OF THE ART

Tidal landscapes are transition zones between marine and terrestrial systems. They can be divided into three main sub-environments (Figure 1.1): channel networks, salt marshes and tidal flats. In specific, channel networks cut through salt marshes, forming the main paths for the exchange of water, sediments, nutrients and energy between marshes and open water (Marani et al., 2003a; Moffett et al., 2010; Ursino et al., 2004; Xin et al., 2013). Tidal flats are located between mean sea level (MSL) and mean low water level (MLWL), acting as the nursery of seagrass (Donatelli et al., 2018; McLeod et al., 2011). Finally, salt marshes, located in areas with elevations higher than MSL but lower than the mean high water level (MHWL) (Allen, 1995; Anisfeld et al., 2017; Bockelmann et al., 2002), are the main habitats of halophytic vegetation (Allen, 2000; Marani et al., 2010a, 2004; Watson and Byrne, 2009).

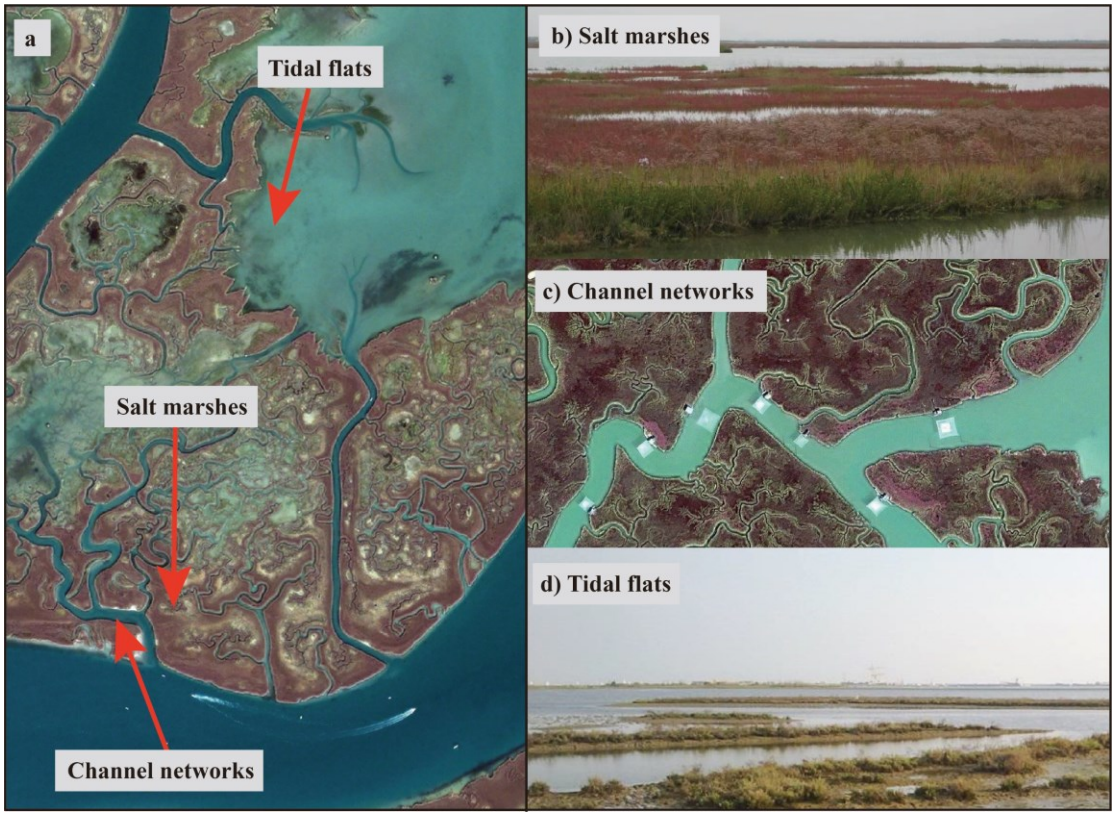

Figure 1. 1: An example of sub-environments of the tidal landscape.

Salt marshes are of critical importance for the ecological and geomorphological processes acting in tidal landscapes (Callaghan et al., 2010; D'Alpaos et al., 2007b; Kirwan and Mudd, 2012; Koppel et al., 2005; Osland et al., 2014; Taramelli et al., 2021; Vittori Antisari et al., 2017; Zhao et al., 2019). Salt marshes provide valuable ecosystem services. They host high primary production and serve as nursery areas for fish (Erickson et al., 2007; Ghosh et al., 2016; Morris, 1990; Scarton et al., 2002), improve water quality by filtering nutrients and pollutants (Stefanon et al., 2012), prevent coastal areas from waves and storms (Möller et al., 2014; Möller and Spencer, 2002; Rupprecht et

al., 2017), and also serve as important global carbon sinks (Erickson et al., 2007; Ghosh et al., 2016; Kulawardhana et al., 2014; Mudd et al., 2009; Mueller et al., 2016; Negrin et al., 2015). Unfortunately, salt marshes are disappearing fast in the last centuries, because of the accelerating relative sea-level rise (RSLR), reduction in sediment availability, lateral erosion caused by waves, and increasing human interferences (Marani et al., 2011a, 2010a; Schulze et al., 2021; Silvestri et al., 2018; Tommasini et al., 2019; Volpe et al., 2011a).

Marsh vulnerability in the vertical plane is mainly controlled by the balance between marsh accretion and relative sea level rise (RSLR), which has become an urgent issue in recent decades, because the rate of RSLR in the 21st century has been predicted to be higher than in previous centuries (Donnelly et al., 2004; Kirwan et al., 2010; Nicholls and Cazenave, 2010). Marsh accretion rate (R_{acc}) is partially controlled by local topography, i.e., lower elevations have a higher probability to be inundated and therefore receive more sediments delivered by tides (D'Alpaos et al., 2011, 2007b; Kirwan and Murray, 2007; Temmerman et al., 2003b). Marsh accretion rates are also controlled by the channel networks. Indeed, R_{acc} generally decreases with distance from channels to the inner marsh portions, due to the fact that sediment concentration is reduced towards the inner marsh portions (D'Alpaos et al., 2007; Temmerman et al., 2003a, 2003b).

Halophytic vegetation species, the plants that grow in salty and periodically inundated environments (Li et al., 2008; Pennings and Moore, 2001; Watson and Byrne, 2009), largely control marsh erosional and depositional patterns, due to their ability to directly trap sediment (Bouma et al., 2010; Fagherazzi et al., 2012; Mudd et al., 2010), attenuate waves (Koftis et al., 2013; van Veelen et al., 2020), and control sediment resuspension (D'Alpaos et al., 2013; Green and Coco, 2014). Besides their effects on hydrological forcings, halophytic vegetation species also influences marsh survival through the species-specific productivity and decomposition rates (Curcó et al., 2002; Hemminga and Buth, 1991; Kirwan et al., 2013; Kirwan and Mudd, 2012; Liao et al., 2008; Mudd et al., 2009; Mueller et al., 2016; Negrin et al., 2015; Pozo and Colino, 1992). It clearly emerges that a better knowledge of halophytic vegetation distribution and dynamics, intertwined with marsh elevation patterns and dynamics, is of central importance to improve the current understanding of marsh eco-morphodynamics and evolution.

Halophytic vegetation is organized by sharply defined patches composed of single species or typical species associations, i.e., so-called *zonation* patterns, which are the net result of edaphic conditions (Álvarez Rogel et al., 2001; Anisfeld et al., 2017; Fariña et al., 2018; Steven C Pennings and Callaway, 1992), species-competition (Bertness and Ewanchuk, 2002; Engels et al., 2011; Pennings et al., 2003), and the capability of halophytes to engineer salt-marsh landscapes via bio-geomorphic feedbacks (Da Lio et al., 2013; Marani et al., 2013). It should be recalled that the halophytic vegetation distribution is strongly linked to the marsh morphology (Silvestri et al., 2003), i.e., each species lives within typical elevation ranges (ecological niches), constituting a species sequence in

the vertical frame. Such sequences have currently been reported in many marshes worldwide (Granse et al., 2021; Hladik et al., 2013; Janousek et al., 2019; Silvestri et al., 2005). In addition, the vegetation-elevation relationship has become an important ingredient to set up models focused on marsh evolution considering landscapes encroached by multiple species (D'Alpaos and Marani, 2016; Da Lio et al., 2013; Feagin et al., 2010; Marani et al., 2013; Morris, 2006).

Increasing rates of relative sea level rise (RSLR) can directly increase flooding and ultimately intensify physical stress (Donnelly and Bertness, 2002; Janousek et al., 2016; Steven C. Pennings et al., 2005; van Dobben et al., 2022; Visser et al., 2003), thus possibly leading the species occupying lower marsh portions to migrate to higher marsh areas and substitute higher species (Anisfeld et al., 2017; Donnelly and Bertness, 2002; Qi et al., 2021; Schieder et al., 2018; Stralberg et al., 2011). However, vegetation migration and inter-specific replacements are strongly species- and site-specific, because they are controlled by physiological adjustments (Alber et al., 2008; Janousek et al., 2016, 2020; Pellegrini et al., 2020a, 2018a, 2017; Strain et al., 2017; Vittori Antisari et al., 2017) and inter-specific activities (Huckle et al., 2000; Pennings et al., 2003; Pennings and Callaway, 1996; Pennings and Moore, 2001). The determination of how typical species change their preferable elevation ranges in response to RSLR in the marsh landscapes is crucial to understand community changes and marsh evolutions, but it has seldom been explored (Anisfeld et al., 2017; Donnelly and Bertness, 2002; Langston et al., 2020; Wasson et al., 2013). Our analyses address this important issue. The main goal of this Ph.D. thesis is to contribute to filling this gap through the analysis of a dataset recording changes in marsh surface elevations conditioned by the appearance of different species in different years to test the stability of the vegetation-elevation relationship over a period of about 20 years.

The available documented vegetation sequences (Janousek et al., 2019; Marani et al., 2006a; Qi et al., 2018; Schoutens et al., 2020; Silvestri et al., 2005, 2003) are mainly obtained from *in-situ* field campaigns, i.e., marsh elevations and vegetation cover were measured and recorded at a limited number of sites, while whether this sequence can also be observed at the whole marsh scale is still unknown, because marsh surface elevation is not the only factor controlling vegetation distribution (Moffett and Gorelick, 2016; Sanderson et al., 2001; Zheng et al., 2016). The possibility to extend the observed species sequence at large spatial scales is challenged by the use of using *in-situ* measurements, because field campaigns involving a large number of field collections are labor-intensive and time-consuming (O'Neil et al., 2018; Palubinskas, 2013; Tinkham et al., 2014). The latest remote sensing techniques represent an efficient tool to address this issue, because they can accurately record spectral and elevation information over large areas (Goodin et al., 2015; Moffett and Gorelick, 2013; Thenkabail et al., 2004). Thus, the suitable utilization of remote sensing data implies the possible opportunity to validate the *in-situ* measured vegetation-elevation relationship at the whole marsh scale. This is a crucial step to inform and test ecomorphodynamic models of marsh evolution.

It is worth emphasizing that vegetation distribution information over the marsh is a necessary input in the vegetation-elevation relationship extension. Taking advantage of the development and application of vegetation species classification methods, halophytic vegetation species have been mapped in the form of pixel-based (Belluco et al., 2006; Timm and McGarigal, 2012; Van Beijma et al., 2014) and object-based (Berhane et al., 2019; Fournier et al., 2007; Juel et al., 2015; Lantz and Wang, 2013; Moffett and Gorelick, 2013; Yeo et al., 2020) schemes. The majority of these schemes are mainly based on the traditional hard classification algorithms, which identify the dominant species or associations in each pixel. However, halophytic vegetation species are highly mixed at the scale of typical satellite sensor resolutions (Silvestri et al., 2003; Wang et al., 2007).

Fractional abundance (FA), i.e., the fractional projection area of each species or bare soil, is a critical representer of halophytic vegetation distribution (Melville et al., 2019; Wang et al., 2007), which is strongly linked to the above- and below- ground biomass production (O'Connell et al., 2021; Roelfsema et al., 2014), marsh evolution and vulnerability (Fivash et al., 2021; Ganju et al., 2017). Yet, the number of studies focused on retrieving the FA of halophytic vegetation species or bare soil in each pixel is still limited (Reschke and Hüttich, 2014; Silvestri et al., 2003; Wang et al., 2007). In addition, most of the available methods aiming at FA estimation are based on neural network algorithms (Costa et al., 2017; Wang et al., 2007), whose performance heavily depends on their interior design. Indeed, minor changes in the number of layers and neurons can significantly affect the final results and the accuracy, such that it is difficult to provide a general neural network architecture that can be easily applied in different environments furthermore populated by different species. Thus, the development of new methods to estimate FA of each halophytic species or bare soil is a critical step in this study.

It is also worth recalling that the elevation data over the whole marsh are also necessary to extend the vegetation-elevation relationship to large spatial scales. Light Detection and Ranging (lidar) has a great potential as a useful tool to acquire accurate elevation data and construct digital elevation models (DEMs) for the whole marsh, because it has been widely used to estimate elevation in other landscapes (Gilmore et al., 2008a; Passalacqua et al., 2015; Sadro et al., 2007). However, the applications of lidar to marsh-DEM construction and the related vertical distribution analyses are challenged by the low accuracy and the narrow habitat elevation range of halophytic species (Buffington et al., 2016; Hladik et al., 2013; Hladik and Alber, 2012; Klemas, 2011). The inaccuracies of lidar over the marsh are mainly due to the poor laser penetrability through the halophytic vegetation (Klemas, 2011).

To accurately construct lidar-derived DEMs of marsh surface, a large number of algorithms that are used for lidar error reduction have been proposed in recent decades (Buffington et al., 2016; Chassereau et al., 2011; Rogers et al., 2018; Schmid et al., 2011; Wang et al., 2009). For example, the minimum-bin gridding method (MBG) uses the lowest lidar return to change the size of the

moving window in order for the return to penetrate the vegetation canopy and reach the marsh surface. This method then uses some gridding schemes to generate the final DEM. The main shortcoming of this method is that it would lose a lot of point-cloud information, and the gridding process could cause some errors. Hladik and Alber (2012) developed a vegetation correction factor (VCF) method, e.g., correct lidar-derived DEM by the application of species-specific factors, but the high heterogeneity of halophyte organizations might limit its broad application to marsh landscapes populated by many species. Buffington et al., (2016) considered the NDVI as the main representer of halophyte biomass and structure thus linking these properties to the error of lidar (so-called LEAN method). However, the large areas inundated by water over the marsh would prevent NDVI from conveying correct information on vegetation structure and biomass (Kearney et al., 2009), further attenuating the accuracy of this method.

Both VCF and LEAN methods indicate that the key step to construct an accurate lidar-derived DEM is to accurately estimate the vegetation biomass and composition. As mentioned before, the FA of each species and multi-spectral data-derived NDVI are important indicators of vegetation biomass and structure. There is a clear gap that might be filled by fully using accurate vegetation information to develop a new method to correct lidar-derived marsh surface elevation. Thus, in this study, we contributed to fill this gap by considering the FA of each species and NDVI in a nonparametric regression model (Random Forest regression, RFR) to correct lidar-derived DEM.

Some authors have reported that channel networks also control the distribution of halophytic vegetation, by affecting edaphic conditions and sediment transport (Moffett et al., 2010; Sanderson et al., 2001, 2000, 1998; Ursino et al., 2004; Xin et al., 2013), while the relevant evidence in the literature is still lacking (Sun et al., 2020; Zheng et al., 2016). On the other hand, some *in-situ* observations suggest that the distribution of halophytic vegetation species is not strongly linked to channel network patterns (Silvestri et al., 2005), due to the fact that the observed effects of channel networks on edaphic conditions are limited to a narrow range (Ursino et al., 2004). It therefore emerges that the link between halophytic vegetation and channel networks is still unclear, calling for further evidence at the whole marsh scale.

Changes in the halophytic vegetation spatial distribution also retain signatures of changes in the ecological and morphological processes over the marsh. In particular, vegetation species replacement at a given place suggests that the occurrence of changes in the local elevation referred to relative mean sea level (RMSL) (Kirwan and Gedan, 2019; Qi et al., 2021). Moreover, the transitions between vegetated configurations and bare soil are strongly linked to changes in marsh surface elevations (Donnelly and Bertness, 2002; Fivash et al., 2021; Qi et al., 2021) and edaphic chemical conditions (Alber et al., 2008; Kearney, 2015; Raposa et al., 2017) such that become important indicators of marsh health and survival. In addition, changes in the patch-size distribution of halophytic species also indicate variations in environmental conditions, although such

distributions are consistent with power laws (Marani et al., 2006a; Zhao et al., 2019) within a period of multiple years (Taramelli et al., 2018). The patch-size distribution has been characterized as an indicator of the self-organization processes of the salt-marsh ecosystem (Pascual et al., 2002; Scanlon et al., 2007; Schwarz et al., 2018; Taramelli et al., 2018, 2017, 2013; Weerman et al., 2012; Zhao et al., 2019), representing the physical stress and inter-specific feedbacks (Kéfi et al., 2007; Scanlon et al., 2007; Taramelli et al., 2021, 2013).

Many previous analyses that focused on marsh vegetation spatial changes were mainly based on remote sensing images with coarse resolutions (O (10 m)) or on some vegetation indexes (such as NDVI) (Doughty et al., 2021; Givnish et al., 2008; Pan et al., 2018; Patil et al., 2015; Wei et al., 2018; Wu et al., 2020). Due to the fact that halophytic vegetation species are highly mixed at the scales of these pixels, previous studies lost a lot of information on species replacement and associated environmental changes. Thus, the bio-geomorphic dynamics caused by the species replacement are more likely to be neglected. In addition, the presence of water on the marsh tends to increase the noise in the vegetation information induced from vegetation indexes (Kearney et al., 2009). Moreover, the detection of vegetation self-organization processes through the analysis of patch-size distribution is seldomly documented (Taramelli et al., 2018), although it has been widely carried out in arid zones to analyze environmental changes (Kéfi et al., 2007; Lin et al., 2010; Pueyo, 2011; Scanlon et al., 2007). Thus there is also a clear gap hindering one to analyze changes in halophytic vegetation spatial distribution to detect marsh eco-morphodynamic processes. We contribute to filling this gap by the application of the latest vegetation classification method to a temporal series of remote sensing data with high spatial resolutions (O (1 m)) to monitor variations in halophytic vegetation spatial distribution, thus further detecting changes in environmental forcing.

The above-ground biomass (AGB), which is intrinsically related to the below-ground biomass (BGB) (Adam Langley et al., 2013; Curcó et al., 2002; Daleo et al., 2008; O'Connell et al., 2021; Penk et al., 2020), controls the marsh eco-morphodyanmic processes and survival (D'Alpaos et al., 2011; Kirwan & Murray, 2007; Morris et al., 2002; Wu et al., 2020). However, the spatial distribution of the AGB over a typical marsh and its dynamics have seldomly been documented (Jensen et al., 2020). This issue could be addressed FA map of each species together with field observations (Roelfsema et al., 2014). Therefore, the final aim of this study is to detect the changes in AGB at the whole marsh scale to analyze eco-morphodynamic feedbacks.

To address all the above recalled issues, we analyzed the link between halophytic species and marsh elevation over a wide range of spatial scales, from the local scale through *in-situ* measurements to the whole marsh scale, through the coupling of field surveys and remote sensing data. Vegetation vertical distribution and dynamics were mainly addressed through the analysis of a unique local elevation-vegetation dataset (including vegetation-elevation information measured at more than

2200 sites) dating back to 2000. The coupling of lidar data and vegetation classifications (obtained through a newly developed method) allowed us to extend the vegetation-elevation relationship from the local observations (O (m^2)) to the whole marsh scale (O (km^2)). Finally, temporal changes in vegetation spatial distribution and above-ground biomass were analyzed by coupling the application of the newly developed classification method to a series of remote sensing data and field observed AGB dataset.

1.3 THE VENICE LAGOON & THE SAN FELICE MARSH

The Venice lagoon (Fig 1.2a) is a typical example of a tidal landscape, which is shaped by the above-mentioned complex ecological, physical, and geomorphological processes together with the increasing human activities.

The Venice lagoon is located in the north-eastern part of Italy, and has a waterbody of about 550 km^2, being the largest lagoon in the Mediterranean. The lagoon, characterized by a semidiurnal tide with an average tidal range of about 1.0 m and a maximum spring tidal range of approximately 1.5 m, is connected to the Adriatic Sea through three inlets: Lido, Malamocco and Chioggia (Belluco et al., 2006; Day et al., 1998; Defina et al., 2007; Marani et al., 2006a, 2004; Roner et al., 2016; Silvestri et al., 2005). The marsh area in the Venice lagoon decreased significantly during the last centuries (Carniello et al., 2009) due to the decrease in the sediment availability, determined by the diversion of the main rivers into the sea in the XVI–XIX centuries (D'Alpaos, 2007), and to the lateral erosion, caused by wave attack (Allen, 1989; Bendoni et al., 2016).

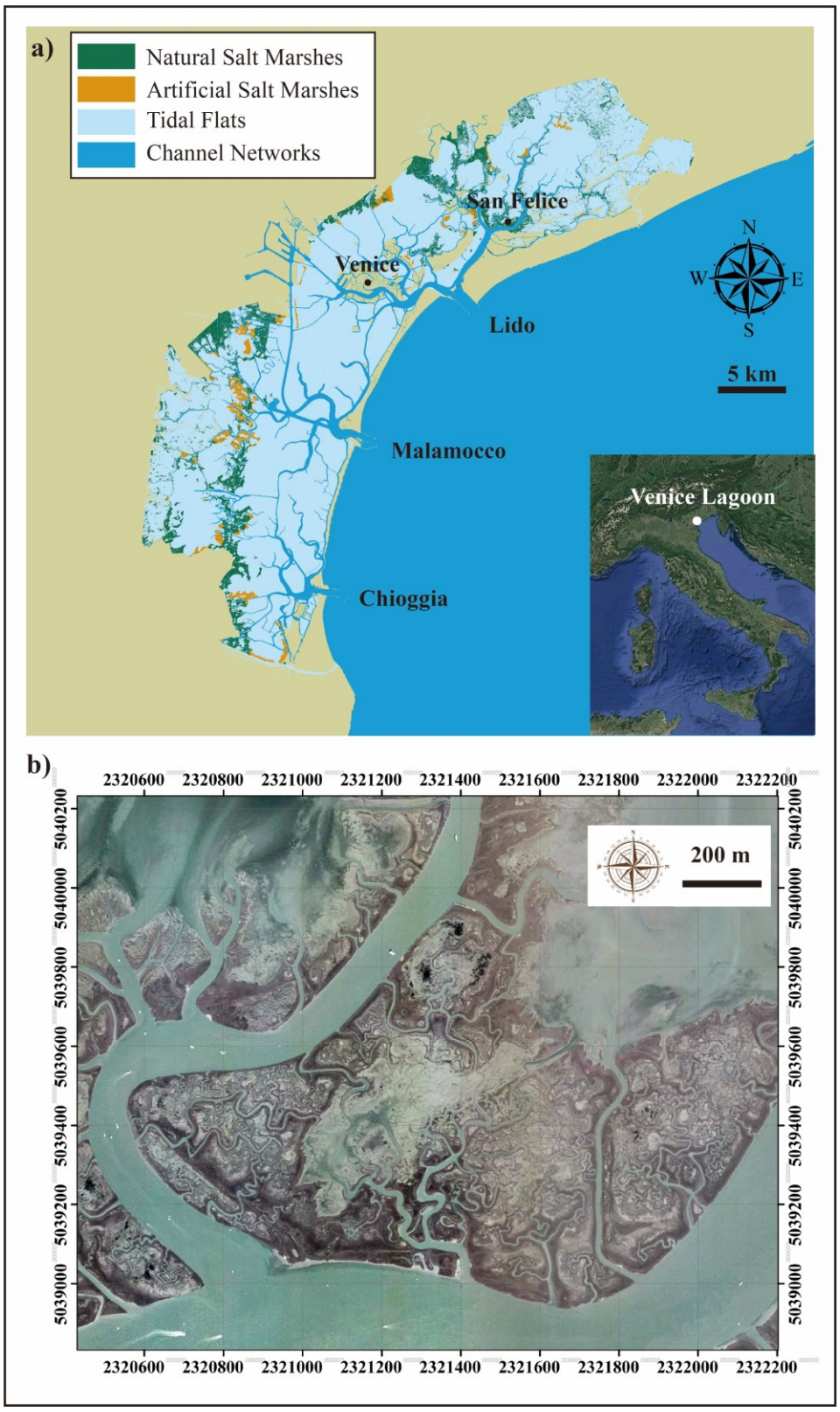

255 **Figure 1. 2**: Research area. (a) is the map of the Venice lagoon, indicating the distribution of each sub-environment and the position of the San Felice marsh in the lagoon; (b) is the map of the San Felice marsh (the base map is IKONOS image acquired in 2006).

This study is mainly carried out by considering the San Felice marsh as a study case (Fig 1.2b). The San Felice marsh is located in the northern lagoon at a short distance from the Lido inlet. This marsh

maintained its main characteristics, because of few human interventions, thus being considered as one of the most naturally preserved areas in the lagoon (Marani et al., 2006a; Roner et al., 2016).

This marsh is mainly encroached by the following species: *Salicornia veneta* (hereafter "*Salicornia*"), *Spartina maritima* (hereafter "*Spartina*"), *Limonium narbonense* (hereafter "*Limonium*"), *Sarcocornia fruticosa* (hereafter "*Sarcocornia*") and *Juncus maritimus* (hereafter "*Juncus*") (Belluco et al., 2006; Marani et al., 2003b; Silvestri et al., 2005; Silvestri and Marani, 2004; Taramelli et al., 2021; Wang et al., 2009, 2007). In specific, *Salicornia* (Fig. 1.3a) is an edible herbaceous succulent plant with a height of about 15 – 40 cm. *Salicornia* is an annual species and blooms in the late summer (July - October). *Spartina* (Fig. 1.3b) is a perennial herbaceous species with erect stems of about 30 - 70 cm high and creeping rhizomes. *Limonium* (Fig. 1.3c) has basal fleshy leaves in rosettes and a deep root system connected to a vertical rhizome storing carbohydrate reserves. It is a perennial species with a height of about 30 - 70 cm. *Limonium* has purple flowers which bloom between June and September. *Sarcocornia* (Fig. 1.3d) is a semi-woody plant with modified photosynthetic succulent stems and a superficial root system. *Juncus* (Fig. 1.3e) is a perennial bushy species with a height of about 100 cm, constituted by green stems and leaves (Pellegrini et al., 2018a; Wang et al., 2009).

Figure 1. 3: Main species in the San Felice marsh: (a) – (e) are *Salicornia*, *Spartina*, *Limonium*, *Sarcocornia* and *Juncus*, respectively.

Existing literature suggests that halophytic species in this marsh are strongly linked to the marsh geomorphology, i.e., each species lives at preferable elevation ranges thus constituting a species sequence. In specific, *Salicornia* and *Spartina* prefer to encroach marsh portions close to marsh lowest boundaries; *Limonium* is more likely to be observed on marsh portions with moderate elevations; *Sarcocornia* is usually found in areas with *Limonium* but it also can be observed on even

higher marsh portions; *Juncus* prefers to encroach marsh platforms with the highest elevations (Silvestri et al., 2005; Silvestri and Marani, 2004). It should be pointed out that *Juncus* encroaches the least area of this marsh, compared with the remaining four species (Belluco et al., 2006).

1.4 GOALS OF THE CURRENT STUDY

Aiming at analyzing eco-morphodynamic processes over the marsh platforms, this study investigates the changes in marsh platform morphology, vegetation-elevation relationship, changes in halophytic vegetation spatial distribution and above-ground biomass between 2000 and 2019 in a salt marsh in the Venice Lagoon.

The distribution and dynamics of halophytic vegetation in the vertical plane were detected through the analyses of newly collected *in-situ* measurements, together with a unique dataset dating back to 2000. The vegetation-elevation relationship was then extended to the whole marsh scale by coupling multi-spectral and corrected lidar-derived DEM. Finally, the dynamics in the spatial distribution of halophytic vegetation and above-ground biomass (AGB) were detected through the coupling of a series of remote sensing data and field observations.

Results and conclusions derived from the current analysis are of critical importance to improve our current knowledge of the marsh eco-morphodynamic processes, especially on landscapes populated by multiple species.

1.5 THESIS OUTLINE

The present work is presented in six chapters.

- Chapter 2: This chapter mainly deals with the temporal changes in the vegetation-elevation relationship. We analyzed a dataset including a series of accurate measurements of vegetation-elevation data collected over the San Felice marsh (Venice lagoon, Italy) between 2000 and 2019. Specifically, the responses of marsh surface elevation to the relative sea level rise (RSLR) is explored by analyzing changes in elevations along stable transacts and within patches with high data site densities over the monitored period. Temporal changes in the elevations of each halophytic vegetation species were analyzed to detect the dynamics in the dependency of vegetation presence on marsh elevations over multiple years.

- Chapter 3: In this chapter, we developed a novel approach to estimate the fractional abundance of halophytic species and bare soil, based on Random Forest (RF) soft classification. The main advantage of this method is that it can fully use the information contained in the frequency of votes generated by each specific decision tree. The method was then applied to the WorldView-2 (WV2) data acquired over the San Felice marsh and the estimated fractional abundance was tested against observed FA in the field survey. Our results suggest that this new approach allows one to retrieve the fractional abundance of marsh-vegetation species with high accuracy (6.7% < root-mean-square error (RMSE) < 18.7% and $0.65 < R^2 < 0.96$).

- Chapter 4: This chapter mainly deals with the extension of the vegetation-elevation relationship, derived from local-scale measurements, to large spatial scales. We first proposed a new approach by fully considering the vegetation information contained in the fractional abundance and normalized differential vegetation index (NDVI) to correct lidar-derived DEM. We then applied this method to lidar point-cloud data collected in 2003 over the San Felice marsh. The corrected DEM was then tested against marsh surface elevations measured during the field campaigns, indicating that this method is reliable because the final DEM is of high accuracy ($R^2 = 0.79$ and RMSE = 3.5 cm). The final DEM was coupled with FA maps derived from multi-spectral data acquired in 2001, which were independent from DEM, and the multi-spectral data acquired in 2003, which was used for DEM correction, to analyze the vegetation-elevation relationship at the whole marsh scale.

- Chapter 5: The focus of this chapter is to explore the marsh eco-morphodynamic processes through the analysis of the changes in the spatial distribution of halophytic vegetation. In specific, based on the application of the FA estimation method in Chapter 3 to a temporal

series of remote sensing images (2001, 2003, 2006, 2013, and 2019), we analyzed the spatial position of halophytic vegetation referred to channels, vegetation replacement and changes in the patch-size distribution. In addition, we also analyzed the changes in above-ground biomass (AGB) over the San Felice marsh together with field observed AGB of each species.

- Chapter 6 summarizes the main results of this study and draws a set of conclusions.

These chapters are intrinsically related to each other to improve our understanding of marsh eco-morphodyamic feedbacks by considering marsh platform morphology, the vegetation-elevation relationship, changes in halophytic vegetation spatial distribution and above-ground biomass in the San Felice marsh in the Venice lagoon. In particular, in Chapter 2 we support the vegetation-elevation relationship measured at local-scales and for the first time we show that the same relationship holds consistently for multiple years. Chapters 3 and 4 aim to extend the local-scale vegetation-elevation relationship (described in Chapter 2) to the whole marsh scale by coupling multi-spectral images and lidar data. More in detail, Chapter 3 proposes a new vegetation classification method to map vegetation species at the whole marsh scale. Chapter 4 provides a new method to correct lidar-derived DEM over the marsh. These two methods are key steps to extend the vegetation-elevation relationship at the whole marsh scale. In addition, Chapter 4 also shows that the vegetation-elevation relationship reported in the second chapter is still reliable at the whole marsh scale. Thanks to the methods proposed in Chapters 3 and 4, we also suggested that the above-ground biomass is tightly linked to the marsh surface elevations. Due to the fact that the vegetation-elevation relationship is consistent in space and time, we explored the marsh ecomorphodynamic processes at a large scale by analyzing the dynamics of spatial distributions of vegetation species and above-ground biomass, as described in Chapter 5. Based on analyses in previous chapters, Chapter 6 draws a set of conclusions.

Chapter 2: Long term monitoring of salt-marsh vegetation elevation changes in response to sea level rise in a microtidal system

This chapter is a manuscript ready to be submitted to Journal of Geophysical Research: Biogeosciences. The marsh surface vulnerability and the vegetation-elevation relationship were analyzed by a unique dataset including *in-situ* measured and recorded and marsh surface elevation vegetation information dating back to 2000. We first analyzed the changes in the marsh surface elevation (above the absolute datum and relative mean sea level) to explore marsh resilience and response to relative sea level rise. The temporal changes in preferable elevation ranges (above the absolute datum and relative mean sea level) of each halophytic vegetation species were analyzed to detect how halophytic vegetation species respond to changes in relative sea level. We finally validate, for the first time, the consistency of the known vegetation species sequence with increasing elevations over a period of 20 years.

PAPER

Long term monitoring of salt-marsh vegetation elevation changes in response to sea level rise in a microtidal system

Zhicheng Yang[1], Davide Tognin[2], Enrica Belluco[2], Alice Puppin[1], Alvise Finotello[1, 3], Sonia Silvestri[4], Marco Marani[2], and Andrea D'Alpaos[1*]

[1] *Department of Geosciences, University of Padua, Padua, Italy*

[2] *Department ICEA, University of Padua, Italy*

[3]*Department of Environmental Sciences, Informatics and Statistics, Ca' Foscari University of Venice, Venezia Mestre, Italy*

[4] *Department of Biological, Geological, and Environmental Sciences, University of Bologna, Bologna, Italy*

Abstract

Salt marshes are coastal ecosystems which provide fundamental ecosystem services. These ecosystems have been disappearing fast in the last decades due to climate changes and human

interferences. Improving current knowledge of salt-marsh response to changes in the environmental forcing is a key step to understand and predict salt-marsh biomorphodynamic evolution. Towards this goal, we analyzed the coupled elevation-vegetation response to changes in relative mean sea level (RMSL) in the microtidal Venice Lagoon, through accurate elevation measurements and vegetation cover information between 2000 and 2019. Our results suggest that: i) although almost all marsh sites increased their absolute elevations in time (relative to a fixed datum), elevations referred to the current RMSL decreased. Most of the marsh sites were not able to keep pace with the current rate of relative sea level rise (RSLR), thus suggesting progressive marsh drowning; ii) accretion rates, which range between 1.7 and 4.3 mm/year, are generally lower than the rate of RSLR (4.4 mm/year) and are strongly site-specific and vary at sites within distances of a few tens of meters, being controlled by local elevations and sediment availability from eroded marsh edges; iii) vegetation species respond to changes in the environmental forcing by modifying their preferential elevation ranges, and their response is species-specific. For the first time, we observe the consistency of a vegetation-species sequence with increasing elevations over a period of 20 years. We suggested that this is the signature of vegetation resilience to changes in the forcings. Our results point at a strong coupling between geomorphological and ecological dynamics, and call for spatially distributed marsh monitoring and properly informed spatially-explicit biomorphodynamic models of marsh evolution.

Key points:

- Marsh elevations need to be monitored with reference to the local, current relative mean sea level.
- Accretion rates are strongly site specific and vary at sites within distances of a few tens of meters.
- Vegetation species respond to changes in the environmental forcing by modifying their preferential elevation ranges, their response being species-specific.

2.1 Introduction

Tidal salt marshes are typical biogeomorphic features of tidal landscapes, usually located between mean sea level (MSL) and mean high water level (MHWL), thus being regularly inundated by the tide (Balke et al., 2014; Fagherazzi et al., 2012; Silvestri et al., 2005; van Belzen et al., 2017; Van der Wal et al., 2008). Salt marshes are important ecosystems between marine and terrestrial landscapes (Kirwan & Guntenspergen, 2012; Marani et al., 2003b, 2006; Schuerch et al., 2018), providing valuable ecological and geomorphological services in tidal landscapes. Marshes host high biodiversity and primary productivity (Janousek et al., 2016; Kirwan & Guntenspergen, 2010; Morris et al., 2002; Thorne et al., 2018); attenuate wave action on the coast (Möller and Spencer, 2002; Rupprecht et al., 2017; Schoutens et al., 2020); reduce flow velocities (Bouma et al., 2007, 2005; Leonard and Croft, 2006); and act as sediment trapping zones (D'Alpaos & Marani, 2016; Ganju et al., 2015; Kirwan et al., 2010; Da Lio et al., 2013; Marani et al., 2013; Mudd et al., 2010; Tang et al., 2020; Temmerman et al., 2005). Salt marshes also serve as organic carbon sinks due to their ability to sequester and store large amounts of carbon (Chmura et al., 2003; Kirwan & Mudd,

2012; McLeod et al., 2011; Mudd et al., 2009; Mueller et al., 2019; Spivak et al., 2019; Roner et al., 2016). However, these valuable ecosystems are currently disappearing fast over the world (Campbell et al., 2017; Carniello et al., 2009; Jankowski et al., 2017; Schuerch et al., 2018; Tommasini et al., 2019; Marani et al., 2007), being threatened by increasing rates of relative sea level rise (RSLR) (Blum & Roberts, 2009; Horton et al., 2018; Kirwan et al., 2010), decreasing sediment supply (Boyd et al., 2017; Silvestri et al., 2018), wave attack (D'Alpaos et al., 2013; Marani et al., 2011; Leonardi & Fagherazzi, 2014; Giulio Mariotti & Fagherazzi, 2013) and increasing human activities (Enwright et al., 2016). Their evolution and survival are controlled by the complex biomorphodynamic feedbacks (D'Alpaos & Marani, 2016; Fagherazzi et al., 2012; Murray et al., 2008).

Rates of sea level rise in the 21st century have been higher than in the previous centuries (Enwright et al., 2016; Nicholls and Cazenave, 2010), representing a great threat to marsh survival. Previous analyses have documented that marshes can keep pace with Relative Sea Level Rise (RSLR) up to a given threshold rate, through inorganic and organic deposition, controlled by complex eco-morphodynamic feedbacks (D'Alpaos et al., 2011; Fagherazzi et al., 2012; Kirwan et al., 2016; Mudd et al., 2009; Temmerman et al., 2003; Marani et al., 2007). However, tidal marshes will drown if the rate of RSLR exceeds a threshold value, which depends on local conditions such as the subsidence rate, sediment supply and the tidal range (e.g., Kirwan et al., 2010; Marani et al., 2010; D'Alpaos et al., 2011). Marsh vulnerability is highly controlled by the balance between the accretion rate (R_{acc}) and the rate of RSLR, which are agreed to change at large spatial scales and long temporal scales (Boyd et al., 2017; Brinson et al., 1995; Day et al., 1998; Détriché et al., 2011; Shi et al., 2012; Temmerman et al., 2003). In particular, modelling results suggest that marshes in microtidal environments are characterized by high vulnerability to RSLR, because the local inorganic and organic deposition rates are usually lower within these areas (D'Alpaos et al., 2011; Kirwan & Guntenspergen, 2010) compared to meso- and macrotidal ones. However, analyses on how microtidal marshes respond to increasing rates of RSLR, in particular through detailed field observations, are still lacking and deserve further analyses of the type proposed herein.

Halophytic vegetation, which grows environmental conditions typical of coastal landscapes, i.e., frequent inundation and high salinity, plays a key role in the eco-morphodynamic evolution of salt marshes, due to its influence on erosional and depositional patterns (e.g., Morris et al., 2002; D'Alpaos et al., 2007; Kirwan and Murray, 2007; Marani et al., 2007; Fagherazzi et al., 2012). A large body of analyses has emphasized that halophytic vegetation can support marsh survival by reducing surface erosion (Bouma et al., 2007; Bouteiller & Venditti, 2015; Collins, 2004) and water flow velocities (Leonard and Croft, 2006; Leonard and Luther, 1995; Lightbody and Nepf, 2006; Zong and Nepf, 2010) and by attenuating lateral retreat (Brisson et al., 2014; Möller et al., 1999) and increasing marsh vertical accretion (D'Alpaos et al., 2012; Kirwan & Murray, 2007; Kirwan et al., 2010; Morris et al., 2002; Reents et al., 2021). Marsh surface elevations are strongly linked to

vegetation presence and therefore, a better understanding of such a tight relationship can help one to better understand and predict marsh response to the increase in RMSL.

Salt-marsh vegetation is usually organized in a single species or typical species associations, a process known as *zonation* (Belluco et al., 2006; Collin et al., 2010; Fariña et al., 2018; Marani et al., 2006; Pennings et al., 2005; Pennings & Callaway, 2015; Silvestri et al., 2005; Snow & Vince, 1984; Engels et al., 2011). Halophyte zonation can be considered as the result of vegetation adaptation to edaphic conditions (Janousek et al., 2016; Marani et al., 2006; Moffett & Gorelick, 2016; Muñoz-Rodríguez et al., 2017; Pennings et al., 2003; Schile et al., 2011; Xin et al., 2013) and species competitions (Huckle et al., 2000; Steven C Pennings et al., 2005; Steven C. Pennings and Callaway, 1992). Marani et al. (2013) and Da Lio et al. (2013) highlighted through biomorphodynamic modelling and field observations that zonation patterns are the result of the interaction and mutual adjustment between biomass production and soil accretion, and that halophytes actively tune soil elevation to maintain them to live within ranges of optimal adaptation. The observed zonation bio-geomorphic patterns are therefore the signature of multiple stable states, generated by competing vegetation species adapted to different elevation ranges. Indeed, halophytic vegetation distribution is intertwined with marsh morphology. A large number of the existing literature has documented that each halophytic vegetation species has lives within specific elevation ranges, which can be considered as the ecological niche (Granse et al., 2021; Janousek et al., 2019; Silvestri et al., 2005). As a result, halophytic species over the same marsh compose a species sequence with increasing elevations, which has been observed in many marshes over the world (Donnelly & Bertness, 2002; Schoutens et al., 2020; Silvestri et al., 2005; Todd et al., 2010). Silvestri et al. (2003) also suggested that halophytic vegetation species can be considered as an indicator of marsh elevation.

RSLR also affects the growth and distribution of halophytic vegetation through the increase in physical stress (Colmer & Flowers, 2008; Fagherazzi et al., 2019; Jensen et al., 2020; Kirwan et al., 2016; van Regteren et al., 2020), allowing species occupying lower marsh portions to replaced their higher counterparts (Donnelly and Bertness, 2002; Qi et al., 2021). However, such displacements and the responses of vegetation to RSLR might be site- and species-specific (Janousek et al., 2016; Morris et al., 2002), and possibly determined by the tolerance to increasing stress (Pellegrini et al., 2017, 2018a; Strain et al., 2017), inter-specific cooperation or competition (Pennings et al., 2005) and environmental conditions (Pennings et al., 2009; Qi et al., 2021). The determination of how typical species respond to RSLR in microtidal marshes is a key step to understand vegetation community changes and marsh evolution, an issue that has rarely been explored (Pellegrini et al., 2020; Strain et al., 2017) and that is one of the main issues addressed this paper.

Towards the goal of better understanding how marsh surface elevations and halophytic vegetation species respond to RSLR, we analyzed a multi-year dataset of coupled marsh elevation-vegetation

field observations which were collected over a salt marsh in the Venice lagoon (Italy) between 2000 and 2019. Specifically, two main questions are addressed in this paper: i) how do marsh respond to changes in the rate of RSLR? How can one quantitatively address this response? Is the response space-dependent? ii) How are halophytic vegetation species adjusting to RSLR?

2.2 Materials and Methods

2.2.1 Research area

The Venice lagoon (Italy), is the largest lagoon in the Mediterranean Sea (Fig. 2.1a). It is characterized by a waterbody area of about 550 km^2, a semi-diurnal tide with an average tidal range of about 1.0 m, and a maximum spring tidal range of approximately 1.5 m (Roner et al., 2016; Tommasini et al., 2019; Yang et al., 2020). The lagoon is connected to the Adriatic Sea by three inlets: Lido, Malamocco, and Chioggia. The total inputs of freshwater and sediments are modest, because the main rivers that used to debouch into the lagoon were diverted directly to the sea in the XVI–XIX centuries (D'Alpaos, 2010). The lagoon has been experiencing a severe morphological erosion in the last century, due to a number of processes among which human alterations to sediment supply, the construction of jetties at the inlets, the excavation of large navigable channels, and the increase in the rate of RLSR (including both eustatism and subsidence) promoted a significant decrease in salt marsh area (Carniello et al., 2009; D'Alpaos, 2010; Day et al., 1998; Laengner et al., 2019; Silvestri et al., 2018; Tommasini et al., 2019).

The considered dataset was collected over the San Felice marsh (Figures 2.1a and b), which is located in the northern part of the lagoon. This area is mainly bounded by the San Felice channel and by the Spacco Tralo channel (Figure 2.1b). The San Felice marsh is one of the most naturally preserved areas within the lagoon (Marani et al., 2003a; Roner et al., 2016). Marsh surface geomorphology in the San Felice marsh is linked to the channels (Silvestri et al., 2005; Roner et al., 2016), showing that marsh surface elevations decrease with increasing distance to main channels. The marsh area decreased significantly in the last century mainly due to the inner pond enlargement and wave attack (Day et al., 1998), highlighting the importance of further analyses on marsh vulnerability in this area.

The San Felice marsh is encroached by typical halophytic vegetation species of the Venice Lagoon, such as *Salicornia veneta* (hereafter "*Salicornia*"), *Spartina maritima* (hereafter "*Spartina*"), *Limonium narbonense* (hereafter "*Limonium*"), and *Sarcocornia fruticosa* (hereafter "*Sarcocornia*") (Belluco et al., 2006; Marani et al., 2003b; Marani et al., 2006; Silvestri et al., 2005; Wang et al., 2007; Yang et al., 2020). Previous field campaigns (Silvestri & Marani, 2003; Silvestri et al., 2005) documented a typical species sequence with elevation, i.e., *Salicornia* and *Spartina*

usually encroach lower elevations, *Limonium* is more likely to be observed on areas with moderate elevations, and *Sarcocornia* prefers to occupy the highest marsh portions.

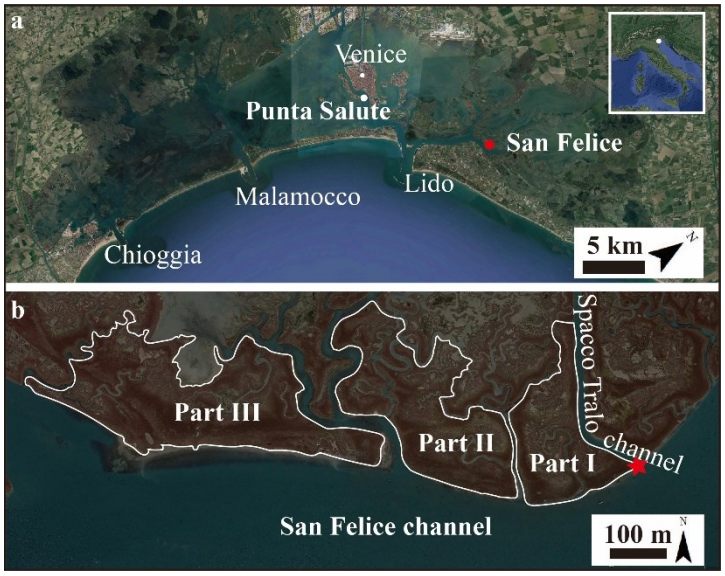

Figure 2. 1: Research area: the Venice Lagoon, Italy; (a) shows the map of the Venice lagoon and the location of the San Felice marsh; (b) shows different parts of the San Felice marsh considered in our analyses. The red star is the crossover point of marsh boundaries along the San Felice and Spacco Tralo channels (base maps are collected from Google Earth, https://www.google.com/earth/).

2.2.2 Methods

To answer the research questions recalled in the Introduction section, the rate of RSLR, marsh accretion rate, and halophytic vegetation migration rate in the corresponding period need to be estimated.

2.2.2.1 Sea level measurements

Long-term analyses of sea level changes in the Venice lagoon can be assessed based on water level measurements performed by a network of tide gauges managed by the Venice municipality (https://www.comune.venezia.it/it/archivio/1653). Water levels recorded by Punta Salute (PS) tidal gauge station (Fig. 2.1a) are considered in our analyses to represent the conditions of the San Felice marsh due to the short distance between the P.S. tidal gauge and the long monitoring history of the P.S. tidal gauge (https://www.comune.venezia.it/content/1-punta-salute-canal-grande). It is worth recalling that, even though the PS tidal gauge is 10 km far from the San Felice salt marsh, the hydrodynamic model developed by D'Alpaos & Defina (2007) shows that the water level differences between the two sites are small (O(1cm)).

Tidal gauge measurements are referred to a benchmark at Punta della Salute (ZMPS, https://www.comune.venezia.it/it/content/riferimenti-altimetrici). The ZMPS was referred to the Italian IGM benchmark, the unique zero benchmark in Genova where IGM stays for "Istituto

Geografico Militare" (Military Geographic Institute). The IGM benchmark was observed to be higher than the ZMPS of 23.56 cm in 1968. However, it has been documented that the elevation of ZMPS decreased in time with a rate of about 0.5 mm/year due to natural and human-induced subsidence (Carbognin et al., 2004; da Lio et al., 2017; Tosi et al., 2018; Trincardi et al., 2016). On the contrary, the elevation of the IGM datum is stable. To correctly estimate changes in RMSL, the annual average values of tidal gauge records from the PS station were then referred to the IGM datum, accounting for the above-recalled subsidence rate.

Water levels in the lagoon are influenced by storm events and waves on the short term (O(days)) (Mel et al., 2014), by astronomic forcing on longer timescales (O(1-10 years) (Valle-Levinson et al., 2021), and by human activities at even longer time scales (O(10-100 years). Valle-Levinson et al. (2021) demonstrated that the interannual variability of mean sea-level in the northern Adriatic sea is associated with lunar precessions, solar activity, and the interaction, or interference, between them. However, marsh elevations and the related accretion rates have been shown unable to record annual or interannual fluctuations in RMSL (D'Alpaos et al, 2011). Therefore, in order to investigate changes in marsh elevations with reference to the IGM datum, but most importantly to the current RMSL, we considered a linear approximation of annual RMSLs (above the absolute IGM datum) between 2000 and 2019 and considered the approximated RMSL values of each year to determine marsh elevations relative to MSL. Therefore, changes in marsh surface elevations (and of the elevations encroached by the different vegetation species) above the current RMSL were obtained by referring to the measured elevations (above the absolute IGM datum) to the approximated RMSL of each specific year.

2.2.2.2 Elevation of marsh surface

Accurate topographic measurements were carried out on randomly selected sites (Figure 2.2) on different marsh portions. The San Felice marsh was surveyed 7 times in different years between 2000 (Silvestri et al., 2005) and 2019 (e.g., 2000, 2002, 2003, 2004, 2006, 2013 and 2019, as shown in Table 1). It should be noticed that data points in 2000, 2013 and 2019 are evenly distributed over the marsh, while data collected in 2002, 2003, 2004 and 2006 are mainly of some typical homogeneous halophyte species patches. In specific, geographic positions and soil elevations were measured through a total station with a high precision (O (2 mm)). All the total station measurements are referred to the IGM datum, which has been used to determine the rate of RSLR in Section *2.2.1*, allowing us to estimate the relative positions of marsh platform and vegetation above MSL for each specific year.

In order to explore the spatial variability of the marsh vertical displacement, the research area was divided into three parts (Part I, II and III in Figure 2.1b).

Table 2. 1: Number of data point of the field work collection

Number of Sites	2000	2002	2003	2004	2006	2013	2019
Part I	88	--	82	--	30	138	284
Part II	51	247	93	76	--	--	104
Part III	99	335	332	149	120	--	108

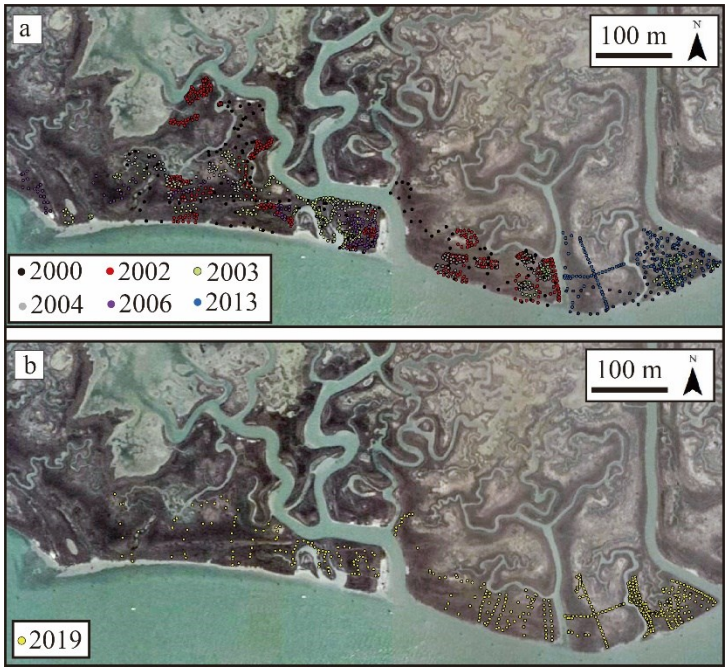

Figure 2. 2: The position of the surveyed points; (a) shows the position of data sites collected in 2000, 2002, 2003, 2004, 2006 and 2013; (b) shows the position of data sites collected in 2019. The base map is the composition of RGB bands of an IKONOS image acquired on August 31, 2006.

Soil elevations and vegetation cover of ten stable transects, all starting on the marsh boundary and ending in either inner marsh portions or at minor creek edges were monitored between 2000 and 2019. Five transects (Figure 2.3a) were surveyed two times in 2000 and 2019, and other five transects were surveyed twice in 2013 and 2019. These transects allow us to analyze marsh surface elevations and their changes (the accretion rates, R_{acc}) together with changes in vegetation cover. The local accretion rate, R_{acc} (mm/year), was estimated as the ratio between the difference in elevations measured in different years (referenced to IGM datum) and the considered time interval Three patches with high data-point density were also selected in each part to estimate marsh surface accretion and to analyze marsh platform vulnerability to RSLR. Then, a paired point sub-dataset composed of corresponding data points in 2000 and 2019 was also used for the further observation of the marsh surface changes in Part III. In specific, we constructed a buffer zone with a radius of 5 m around data points in 2000 in this part. The data points visited in 2019 which fall in such buffers are selected to construct the 2019-part of this sub-dataset. Then data points in 2000 that have near neighbors (<5 m) collected in 2019 are considered as the 2000-part in this sub-dataset. Finally, platform elevations measured from transects, patches and paired points were projected to the current RMSL of the specific considered year to detect the relative elevation changes. The number of data sites in patches and pair-point are listed in Table 2.2.

To address vegetation elevation changes, vegetation observations were carried out at the same time as the marsh elevation measurements. *Salicornia*, *Spartina*, *Limonium* and *Sarcocornia* are the main species in this area (Silvestri et al., 2003, 2002) and their fractional abundance was estimated using the standard Braun-Blanquet visual method, which records the presence of each species in an area of about 1 m^2 by 10 intervals between 0% and 100% (Silvestri et al., 2005). The numbers of times that each species was recorded are listed in Table 3. The elevation change rate (R_c) of each species is also determined by the linear fitting of its yearly mean elevation (above the IGM datum). The submergence trend of each species is estimated by the differences between R_c and R_{rsl}.

2.2.2.3 Marsh boundary retreat estimation

We employed the DSAS (Digital Shoreline Analysis System) extension 5.0 (Himmelstoss et al., 2018) for ArcGIS 10.5 to estimate the marsh boundary retreat rate in the last 20 years. In specific, we digitalized marsh boundaries along the San Felice channel from its cross point (red star in Fig. 2.1b, hereafter 'cross point') with Spacco Tralo channel in an east direction on the remote sensing images acquired over this marsh acquired in 2001 (IKONOS, spatial resolution = 1 m) and 2019 (WV 2, spatial resolution = 0.5 m). To accurately describe the marsh boundary retreat trend in each marsh portion, transects were evenly generated with a small space of 5 m. Consequently,162 transects (e.g., 39, 41 and 82 transects for Part I, Part II and Part III, respectively) starting from the cross point (Fig. 2.1b) were used in marsh retreat rate estimation.

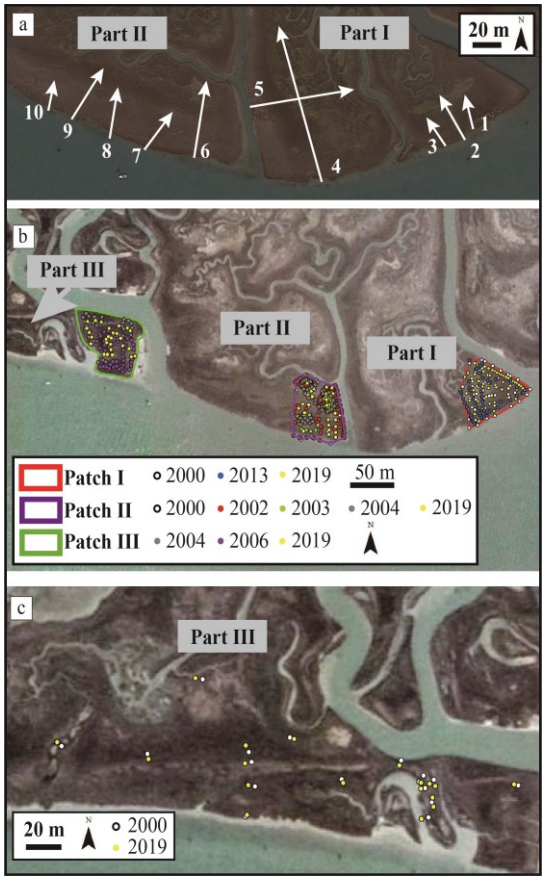

Figure 2. 3: Position of marsh sites considered to determine marsh vertical accretion; (a) position of the selected transects; (b) position of patches; (c) position of paired data points in Part III. Base map of (a) is collected from Google Earth (https://www.google.com/earth/) and base maps of (b) and (c) are collected from IKONOS data acquired in 2006.

Table 2. 2: Number of data points (n) of the elevation dataset, collected in the different parts of the San Felice marsh, at different years.

	Transects				**Patches**											**Paired-point**	
Part	Part I		Part II		Part I			Part II					Part III			Part III	
Year	2013	2019	2000	2019	2000	2013	2019	2000	2002	2003	2004	2019	2004	2006	2019	2000	2019
n	73	71	21	21	48	49	97	18	129	57	40	36	42	56	27	17	18

Table 2. 3: Number of data sites for each vegetation species in the in the different parts of the San Felice marsh, at different years. I = Part I; II = Part II; III = Part III.

Number of data sites	**2000**			**2002**			**2003**			**2004**			**2006**			**2013**			**2019**		
	I	II	III	I	II	III	I	II	III	I	II	III	I	II	III	I	II	III	I	II	III
Salicornia	-	-	-	-	-	-	-	-	-	-	-	-	23	-	-	23	-	-	48	13	12
Spartina	18	11	15	-	87	68	47	17	50	-	24	37	-	-	-	27	-	-	33	5	12
Limonuim	46	24	36	-	100	206	--	68	149	-	38	125	-	-	55	77	-	-	170	81	59
Sarcocornia	51	36	56	-	174	211	31	65	126	-	38	56	-	-	98	62	-	-	185	79	75

2.3 Results

2.3.1 Sea level changes of the San Felice Marsh

We first analyzed the changes in relative mean sea level (RMSL). The annual average values of sea level (MSL) generally increased in the considered period, indicating the San Felice marsh is subjected to a RSLR trend, with an average rate of about 4.4 mm/year (black dashed line in Figure 2.4). In fact, the measured annual average value of sea level (black dots in Figure 2.4) fluctuated around this trend, being the result of astronomic forcing, storms and human activities (Mel et al., 2014; Silvestri et al., 2018; Valle-Levinson et al., 2021). Whereas numerical modelings have suggested that marsh surface cannot record such fluctuations (D'Alpaos et al., 2011; Kirwan & Murray, 2008). Thus, values in the trend (red dots in Figure 2.4) can represent the RMSL in each specific year and allow us to analyze the marsh and vegetation elevations above RMSL.

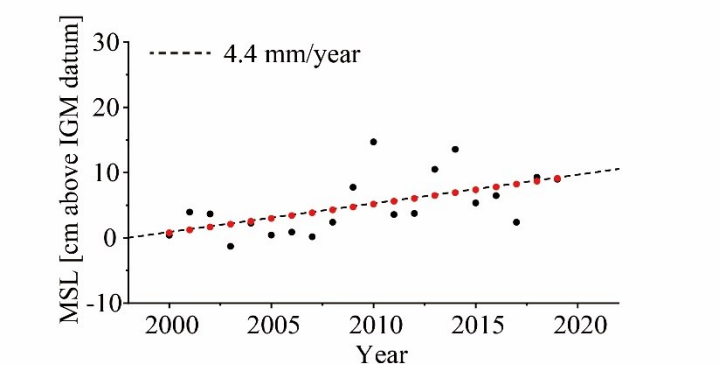

Figure 2. 4: Mean annual RMSLs (measured by the Punta Salute station) referred to the IGM datum, measured between 2000 and 2019. Black dots represent measured data, red dots represent RMSLs used in the analyses.

2.3.2 Marsh surface elevation changes between 2000 and 2019

We first analyzed changes in marsh elevation along the ten transects shown in Fig. 2.3a. Fig. 2.5 shows the mean marsh elevation along the ten transects measured with reference to the IGM datum between 2013 and 2019 (Fig. 2.5a for Part I) and between 2000 and 2019 (Fig. 2.5b for Part II). Elevations measured with reference to the IGM datum display an increase in time for Part I and II, although with different accretion rates. Indeed, inorganic and organic sediment deposition allowed the marsh to increase its elevation in this 20-year period with rates of about 1.7 mm/year (Part I, Fig. 2.5a) and 4.3 mm/year (Part II, Fig. 2.5b). However, if one considers marsh elevations referenced to the RMSL of the specific considered year (Fig. 2.4), it emerges that only Part II (Fig. 2.5d) is characterized by accretion rates that tend to balance the rate of RSLR (4.4 mm/yr, Fig. 2.4). Indeed Part I displays a constant decrease in elevations referenced to the RMSL (Fig. 2.5c), thus suggesting that this portion of the marsh cannot keep pace with the increase in RMSL. Although for both transects in Part I and II one can observe an increase in the absolute marsh

elevations (referred to the IGM datum), changes in marsh elevations relative to MSL show that only Part II can keep pace with the incr4ease in RMSL.

More in detail, the analysis of the behavior of the single transects in Part I (transects 1-5 in Fig. 2.6) and Part II (transects 6-10 in Fig. 2.7) confirms the above general trend, but furthermore allows one to further investigate the spatial dependency of marsh response to changes in the forcing. Figs 2.6 and 2.7 show marsh elevations along the transects together with vegetation cover for the considered surveys. Our data show that marsh platform elevations generally decrease with distance from channels (Figs 2.6 and 2.7), mainly due to the fact that sediment concentration decreases towards the inner marsh portions (Coleman et al., 2020; Kirwan & Murray, 2007; Roner et al., 2016; Schuerch et al., 2019; Temmerman et al., 2003; D'Alpaos et al., 2007; Marani et al., 2013).

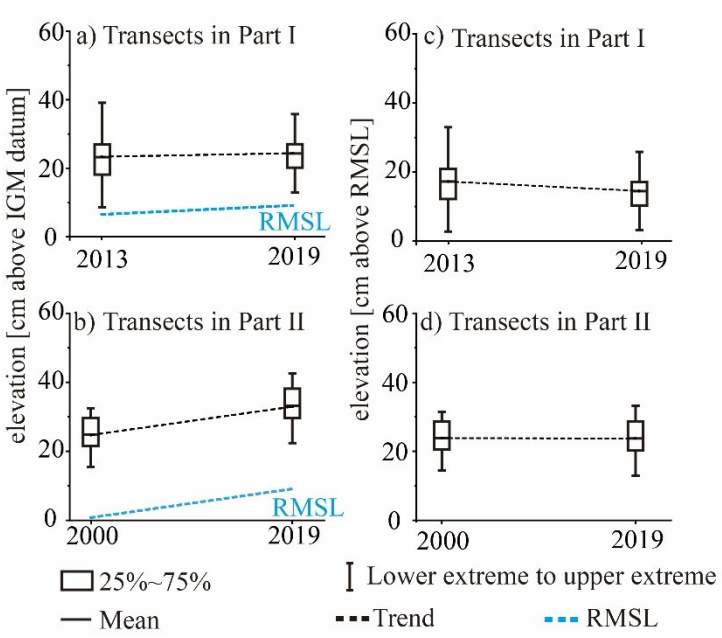

Figure 2. 5: Box whisker plots of average marsh elevations along transects in Part I and Part II at different years; (a) and (b) show absolute elevations above the IGM datum; (c) and (d) show elevations above RMSL. The dashed blue line in panels (a) and (b) represents RMSL.

Data for the specific transects in Part I (Fig. 2.6) show that while marsh elevations referenced to the IGM datum did not display notable changes in time (consistent with the average accretion rate of 1.7mm/yr described above), marsh elevations referenced to RMSL decreased in time, thus suggesting that these marsh sites lost elevation above RMSL and were not able to pace with the increase in RMSL. Vegetation cover along transects displayed minor changes. In transect 2, *Limonium* was replaced by *Sarcocornia* at the margins of the transect, whereas a transition from *Limonium* to bare soil was observed in the inner marsh. In transect 3, bare soil spots in the inner marsh portion were encroached by *Sarcocornia* and *Limonium*. In transect 4 a transition from vegetated configurations (populated by *Limonium* and/or *Salicornia* and/or *Spartina*) to bare soil new states were observed.

Fig. 2.7 shows changes in marsh elevations along every single transect in Part II. Marsh sites along Transects 6 – 10 (Fig. 2.3a) display a notable increase in marsh elevations referenced to the IGM datum (Fig. 2.7 a-e), which tends to balance the rate of RSLR, thus suggesting that these sites are able to keep pace with the increase in RMSL (Fig. 2.7f-j) their average accretion rate (4.3 mm/yr) being quite close to the rate of RMSL rise (4.4 mm/yr). In terms of vegetation cover along these transects, minor dominant species replacements were observed. In transect 6 (Fig. 2.7f), a transition from vegetated configurations populated by *Limonium* to bare soil new states was observed, together with the replacement of vegetation species characteristic of higher elevations to lower elevation species were observed (transitions from *Sarcocornia* to *Limonium*) were local decrease in elevations relative to RMSL were observed.

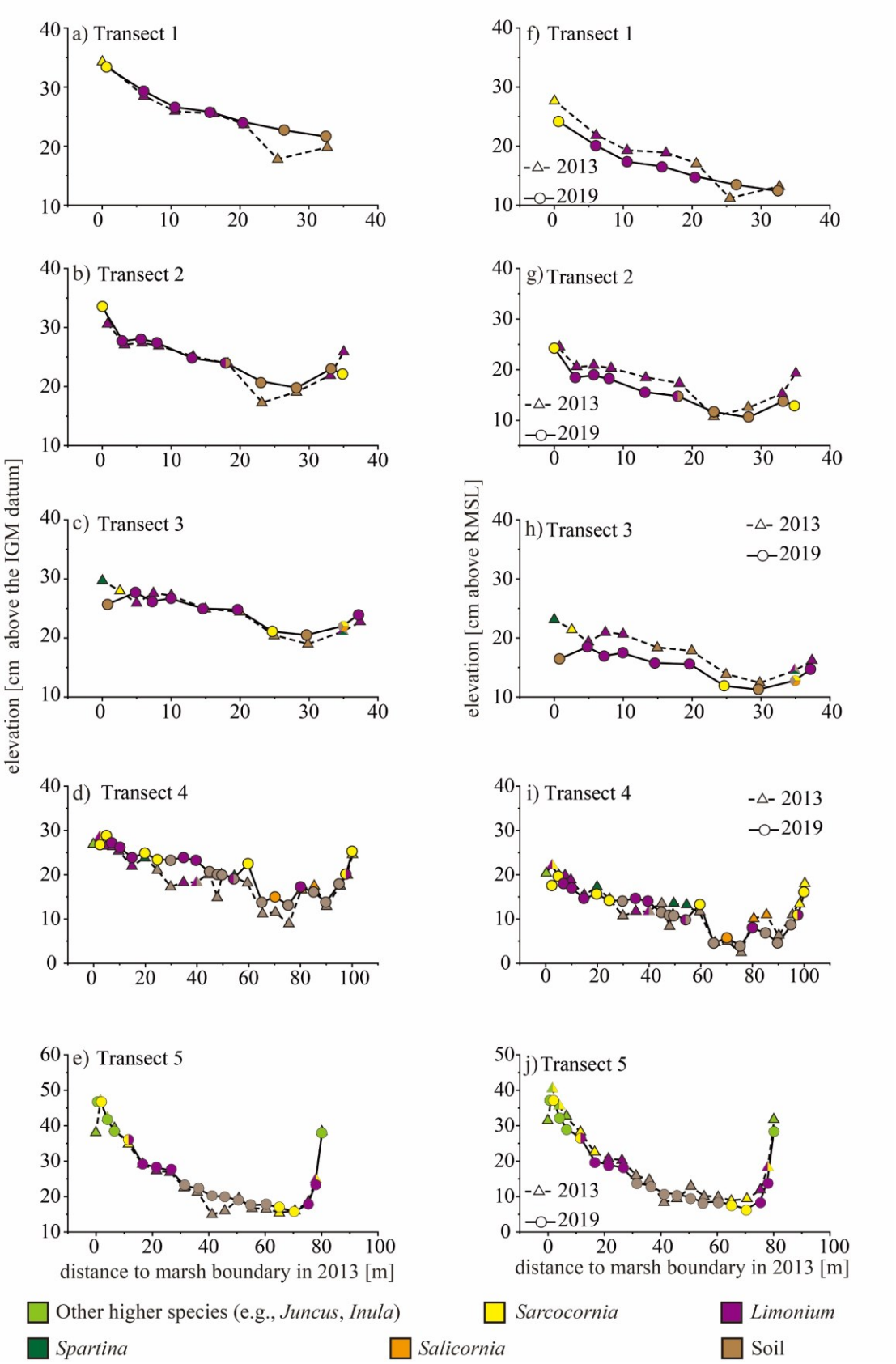

Figure 2. 6: Marsh elevations along transects 1 – 5 between 2013 and 2019, together with local dominant vegetation species surveyed in the same years. The left column shows elevations above the IGM datum, whereas the right column shows elevations above RMSL (Fig. 2.4).

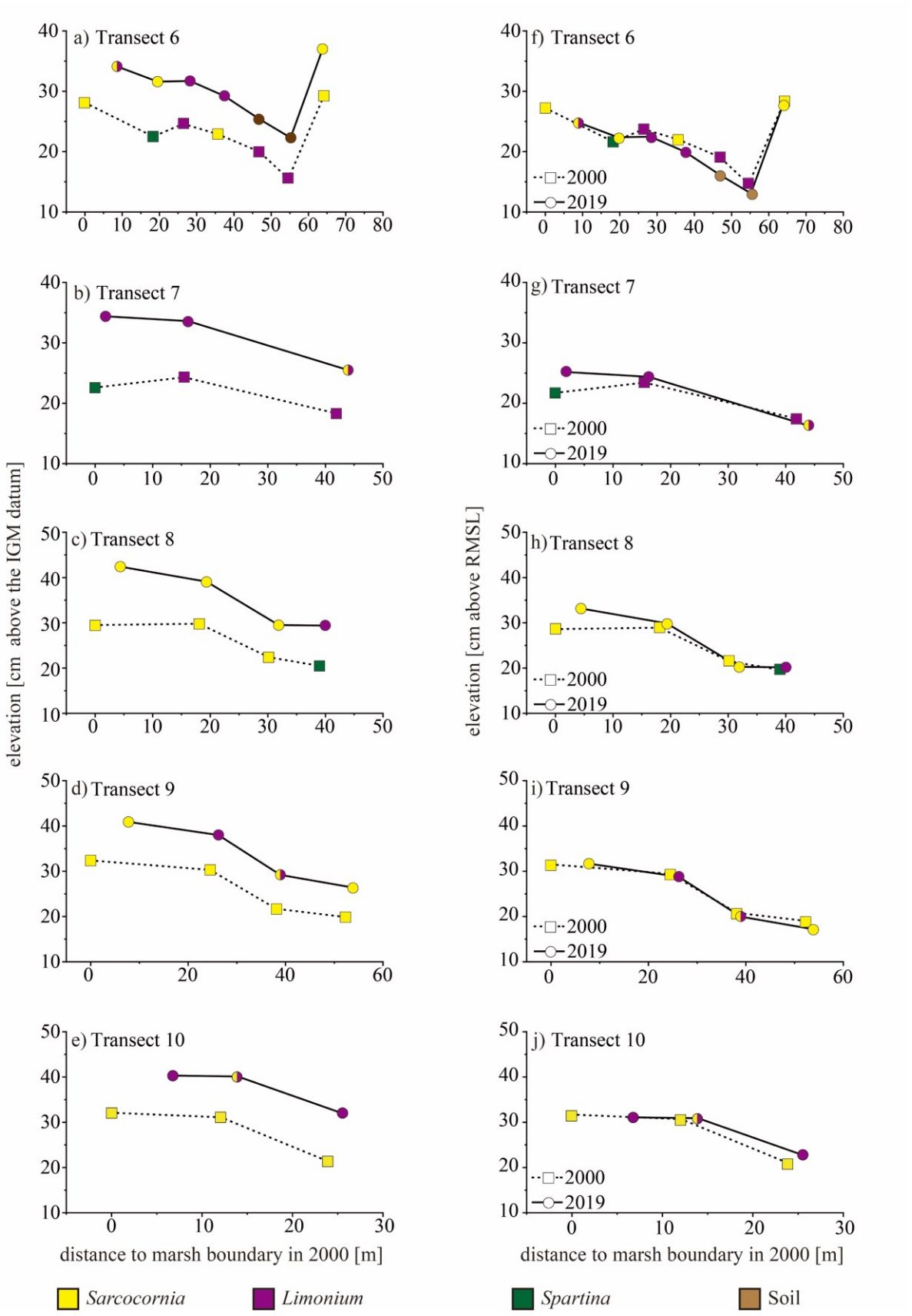

705 **Figure 2. 7:** Marsh elevations along transects 6 – 10 between 2000 and 2019, together with local dominant vegetation species surveyed in the same year. The left column shows elevations above the IGM datum, whereas the right column shows elevations above RMSL (Fig. 2.4).

Elevation measurements at the same marsh sites allow one to analyze the dependency of accretion rates (R_{acc}) on marsh geomorphology. Fig. 2.8 suggests that R_{acc} generally decreases with increasing elevations, indicating that organic and inorganic sediment deposition is higher at sites with lower elevations, allowing lower marsh portions to keep pace with the increase in RMSL. A few marsh sites, located in Part I along transects 3, 4, and 5, displayed a temporal decrease in elevation relative to the IGM datum, likely due to local subsidence (Da Lio et al., 2018; Tosi et al., 2018, 2013). However, when comparing accretion rates with the rate of RSLR, it clearly emerges that most of the sites along transects in Part I cannot keep pace with the increase in RMSL and are therefore subjected to drowning or submergence. Sites along transects in Part II are characterized by accretion rates that tend to match the rate of RSLR, consistently with the elevation analyses in Figs. 2.5-2.7.

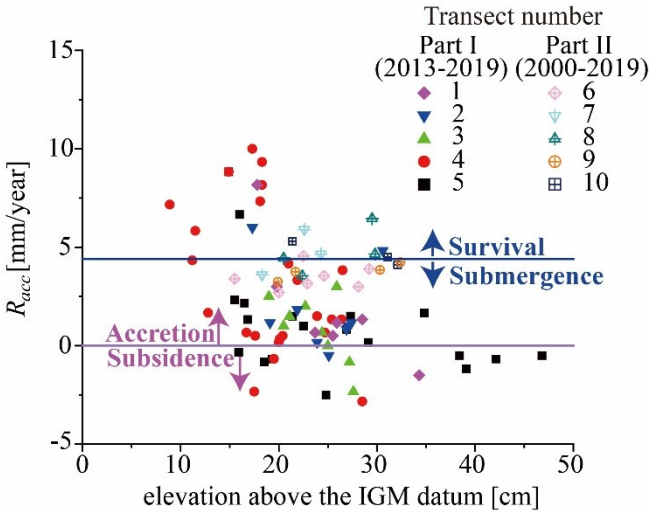

Figure 2. 8: Variations in the accretion rate, R_{acc}, as a function of local elevations. The purple line shows the null accretion state R_{acc} = 0 mm/year; i.e., points above or below the purple line experienced accretion or subsidence, respectively. The blue line portrays the rate of RSLR, R_{rsl} = 4.4 mm/year, and allows one to distinguish points that can keep pace with the increase in RMSL (survival, i.e. above the blue line) from points that progressively drown (submergence, i.e. below the blue line).

We then analyzed changes in marsh elevations within patches (Fig. 2.3b) and at paired points (Fig. 2.3c). Fig. 2.9 shows that the mean marsh elevations, referenced to the absolute IGM datum, within patches and in correspondence of paired points increased in time (Fig. 2.9a-d) with rates of about 2.2 mm/year (Part I, Fig. 2.9a), 3.4 mm/year (Part II, Fig 2.9b) and 2.4-2.9 mm/year (Fig. 2.9c-d, Part III). On the one hand, this first indicates that the marsh increased in elevation due to organic and inorganic deposition, confirming the general trend observed for mean elevations along transects (Fig. 2.5). It also suggests that the R_{acc} in Part II is higher than R_{acc} in Part I and III, furthermore emphasizing that the R_{acc} is strongly site-specific. On the other hand, however, our results show that if one considers elevations above the RMSL in the specific year (Fig. 2.4), all of these three marsh portions lost elevations relative to RMSL, thus highlighting that they cannot keep pace with the increase in RMSL (Fig. 2.9 e-h), being the R_{acc} observed in these patches (ranging from 2.2 to 3.4 mm/yr) lower than the rate of RMSL (4.4 mm/year).

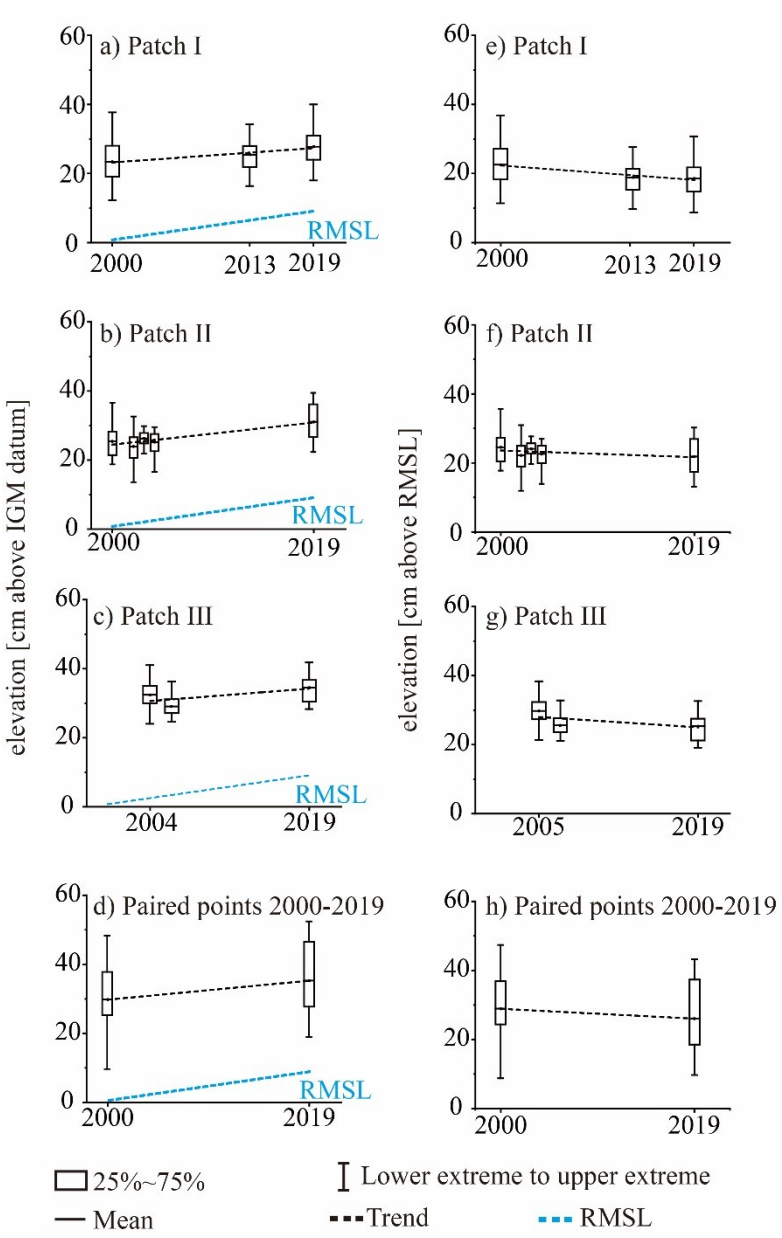

Figure 2. 9: Box whisker plots of average marsh elevations within patches and at paired points; (a)-(d) show elevations above the IGM datum; (e)-(h) show elevations above RMSL. The dashed blue line in panels (a)-(d) represents RMSL.

One might however wonder why different marsh portions, very close one to the other, display different behavior when adapting to RSLR. We suggest that the higher accretion rates in Part II are associated with the larger marsh retreat rate in this portion (Fig. 2.10), with collapsing marsh edges that provide sediments for the marsh surface to accrete vertically (Mariotti and Carr, 2014; Priestas et al., 2015). Indeed, the average boundary retreat rate in Part II was found to be equal to about 39 cm/year, and it was higher than the average boundary retreat rate in Part I (29 cm/year) and in part III (11 cm/year). We speculate this supports the hypothesis that Part II receives more sediments from eroded edges, which allows it to increase its elevations in time with larger accretion rates (Mariotti & Carr, 2014).

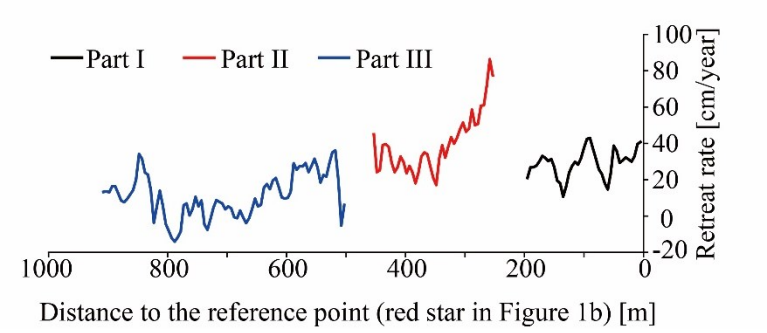

Figure 2. 10: Lateral marsh retreat rates between 2000 and 2019

2.3.3 Changes in halophytic vegetation elevation between 2000 and 2019

We then analyzed the dependence of vegetation presence on soil elevation, i.e. the range of marsh elevations encroached by each vegetation species. Our analysis shows that a species sequence with increasing elevations exists (Marani et al., 2004; Silvestri et al., 2005; Silvestri & Marani, 2004) due to the fact that each vegetation species tends to live within specific elevation ranges (i.e., ecological niches). Indeed, *Salicornia* tends to encroach the lowest marsh elevations; *Spartina* occupies marsh portions with slightly higher elevations compared to *Salicornia*; *Limonium* tends to encroach areas with moderate elevations and *Sarcocornia* is more likely to be observed on higher marsh portions (Fig. 2.11). Differences and overlaps between elevation ranges typical to each halophytic species are summarized in Fig. 2.11 for the different marsh portions considered in our analysis. Interestingly, for the first time we show that the recalled sequence displays a consistent behavior over time, since the same sequence is maintained in all marsh portions in the considered period. Although minor temporal changes in the preferred elevations for each species are observed, these changes do not alter the species sequence described above (Fig. 2.11). Moreover, we show that a given halophytic species is observed at preferential elevations which are different in the three considered marsh portions, although separated by a few hundred meters. The same sequence is shifted vertically at the three different considered marsh portions thus suggesting the development of site-specific biogeomorphic patterns.

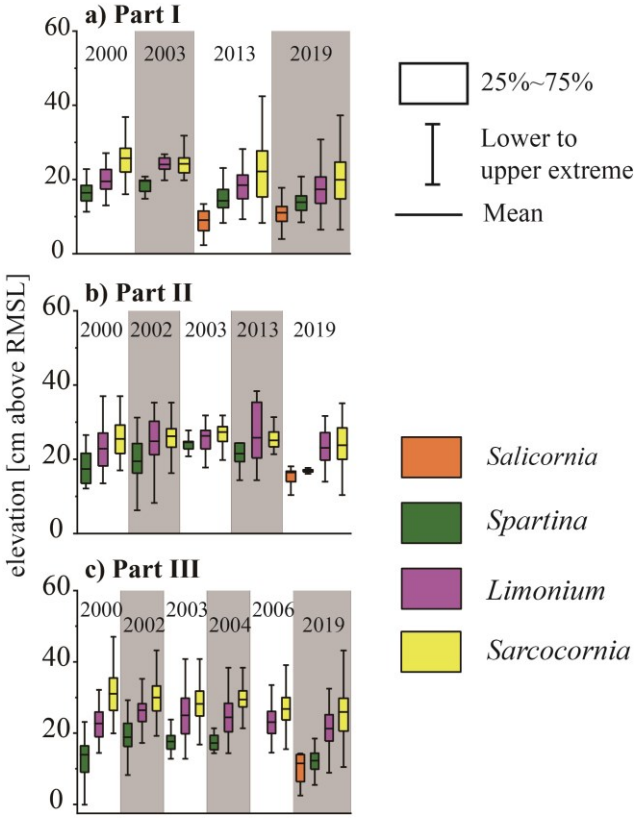

Figure 2. 11: Vegetation species sequence with increasing elevations; (a), (b) and (c) are box whisker plots of average elevations of each species above the RMSL in Part I, Part II and Part III, respectively.

Figs 2.12-2.14 display the mean elevations of each species in different marsh portions over the monitored period (Fig. 2.12 for Part I, Fig. 2.13 for Part II and Fig. 2.14 for Part III). Absolute vegetation elevations measured above the fixed IGM datum increase in time (Fig. 2.12a-d for Part I, Fig. 2.13a-c for Part II, and Fig. 2.14a-c for Part III), suggesting that halophytic vegetation tends to increase its elevation with species-specific rates (R_c, Table 2.4). *Sarcocornia* and *Limonium* are the species which tend to better adapt to the observed current rates of RSLR (Table 2.4). However, if one considers the elevations encroached by each species referred to the RMSL in the specific year, it clearly emerges that in most cases elevations tend to decrease in time (Fig. 2.12e-h for Part I and Fig. 2.14d-f for Part III) or stay nearly constant (Fig. 2.13d-f for Part II).

Records of vegetation cover across the marsh over the monitored period also allow one to analyze vegetation composition changes in time. More in detail, *Salicornia* was not recorded over the marsh between 2001 and 2004, but was observed between 2006 and 2019 in Part I (Table 2.3 and Fig. 2.12), suggesting that this invasive species that started to encroach this marsh in between 2004 and 2006. In addition, *Spartina* was not observed in 2004 and 2006 but it was recorded in the remaining years, indicating the occurrence of a dieback event for this species. These observed composition-change events are consistent with previous remote sensing observations over the same marsh before 2006 (Belluco et al., 2006).

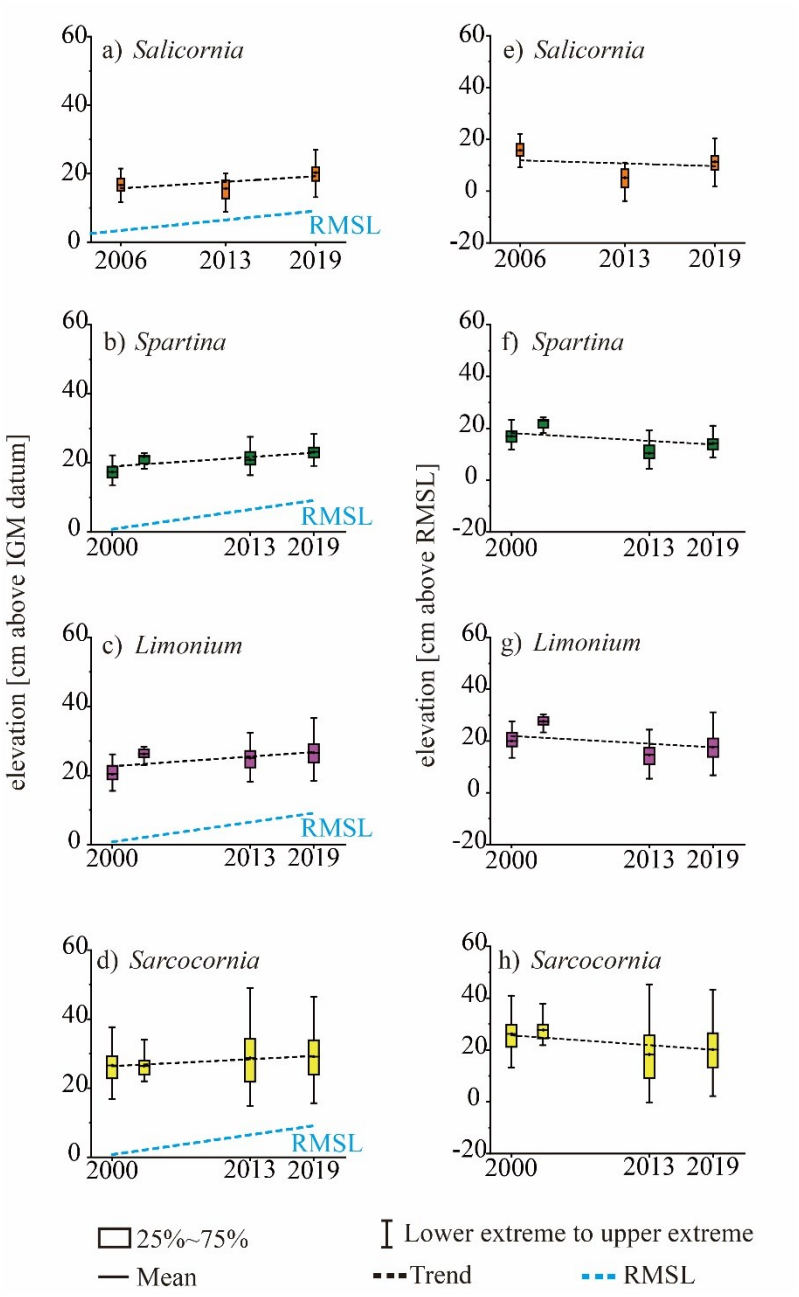

785

Figure 2. 12: Box whisker plots of average elevations encroached by each species in Part I. (a)-(d) show elevations above the IGM datum; (e)-(h) show elevations above the RMSL. The dashed blue line in panels (a)-(d) represents RMSL

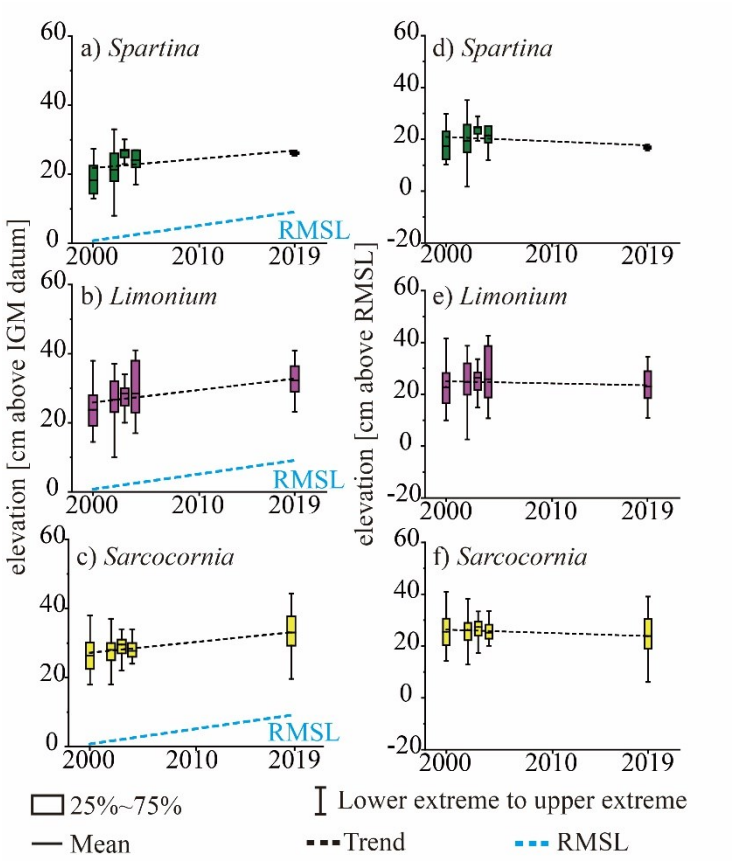

790 **Figure 2. 13:** Box whisker plots of average elevations encroached by each species in Part II; (a)-(c) show elevations above the IGM datum; (d)-(f) show elevations above the RMSL. The dashed blue line in panels (a)-(c) represents RMSL.

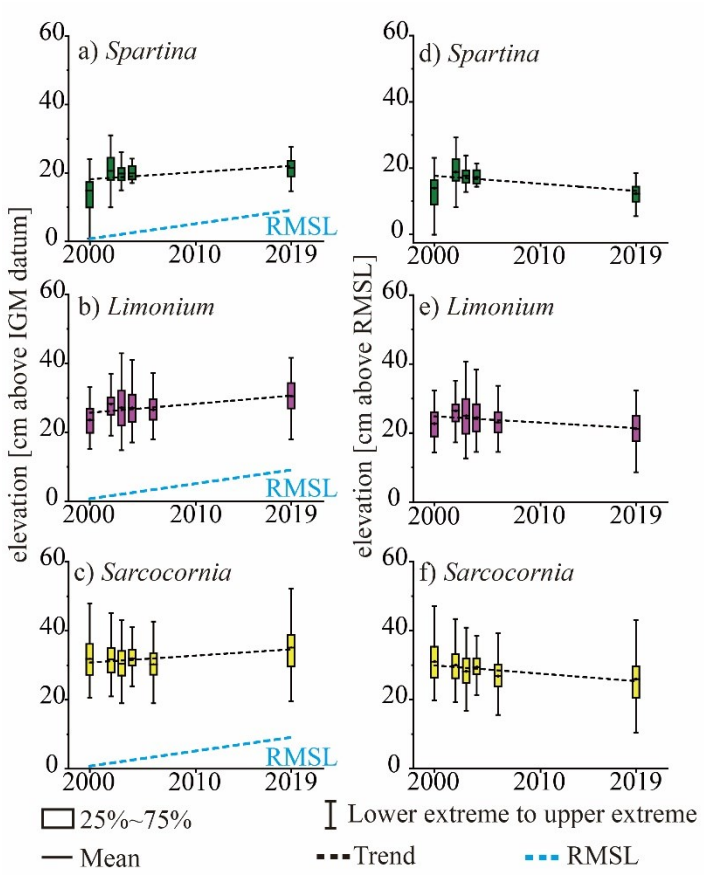

Figure 2. 14: Box whisker plots of average elevations encroached by each species in Part III; (a)-(c) show elevations above the IGM datum; (d)-(f) show elevations above the RMSL. The dashed blue line in panels (a)-(c) represents RMSL.

Table 2. 4: The elevation change rate (Rc) of each species between 2000 and 2019

R_c (mm/year)	Part I	Part II	Part III	R_{rsl} (mm/year)
Salicornia	2.7	--	--	4.4
Spartina	2.1	2.7	2.0	
Limonium	2.1	3.6	2.6	
Sarcocornia	1.5	3.1	2.0	

2.4 Discussion

2.4.1 Marsh vulnerability to current environmental forcing

Elevations measured with reference to the IGM datum suggest that organic and inorganic deposition allow the marsh to increase its elevation in the monitored period. However, it is important to note that most of the marsh areas display a decrease in the mean elevations with reference to RMSL for the specific year, suggesting a possible drowning of the marsh. Analyses of changes in marsh elevation need to consider marsh

elevations relative to the current, local value of mean sea level. Possible reasons for the alarming trend described above are: 1) the higher current rate of RSLR (R_{rsl} = 4.4 mm/year), compared to the lower rate (3.5 mm/year) observed in the Venice lagoon in the last century (Carbognin et al., 2004; Marani et al., 2007); 2) the low sediment concentration (C_0=10~30 mg/L) in the water of the lagoon (Venier et al., 2014), due to the fact that the main rivers that used to debouch into the lagoon were diverted directly to the sea in the last centuries (Marani et al. 2007; Tommasini et al., 2019), and 3) the microtidal setting, which is known to limit marsh resilience to changes in the rate of RSLR and sediment supply (D'Alpaos et al., 2011; Silvestri et al., 2018; Kirwan et al., 2010; Marani et al., 2010).

Interestingly, our results also suggest that the accretion rate (R_{acc}) and marsh response are strongly site-specific, displaying important variations also among sites separated by a few hundred meters. In particular, marsh elevation measurements along the transects suggest that the R_{acc} increases with lower marsh elevation (Fig. 2.8). In fact, lower marsh portions can receive more inorganic sediment due to the longer waterlogging period (D'Alpaos et al., 2011; Temmerman et al., 2003). Lower elevations also represent higher water-depth when the marsh is flooded by tide, which can enhance biomass production (Janousek et al., 2020; Morris et al., 2002), further improving the organic deposition. Furthermore, the R_{acc} in Part II is higher than Part I and III (Figs. 2.5 and 2.9), indicating that the accretion rate might be intrinsically related to the marsh retreat rate (Fig. 2.10). Sediments eroded from the marsh boundary can be redistributed over the marsh platform by waves and tides, thus helping the marsh to vertically keep pace with RSLR, while retreating horizontally. However, quantitatively descriptions of the link between marsh boundary retreat and vertical deposition are still lacking (Mariotti and Carr, 2014; Priestas et al., 2015), thus calling for spatially-extended field observations and modeling to facilitate analyses focused on future marsh biomorphodynamic evolution. In fact, different marshes over the world are in different submergence or resilience situations (Table 2.5).

Table 2.5: Marsh conditions in different parts of the world

Area	Condition	Reference
Delaware Bay	R	Boyd et al., (2017)
Barnegat Bay	S	Boyd et al., (2017)
Deal Island	S	Qi et al., (2021)
Mississippi Delta	S	Blum et al., (2009)
Exmouth Gulf	S	Lovelock et al., (2021)
New England salt marsh	S	Donnelly & Bertness (2001)
Yangze Estuary	R	Yang (2005)

R= resilience, S=submergence.

The marsh drowning trend suggested by the higher value of RMSL rise compared to the accretion rate, does not imply that the San Felice marsh will disappear and experience a transition to tidal flat. Indeed, marshes have strong resilience to increasing RMSLs thanks to biomorphodyanmic feedbacks. The marsh might decrease its elevation in order to increase the accretion rate and balance the rate or RSLR, up to a given threshold that, when exceeded, will lead to progressive marsh drowning. Improving sediment supply by

redirecting rivers into the lagoon or artificially adding sediments that could be later reworked and redistributed by waves and tides can be possible methods to prevent the drowning trend of the marsh.

2.4.2 Halophytic vegetation response to the increase in RMSL

Vegetation cover along the single transects in Part I (Fig. 2.6) did not display relevant species replacement, although the marsh is likely subjected to drowning, which is out of our expectations and observations in the literature (Donnelly and Bertness, 2002; Qi et al., 2021). The possible reason for the stable vegetation configuration along transects 1 - 5 can be that vegetation can tolerate the deterioration of the edaphic conditions caused by the increase in RMSL in the monitored period (6 years, between 2013 - 2019). In addition, dominant species replacement was not observed along transects 6 - 10 (Fig. 2.7) in Part II, suggesting that vegetation can persist in its position when the accretion rates can balance the increase in RMSL. Thus, we speculate that, after the increase in RMSL in a few years within a threshold (e.g., 6 years in this case), halophytic vegetation can tolerate the deterioration of physical conditions within a threshold value, and responds to RSLR mainly through the persistence in its position, instead of the vertical displacement.

The observed disappearance of *Spartina* between 2004 and 2006 due to the sudden dieback of *Spartina*, was likely associated with the drought conditions related to the heat-wave event in 2003 (Alber et al., 2008; Hughes et al., 2012; Strain et al., 2017). Salt marsh encroachment by *Salicornia* at the San Felice site after 2006 is likely due to the fact that this species is widely distributed over other marshes in the lagoon (Silvestri et al., 2005), which provides available seeds for it to encroach the platform.

Our analyses suggest that there is a typical species sequence with increasing elevation, which, for the first time, we observe to be consistent over the 20-year period (Fig. 2.11). The consistency of this sequence is of critical importance to inform marsh evolution models by considering high bio-diversity conditions (e.g., Marani et al., 2013; Dalio et al., 2013; D'Alpaos and Marani, 2016), while most of the available models mainly consider one single species (Kirwan et al., 2007, 2016; Mudd et al., 2009; D'Alpaos et al., 2011; Morris et al., 2002). Our unique time record of vegetation-elevation changes over a period of a few decades in the Venice lagoon, allowed us to highlight that vegetation respond to changes in RSLR by increasing its preferential elevation over the marsh, but with species-specific rates, possibly due to the fact that halophytic vegetation response is strongly species-dependent (Janousek et al., 2020).

The observed species sequence can be considered as a combination of vegetation adaptation to soil properties and species competition (Pennings et al., 2005). In specific, higher marsh portions, characterized by relatively lower physical stress due to lower waterlogging periods, are more likely to be occupied by species with higher compatibilities (such as *Limonium* and *Sarcocornia*), while lower marsh portions, characterized by relatively higher stress due to long-time inundation, are more likely to be encroached by species with

higher adaptability to higher physical stresses but lower compatibility (such as *Spartina* and *Salicornia*). We speculate this explains the consistency of the species sequence although elevations encroached by each species changed with species-specific rates. In particular, *Limonium* and *Sarcocornia* cannot adjust to, and live within, areas with high inundation periods, thus they tend to populate relatively higher marsh portions with hydrological stresses they can tolerate. We suggest although increasing sea levels will likely lead to a loss in marsh elevations, *Limonium* and *Sarcocornia* would still occupy positions higher than those occupied by *Spartina* and/or *Salicornia*. However, if elevations fall below a given threshold below which these species cannot survive, they will likely disappear from the marsh. At that time, the marsh will be populated by only *Spartina* and *Salicornia*, species with higher tolerance to large waterlogging stress. Further research efforts and evidence from long-time observations are needed to support these speculations.

An important source of uncertainty in our analysis might be related to the randomly selected sites over the marsh. The position and number of surveyed sites in the dataset, at which marsh surface elevation was measured and vegetation cover was recorded changed in time. This might have affected the accuracy of the estimated marsh accretion rates and vegetation elevation changes, thus calling for further field observations. Another limitation of this study is associated with the large (2237) but the relatively limited number of *in-situ* observations. Field observations of the type considered in our analyses are time-consuming, and larger-scale analyses are needed to extend our results to the whole lagoon scale, where the presence of each species is also controlled by soil properties, subsurface water dynamics, oxygen availability, reduced conditions and high sulfide concentrations (Alber et al., 2008; Marani et al., 2006; Xin et al., 2013). Our analyses also show that the specific sequence is shifted vertically also at adjacent sites and therefore it is expected to be shifted when considering different marshes in the lagoon (Silvestri et al., 2005). This calls for observations over large areas, which are possible by coupling vegetation species maps obtained through multi- or hyper-spectral data (Belluco et al., 2006; Yang et al., 2020) and digital elevation models obtained by lidar observations (Buffington et al., 2016; Hladik et al., 2013; Hladik and Alber, 2012; Wang et al., 2009).

2.5 Conclusions

We analyzed the coupled elevation-vegetation response to changes in relative mean sea level in a microtidal system (the Venice Lagoon) by using accurate elevation measurements and vegetation cover information. Our data from the San Felice marsh included data surveyed 7 times between 2000 and 2019.

Analyses of marsh elevations suggest that almost all marsh points increased their absolute elevations (relative to a fixed datum in time, the IGM datum) thanks to the coupled organic and inorganic deposition over the surface. However, when elevations referred to the current RMSL were considered, it emerged that most of the marsh sites were not able to keep pace with the current rate of RSLR, thus suggesting progressive marsh drowning. This suggests the need to refer to local marsh elevations referenced to RMSL when monitoring marsh evolution and response to changes in the environmental forcing.

In addition, we observe that marsh accretion rates are strongly site-specific and change at sites within distances of a few tens or hundreds of meters. At adjacent sites accretion rates range between 1.7 and 4.3 mm/year, with differences that crucially affect marsh response to the current rate of RSLR (4.4 mm/yr). Differences are related to local conditions, such as local marsh elevations (accretion rates are larger for lower marsh elevations) or sediment availability due to marsh lateral erosion. In the latter case, sediments eroded from the marsh edge are later deposited over the platform by waves and tides. This crucially calls for spatially distributed marsh monitoring and properly informed spatially-explicit biomorphodynamic models of marsh evolution.

Finally, we showed that vegetation species respond to changes in the environmental forcing by modifying their preferential elevation ranges. Different species vertically migrate with different rates, according to species-specific characteristics. Indeed, each species lives within specific elevation ranges, thus displaying a species sequence with increasing elevations. For the first time, we observe the consistency, over a period of 20 years, of such vegetation-species sequence. This is suggested to be a signature of vegetation resilience to changes in the forcings. We observed a dieback of *Spartina* between 2003 and 2006, and its reappearance 2013, whereas *Salicornia* started to encroach the marsh between 2003 and 2006. All these observations point at a strong coupling between geomorphological and ecological dynamics, with relevant implications for the further eco-morphodynamic analyses.

Author Contributions: Conception or design of the work, Z.Y., A.D., M.M., and S.S.; Data collection, A.D., M.M., S.S. D.T., E.B., A.P., A.F., and Z.Y.; Data analysis and interpretation A.D., M.M., S.S. and Z.Y.; Drafting the article, Z.Y. A.D. S.S. and M.M.; Critical revision of the article Z.Y. A.D. S.S. and M.M..

Chapter 3: Assessing the fractional abundance of highly mixed salt-marsh vegetation using Random Forest soft classification

This chapter is a manuscript published on Remote Sensing. We proposed a novel approach that is based on the Random Forest Soft classification algorithm to estimate the fractional abundance (FA) of each species and bare soil in plant associations. The method can fully use the votes from each decision tree and interpret the frequency of the vote to each species as the fractional abundance of paired species or bare soil. This method was shown to yield FA maps with high accuracy ($6.7\% < RMSE < 18.7\%$ and $0.65 < R^2 < 0.96$) when it was applied to the WorldView-2 data acquired for San Felice marsh. In addition, this method performs better than the previous ones based on Random Forest Regression (Immitzer et al., 2018).

PAPER

Assessing the fractional abundance of highly mixed salt-marsh vegetation using Random Forest soft classification

Zhicheng Yang [1,*], Andrea D'Alpaos [1], Marco Marani [2] and Sonia Silvestri [4]

[1] *Department of Geosciences, University of Padova, Via G. Gradenigo 6, IT-35131 Padova, Italy; zhicheng.yang@phd.unipd.it*

[2] *Department of Geosciences, University of Padova, Via G. Gradenigo 6, IT-35131 Padova, Italy; andrea.dalpaos@unipd.it*

3 Department of Civil, Environmental and Architectural Engineering, University of Padova, via Marzolo 9, IT-35131 Padova, Italy; marco.marani@unipd.it

4 Department of Biological, Geological, and Environmental Sciences, University of Bologna, via S. Alberto 163, IT-48100 Ravenna, Italy; sonia.silvestri5@unibo.it

Abstract: Coastal salt marshes are valuable and critical components of tidal landscapes, currently threatened by increasing rates of sea level rise, wave-induced lateral erosion, decreasing sediment supply, and human pressure. Halophytic vegetation plays an important role in salt-marsh erosional and depositional patterns and marsh survival. Mapping salt-marsh halophytic vegetation species and their fractional abundance within plant associations can provide important information on marsh vulnerability and coastal management. Remote sensing has often provided valuable methods for salt-marsh vegetation mapping; however, it has seldom been used to assess the fractional abundance of halophytes. In this study, we developed and tested a novel approach to estimate fractional abundance of halophytic species and bare soil that is based on Random Forest (RF) soft classification. This approach can fully use the information contained in the frequency of

decision tree ‘votes’ to estimate fractional abundance of each species. Such a method was applied to WorldView-2 (WV-2) data acquired for the Venice lagoon (Italy), where marshes are characterized by a high diversity of vegetation species. The proposed method was successfully tested against field observations derived from ancillary field surveys. Our results show that the new approach allows one to obtain high accuracy (6.7% < RMSE< 18.7% and 0.65 < R^2 < 0.96) in estimating the sub-pixel fractional abundance of marsh-vegetation species. Comparing results obtained with the new RF soft-classification approach with those obtained using the traditional RF regression method for fractional abundance estimation, we find a superior performance of the novel RF soft-classification approach with respect to the existing RF regression methods. The distribution of the dominant species obtained from the RF soft classification was compared to the one obtained from a RF hard classification, showing that numerous mixed areas are wrongly labeled as populated by specific species by the hard classifier. As for the effectiveness of using WV-2 for salt-marsh vegetation mapping, feature importance analyses suggest that Yellow (584 – 632 nm), NIR 1 (765-901 nm) and NIR 2 (856 – 1043 nm) bands are critical in RF soft classification. Our results bear important consequences for mapping and monitoring vegetation-species fractional abundance within plant associations and their dynamics, which are key aspects in biogeomorphic analyses of salt-marsh landscapes.

Keywords: Halophytic vegetation; Fractional abundance; Random Forest; Unmixing; Percentage cover

3.1 Introduction

Salt-marsh ecosystems are transition zones between aquatic and terrestrial systems and provide critical ecological and geomorphological functions in tidal landscapes (D’Alpaos et al., 2007b; Fagherazzi et al., 2012; FitzGerald and Hughes, 2019; Cronk; MS, 2001; Marani et al., 2006a). Salt-marsh ecosystems host high primary productivity (Mitsch and Gossilink, 2000; Morris and Haskin, 1990; Zedler and Kercher, 2005), attenuate waves, protect coastal areas from storms (Howes et al., 2010; Loder et al., 2009; Möller et al., 2014; Möller and Spencer, 2002; Silinski et al., 2016), and act as important global carbon sinks (Chmura et al., 2003; FitzGerald and Hughes, 2019; Kirwan and Mudd, 2012; McLeod et al., 2011; Mudd et al., 2009; M. Roner et al., 2016). Unfortunately, salt marshes are also threatened by accelerating sea-level rise, reduced sediment availability at the coast, wind-wave erosion, and human interventions, especially in recent decades. Salt-marsh deterioration is a consequence of lateral erosion (Leonardi et al., 2016; Marani et al., 2011a; Mariotti and Fagherazzi, 2013; Tommasini et al., 2019) and retreat in the horizontal plane (D’Alpaos et al., 2011; Kirwan and Murray, 2007; Marani et al., 2011b; Balke et al., 2016), although these processes are rarely studied in a coupled way (Hopkinson et al., 2018; Mariotti and Carr, 2014; Yousefi Lalimi et al., 2020, 2017).

Halophytic vegetation populates marsh areas between mean sea level (MSL) and mean high tide (MHT) (Kirwan and Guntenspergen, 2010). Halophytes can strongly influence erosional and deposition processes, by reducing flow velocity, by attenuating waves, and by trapping suspended sediments (Bouma et al., 2007; Brisson et al., 2014; Fagherazzi et al., 2012; Leonard and Croft, 2006; Leonard and Luther, 1995; Marani et al., 2010a; Mudd et al., 2010). Indeed, halophytes can support salt-marsh survival through biomorphic

feedbacks, increasing organic and inorganic deposition (D'Alpaos et al., 2011; D'Alpaos and Marani, 2016; Kirwan et al., 2016a, 2010; Kirwan and Murray, 2007; Marani et al., 2007; Morris et al., 2002). Vegetation spatial patterns are characterized by sharply-defined patches of typical species associations (Belluco et al., 2006; Costa et al., 2003; Marani et al., 2013; Moffett et al., 2012, 2010; Pennings et al., 2003; Ratliff et al., 2015; Silvestri et al., 2005; Wijnen et al., 1997). This spatial organization, or zonation, can be attributed to the adaptation of halophytes to edaphic conditions (Adams and Bate, 1995; Álvarez Rogel et al., 2001; Bockelmann et al., 2002; Fariña et al., 2018; Marani et al., 2006b, 2004; Moffett and Gorelick, 2016; Silvestri and Marani, 2004; Watson and Byrne, 2009), species competition (Marani et al., 2006c; Steven C Pennings et al., 2005; Steven C. Pennings and Callaway, 1992; Strain et al., 2017), and the capability of halophytes to engineer salt-marsh landscapes via biogeomorphic feedbacks (D'Alpaos and Marani, 2016; Da Lio et al., 2013; Marani et al., 2013; Ratliff et al., 2015).

Fractional abundance, i.e. the fraction of the area – projected on the horizontal plane – occupied by plants of a given species, is an important indicator of vegetation distribution (Silvestri et al., 2005), with strong links to biomass and salt-marsh surface geomorphology (M. Roner et al., 2016) and its time evolution (D'Alpaos and Marani, 2016; Da Lio et al., 2013; Fagherazzi et al., 2012; Marani et al., 2013; Morris et al., 2002; Taramelli et al., 2018; Temmerman et al., 2007; Zhu et al., 2020). Fractional abundance of bare soil is also an important property of the marsh landscape that has been connected to the marsh sediment budget and marsh vulnerability (Ganju et al., 2017; Ladd et al., 2019). Hence, accurate vegetation and bare soil mapping is of central interest to understand marsh dynamics and to support coastal management strategies.

Due to the profound influence of halophytic vegetation on ecological and geomorphological processes and their spatial and temporal dynamics (Bernhardt and Leslie, 2013; Kirwan et al., 2016a; Kirwan and Guntenspergen, 2012; Koppel et al., 2005; Morris et al., 2002; Silvestri et al., 2005; Van der Wal et al., 2008), analyses of the fractional abundance of salt-marsh vegetation species are required over a large range of spatial scales, from the local (plant) scale to the whole-marsh scale (up to several km^2). Remote sensing is an ideal tool to obtain this type of quantitative information and there is an ever-growing amount of research work focusing on the application of remote sensing methods to map the fractional abundance of halophytic vegetation in space and time (Artigas and Yang, 2006; Belluco et al., 2006; Berhane et al., 2019; Gilmore et al., 2008b; Van der Wal et al., 2008; Wang et al., 2007).

Classification methods applied to salt marshes have been developed for and applied to multi- and hyperspectral remote sensing data in a diverse set of biomes worldwide (Berhane et al., 2019; Costa et al., 2017; Cutler et al., 2007; Goodin et al., 2015; Kulkarni and Lowe, 2016; Kumar et al., 2017; Pal, 2005). The large majority of previous approaches to halophytic vegetation mapping determined vegetation abundance by identifying the dominant species in each pixel, using traditional supervised and unsupervised classification algorithms (Belluco et al., 2006; Berhane et al., 2019; Campbell et al., 2017; Marani et al., 2006a; Moffett et al., 2015; Silvestri et al., 2003; Van Beijma et al., 2014). Nonparametric mapping methods, such as Random Forest (RF) algorithms, have also been applied to halophytic vegetation mapping in the

form of pixel-based (Timm and McGarigal, 2012; Van Beijma et al., 2014) and object-based methods (Berhane et al., 2019; Campbell et al., 2017; Juel et al., 2015). However, halophytic vegetation species are highly mixed at the scale of typical satellite sensor resolutions (order of 0.5-1 m) such that the use of hard classification approaches, which attempt to associate a single dominant species to each pixel, is hardly justified. Yet, the number of studies focusing on retrieving the fractional abundance of halophytic vegetation species and bare soil at the sub-pixel scale, i.e. the problem of unmixing, is still limited (Silvestri et al., 2003; Taramelli et al., 2018). This is a clear gap that hinders the usefulness of remote sensing retrievals of vegetation distribution and change in salt-marsh studies. Here we contribute to filling this gap by developing and applying a novel RF-based soft classification method to infer relative species abundance at the sub-pixel scale.

Wang et al. (Wang et al., 2007) used artificial neural network models to map the fractional abundance of species within associations in salt-marsh landscapes. Artificial neural networks, however, require relatively a time-consuming training phase and the definition and identification of their parameters can be a difficult task. Additionally, artificial neural network performance heavily depends on their structure and design (Verrelst et al., 2015), i.e., the number of layers and neurons can significantly influence the accuracy of the method, such that it is difficult to provide a general neural network architecture that can be easily applied in different environments furthermore populated by different species.

RF algorithms (Breiman, 2001) have been applied to detect land-use fractional cover (Immitzer et al., 2018; Sanpayao et al., 2017). However, to our knowledge, the RF approach has never been applied to estimating the fractional abundance of salt-marsh halophytic species at the sub-pixel scale. Because marsh vegetation species are particularly highly-mixed, here we wonder whether the RF methods may have the ability to provide reliable unmixing results. Furthermore, typical applications of the RF unmixing method to other environments separately estimate single species abundances through regression and subsequently normalize them to sum to 100% (Immitzer et al., 2018). This leads to increased estimation errors, which may be avoided if the RF formulation were better leveraged. To address the latter issue, in this work, we propose a new approach which uses the frequency with which individual ‘trees’ in the RF assign a pixel to each species as reflective of its relative abundance at the sub-pixel scale. This new approach substantially differs from previous analyses based on the RF regression algorithm to estimate fractional abundance at the sub-pixel level, because those analyses do not take advantage of the information contained in the individual tree “votes” and rely on empirical regressions based on field observations. Towards the goal of improving current capability to accurately map fractional abundance of halophytic vegetation in space and time in salt-marsh landscapes, we first explored the possibility of applying the new algorithm based on RF soft classification and then compared the performance of the newly proposed approach to that characterizing existing RF regression methods.

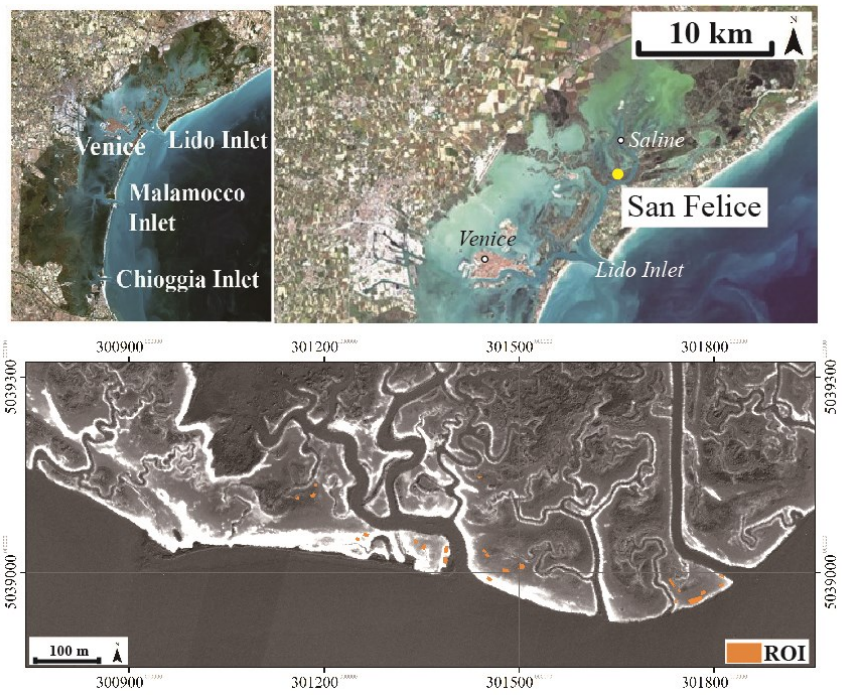

Figure 3. 1: Research area: the top panels show the map of the Venice lagoon and the position of the San Felice salt marsh; the bottom panel shows the map of the San Felice marsh acquired by WV-2 (Red Edge, Central Wavelength: 724 nm) in 2019 and the positions of the Regions Of Interest (ROIs).

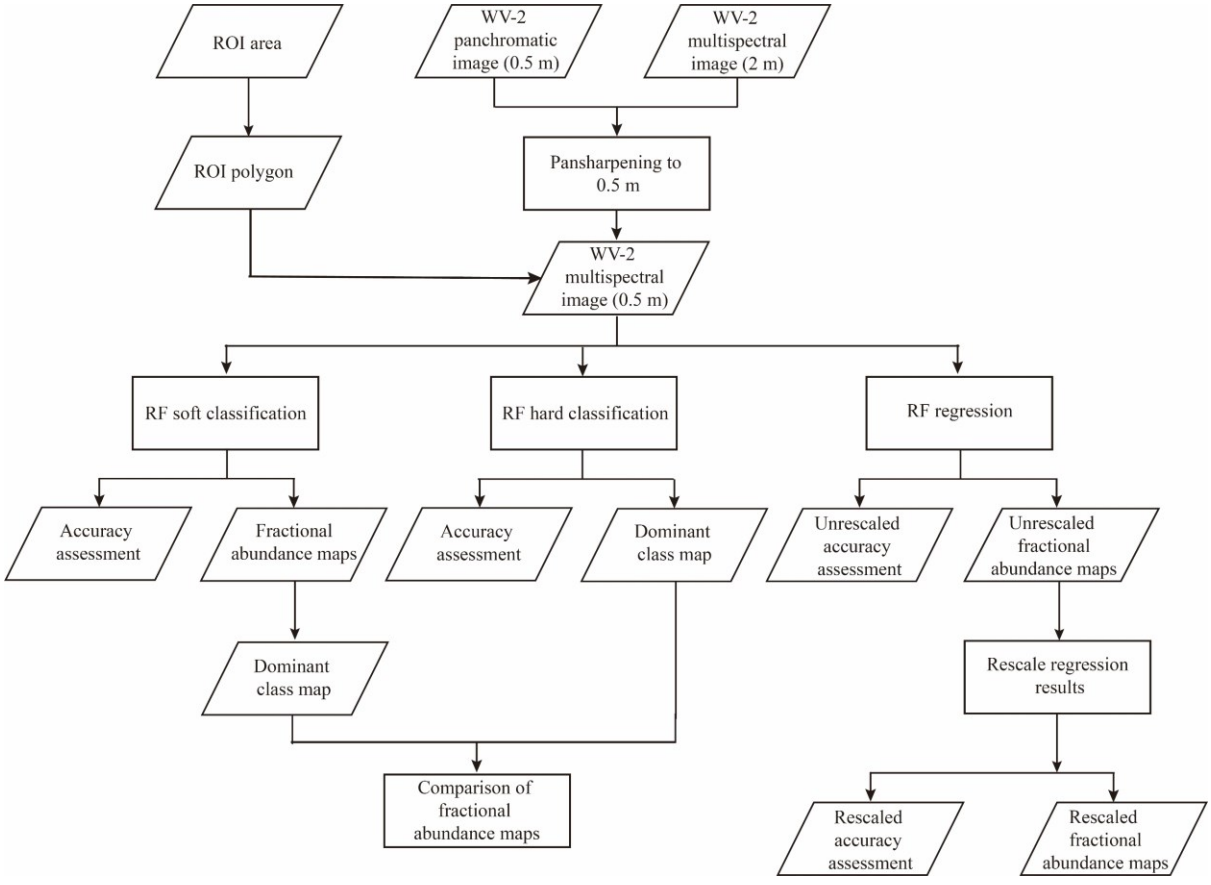

Figure 3. 2: The Workflow of the present study.

3.2 Methods

3.2.1. Study site – the San Felice salt marsh (Venice lagoon, Italy)

The Venice lagoon (top panels in Figure 3.1) is located in northeastern Italy and is connected to the Adriatic Sea by three inlets: Lido, Malamocco, and Chioggia. The main rivers that used to debouch into the lagoon were diverted directly to the sea in the XVI-XIX centuries (D'Alpaos, 2010), and only a few small rivers now remain, carrying modest amounts of freshwater and sediments into the lagoon. The Venice lagoon has an area of about 550 km^2 and is characterized by a semidiurnal tide with an average tidal range of about 1.0 m and a maximum spring tidal range of approximately 1.5 m (D'Alpaos et al., 2013; Silvestri et al., 2018).

The present study focuses on the San Felice salt marsh (bottom panel in Figure 3.1), one of the most naturally preserved areas within the northern part of the lagoon, close to the Lido inlet. The San Felice marsh is characterized by relatively healthy vegetation conditions (Marani et al., 2003c; M. Roner et al., 2016) and is colonized by halophytic vegetation associations dominated by the following species: *Salicornia veneta* (hereafter '*Salicornia*'), *Spartina maritima* (hereafter '*Spartina*'), *Limonium narbonense* (hereafter '*Limonium*'), *Sarcocornia fruticosa* (hereafter '*Sarcocornia*') and *Juncus maritimus* (hereafter '*Juncus*') (Belluco et al., 2006; Silvestri et al., 2005, 2002; Wang et al., 2007). Silvestri et al. (Silvestri et al., 2005) reported that each species occupies a preferential range of possible elevations, thus leading to a typical species sequence with increasing elevation. Moreover, due to the strong link between marsh elevation and distance to channels (D'Alpaos and Marani, 2016), the distribution of halophytic species also varies from the channel edges to the inner portions of the marsh. Specifically, *Salicornia* and *Spartina* are preferably found in the lowest areas (inner portions of the marsh), *Limonium* tends to occupy intermediate marsh elevations, and *Sarcocornia* is more likely to colonize higher marsh areas, close to marsh edges. *Juncus* tends to develop where creeks bring litter and organic matter accumulates over time. In general, the density of halophytic vegetation decreases with distance to marsh edges (M. Roner et al., 2016).

As mentioned above, halophytic vegetation distribution is strongly linked to marsh morphology through a landscape-forming bio-morphologic process, and species are associated with (possibly overlapping) characteristic elevation ranges (Marani et al., 2013; Silvestri et al., 2005), the result of species adaption to edaphic factors (Adams and Bate, 1995; Moffett and Gorelick, 2013; Pennings et al., 2003) and of interspecific competition (Morris, 2006; Steven C Pennings et al., 2005). Productivity and bio-diversity of halophytic vegetation are also linked to elevation (Janousek et al., 2016; Kirwan and Guntenspergen, 2012; Morris et al., 2002). The presence of these links between morphological and ecological patterns highlights the great value of robust fractional-abundance mapping methods to monitor and analyze salt-marsh bio-morphodynamics. This suggests that robust fractional abundance mapping algorithms are of critical importance to analyze halophytic vegetation distribution patterns and temporal dynamics at large spatial scales (indicatively 10 m – 10,000 m).

Finally, halophytic vegetation distribution has been observed to change over time scales of a few years (Belluco et al., 2006; Schepers et al., 2017; Strain et al., 2017; Taramelli et al., 2018; Van der Wal et al., 2008; Zhu et al., 2012), especially in the current accelerating sea-level rise scenario (Donnelly and Bertness, 2002; Fagherazzi et al., 2019a; Feagin et al., 2010; Ge et al., 2016; Kirwan et al., 2016b). Hence, a proper quantitative description of marsh vegetation space-time dynamics would greatly benefit from robust and highly repeatable quantitative mapping.

3.2.2. Data sets

3.2.2.1. WoldView-2 data

We develop and test RF unmixing methods with application to WorldView-2 (WV-2) data. WV-2 sensors include a panchromatic spectral band with a high spatial resolution (0.5 m) and 8 multispectral bands (Table 3.1) with a lower spatial resolution (2 m), spanning 4 standard bands (red, green, blue, and near-infrared 1) and 4 other application-oriented bands (coastal, yellow, red edge, and near-infrared 2). The sensor acquires data from an altitude of about 770 km. The data analyzed in this study were acquired at 10:23:00 on Nov 7, 2019. At the time of acquisition, the tidal level, measured at the Saline tide gauge station, close (about 3 km) to the San Felice marsh, was about 0.76 m above the Punta della Salute datum. Because the current MSL is 31 cm higher than the Punta della Salute datum, the water level was about 0.45 m above the MSL at the time of acquisition, which corresponds to water depths ranging between 0 and 30 cm over the marsh platform.

Table 3. 1: WorldView-2 Spectral Band Edges and Center Wavelengths

Band Name	Center Wavelength (nm)	Lower Band Edge (nm)	Upper Band Edge (nm)	Spatial Resolution (m)
Panchromatic	627	447	808	0.5
Coastal Blue	427	396	458	2.0
Blue	478	442	515	2.0
Green	546	506	586	2.0
Yellow	608	584	632	2.0
Red	659	624	594	2.0
Red Edge	724	699	749	2.0
NIR 1	833	765	901	2.0
NIR 2	949	856	1043	2.0

3.2.2.2. Field observations

Field vegetation mapping was performed on Jan 9, 2020. Twenty-four Regions Of Interest (ROIs, i.e. field areas used for training and validating the classification model), were selected, with areas ranging between 18.0 m^2 and 106.5 m^2 (Table 3.2 and bottom panel in Figure 3.1). ROIs were randomly selected across the marsh to include all typical homogeneous associations of species that encroach the San Felice salt marsh. For each ROI the percentage cover of vegetation species and bare soil was estimated using the standard

Braun-Blanquet visual method, which records the presence of each species by 10 intervals between 0% and 100% (Belluco et al., 2006). The boundaries of the ROIs were accurately delimited through differential GPS (Leica CS15 in RTK mode, minimum accuracy of ±1 cm) (see Table 3.2 for ROI properties). ROIs were then overlaid on the WV-2 georeferenced image (using ArcGIS 10.5) and only pixels falling entirely within a ROI were used to build the classification dataset, which was then divided into two independent training and validation subsets, as explained in Section 3.2.3 (Wang et al., 2007).

Table 3. 2: Field measurements of fractional abundance of each class in the San Felice salt marsh (Venice, Italy). Jun = *Juncus*, Lim = *Limonium*, Sali = *Salicornia*, Sarc = *Sarcocornia* and Spar = *Spartina,*

ROI	Area (m^2)	Fraction (100%)					
		Jun	Lim	Sali	Sarc	Soil	Spar
1	25.1	--	5	--	95	--	--
2	106.5	--	80	--	20	--	--
3	44.8	--	80	--	20	--	--
4	18.7	--	15	--	85	--	--
5	28.4	--	80	--	20	--	--
6	55.0	--	40	--	60	--	--
7	18.2	--	--	80	--	20	--
8	23.6	--	--	--	100	--	--
9	30.4	--	--	80	--	20	--
10	48.2	100	--	--	--	--	--
11	28.7	100	--	--	--	--	--
12	58.2	--	--	--	--	100	--
13	56.1	--	--	--	--	100	--
14	41.3	--	--	--	100	--	--
15	22.2	--	50	--	50	--	--
16	16.4	--	10	--	--	10	80
17	43.1	--	10	--	--	10	80
18	20.2	--	60	--	--	20	20
19	18.0	--	--	90	--	10	--
20	31.6	--	50	--	50	--	--
21	28.6	--	30	--	30	10	30
22	45.6	--	--	--	100	--	--
23	58.9	--	90	--	10	--	--
24	68.4	--	20	20	20	20	20

3.2.2.3. WorldView-2 data preprocessing

Even though the atmospheric correction may not influence the result and accuracy of classifications (Hoffbeck and Landgrebe, 1994), we applied such a correction to obtain more accurate spectral information to favor the interpretation of the results, and for possible comparisons with past or future acquisitions. The Fast Line-of-sight Atmospheric Analysis of Spectral Hypercubes (FLAASH) algorithm (Cooley et al., 2002; Matthew et al., 2002) was employed to perform atmospheric correction in Envi 5.4. In FLAASH, the 'Mid-Latitude Winter' Atmospheric Model and the 'Maritime' Aerosol Model were used. Due to the lack of

aerosol optical thickness data at the nearest AERONET station on the acquisition date (https://aeronet.gsfc.nasa.gov/) and good weather conditions, according to the instruction (Visual Information Solutions, 2009) the visibility was set to 'Clear', corresponding to 40 km. After atmospheric correction, the multi-spectral bands were pan-sharpened using the panchromatic band, which has a spatial resolution of 0.5 m, through the Gram-Schmidt Pan Sharpening algorithm (Maurer, 2013; Palubinskas, 2013). Both Atmospheric correction and pan-sharpening were performed in ENVI 5.4. Water bodies were masked based on negative values of the NDVI (Normalized Differential Vegetation Index) (Rouse et al., 1974) derived from 'NIR1' and 'Red' channels (Table. 3.1).

3.2.3. Algorithm description

In this work, the RF algorithm is applied using the Scikit-learn package (Pedregosa et al., 2011), a freely-available machine learning library for the Python programming language.

RF is a machine-learning algorithm based on the Decision Tree method (Breiman, 2001), which is being increasingly and successfully used in remote sensing analyses of vegetation species and habitats (Belgiu and Drăgu, 2016; Berhane et al., 2019; Immitzer et al., 2018, 2016; Pal, 2005; Van Beijma et al., 2014). RF classification is a supervised nonparametric classification method that makes predictions through a set of decision trees (Breiman, 2001) which form a so-called "forest". Each decision tree is composed of a set of internal nodes and terminal nodes. Given a set of pixels known to belong to different information classes (i.e. the different vegetation species in the present application), training is performed by feeding each tree with the input spectral reflectance and the associated class for each pixel. Training pixels (samples) are then split into two groups ('left' and 'right') at each node, based on so-called 'best split' binary rules (Breiman, 2001; Xu et al., 2005) and decreasing the Gini impurity index ($G(I)$), which is defined as :

$$G(I) = 1 - \sum_{i=1}^{n} p_i^2, \tag{3.1}$$

where p_i is the frequency of occurrence of the ith class among the n total classes. $G(I)$ represents the impurity level of information in the current node. Specifically, the highest value of $G(I)$, $G(I)$=1-1/n, shows each class is equally distributed in this node, while the minimum value of $G(I)$ shows all pixels in this node belong to one class. The best-split is chosen by maximizing the impurity decrease (ID), which can be expressed as:

$$ID = \frac{Nt}{N*(G(I)-\frac{Ntr}{Nt}*G(I)_{right}-\frac{Ntl}{Nt}*G(I)_{left})}, \tag{3.2}$$

where N is the total number of samples in the training set, Nt is the number of samples at the current node, Ntl is the number of samples in the left child node, and Ntr is the number of samples in the right child node, and the $G(I)_{right}$ and $G(I)_{left}$ are $G(I)$ in the right and left child node respectively (Pedregosa et al., 2011). In a decision tree, the nodes will be split if this split induces a decrease in the impurity larger than or equal to a determined value, named 'min impurity decrease' (hereafter *mid*). The value of *mid* is pre-determined

as 0, which is the default value in Scikit-learn package. If the growth of a tree is not bounded, the tree would keep growing until there is a terminal node for every single pixel.

In the RF classification, a user-defined large number of decision trees (*ntree*) is chosen, but each tree has limitations in growth given by specific rules. In particular, each tree learns from a subset of pixels randomly selected from the training data set. Two-thirds of the pixels present in the training dataset are drawn with replacement (i.e. bootstrapping) to construct each decision tree; thus decision trees are trained on different subsets of the data (Breiman, 2001). Each tree is fed with a subset of the training pixels, those that are left out (out of bag, OOB) are used as validation datasets to test the predictive ability of that individual tree. The proportion of times that OOB samples are incorrectly predicted is recorded and averaged over all cases to produce an OOB error estimate (OOB score). The OOB error estimation has been proven to be unbiased (Breiman, 1996).

The training process also makes it possible to evaluate the importance of each spectral band in reducing the classification error. Specifically, at each split, the decrease in $G(I)$ is recorded for each band (X_i) that was used to form the split. The average of all decreases in the $G(I)$ in the forest where band (X_i) is involved yields the Gini variable Importance Value (*IV*) (Archer and Kimes, 2008; Jiang et al., 2009; Menze et al., 2009). Scikit-learn normalizes *IVs* of each band to a value between 0 and 1 by dividing by the sum of all importance values (Pedregosa et al., 2011). As for other supervised classification methods, the training dataset may come from ROIs selected in the image. If the ROIs contain mixed vegetation and bare soil areas, as it often happens with marsh sites, the RF classifier allows to include 'sample weights', which, in this study, correspond to the fractional abundance of different vegetation species and bare soil estimated for each ROI during field surveys. Once 'sample weights' are defined, the split is determined by the weight of each class at the current node, instead of the number of samples. *N*, *Nt*, *Ntr,* and *Ntl* in equation (3.2) will be the sum of the weight of all species at their corresponding nodes. For example, a node including *n* pixels, in which fractional abundance belongs to *i*th species is *Fi*. *N* at this node can be obtained by $N = \sum_n Fi$. Once this node acts as a mother node to split, the calculation of *Nt*, *Ntr,* and *Ntl* will follow the same method. Moreover, we use another parameter, i.e. the 'min weight fraction', to control the split process. 'Min weight fraction' is defined by Pedregosa et al. (Pedregosa et al., 2011) as the minimum weighted fraction of the total sum of the weights (of all the input samples) at each child node. Here we prefer to interpret it as a threshold value to determine whether the child node should be created or not. Specifically, the weight fraction (*wf*) of each child node creation is defined as follows:

$$wf = \frac{weight_{child}}{weight_{mother}}, \tag{3.3}$$

where $weight_{child}$ and $weight_{mother}$ are the weight sum of classes in the child and mother node, respectively. A child node whose *wf* is lower than 'min weight fraction' should not be created. In this study, the 'min weight fraction', is set to 0. The RF is trained based on the provided classes and sample weights (fractional abundances), generating the pruning decision trees. After the training, when an unknown pixel value is input

into the model, each decision tree assigns it to a specific class independently. This is usually explained by saying that each tree "votes" for a class, thus suggesting the possibility to consider it as a voting process. The RF classifier records the number of votes associated with the classified pixel for all the classes and the pixel is usually assigned to the class with the highest number of votes. Instead of considering the final association of each pixel to the most-voted class, in this work, we consider the number of votes as the probability value that the pixel belongs to one specific class (Breiman, 2001), and then we interpret such probability value as the sub-pixel relative fractional abundance.

An important advantage of the RF classification is that it can manage a large number of input bands (Juel et al., 2015; Ma et al., 2017; Van Beijma et al., 2014) and minimize data dimensionality issues, such as the Hughes phenomenon (Belgiu and Drăgu, 2016), that makes the large amount of information contained in multispectral data difficult to exploit fully. Moreover, unlike some supervised parametric classifiers, such as the Maximum Likelihood method which assumes data are normally distributed (Liu et al., 2011), RF is also capable of handling multi-modal datasets, whose variables display more than one maximum in their probability distribution (Belgiu and Drăgu, 2016).

In this work, in order to test the accuracy of our results, we have randomly divided the original dataset into two independent groups, i.e. 75% of the pixels (2804 pixels) from the ROIs were used for model training and 25% of the pixels (935 pixels) were used for testing. Sample weights of training data were passed to the model according to fractional coverages of vegetation species recorded in the field. At the end of the process, we assumed that the predicted probability of each vegetation class (i.e. species) equals its fractional abundance. Results were validated using the fractional abundance of the validation dataset and the error for each vegetation species was calculated.

With the purpose of verifying the effectiveness of this new approach based on RF soft classification for sub-pixel fractional abundance assessment, we used the same dataset to train and test a traditional RF regression method. The workflow of this study is shown in Figure 3.2.

Similarly to the RF classification, the RF regression is an ensemble of decision trees, and it is based on the assumption that the relationship between input variables (spectral reflectance) and sub-pixel fractional abundance can be described through a non-linear correspondence (Breiman, 2001). Following the above description of RF classification, it is easy to understand the processes of RF regression, which shares many of the advantages of the RF classifier. RF regression is always characterized by a relatively low risk of overfitting, compared with other regression methods, especially the Decision Tree regression. Similar to its classification counterpart, RF regression can provide a relatively unbiased evaluation of the model (through OOB information). In the RF regression process, the same training and validation datasets of RF soft classification were used to construct and test the RF regression model.

The main steps of the RF regression are: 1) the RF generates a regression model for each vegetation species based on the training dataset; 2) for each unknown pixel, the RF regression model is used to predict the

fractional abundance of vegetation species and soil, and the prediction error is calculated using the validation dataset; 3) the results obtained for each pixel are then rescaled to sum to unity because the method predicts vegetation fractional abundance separately for each vegetation species; 4) the accuracy of the predicted percentage for each class (obtained in Step 3) is again quantified using the validation dataset.

Considering that traditional approaches to mapping halophytic vegetation usually assign pixels to the dominant species (Belluco et al., 2006; Marani et al., 2006a, 2003c; Van Beijma et al., 2014) and that some of species associations are dominated by one species, we used the fractional abundance maps obtained with the RF soft classification method to produce a map of the most abundant halophytic species across the study site. Specifically, the pixels with percentage cover larger than 60% were considered as colonized by the dominant species (Belluco et al., 2006). The results were then compared to a map obtained using a RF hard classification trained using only ROIs characterized by relative homogeneous vegetation communities (or bare soil) with the dominant species (or soil) covering more than 60% of the area. A dataset of 2829 pixels was used, but to allow for error assessment, it was randomly divided into two groups: 2121 pixels (about 75% of the dataset) were used in model training and 708 pixels (about 25% of the dataset) were used in model validation. We notice that the number of data used for the hard classification is smaller than that used for soft classification and regression because hard classification just includes pixels with percentage cover greater than 60% (Belluco et al., 2006) while all pixels are used in soft classification and regression processes.

3.2.4. Estimation of accuracy

The confusion Matrix was used to evaluate the performance of the hard classification, which can provide Overall Accuracy (*A*), describing the ratio between the number of correctly classified validation points and the total number of validation points irrespective of the class (Foody, 2002). We also used the Kappa coefficient, *K*, which is defined by the proportion of correctly classified validation sites after random agreements are removed (Rosenfield, 1986). The root-mean-square error (RMSE) and the coefficient of determination (R^2) between predicted fractional abundance and test data were calculated for each class to estimate model performance:

$$\mathrm{RMSE} = \sqrt{\frac{\sum_{i=1}^{n}(y_i - \hat{y}_i)^2}{n}}, \tag{3.4}$$

$$R^2 = \frac{\sum_{i=1}^{n}(\hat{y}_i - \bar{y})^2}{\sum_{i=1}^{n}(y_i - \bar{y})^2}, \tag{3.5}$$

where y_i is the ground referential value, $\hat{y}_i$ represents the predicted value, $\overline{y}$ is the average of the observed values, and *n* is the number of test points.

3.3 Results

3.3.1. Selection of ntree

In this work we selected *ntree* based on the accuracy of hard classification, testing the overall Accuracy (*A*) variations when the number of trees ranged from 10 to 1000. Figure 3.3 shows the results obtained when the number of trees is in the 10 to 1000 range. We notice that the training accuracy *A* rapidly increases and stays stable once *ntree* is larger than 150. The steady increase of *A* with *ntree* can be attributed to the reduced risk of overfitting. Indeed, the peak value of *A* is approached when *ntree* ranges from 460 to 490. Because the RF is a computationally efficient algorithm and a larger ensemble of trees can reduce the risk of overfitting, *ntree* should be set as large as possible (Guan et al., 2013). Considering that several applications of the RF to remote sensing image classification used *ntree* = 500 (Díaz-Uriarte and Alvarez de Andrés, 2006; Ghosh et al., 2014; Immitzer et al., 2018, 2012), we decided to use *ntree* close to 500 to compare the results obtained with our method to those from previous analyses. We thus select *ntree* equal to 490, which is close to the value used in previous studies and also provides the highest value of *A* in this study. Even though *ntree* was selected based on RF hard classification, to consistently compare the results, we have maintained *ntree* = 490 also for RF soft classification and RF regression.

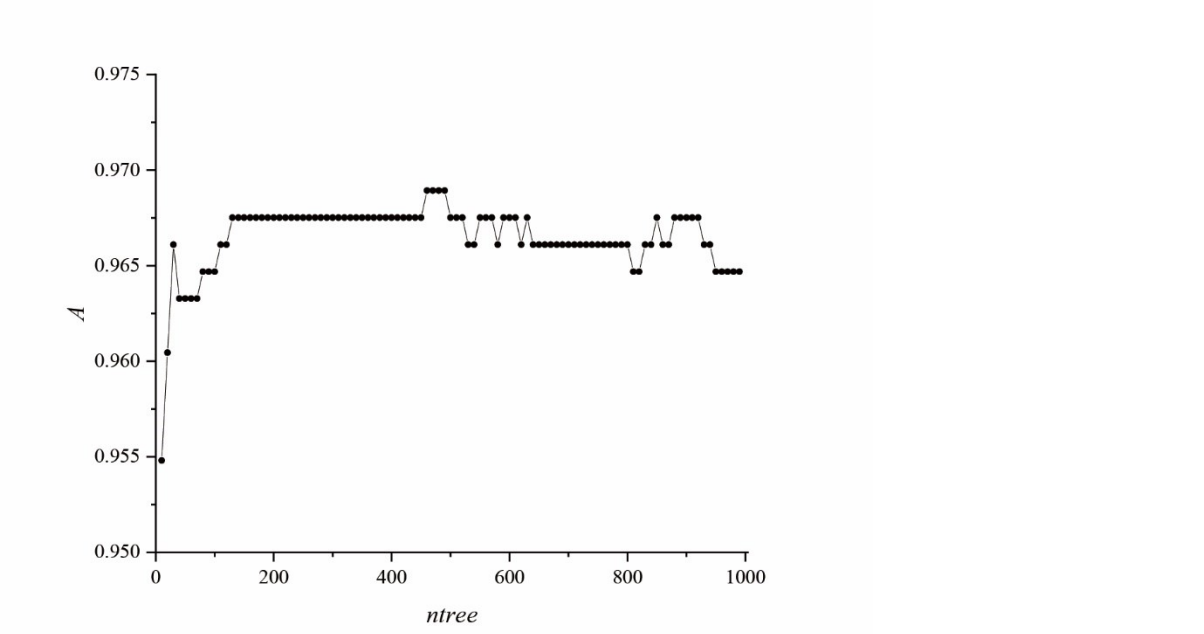

Figure 3. 3: Overall accuracy (A) of hard classification variations as a function of the number of trees (ntree).

3.3.2. Fractional abundance based on RF soft classification method

As discussed in the Methods section, we use the number of votes resulting from the RF soft classification to determine the probability of each vegetation species. The main advantage of this new approach is that, for each pixel, the sum of the predicted probability of each class is equal to 100%. Indeed, by assuming that the probability of each species represents its fractional abundance, there is no need to rescale the abundance of the different species. This is consistent with the collection of ancillary data because we emphasize that the

method used in the field for determining the fractional abundance (i.e. the Braun-Blanquet visual method, commonly used in ecology) is also essentially related to the occurrence probability of each class.

Maps of fractional coverage of *Juncus*, *Limonium*, *Salicornia*, *Sarcocornia*, Soil, and *Spartina* generated using the RF soft classification method are shown in Figure 3.4, while Table 3.3 shows R^2 and RMSE for fractional abundance. We notice that the R^2 and RMSE values for the RF soft classification range from 0.652 to 0.956 and from 6.753 to 18.667, respectively. This suggests that the RF soft classification method can successfully predict the fractional abundance of each species and bare soil.

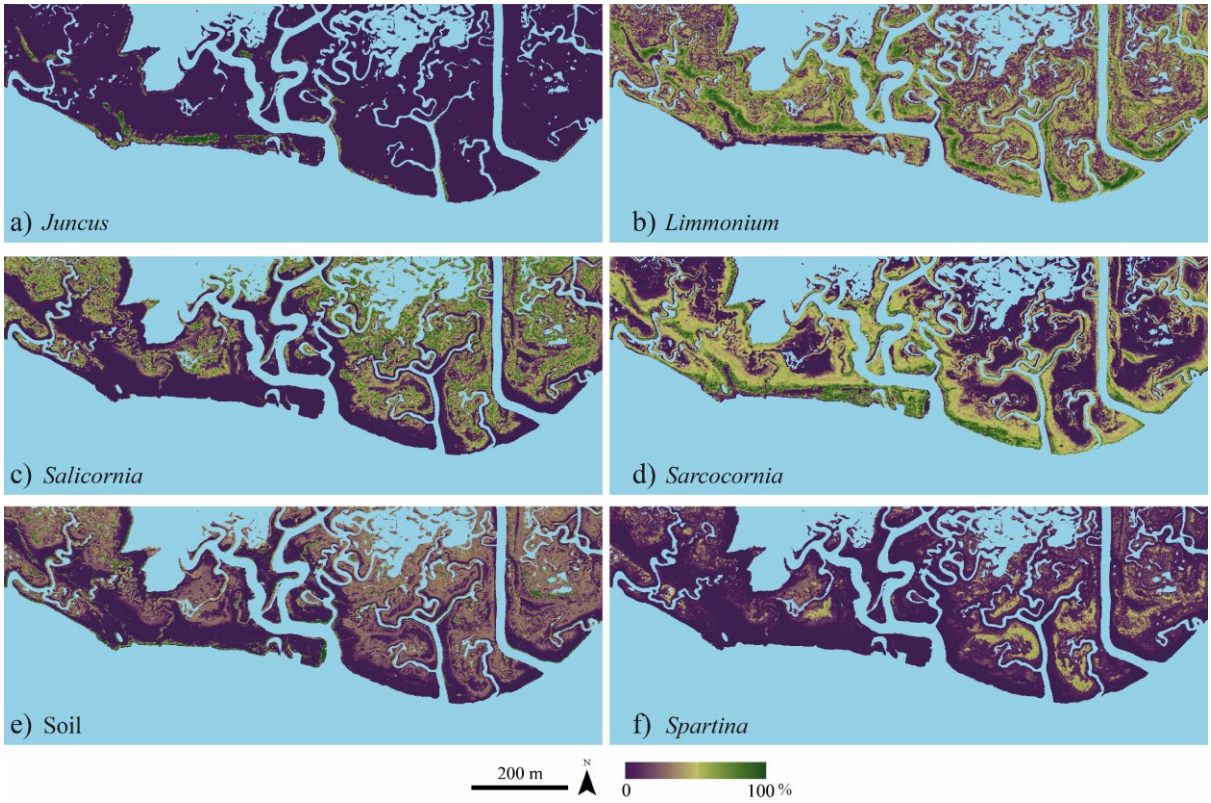

Figure 3. 4: Maps of fractional abundance of each species and bare soil obtained based on the RF soft classification method. Light blue areas represent water.

Table 3. 3: Accuracy information for RF soft classification. Jun = *Juncus*, Lim = *Limonium*, Sali = *Salicornia*, Sarc = *Sarcocornia* and Spar = *Spartina*:

Classes	R^2	RMSE
Jun	0.896	8.971
Lim	0.784	15.522
Sali	0.652	11.870
Sarc	0.715	18.667
Soil	0.956	6.753
Spar	0.884	7.069

3.3.3. Subpixel classification through RF regression method

It has been shown that RF regression can perform well for vegetation species mapping when *ntree* is large (for example 500 trees) (Immitzer et al., 2018). To compare the performance of the RF regression method with the soft method, 490 decision trees (i.e. *ntree* = 490) were used to predict the abundance of the six vegetation species individually. Table 3.4 provides the accuracy retrieved for each class, showing that R^2 and RMSE range from 0.74 to 0.98 and from 4.5 to 15.0, respectively. These results confirm that the RF regression is an accurate predictor of percentage for each class when we consider one class at a time (Figure 3.5). However, once the predicted abundance of each class is simply rescaled to 100% (i.e., the percentage values of the classes are rescaled to sum to 100% for each pixel), the accuracy decreases (Table 3.4), suggesting that the RF regression method may not be suitable to provide quantitative information on the fractional abundance for highly mixed vegetation species. Because of their low accuracy, the rescaled fractional abundance maps are not shown in this paper.

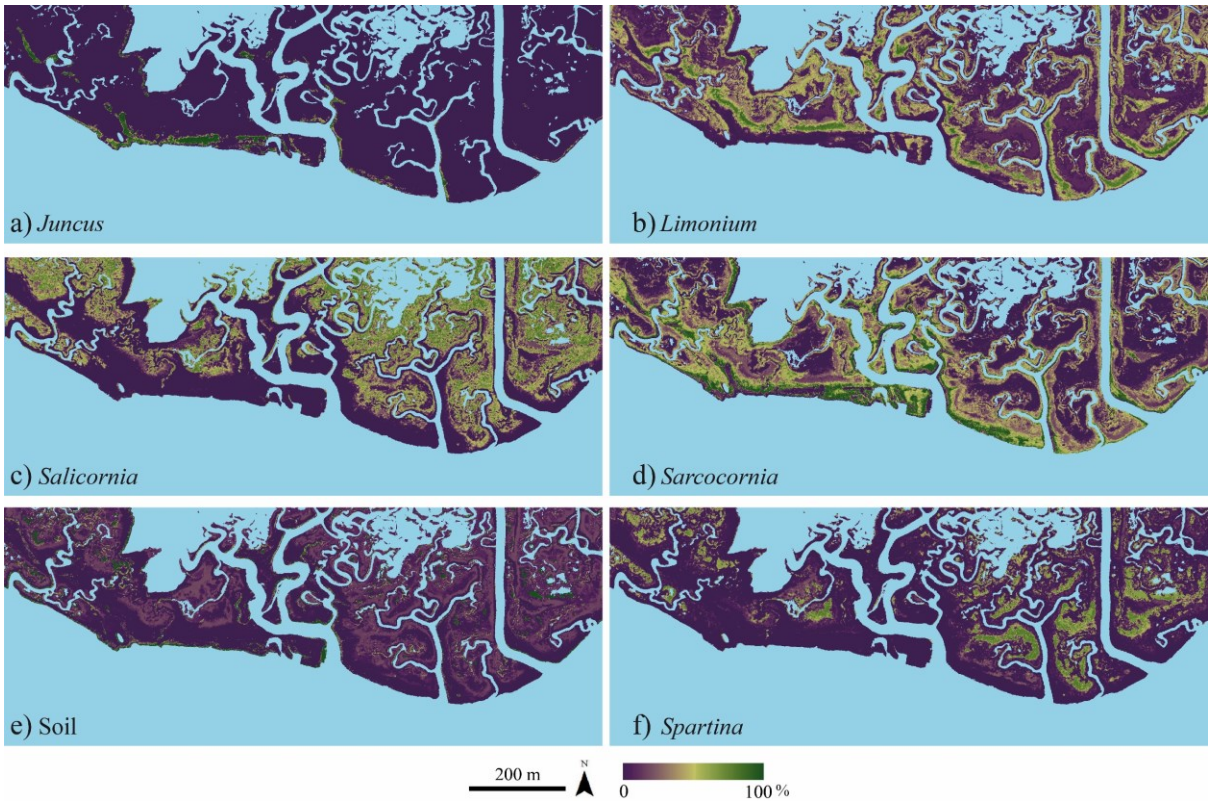

Figure 3. 5: Maps of the individually predicted abundance of vegetation species obtained based on the RF regression. Light blue areas represent water.

Table 3. 4: Accuracy information for RF regression. Jun = *Juncus*, Lim = *Limonium*, Sali = *Salicornia*, Sarc = *Sarcocornia* and Spar = *Spartina*.

Classes	Unrescaled		Rescaled	
	R^2	RMSE	R^2	RMSE
Jun	0.917	8.018	0.547	18.713
Lim	0.943	8.120	0.342	27.602
Sali	0.738	10.987	0.140	19.901
Sarc	0.814	15.033	0.201	31.131

Soil	0.975	4.984	0.579	20.465
Spar	0.950	4.528	0.397	15.784

3.3.4. RF hard classification

Figure 3.6 shows the results of a RF hard classification with *ntree* = 490, trained with the same dataset used for the RF soft classification (Figure 3.6a). The OOB, A, and Kappa of the RF hard classification are 0.96, 0.97, and 0.96, respectively. Figure 3.6b shows a majority map created using fractional abundance predicted by the RF soft classification, i.e. a map that shows the spatial distribution of species with fractional abundance higher than 60%. Black pixels in the map indicate the highly-mixed locations, where the percentage cover of all classes is lower than 60%. The Confusion Matrix for the RF hard classifier is displayed in Table 3.5. Our results show that the RF hard classifier can efficiently distinguish different vegetation associations based on the dominant species and bare soil.

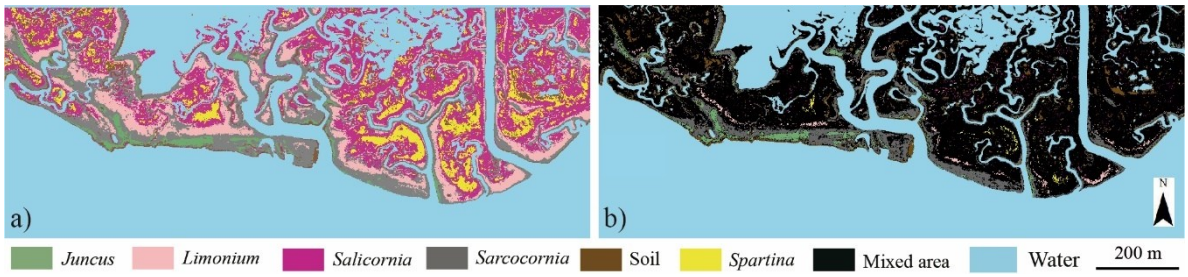

Figure 3. 6: Maps for dominant species and soil: (a) RF hard classification map results; (b) majority map based on RF soft classification.

Table 3. 5: Confusion Matrix for WV-2 classification of San Felice marsh through Random Forest (RF) hard classifier. Jun = *Juncus*, Lim = *Limonium*, Sali = *Salicornia*, Sarc = *Sarcocornia* and Spar = *Spartina*.

Classes	**Test areas (pixel)**						
	Jun	**Lim**	**Sali**	**Sarc**	**Spar**	**Soil**	**total**
Jun	78	0	0	1	0	0	79
Lim	0	234	0	4	0	0	238
Sali	0	0	60	6	0	0	66
Sarc	2	2	6	146	0	0	156
Spar	0	0	0	1	108	0	109
Soil	0	0	0	0	0	60	60
total	80	236	66	158	108	60	708

3.4 Discussion

We developed and tested a new method that uses the frequency with which an individual 'tree' in a RF algorithm assigns a pixel to each species as reflecting the fractional abundance of the corresponding species. A comparison of results from the new algorithm to those from existing RF regression methods (Liu et al., 2017; Liu et al., 2017; Schwieder et al., 2014) shows a superior performance of the proposed method (Table 3.3), which thus constitutes a powerful method for the analysis of vegetation patterns and their dynamics in salt-marsh landscapes.

3.4.1. Halophytic vegetation distribution patterns on the San Felice marsh

The application of the new method of vegetation abundance mapping to marshes in the Venice lagoon allows the quantitative description of some characteristic patterns exhibited by halophytic vegetation. Figure 3.4 (a) shows that *Juncus* is more likely to populate marsh edges, while *Limonium* and *Sarcocornia* (Figs. 3.4b and d) tend to compete for the same area, located at a moderate distance from the tidal channels. Figures 3.4 (c) and (f) show that *Salicornia* and *Spartina* tend to cover the inner portions of the marsh. Such patterns nicely agree with those documented through field observations (Belluco et al., 2006; Silvestri et al., 2005). Indeed, as discussed in Section 3.2, halophytic vegetation distribution is associated with salt-marsh surface morphology. Silvestri et al. (Silvestri et al., 2005) showed that, in the study marsh considered, *Spartina* colonizes the inner and lower part of the marsh, *Limonium* and *Sarcocornia* are more likely to be observed at intermediate surface elevations, and *Juncus* tends to occupy higher-elevation marsh areas. Indeed, the fractional abundance of each species has been considered as an indicator of marsh morphology (Silvestri and Marani, 2004) and of distance to channels (Sanderson et al., 2001). Consistently with observational evidence (Marani et al., 2006a; Silvestri et al., 2005; Silvestri and Marani, 2004; Wang et al., 2007) maps of fractional abundance of each species provided by the "soft" RF algorithm (Figure 3.4) emphasize the clear link between vegetation distribution and marsh surface morphology, which is strongly related to the distance to main channels representing the source of sediments delivered to the platform (D'Alpaos et al., 2007a). Indeed, inner marsh portions, that are mainly occupied by *Salicornia* and *Spartina* (Figures. 3.4c and f), display lower elevations; areas at moderate distance to the channels, that are encroached by *Limonium* and *Sarcocornia*, (Figures. 3.4b and d) are characterized by intermediate surface elevations; and finally marsh edges, which are mainly occupied by *Juncus*, are characterized by higher elevations. The link between plant distribution and marsh morphology, described in Figure 3.4 is consistent with observational evidence (M. Roner et al., 2016; Silvestri and Marani, 2004), and therefore further confirms the robustness of the RF soft classification. The repeated application of the novel soft RF algorithm to a temporal series of remote sensing data from the same marsh can thus allow a quantitative and repeatable monitoring of marsh eco-morphodynamic processes.

3.4.2. The RF soft method performance compared to existing regression models

It is worth recalling that the RF regression method (Liu et al., 2017; Liu et al., 2017; Lopatin et al., 2016; Melville et al., 2019; Schwieder et al., 2014), after simply rescaling abundance of each class to sum to 100%, was observed to perform well when applied, e.g., to map fracitonal abundance of tree species in Bavaria (Germany) ($0.72 < R^2 < 0.82$) (Immitzer et al., 2018) and plant types ($0.47 < R^2 < 0.78$) in east Asia steppe (China, Mongolia, and Russia) (X. Liu et al., 2017). However, in our case the accuracy of the RF regression model was not satisfactory ($0.14 < R^2 < 0.58$). This relatively worse performance, can be probably attributed to the high small-scale heterogeneity that characterizes marsh vegetation. In particular, the number of classes in Bavaria (2 tree species and 1 class labeled as 'other' considered in (Immitzer et al., 2018)) and in east Asia steppe (2 plant types: woody and herbaceous) was lower than that of the Venice lagoon (5 vegetation

species and 1 class representing the bare soil on the marsh). Furthermore, the renormalization of RF regression results summing to 100%, which is necessary to obtain fractional abundances, is likely to increase the estimation error (Table3. 4 and Figures 3.7-9). Indeed, as Immitzer et al. (Immitzer et al., 2018) reported when they estimated fractional abundance of tree species in Bavaria via the RF regression, the highest value of the sum of the relative abundance of the three considered classes in each pixel was about 102%, while such a value increased to more than 200% in our case. It should be noticed that the renormalization process in the application of the RF regression is performed in this study by assuming that all RF regression models for single species contribute equally, e.g. considering that the sum of the predicted abundance is 100 % (Guerschman et al., 2015). In order to improve the accuracy of the RF regression, a weighted contribution of each model on the basis of the documented vegetation distribution patterns could be considered.

Figures 3.7-9 and Table 3.4 suggest that, although the RF regression model predicts reasonably the relative distribution of each class taken separately, the method that is usually adopted (Immitzer et al., 2018; Liu et al., 2017; Liu et al., 2017; Melville et al., 2019) can hardly be applied to accurately estimate the fractional abundance of each species in the case of highly mixed species. Values of R^2 and RMSE for fractional abundance derived from RF soft classification and RF regression respectively (Tables 3.3 and 3.4), suggest that the RF soft classification performs slightly worse than RF regression for single classes, while its performance is considerably higher compared to the rescaled RF regression method. Figures 3.7-9 show the outcome of the test performed to compare field observations with the results obtained with the three different methods (RF soft classification, RF regression, and rescaled RF regression models) for *Juncus* and *Limonium* (Figure 3.7), *Salicornia* and *Sarcocornia* (Figure 3.8), Soil and *Spartina* (Figure 3.9) and highlight that the RF soft classification method performs much better than the rescaled RF regression method.The superior performance of the RF soft classification can be attributed i) to the full use of the information provided by each decision tree; and ii) to the simultaneous consideration of all classes which avoids the need to perform *ad hoc* renormalizations.

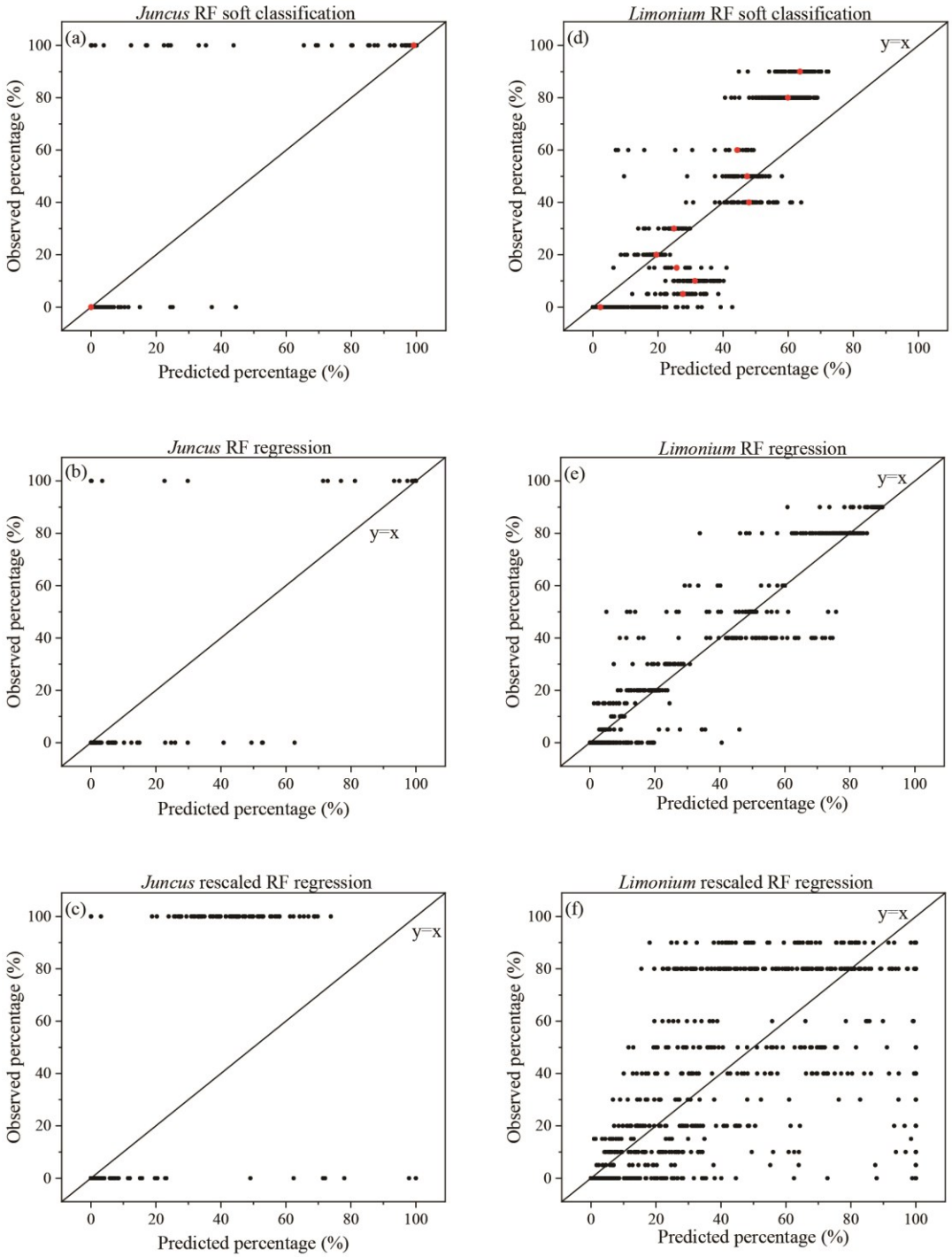

Figure 3. 7: Validation results for *Juncus* and *Limonium*: (a) and (d) are predicted probabilities (x-axis) plotted against the validation data; (b) and (e) are regression results (x-axis) plotted against the validation data; (c) and (f) are rescaled regression results (x-axis) plotted against the validation data. Red dots represent the mean of the predicted percentage using the RF soft classification.

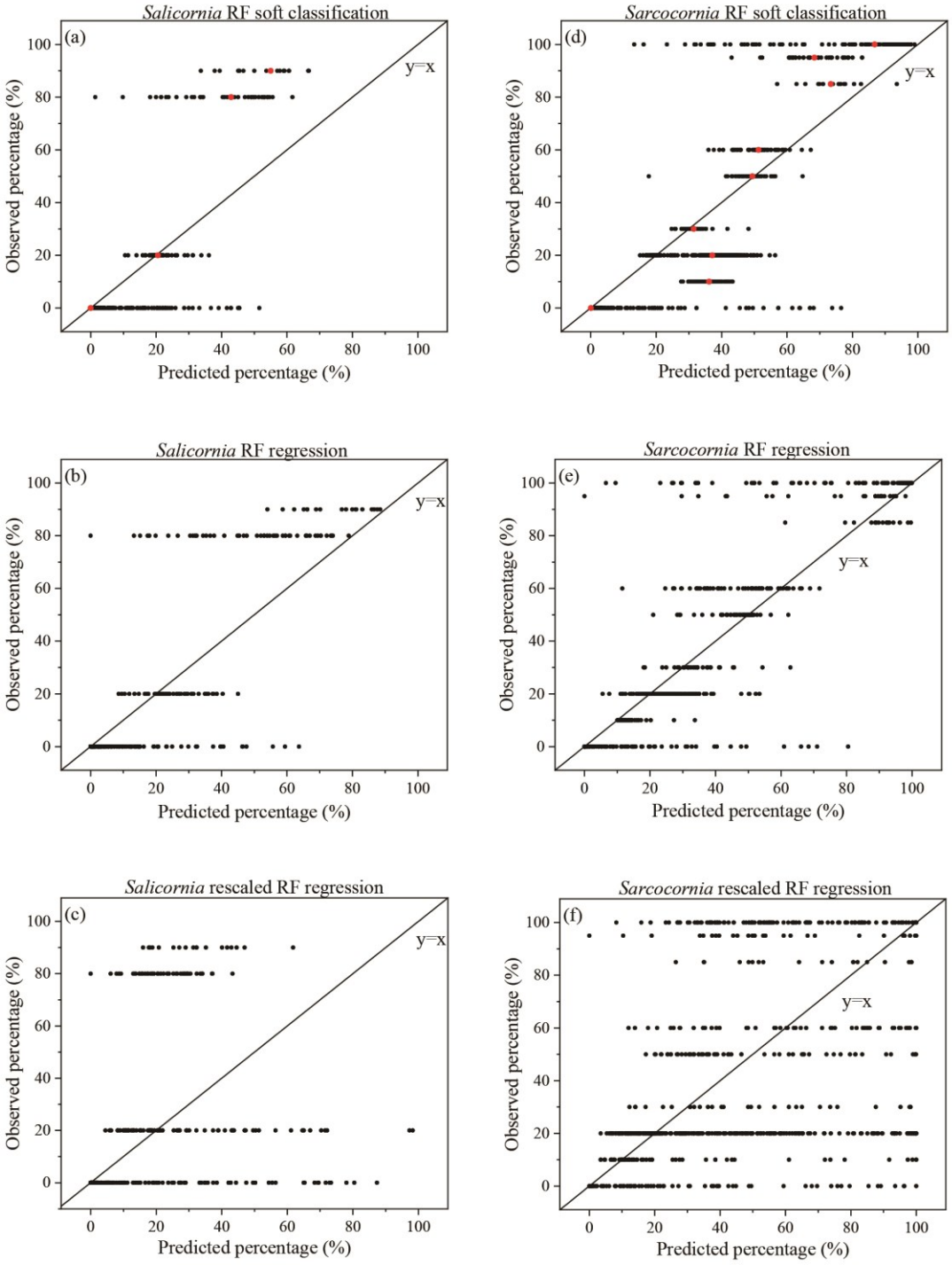

Figure 3. 8: Validation results for *Salicornia* and *Sarcocornia*: (a) and (d) are predicted probabilities (x-axis) plotted against the validation data; (b) and (e) are regression results (x-axis) plotted against the validation data; (c) and (f) are rescaled regression results (x-axis) plotted against the validation data. Red dots represent the mean of the predicted percentage using the RF soft classification.

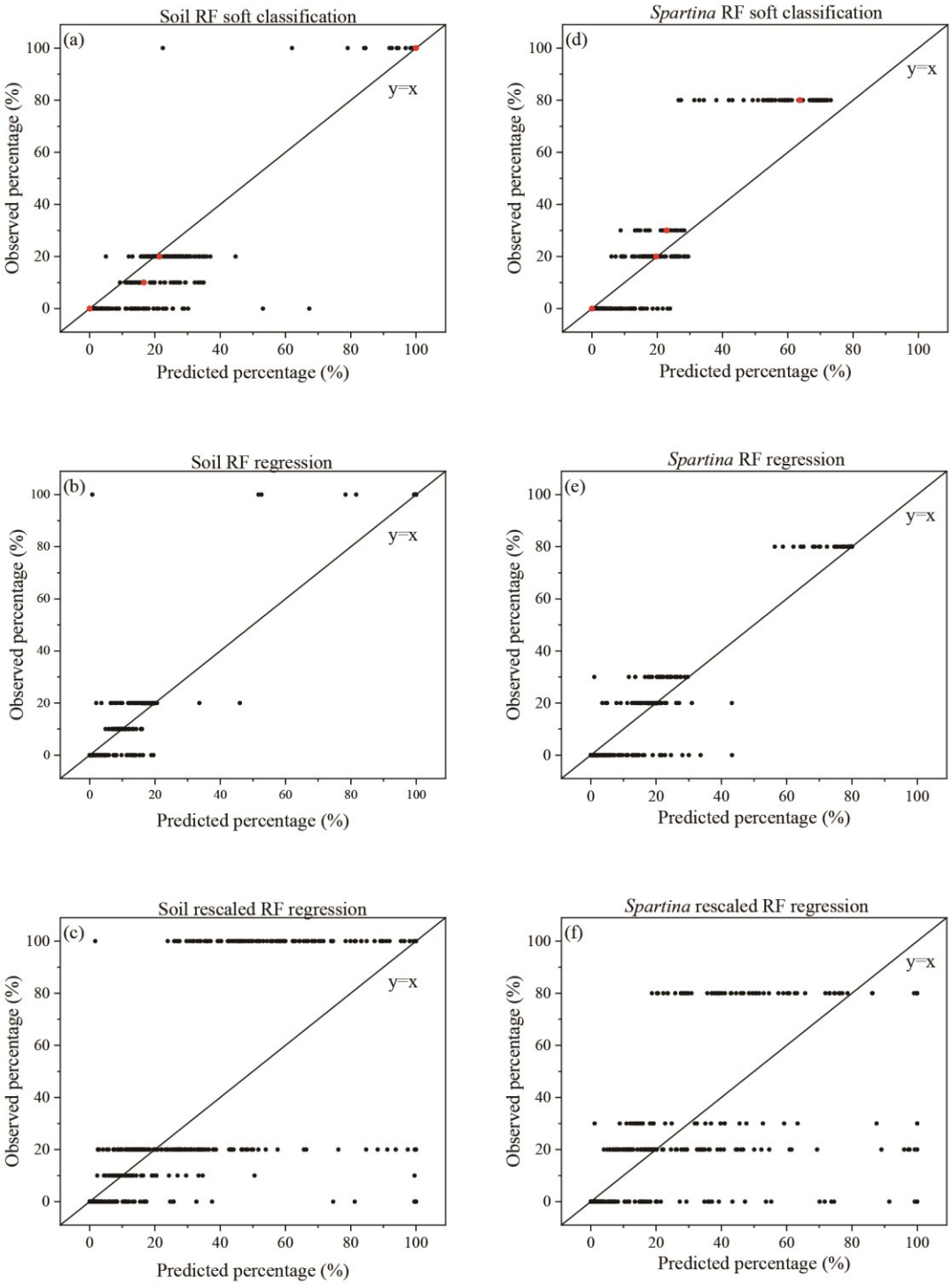

Figure 3. 9: Validation results for Soil and *Spartina*: (a) and (d) are predicted probabilities (x-axis) plotted against the validation data; (b) and (e) are regression results (x-axis) plotted against the validation data; (c) and (f) are rescaled regression results (x-axis) plotted against the validation data. Red dots represent the mean of the predicted percentage using the RF soft classification.

3.4.3. Drawbacks of dominant species maps

Due to the high biodiversity of halophytic vegetation species on marshes, we argue that traditional hard classification methods (i.e., where classifiers tend to associate each pixel to an individual species or to bare soil) (Belluco et al., 2006; Van der Wal et al., 2008) cannot provide accurate information on vegetation distribution. Indeed, pixels (whose size is in the order of 0.5 - 1 m) in remote sensing images are often composed of highly mixed vegetation associations (Silvestri and Marani, 2004; Wang et al., 2007), particularly over salt marshes.The results obtained with the hard classification (Figure 3.6a) allow us to perform a further analysis of the results obtained with the RF soft classification (Figure 3.6b). Specifically, we notice that the position of patches occupied by dominant classes agrees quite well with those obtained with a RF hard classification, thus suggesting the robustness of the RF soft method. Furthermore, we notice that some large mixed areas, composed by more than one species (or bare soil), cannot be detected by the hard classification method. These areas are mostly located in the inner portions of the marsh, where topographic elevations are relatively low (M. Roner et al., 2016; Silvestri et al., 2005) and inner species (*Salicornia* and *Spartina*) are always mixed with bare soil. Finally, we also notice that mixed areas are observed in *Limonium*- dominated areas in the hard classification results. This can be attributed to the fact that *Limonium* and *Sarcocornia* tend to colonize the same areas.

We further compared our results to those obtained by Belluco et al. (Belluco et al., 2006) using ML (Maximum Likelihood) and SAM (Spectral Angle Mapper) hard classifiers applied to a 2001 IKONOS dataset over the same study site. The map obtained with the RF hard classification and the majority map obtained from the RF soft classification are both very similar to that of ML and slightly better than its SAM counterparts, based on the comparison of A and Kappa, indicating that RF is a reliable classifier for halophytic species.

We therefore conclude that, in highly mixed vegetation environments like salt marshes, traditional hard classification methods do not provide sufficient information on species distribution since they must necessarily label mixed areas with the dominant species. On the contrary, soft classification methods, when properly applied, provide essential information about species presence (also within mixed pixels). Majority maps obtained by from RF soft methods are consistent with those produced with hard classification methods, lending further support to the method introduced here.

3.4.4. Feature importance analyses

An advantage of the RF algorithm is that it allows the quantification of the importance of each spectral band (i.e. feature) used in the classification. In our case, we analyzed IV values of each WV-2 band for the detection of salt marsh vegetation and bare soil. As for the hard classification method, Figure 3.10 (a) shows that the Yellow band (Wavelength: 584 – 632 nm) is the most important band among those provided by WV-2. One possible explanation for this could be that the Yellow band facilitates the detection of bare soil, which has higher reflectance at this wavelength compared to vegetation (Figure 3.10c). As for the subpixel classification based on RF soft method, Yellow band, NIR 1, and NIR 2 bands are those that provide the majority of information (Figure 3.10b), possibly due to the difference of reflectance characteristics in the

NIR 1 and NIR 2 bands of different vegetation species (Figure 3.10c). Table 3.6 suggests that the Yellow band is of critical importance in Soil and *Limonium* percentage regression. Moreover, Table 3.6 also shows that the NIR 1 and NIR 2 bands are critical in regression practice for other classes. These analyses suggest the NIR 1 and NIR 2 bands provided by WV-2 can improve the accuracy of halophytic classification. This can be explained because, as shown in Figure 3.10 (c), in the visible range, reflectance values of vegetation species are similar, while the variability increases in NIR 1 and NIR 2 bands.

Table 3. 6: Feature importance of each band in RF regression (CB is Coastal Blue). Jun = *Juncus*, Lim = *Limonium*, Sali = *Salicornia*, Sarc = *Sarcocornia* and Spar = *Spartina*.

Band Importance	Classes					
	Jun	**Lim**	**Sali**	**Sarc**	**Soil**	**Spar**
CB	0.028	0.016	0.074	0.034	0.004	0.028
Blue	0.014	0.017	0.142	0.033	0.006	0.043
Green	0.008	0.016	0.055	0.234	0.009	0.024
Yellow	0.010	0.670	0.087	0.047	0.930	0.011
Red	0.033	0.022	0.133	0.094	0.004	0.212
Red Edge	0.010	0.128	0.098	0.100	0.007	0.068
NIR 1	0.037	0.093	0.274	0.354	0.009	0.516
NIR 2	0.861	0.038	0.135	0.104	0.030	0.099

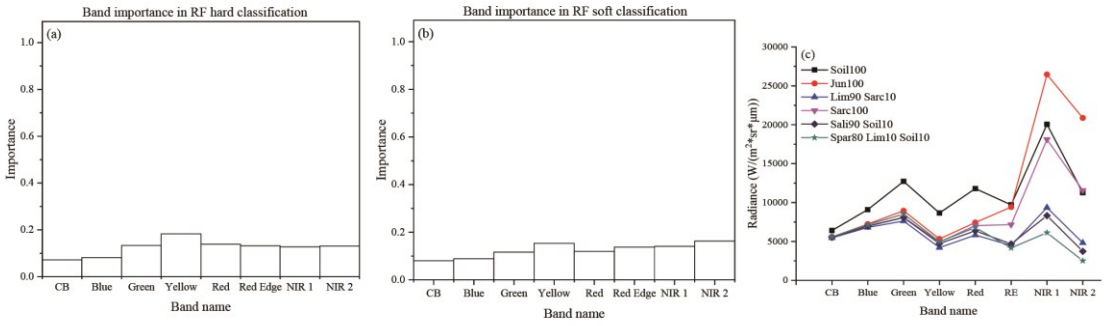

Figure 3. 10: Band importance for different methods and reflectance characteristics of each class: (a) and (b) is the relative importance of each band for RF hard classification and RF soft classification, respectively; (c) is calculated by average radiance value of corresponding ROI (CB is Coastal Blue, RE is Red Edge).

An important source of uncertainty in this study may be related to the interference of water with species reflectance. The tidal elevation at the time of acquisition was about 0.45 m above MSL, suggesting that large portions of the marsh, whose elevations range from 0.15 m to 0.60 m above MSL, were flooded with water depths up to 30 cm. Kearney et al. (Kearney et al., 2009) documented that tidal inundation can result in a significant reduction in NIR 2 (856-1043 nm) and greatly affects the Red Edge band (699-749). High water levels thus increase noise in spectral reflectance information, in particular for NIR bands and significantly affect the outcome of hard and soft classifiers.

3.5 Conclusions

Halophytic vegetation, an important component of salt marshes, is typically organized in patches of species associations. In this study, we focus on the development of a new approach based on the application of RF soft classification for estimating fractional abundance of each species within vegetation associations and applied it to a WV-2 multispectral image. In particular, we make full use of the information contained in the distribution of "votes" from individual decision trees and interpret their distribution across classes as the corresponding fractional abundance. This approach yields high classification accuracies (6.7% < RMSE< 18.7% and $0.65 < R^2 < 0.96$). We found that, while the RF regression can predict the percentage of each class accurately when each class is considered separately, the overall accuracy decreases significantly when relative abundances are rescaled to sum to 100%. Comparisons of RF soft classification results to rescaled RF regression results (Figures 3.6, 7 and 8), suggest that the former is more suitable to accurately map fractional abundance in highly-mixed halophytic associations. Our results show that the RF soft-classifier predicted distribution patterns are in very good agreement with halophytic vegetation patterns documented by previous analyses (Belluco et al., 2006; M. Roner et al., 2016; Silvestri et al., 2005, 2003), thus confirming the usefulness of the method.

We show that the results obtained with the RF soft classification can be used to produce a map of the dominant species within the plant association (i.e. with percentage cover higher than 60% in our case). This map nicely agrees with a RF hard classification map (Kappa=0.962, A=0.970) produced for the same study site, thus emphasizing the RF soft-classifier robustness. Our comparison also highlights that the traditional hard classifiers force the pixels to be assigned to a specific class, which is unrealistic when dealing with mixed vegetation associations as in the case of salt marshes, thus neglecting the heterogeneous contribution to the spectral signal associated with the mixture.

In conclusion, we developed a robust RF soft classification approach to assess the fractional abundance of halophytic vegetation and bare soil. This approach uses the frequency of 'votes' to each species to represent corresponding fractional abundance. We applied this method to estimate the fractional abundance of halophytic vegetation species within our study site, which is characterized by high biodiversity of salt-marsh vegetation and where halophytic species are organized in mixed vegetation associations at the scale of the satellite sensor resolution (0.5 m). The proposed method allowed us to obtain high accuracy in the current application, suggesting it can be a valuable tool to analyze the distribution pattern of fractional abundance of salt-marsh vegetation species. The comparison between the results obtained with the RF soft classifier to those drawn from its regression counterpart shows its superior robustness. We suggest that the RF soft classification is a useful tool to describe fractional abundance of halophytic species and bare soil on salt marshes and to provide important information about the spatial distribution of dominant species. Thus, the RF soft classification allows one to monitor the temporal evolution of halophytic vegetation, such as dieback and replacement. We, therefore, suggest that the RF soft classification method should be considered to

analyze salt-marsh response to sea-level changes and for the development and testing of biogeomorphic models.

Author Contributions: Conceptualization, Z.Y., A.D., M.M. and S.S.; Methodology and Validation Z.Y. and S.S.; Formal Analysis, Z.Y.; Investigation Z.Y., A.D., M.M. and S.S.; Data Curation Z.Y., A.D., M.M. and S.S.; Writing- Original Draft Preparation Z.Y. and S.S.; Writing-Review & Editing, Z.Y., A.D., M.M. and S.S.; Funding Acquisition, A.D.. All authors have read and agreed to the published version of the manuscript.

Chapter 4: Large-scale halophytic vegetation vertical distribution from coupled multi-spectral data and LIDAR-derived marsh surface elevations

This chapter is a manuscript ready to be submitted to the Journal of Ecology. This chapter mainly focused on the extension of the *in-situ* observed vegetation-elevation relationship to the whole marsh scale through the use of remote sensing data. In particular, we first developed and tested a novel method to analyze LIDAR data and obtain a Digital Elevation Model (DEM) of the marsh based on the Random Forest Regression algorithm, using information contained by the fractional abundance of each species and Normalized Differential Vegetation Index (NDVI). The vegetation-elevation relationship was then analyzed by coupling the corrected DEM and vegetation maps. Finally, the vertical distribution of above-ground biomass was explored through the analysis of relevant bio-morphodynamic metrics.

PAPER

Large-scale halophytic vegetation vertical distribution from coupled multi-spectral data and LIDAR-derived marsh surface elevations

Zhicheng Yang[1*], Enrica Belluco[2], Xiaxiang Li[3], Davide Tognin[2], Sonia Silvestri[4], Marco Marani[2], Andrea D'Alpaos[1*]

[1] *Department of Geosciences, University of Padua, Padua, Italy*

[2] *Department of ICEA, University of Padua, Italy*

[3]*Key Laboratory of Land Surface Pattern and Simulation, Institute of Geographical Sciences and Natural Resources Research, Chinese Academy of Sciences, Beijing, 100101, China*

[4] *Department of Biological, Geological, and Environmental Sciences, University of Bologna, Bologna, Italy*

Abstract

Salt marshes are critical ecosystems that are vulnerable to the current rates of sea-level rise and increasing human impacts. Halophytic vegetation helps offsetting marsh drowning through complex bio-morphodynamic feedbacks. However, our knowledge on its distribution and biomass production is still limited and mainly based on *in-situ* measurements. To extend knowledge of vegetation biomass distribution at larger scales, we coupled light detection and ranging (lidar) point clouds and multi-spectral data, acquired over the San Felice marsh (Venice lagoon, Italy) to explore the vertical distribution of halophytic vegetation and analyze the relationship between marsh morphology and above-ground biomass production (AGB).

Towards this goal, we first developed and tested a novel method based on the Random Forest Regression algorithm, combining a lidar-derived Digital Elevation Model (DEM) with vegetation fractional abundance (FA) and biomass information. The vertical distribution of halophytic vegetation was then analyzed by coupling the corrected DEM and vegetation maps. Finally, the vertical distribution of AGB was explored through the analysis of relevant bio-morphodynamic metrics (NDVI, sum of the fractional abundance of vegetation (SFA), leaf area index (LAI) and empirical AGB (eAGB)) that were derived from multi-spectral, lidar point cloud data and field observations. Our analyses suggest that: i) the proposed method is reliable and produces a highly accurate DEM of the marsh (R^2 = 0.79 and RMSE = 3.5 cm); ii) previously reported *in-situ* vegetation species sequence with increasing elevations, is found to be consistent and reliable at the whole marsh scale; iii) the AGB generally increases with higher elevations, as suggested by all metrics (NDVI, SFA, LAI and eAGB) displaying higher values at higher marsh portions. For the first time we extended the vegetation-elevation relationship observed by local-scale measurements to the whole marsh scale, a critical step to inform and test eco-morphodyanmic models. Moreover, the proposed lidar-derived method can be a useful tool to further improve our current understanding on marsh ecological and geomorphological dynamics.

4.1. Introduction

Salt marshes are ecosystems periodically inundated by the tide, forming transition zones between marine and terrestrial landscapes (Balke et al., 2014; Fagherazzi et al., 2012; Marani et al., 2004; Silvestri et al., 2005; van Belzen et al., 2017; Van der Wal et al., 2008; Zhu et al., 2020). They exert important roles in the geomorphological and biological processes of intertidal areas (Brinson et al., 1995; Dalrymple and Choi, 2007; Laengner et al., 2019; Raabe and Stumpf, 2016; Schuerch et al., 2019; Shi et al., 2012), but currently experiencing a strong erosional trend worldwide (Horton et al., 2018; Jankowski et al., 2017; Schepers et al., 2017; Sun et al., 2020; Tommasini et al., 2019; Törnqvist et al., 2020) due to the increase in the rates of relative sea-level rise (RSLR), the decrease in sediment supply (Blum and Roberts, 2009; D'Alpaos and Marani, 2016; Kirwan et al., 2010; Marani et al., 2010a), lateral erosion caused by wave attack (Koppel et al., 2005; Priestas et al., 2015; Tommasini et al., 2019) and increasing human interferences (Kearney, 2015; Silvestri et al., 2018).

Halophytic vegetation encroaches coastal marshes because of its high adaptability to periodic inundation and high salty conditions (Costa et al., 2003; Crain et al., 2008; Marani et al., 2003; Pennings and Moore, 2001). Halophytic vegetation affects erosional and depositional patterns over the marsh surface through complex bio-morphodynamic processes (Bouma et al., 2009; Lightbody and Nepf, 2006; Rupprecht et al., 2017; Temmerman et al., 2007; Yang and Nepf, 2019), e.g., producing organic sediments (Curcó et al., 2002; Janousek et al., 2016; Kirwan and Guntenspergen, 2012; Morris, 1990; Mudd et al., 2009; Scarton et al., 2002), reducing flow velocities (Bouma et al., 2007, 2005; Leonard and Croft, 2006) and directly trapping sediments (Fagherazzi et al., 2012). Thus, halophytic vegetation can support marsh survival under increasing sea level scenarios (D'Alpaos et al., 2011; Kirwan et al., 2010; Morris et al., 2002; Mudd et al., 2009).

However, biomass production and halophyte response to RSLR are species-specific (Janousek et al., 2016; Morris et al., 2002; Scarton, 2006; Scarton et al., 2002). As a result, a better understanding of halophytic vegetation speices distribution is of central importance to understand marsh surface processes and to predict marsh evolution (Collin et al., 2010; Janousek et al., 2019; Silvestri et al., 2005).

Halophytic vegetation is organized by sharply defined patches composed of single species or typical species associations, a spatial structure known as zonation. Such zonation patterns can be considered as the net results of edaphic conditions (Bertness and Ewanchuk, 2002; Bockelmann et al., 2002; Daleo et al., 2008; Moffett et al., 2012; Snow and Vince, 1984), interspecific competition (Costa et al., 2003; Pellegrini et al., 2018; Pennings et al., 2005) and the capability of halophytic vegetation species to engineer salt-marsh topography via biogeomorphic feedbacks to maintain they can live within species-specific preferable elevation ranges (Da Lio et al., 2013; Marani et al., 2013). Marsh surface elevation controls the waterlogging frequency and duration, thus regulating the physical stress and edaphic conditions. As a result, the distribution of halophytic vegetation is strongly linked to marsh surface morphology. Previous field observations have reported that each species has its preferable elevation range, which is characterized as its ecological niche, thus constructing species sequence as elevation changes (Donnelly and Bertness, 2002; Janousek et al., 2019; Qi et al., 2021; Silvestri et al., 2005, 2003). Marsh platform morphology also affects biomass production, thus changing the ability of halophytic vegetation to support marsh surface to keep pace with sea-level rise (Kirwan et al., 2010; Kirwan and Guntenspergen, 2012; Marani et al., 2010a; Morris et al., 2002; Mudd et al., 2010). In particular, field measurements of above-ground biomass (AGB) in many marshes worldwide suggest that AGB generally increases with elevations (Roner et al., 2016). However, most of the previous analyses on the vertical distributions of halophytic vegetation species and AGB are mainly measured from a limited number of sites. While marsh elevation is not the only variable controlling vegetation species distribution (Moffett and Gorelick, 2016; Pennings et al., 2005; Qi et al., 2018). Until now, to our knowledge, there is still no observations focused on the species and AGB vertical distributions of at large range of spatial scales (within a whole marsh up to several km^2), because a large number of field collections is labor-intensive and often inner marsh areas are difficult to reach. So there is a clear gap to extend the vegetation-elevation relationship to the whole marsh scale, thus becoming one of the issues in this study.

Remote sensing provides useful tools to address these issues, thus extending such analyses to a large spatial scale (Fagherazzi et al., 2012). Classification methods, aiming at halophyte species discrimination, have been widely developed and also been applied to multi- and hyper-spectral data with high accuracy (Belluco et al., 2006; Marani et al., 2006b). Halophyte species have been classified in the form of pixel-based (Belluco et al., 2006; Timm and McGarigal, 2012; Van Beijma et al., 2014) and object-based (Berhane et al., 2019; Fournier et al., 2007; Juel et al., 2015; Lantz and Wang, 2013; Moffett and Gorelick, 2013; Yeo et al., 2020) scales. Because halophytic vegetation species are always organized with high heterogeneity in typical optical data pixels, the methods to estimate the fractional abundance (i.e., the ratio of the vertical projection area of given vegetation species, FA) of halophyte species have been well developed more recently, allowing us to

yield FA maps with high accuracy (Costa et al., 2017; Silvestri et al., 2003; Wang et al., 2007; Yang et al., 2020).

Remote sensing also allows us to analyze the above-ground biomass (AGB) distribution at the marsh scale by using some reliable representers (Ganju et al., 2017; Marani et al., 2004; Roner et al., 2016; van Belzen et al., 2017; Yousefi Lalimi et al., 2017). In particular, normalized difference vegetation index (NDVI), defined as the normalized difference between infrared and red bands, was proposed in the 1970s (Rouse et al., 1974) and it has been proven to represent vegetation biomass production (Lopes et al., 2020; Pan et al., 2018; Schalles et al., 2013; Sun et al., 2018; Wang et al., 2017) and structure (Feng et al., 2016; Givnish et al., 2008; Jia et al., 2006; Pan et al., 2018). The fractional abundance of halophytes, i.e., the sum of the fractional abundance of each vegetation species (SFA), is another proxy for above-ground biomass (Roner et al., 2016). Leaf area index (LAI), which is defined as the total one-sided leaf area per ground surface area (Zheng and Moskal, 2009), always carry critical information on the structure of vegetation canopy and above-ground biomass (Fedrigo et al., 2018; Korhonen et al., 2011; Richardson et al., 2009; Yousefi Lalimi et al., 2017). In addition, a combination of accurate FA maps and an empirical AGB dataset (obtained from in-site observation and in-lab experiments) is another way to empirically estimate the AGB (eAGB) over the marsh (Roelfsema et al., 2014).

In terms of elevation data, light detection and ranging (lidar) is a common tool to construct digital elevation models (DEMs) for different landscapes (Pinton et al., 2020; Wang et al., 2009; Wulder et al., 2012; Yan et al., 2015; Yousefi Lalimi et al., 2017). The applications of lidar on marsh-DEM construction and related vertical distribution analyses are still challenged by the low accuracy and the narrow habitat elevation range of halophytes (Buffington et al., 2016; Hladik et al., 2013; Hladik and Alber, 2012; Klemas, 2011). The errors of lidar over the marsh are mainly due to poor laser penetrability through halophytic vegetation and to the presence of water flooding the marsh (Klemas, 2011).

To construct lidar-derived DEMs of marsh surface, the development of algorithms that are used for lidar error removal has been one of the central interests to marsh researchers and managers (Buffington et al., 2016; Chassereau et al., 2011; Rogers et al., 2018; Schmid et al., 2011; Wang et al., 2009) and a variety of methods have been proposed in the recent decades. For example, the minimum-bin gridding method (MBG) uses the lowest lidar return in changing the size of the moving window to make sure such return can penetrate the vegetation and reach the marsh surface, and then use some gridding methods to generate a DEM. The main drawback of this method is that it would lose a lot of point-cloud information, and the gridding process could cause some errors in the final DEM. Hladik and Alber (2012) developed a vegetation correction factor (VCF) method, e.g., correct lidar-derived DEM by the application of species-specific factors, but the high heterogeneity of halophyte organizations would hinder its broad application. Buffington et al., (2016) consider the NDVI as the main representer of halophyte biomass and structure thus linking it to the error of lidar (so-called LEAN method). But the wide appearance of the wet area over the marsh would lead to that NDVI cannot convey correct information on vegetation structure and biomass (Kearney et al., 2009), further

attenuating the accuracy of this method.

It clearly emerges that the key step to construct an accurate lidar-derived DEM is to accurately estimate the biomass and vegetation composition. The FA of each species and multi-spectral data-derived NDVI are important indicators of vegetation biomass, structure and the probability of the laser penetrating the vegetation to reach the marsh surface. However, there is still a gap that hinders the utilization of them to facilitate lidar-derived DEM construction. Thus, in this study, we mainly consider both FA and NDVI in a nonparametric regression model (Random Forest regression, RFR) to estimate the marsh surface elevations and then construct a lidar-derived DEM with high accuracy.

The FA maps and lidar-derived DEM allow us to quantitatively describe the vertical distribution of halophytic vegetation and AGB by using eco-morphodynamic metrics on a large spatial scale. Here we mainly test our assumption that marsh surface morphology controls the halophytic vegetation distribution and biomass production. In specific, the variations of dominant species (the most abundant one) and of FA with elevation gradient will be analyzed. Then, we will make further efforts to analyze the vertical distribution of biomass-related metrics (NDVI, SFA, LAI and eAGB).

In the next section, we describe the study area, our lidar point clouds, multi-spectral data and ground-truthing data collected by ancillary field campaigns. Section 4.3 mainly describes the methods to assess the FA of each species, to determine NDVI, to estimate the elevation on the basis of vegetation information and lidar raw data, to analyze the vertical distribution of halophytic vegetation and above-ground biomass production. In Section 4, we analyze the vertical distribution of halophytic vegetation and AGB. Section 4.5 gives some discussion and then we draw a set of conclusions in the final section.

4.2. Study area and data

4.2.1 Study Site—the San Felice salt marsh (Venice lagoon, Italy)

The Venice lagoon (Fig. 4.1a) is located in the northeastern area of Italy. The lagoon has a waterbody area of about 550 km^2 and it is connected to the Adriatic Sea by three inlets: Lido, Malamocco and Chioggia (D'Alpaos et al., 2017; Fagherazzi et al., 2006; Tommasini et al., 2019; Tosi et al., 2018). It is characterized by a semidiurnal tide with a mean tidal range of about 1.0 m and a maximum tidal range of about 1.5 m (Roner et al., 2016; Volpe et al., 2011).

This analysis is carried out over the San Felice marsh (Fig. 4.1b), which is one of the most naturally preserved areas within the northern part of the lagoon (Marani et al., 2003; Roner et al., 2016). The area of this marsh decreased in the last century mainly due to the apperacne and the extension of the inner pond and lateral erosion caused by wave attack (Day et al., 1998). At the year of our remote sensing data acquisition (2003, explained in Section 2.2), this marsh is mainly encroached by 4 species: *Spartina maritima* (hereafter "*Spartina*"), *Limonium narbonense* (hereafter "*Limonium*"), *Sarcocornia fruticosa* (hereafter "*Sarcocornia*") and *Juncus maritimus* (hereafter "*Juncus*") (Marani et al., 2006b; Wang et al., 2009). The spatial distribution

of these species over the San Felice marsh has been analyzed ranging from small spatial scale by in-site measurements (Silvestri et al., 2003) to the whole marsh by using remote sensing images (Belluco et al., 2006; Marani et al., 2006b, 2003b; Wang et al., 2007; Yang et al., 2020); While, until now, our knowledge on the vertical distribution is still limited in a small scale based on some in-site measurements (Silvestri et al., 2005) and cannot extend to a whole marsh scale, thus calling for the further analyses.

4.2.2 Remote sensing data and ancillary field campaigns

The main aim of this study is to analyze the vegetation-elevation relationship at the whole marsh scale through accurate lidar-derived DEM and vegetation distribution maps. In specific, we consider using the vegetation information derived from multi-spectral remote sensing data to correct lidar over the marsh and analyze the vegetation and biomass vertical distribution by coupling the corrected lidar and multi-spectral data.

4.2.2.1 Lidar data

The lidar data collection was carried out over the San Felice (SF) marsh on February 9, 2003. We used the FALCON II sensor here, which provides both first and last returns at a wavelength of 1560 nm. The aircraft acquired point clouds with a density of about 8 points/m^2 at an altitude of about 450 m above ground with a speed of about 60 m/s. The lidar records are composed of 6 flight lines to cover the whole marsh. For further details on the raw lidar data, we refer readers to Wang et al. (2009). Following Wang et al. (2009), last return data were selected in this study mainly because they are more efficient in the discrimination between vegetation and substrate in this area.

4.2.2.2 Multi-spectral data

We use the multi-spectral data (QuickBird 2) to estimate the FA and NDVI over the marsh to facilitate the lidar correction, because it is acquired in the same year (July 2003) of the lidar. The QB sensors include 5 spectral bands (Table 4.1), i.e., a panchromatic spectral band with a higher spatial resolution (0.72 m) and 4 multispectral bands with a lower spatial resolution (2.88 m). The QB sensor acquires data from an altitude of about 450 km.

The IKONOS image acquired in 2001 is also used for the analyses of the vertical distributions of vegetation and above-ground biomass. The IKONOS data is composed of 4 multi-spectral bands, ranging from visible and near-infrared bands with a spatial resolution of 4 m, and a Panchromatic band (409-1048nm) with a finer spatial resolution of 1 m (Belluco et al., 2006).

The general information of these images is summarized and listed in Table 4.1. The vegetation biomass as well as the percentage cover change with seasons (Mudd et al., 2009), which would influence the penetration of lidar thus influencing the accuracy of our correction method. Moreover, the tidal level is an important factor influencing the accuracy of derived vegetation information (Kearney, 2015; Yang et al., 2020). Thus,

the image acquisition date and the tidal level information are also included in Table 4.1. The tidal elevation is measured by Punta Salute (Figure 4.1a) station higher than the “Istituto Geografico Militare” (hereafter “IGM") datum. The MSLs in 2001 and 2003 are about 0-5 cm higher than the IGM datum, indicating that the marsh was not flooded and only very low marsh portions were flooded during acquisitions.

Table 4. 1: Information of the image and of the corresponding acquisitions

Acquisition year	**2001**	**2003**
Sensor	IKONOS	QuickBird
Spatial resolution	P: 1 m M: 4 m	P: 0.72 m M: 2.88 m
Acquisition date	26/06	25/07
Flight time (GMT)	10:00	9:45
Tidal level	−20 cm	+6.7 cm

P=panchromatic; M=multispectral;

4.2.2.3 Field observations for vegetation information

Field observations on vegetation information were performed currently with remote sensing acquisitions to provide accurate vegetation information. For each multi-spectral image, a set of ground reference areas (Region of Interest, ROIs), which will be used for training and testing the vegetation classification models, were randomly selected across the marsh with the target to include all the typical species and associations. The boundary of each ROI was delimited by using differential GPS (Leica CS15 in RTK mode, minimum accuracy of ±1 cm). For each ROI, the fractional abundance of each species and bare soil were estimated by using the standard Braun–Blanquet visual method (Belluco et al., 2006; Biondi et al., 2014; Silvestri et al., 2005; Van der Wal et al., 2008), which records the presence of each species and bare soil by 10 intervals between 0% - 100%. The number of ROIs for vegetation classification in 2001 and 2003 were 11 and 20, respectively.

After the field collection, all ROIs were overlaid on the georeferenced and resampled multi-spectral data (as explained in Section 4.3.2) in Arcmap 10.8 and only pixels falling entirely within each ROI were used to build the classification dataset.

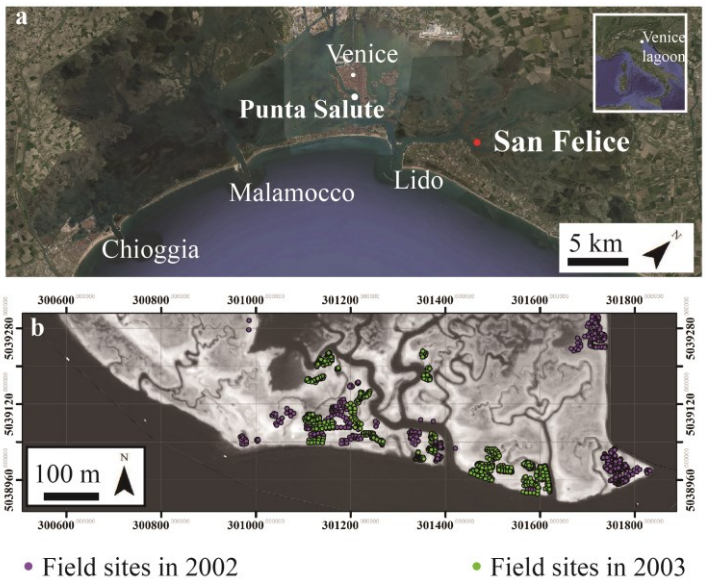

Figure 4. 1: Study area: (a) shows the position of San Felice marsh on a map of Venice lagoon (base map is collected from Google Earth, https://www.google.com/earth/); (b) shows the map of the San Felice marsh and data points used to correct lidar (base map is the NIR band of QB data).

Marsh surface elevation data were collected in 2002 and 2003 with the aim of providing accurate ground reference elevation to construct the DEM. The measured elevation (2 above datasets, Fig. 4.1b) by DGPS and lidar point clouds were with the respect to the IGM datum and with the reference to UTM-WGS84 planar coordinates. The total number of elevation points is 1579. It should be noted that the accretion rate of the San Felice marsh is about 3 mm/year (Day et al., 1998), which cannot be detected by DGPS, thus including data points in both 2002 and 2003 cannot result in any deviations and errors of the final DEM. All those points were then overlaid on and extracted local information from the lidar raw grid data (as explained in Section 3.1), FA maps of each species and NDVI (generated from QB data as explained in Section 3.3.2) to build a final dataset to train the model (explained in Section 3.3.3) to construct a DEM with high accuracy.

4.3. Methods

4.3.1 Lidar data preprocessing

Lidar collection would cause some random errors, thus, following Wang et al (2009), returns from the water body are removed at first. Moreover, all laser returns with an elevation higher than 300 cm or lower than 0 cm are removed. According to the estimation of planimetric offsets by Wang et al (2009), the lidar raw data should be translated of 65 and 110 cm (no rotation), respectively, due to x-axis and y-axis deviations. We also applied the vertical shift provided by Wang et al (2009), as listed in Table 4.2.

Table 4. 2: Summary of vertical shift

Flight lines	z shift (cm)

1	1.14
2	1.13
3	-1.20
4	-1.38
5	-1.75
6	2.05

After the planimetric translation, we generate a grid with a resolution of 1 m by selecting the lowest elevation of the raw lidar data in each pixel (by the use of CloudCompare v2.11.3), because the lowest elevation has the highest probability to represent local marsh surface elevation (Pinton et al., 2020).

4.3.2 Multi-spectral data preprocessing

In order to accurately estimate the FA of each species and construct a dataset for potential comparisons with past and future acquisitions, the multi-spectral data were atmospherically corrected by the use of MODTRAN (Richter and Schläpfer, 2002) and then transformed into reflectance values using the 6S model by the use of a 'Maritime' type of atmospheric profile (Belluco et al., 2006; Vermote et al., 1997). After atmospheric correction, the IKONOS and QB data were pan-sharpened to a spatial resolution of about 1.0 m and 0.72 m, respectively, by using the panchromatic band (Table 4.1) through the Gram–Schmidt Pan-Sharpening algorithm (Maurer, 2013; Palubinskas, 2013). And then the QB data were resampled to a resolution of 1 m through the nearest neighbor method. Pan-Sharpening and resample processes were performed in ENVI 5.4 and Arcmap 10.8, respectively. Then, in order to minimize errors in the final DEM, we geo-referenced the IKONOS and QB data by the usage of 5 points. The final step is the manual digitalization of channel networks on the geo-referenced data.

4.3.3 Lidar-correction algorithm description

Random Forest (RF) is a supervised nonparametric 'ensemble machine learning' algorithm mainly for classification (Random Forest classification, RFC) and regression (Random Forest Regression, RFR) tasks, based on a set of Classification and Decision Trees (CART) (Breiman, 2001). The RF method has been successfully used in habitat, vegetation species, or landscape classification (Belgiu and Drăgu, 2016; Berhane et al., 2019; Rogers et al., 2018; Schwieder et al., 2014), and key ecological parameter prediction (Immitzer et al., 2018; Rogers et al., 2018), due to its outstanding advantages, such as the ability to manage a large number of input bands (Juel et al., 2015; Ma et al., 2017; Van Beijma et al., 2014), to minimize Hughes phenomenon (Hughes, 1968) and to handle multi-modal datasets (Belgiu and Drăgu, 2016). In this work, the RF is carried out using the Scikit-learn package (Pedregosa et al., 2011), an open-source and commercially usable machine learning library for the Python programming language.

The RF is a non-parametric model that makes predictions based on the statistics of predictions by each inside CART. After a user-defined number of CART (*ntree*) is chosen, each CART is trained by about two-thirds of the samples (input data) that are selected randomly with replacement (bootstrapping) (Breiman, 1996).

The bootstrapping method results in each CART is fed with different sub-datasets and those that are left out (out of bag, OOB) can serve as datasets to test the predictive ability of each CART. Once the training data input, training samples are binary split into two groups at each node (internal nodes) based on so-called "best split" binary rules (Breiman, 2001) and the decreasing in Gini impurity index (*Gini*), which can be expressed as:

$$Gini = 1 - \sum_{i=1}^{n} p_i^2 \quad (4.1)$$

where p_i is the frequency (probability) of *i*th class in *n* total classes (Breiman, 2001). If the growth of a CART is not limited, it would keep growing until there is a node (terminal node) for every single class.

In the regression process, the accuracy (R^2, as explained in section 4.3.3) of predicted OOB samples is recorded and averaged over all cases to produce an OOB accuracy estimation (OOB score). The OOB accuracy estimation is unbiased and can be used as a cross-section test (Breiman, 1996).

4.3.3.1 Method to estimate the fractional abundance and map the most abundant species

We perform the Random Forest Soft Classification (RFSC) method to estimate the fractional abundance (*FA*) of each species. Detailed information about this method can be found in Yang et al. (2020). The key steps of this method are 1) using sample weights (observed FA in fieldwork) to change CART split processes; 2) considering the number of votes as the probability value that the pixel belongs to one specific species, and 3) interpreting such probability as FA of each species (Yang et al., 2020). In this work, following Yang et al (2020), we decide to select *ntree* equal to 490, because of its high accuracy. After the estimation of FA of each species, we define the most abundant species in each pixel as the one with the highest FA. The ROI collection allows us to have a dataset of 5649 pixels to construct the model. To estimate the accuracy, the dataset was randomly divided into two groups: 4237 pixels (about 75% of the dataset) were used in model training and 1412 pixels (about 25% of the dataset) were used in model validation. After the estimation of FA of each species and bare soil, the most abundant species were then mapped by the one with the highest FA in each pixel, where can be considered as its habitat (Van Beijma et al., 2014; Zhang, 2015).

4.3.3.2 Computation of NDVI

NDVI is strongly linked to chlorophyll content and can be expressed as:

$$NDVI = \frac{NIR - R}{NIR + R} \quad (4.2)$$

where NIR and R are the spectral reflectances in the NIR and red bands, respectively (Tucker, 1979). Because *NDVI* is an important bio-morphodynamic metric to represent AGB, after the construction of DEM (described in Section 3.3.3), the average value of NDVI (mNDVI) at each elevation will be calculated to

describe its link to elevation.

4.3.3.3 Method to construct the DEM

As mentioned above, FA and NDVI can provide valuable information on lidar error correction. Random Forest Regression (RFR) model was selected to find a relationship between input variables (FA of each species, NDVI, and raw lidar grid data) and the local correct marsh surface elevation. The RFR is similar to the Random Forest Classification method, and it is based on the assumption that the relationship between input variables and the target variable (local 'true' marsh surface elevation) can be described through a non-linear correspondence. The RFR makes predictions by using the average value of the individual CART (Breiman, 2001).

The main steps of the RFR process are 1) information on FA of each species, NDVI, and raw lidar grid data of each field point are extracted in Arcmap 10.8; 2) construct a dataset for RFR by using information obtained from 1) (input variables) and local 'true' elevation (target variable); 3) the dataset in 2) was randomly divided into two groups, i.e., 1180 (about 80%) points were used to train the RFR model and the other 260 (about 20%) were used to test the RFR accuracy.

Before the DEM construction, we decided *ntree* in this part by maximizing the OOB score when the *ntree* ranged from 10 to 1000. Fig. 4.2 shows that the OOB score increases rapidly up to *ntree* = 100 (Fig. 4.2). We select *ntree* equal to 375 since the OOB maintains constant after here (Fig. 4.2).

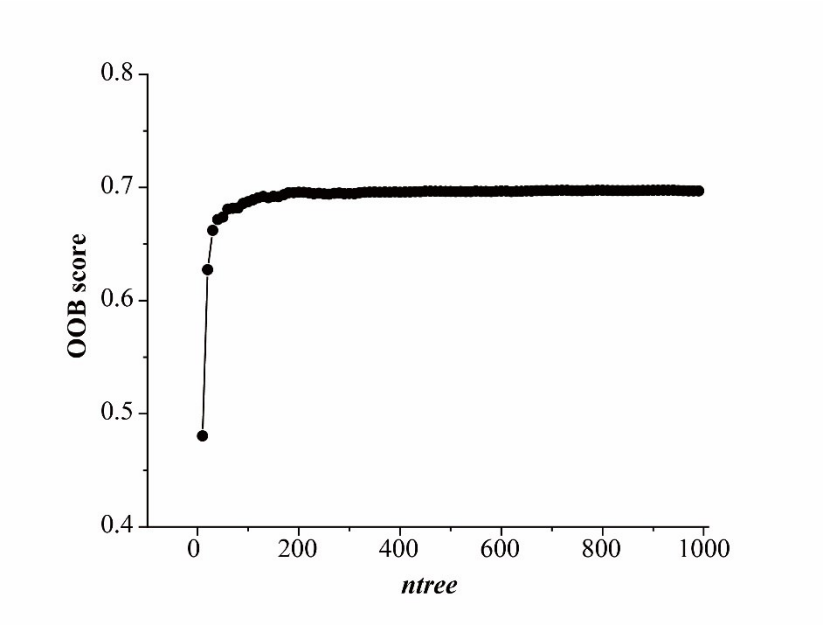

Figure 4. 2: R^2 and OOB score variations with increasing *ntree.*

4.3.3.4 Estimation of accuracy

Both the performances of FA and elevation estimations are tested by two matrics, i.e., the root-mean-square

error (RMSE) and the coefficient of determination (R^2) :

$$\mathrm{RMSE} = \sqrt{\frac{\sum_{i=1}^{n}(y_i - \hat{y}_i)^2}{n}} \tag{4.3}$$

$$R^2 = \frac{\sum_{i=1}^{n}(\hat{y}_i - \bar{y})^2}{\sum_{i=1}^{n}(y_i - \bar{y})^2} \tag{4.4}$$

where y_i $\hat{y}_i$ and $\overline{y}$ represents the ground referential value, the predicted value, and the average of the observed values respectively, and *n* is the number of validation data points.

4.3.4 Analyses of halophyte vertical distribution

After the construction of DEM, the vertical distributions of the most abundant species in 2001 and 2003 were analyzed by coupling the most abundant maps and the DEM. In the next step, the distribution of elevation encroached by each most abundant species was analyzed by using the Kernel Density Estimator (Bowman and Azzalini, 1997) in MATLAB 10.8a. Finally, we use the average value of FA (mFA) of each species and bare soil to show the variations of fractional abundance of each species with different elevations.

4.3.5 Computation of SFA, LAI and AGB

4.3.5.1 Estimation of SFA

SFA is calculated by using the sum of fractional abundance of each halophyte species (or 1 minus *FA* of bare soil). We use the average value of SFA ($\mathrm{mSFA_i}$) at each given elevation (*i*) to show its vertical distribution. *m SFA*$_i$ can be determined by:

$$mSFA_i = \sum mFA_{i,j} \tag{4.5}$$

where $mFA_{i,j}$ is the mean FA of *j* species at a given elevation (*i*).

4.3.5.2 Estimation of LAI

In this study, after proposing a new lidar correction method, we carry out the *LAI* estimation based on the calculation of gap probability, i.e., the probability ($P(\theta)$) that a laser beam can penetrate the vegetation to reach the marsh surface (Richardson et al., 2009; Houl et al., 2005):

$$LAI = -\cos(\theta)\ln(P(\theta))/k \tag{4.6}$$

where θ is the zenith angle (scan angle of the sensor) and *k* is the extinction coefficient (=0.5) (Campbell, 1986; Houl et al., 2005). To keep in line with much of the available literature (Campbell, 1986; Richardson et al., 2009; Lalimi et al., 2017), we here assume $\theta = 0$ for all returns. The penetration of lidar laser of

vegetation canopy in each lidar raw grid is detected by elevation difference between each laser return and elevation value of DEM corrected by RFR method, i.e., if such difference is very small (lower than a specified threshold elevation), we can consider this laser successfully reach the marsh surface through the canopy gap. Based on the field vegetation height measurement (Wang et al., 2009), we assume that the threshold elevation of 20 cm is consistently lower than the returns reflected by the vegetation canopy. And then, similar to other metrics, we use the average value of LAI (mLAI) at each elevation to describe its vertical distribution.

4.3.5.3 Empirical estimation of AGB (eAGB)

Combining an empirical dataset of the biomass of all typical species covering marshes in the Venice lagoon (Scarton, 2006), and the FA maps generated in Section 4.3.3.1, we can calculate the empirical AGB (eAGB) in each pixel. Here, one of the main aims of this article is to characterize the link between marsh surface morphology and above-ground biomass (AGB), thus we describe such link by the calculation of the mean value of empirical AGB (meAGB) at each elevation of *i* cm through the following equation:

$$meAGB_i = mFA_{i,j} \cdot meAGB_{i,j} \quad (4.7)$$

where $meAGB_{i,j}$ is the average empirical AGB (eAGB) of *j* species at a given elevation (*i*), as listed in Table 4.3.

Table 4. 3: The empirical dry weight of each species (g/m^2) based on data by Scarton (2006) used to determine the estimated above-ground biomass (eAGB).

***j* (Species)**	**Dry weight** (g p.s./m^2)
Juncus	1000
Limonium	222
Sarcocornia	887
Spartina	534

4.4. Results

4.4.1 Maps fractional abundance of each species estimated by RFSC s

FA maps of each species and bare soil in 2001 and 2003 are displayed in Fig. 4.3 and Fig. 4.4, respectively, while their accuracy information (R^2 and RMSE) are listed in Table 4.4. The R^2 and RMSE values for the RFSC application to IKONOS data (acquired in 2001) range from 0.72 to 0.94 and from 6.09 to 17.15, respectively. And these two values for the application to QB data (acquired in 2003) range from 0.66 to 0.90 and from 4.22 to 12.55, respectively. This suggests that the RFSC is reliable to estimate the spatial distributions of FA, further confirming the high accuracy of the most abundant species maps in Fig. 4.5.

Figs 4.3 and 4.4 show that *Limonium* and *Sarcocornia* tend to occupy areas along main channels, whereas

Spartina prefers to encroach inner marsh portions, while the areas of marsh sites are encroached mainly by *Juncus* is smaller than the other three species. As to the changes between 2001 and 2003, areas with higher *Spartina* FA values display an obvious decrease in time, while areas with higher soil FA values display a contrasting behavior. This could be due to the heat-wave event starting from April 2003, resulting in extreme drought and high temperature thus further causing the dieback of *Spartina*, as well as a decrease in FA values of other species (Strain et al., 2017).

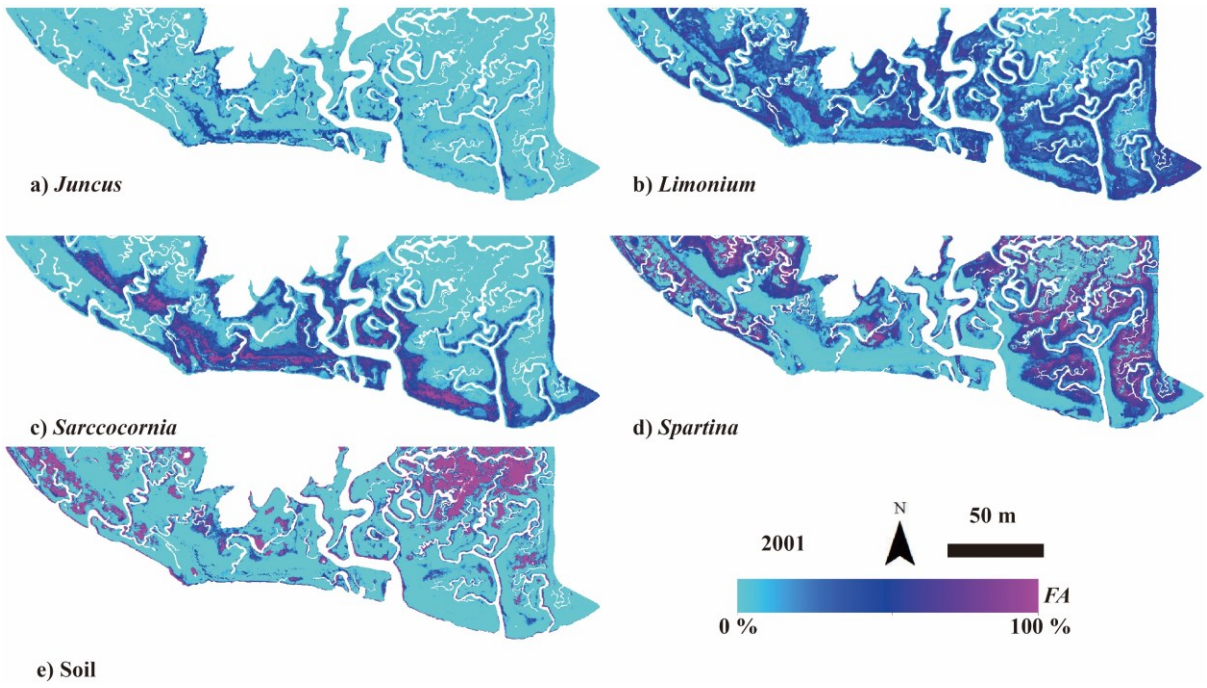

Figure 4. 3: FA maps of each species or bare soil in 2001.

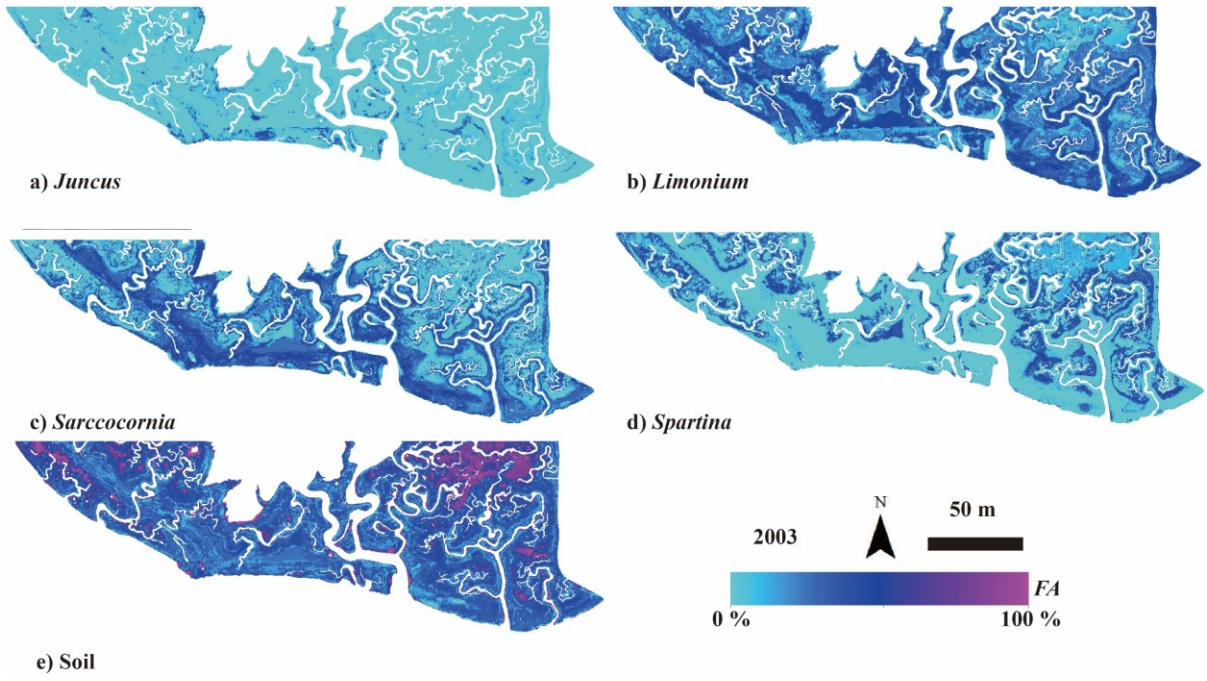

Figure 4. 4: FA maps of each species or bare soil in 2003.

Table 4. 4: Accuracy information for RFSC method

Classes	2001		2003	
	R^2	RMSE	R^2	RMSE
Juncus	0.83	9.76	0.83	4.22
Limonium	0.72	15.88	0.70	12.55
Sarcocornia	0.78	17.15	0.66	9.98
Spartina	0.94	6.09	0.90	4.73
Soil	0.91	10.42	0.75	9.27

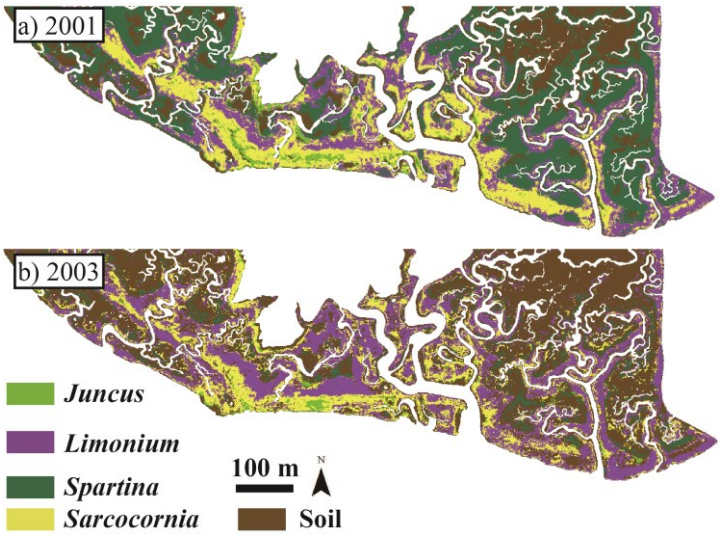

Figure 4. 5: Map of the most abundant species.

The most abundant species maps display that a large area dominated by *Spartina* shifts to the bare soil state, confirming the dieback event observed from FA changes in time (Figs 4.3 and 4.4), which has also been documented by previous remote sensing analyses over the same marsh (Belluco et al., 2006).

4.4.2 NDVI map

Fig. 4.6 shows the NDVI maps over the San Felice marsh in 2001 and 2003 by using equation (4.2). It emerges that NDVI values on marsh portions close to main channels are much higher than inner marsh portions. Indeed, inner marsh portions are more likely to observe the bare soil shown in Figs. 4.3, 4.4 and 4.5, thus reducing the NDVI value. We also notice that NDVI values in inner marsh sites in 2003 were lower than in 2001, which can be attributed to the higher tidal level at the acquisition time of QB data (Table 4.1).

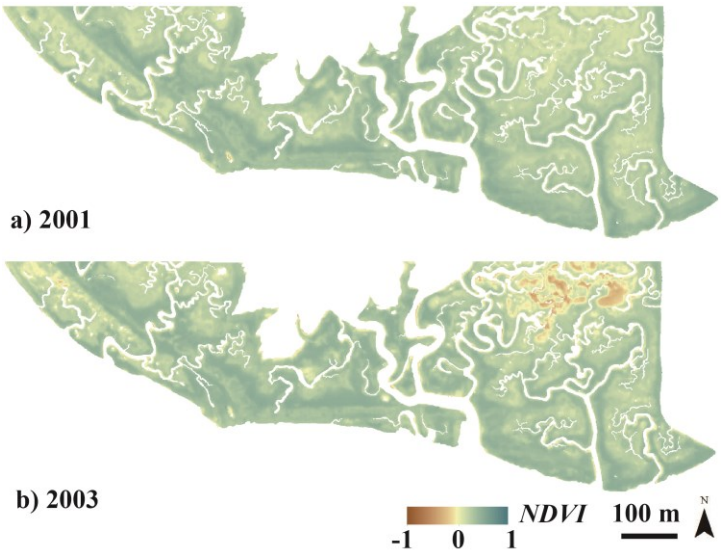

Figure 4. 6: NDVI map over the San Felice marsh

4.4.3 DEM construction by the RFR method

Fig. 4.7 shows the DEM constructed by the RFR method, whose R^2 and RMSE values for this method are 0.79 and 3.5 cm, respectively. It emerges that relatively higher areas border along the main channel on the southern part of the marsh, as well as along the major tidal creeks and the northern tidal flat, whereas the inner portions of the marsh show relatively lower elevation. Visual observation (Figs. 4.5 and 4.7) shows areas dominated by *Spartina* are lower than areas mainly encroached by *Limonium* and *Sarcocornia*, and *Juncus* prefers to encroach highest marsh portions. Bare soil patches are more likely to be observed in inner marsh portions with low elevation.

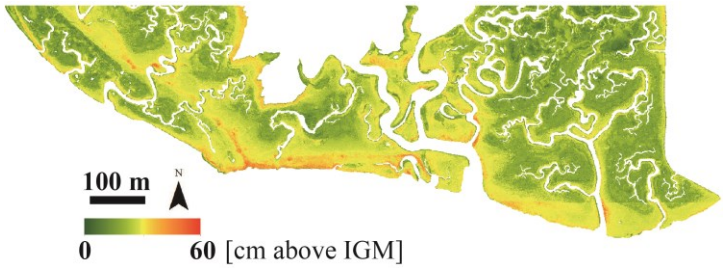

Figure 4. 7: DEM constructed by the proposed RFR method

4.4.4 Vertical distribution of the most abundant species and FA of each species

We first analyzed the vertical distribution of the most abundant species. Fig 4.7a and c show the frequency distributions of marsh elevation of each species habitat in both 2001 and 2003, indicating that the elevations of the habitats of *Spartina*, *Limonium* and *Sarcocornia* can be characterized by the unimodal distribution. While *Juncus* is the only species exhibiting bimodal distribution with two obvious peak frequency values. These suggest that each species lives within typical elevation ranges, which can be considered as its ecological niche (Silvestri et al., 2005, 2003). Interestingly, this leads to the observation of a typical species

sequence with increasing elevations (Fig. 4.8c and 4.8d). More in detail, in these two years, *Spartina* prefers to encroach lower marsh portions with the mean elevation of about 18.2 - 19.1 cm (above the IGM), *Limonium* is more likely to be observed on marsh platforms with the average elevations of about 25.3 – 26.7 cm (above the IGM), whereas *Sacocornia* occupies higher marsh portions with the average elevations of about 29.0 – 28.4 cm (above the IGM), while *Juncus* encroach the highest marsh portions on average (31.0 – 32.5 cm above the IGM).

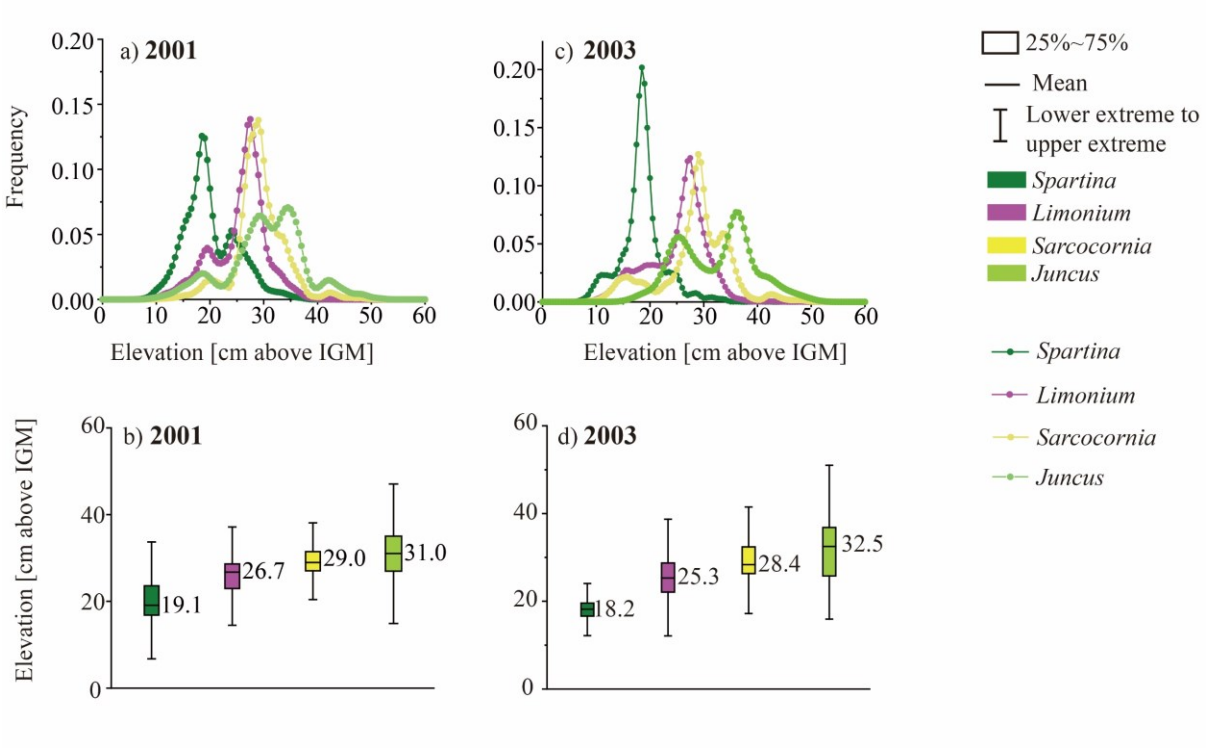

Figure 4. 8: The vertical distribution of the most abundant species: (a) and (b) are the frequency and box-whisker plot of elevation dominant by each species in 2001, respectively; (c) and (d) are the frequency and box-whisker plot of elevation dominant by each species in 2003, respectively.

The coupling of the DEM of high accuracy (Fig. 4.7) and accurate FA maps for each species (Figs 4.3 and 4.4) allows one to analyze the variations in mean FA with increasing elevations. Fig. 4.7 shows a general decrease in FA values of Soil with higher elevation, indicating halophytic vegetation is difficult to occupy marsh portions with elevations similar to MSL, which is about 0-5 cm higher than the IGM in the observation period. Indeed, these sites are characterized by anoxic edaphic conditions that cannot support vegetation encroachment due to higher waterlogging period and frequency (Pennings et al., 2005). As to variations in the mean FA of typical species with increasing elevation, it emerges that the mean FA of each species approaches the peak value in a species-specific elevation range. In specific, the peak value in mFA of *Limonium* can be observed at elevations between 20 and 30 cm (above the IGM), while the mFA of *Sarcocornia* tends to approach its highest value at elevations of around 30 cm and then maintains constant, which is similar to the behavior of mFA of *Juncus* that approaches its peak at marsh sites about 40 cm above IGM and then maintained at higher elevations. These species-specific behaviors did not display an obvious

change between 2001 and 2003. However, in terms of the behavior of mFA of *Spartina* with increasing elevations, it can be characterized as time-dependent. It reached the highest value (about 0.5) at areas with elevations of about 20 cm (above IGM) in 2001, whereas it displayed a flat pattern with peak values of about 0.3 in 2003, resulting in an obvious increase in mFA of bare at areas with elevations range from 10-20 cm (above IGM). These changes also can be attributed to the above-mentioned heatwave event, which results in an obvious decrease in FA of *Spartina* (Figs 4.3 and 4.4).

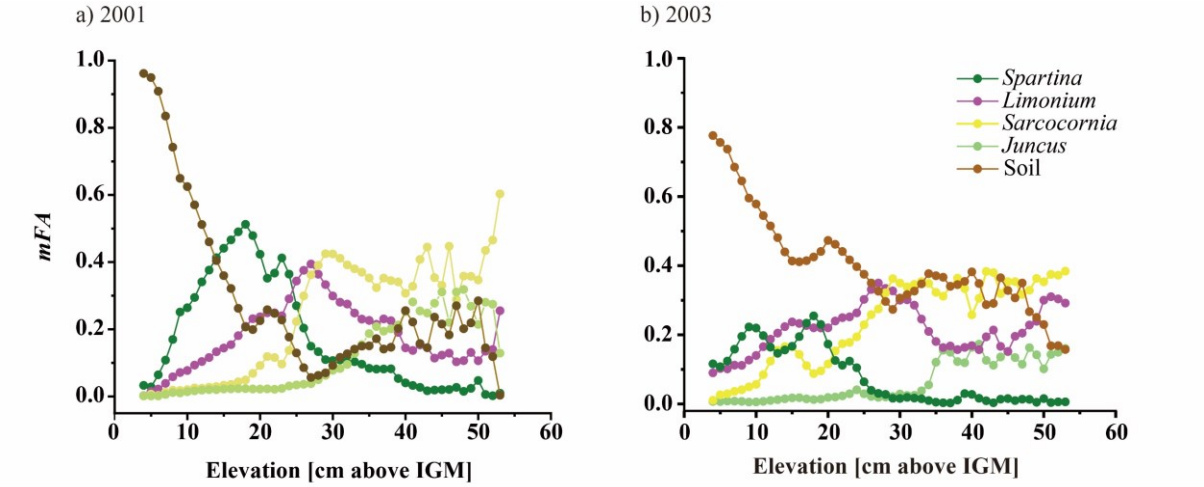

Figure 4. 9: mFA changes of each species with higher elevation

4.4.4 vertical distribution of above ground biomass production

We then analyzed the relationship between above-ground biomass and marsh surface elevation through critical bio-morphodynamic metrics (NDVI, SFA and LAI meAGB). Figures 4.10 and 4.11 show the vertical variations in these metrics, indicating that NDVI, SFA, LAI and meAGB generally increase with higher elevations. This suggests that AGB is generally higher in higher marsh portions. Indeed, the lower physical stress of the waterlogging on the higher marsh portions can facilitate biomass production (Pennings et al., 2005). In addition, the above-ground biomass of *Spartina* and *Limonium*, those who prefer to encroach lower marsh portions (Figs. 4.8 and 4.9), is lower than that of their counterparts on higher marsh portions (Scarton 2006, Table 4.3). In addition, we realized that each metric has a trough value at elevations ranging from 20-30 cm (above the IGM), suggesting the relatively lower AGB here. This can be explained by the reason that these marsh areas are mainly dominated by *Limoniuim* (Fig. 4.8), the one that has the lowest productivity among all species (Scarton 2006).

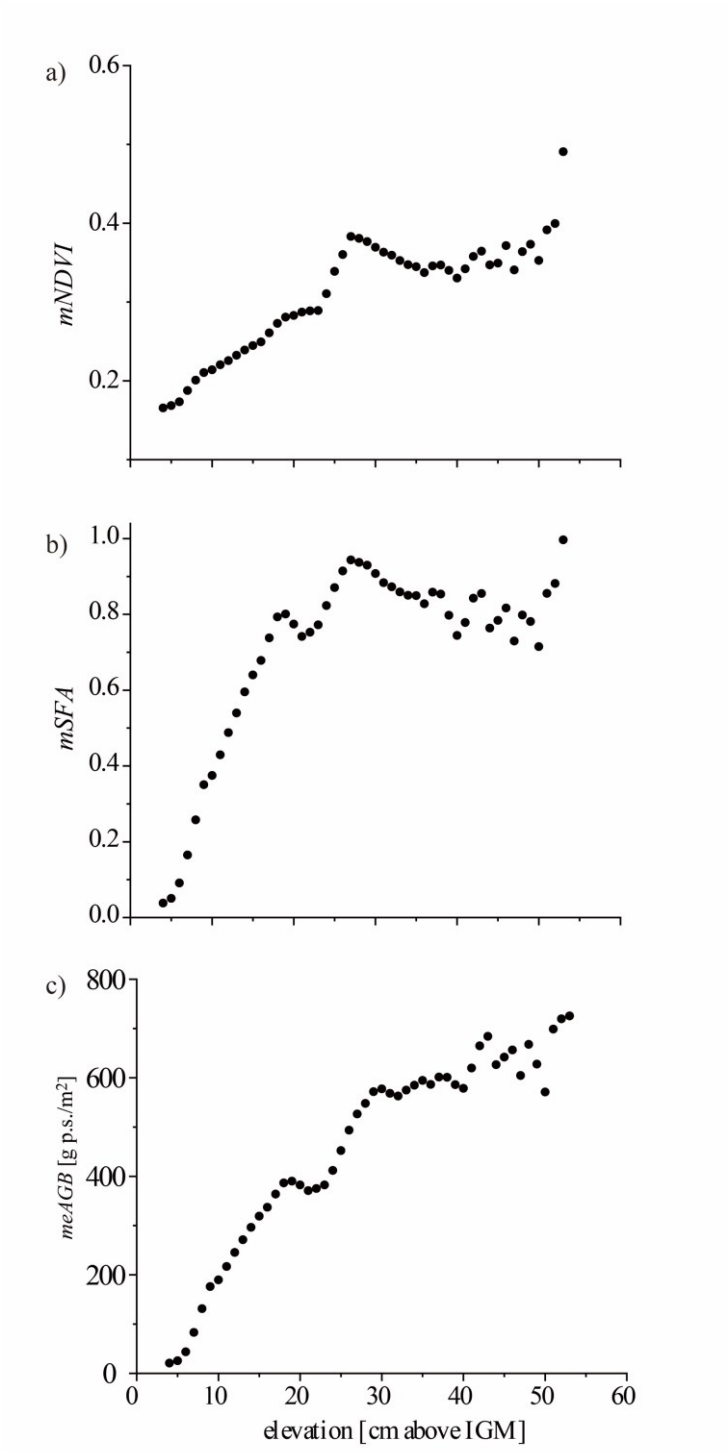

Figure 4. 10: Variations in mNDVI, mSFA and meAGB with increasing elevation observed in 2001.

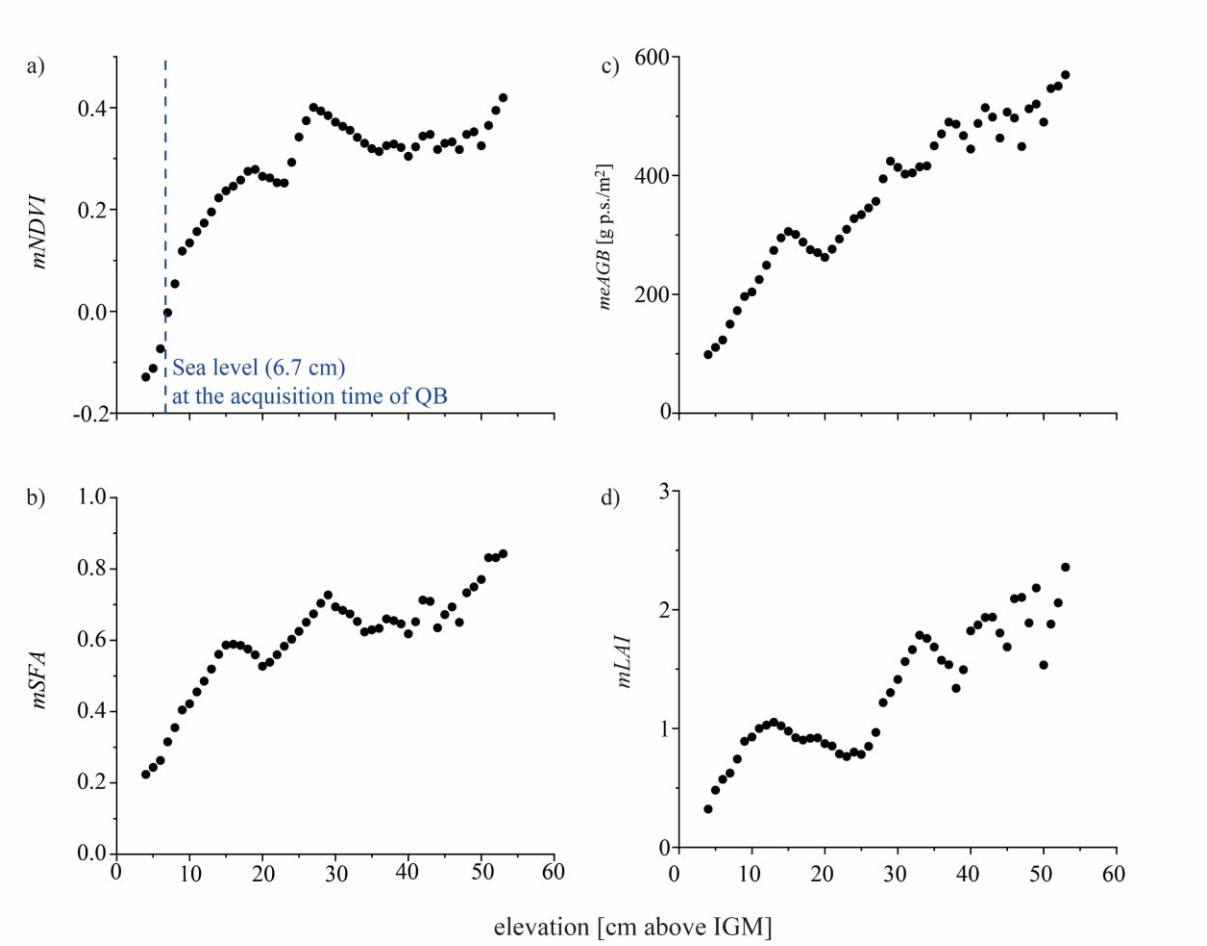

Figure 4. 11: Variations of matrics with increasing elevation.

4.5. Discussion

4.5.1 The RFR method performance compared to existing methods

We made a comparison of the performances of our method and the other methods in the literature. More in detail, the minimum-bin gridding method (MGB, Wang et al., 2009) which has been used to construct a DEM with the same lidar clouds in this analysis by selecting a moving window with a radius of 3.5 m, and the Lidar Elevation Adjustment with NDVI (LEAN) method (Buffington et al., 2016), which constructs a link between the inaccuracies (E) between lidar and ground elevations (l) and NDVI by:

$$E = l + NDVI + NDVI^2 + l * NDVI^2 + NDVI^2 * NDVI + l * NDVI^2 * NDVI \quad (4.8)$$

In specific, the LEAN method was trained using the same training dataset of our RFR method (introduced in Section 3.3.4) but only considering NDVI, grid raw lidar data and ground-truthing elevations. The predicted elevations by MGB and LEAN methods were extracted using the positions of the validation dataset of our RFR method.

Their performances were displayed in Fig. 4.12 together with the accuracy of the lidar raw grid data (Fig.

4.12a), which is more likely to overestimate the marsh surface elevation, mainly due to the poor laser penetrability through vegetation (Hladik and Alber, 2012; Klemas, 2011). Fig. 4.12 shows all these three methods have the ability to improve the accuracy of the lidar-estimated elevation but with different performances. Indeed, our proposed RFR method (RMSE = 3.5 cm) performs better than MGB (RMSE = 6.6 cm) and LEAN methods (RMSE = 5.2 cm), taking advantage of by fully using vegetation information represented by FA and NDVI. Besides the higher accuracy, the RFR method, compared with the MGB method, can preserve more information provided by the lidar point clouds and, compared with the LEAN method, is less likely to be influenced by the appearance of water due to the fact FA also can represent vegetation information in a large degree.

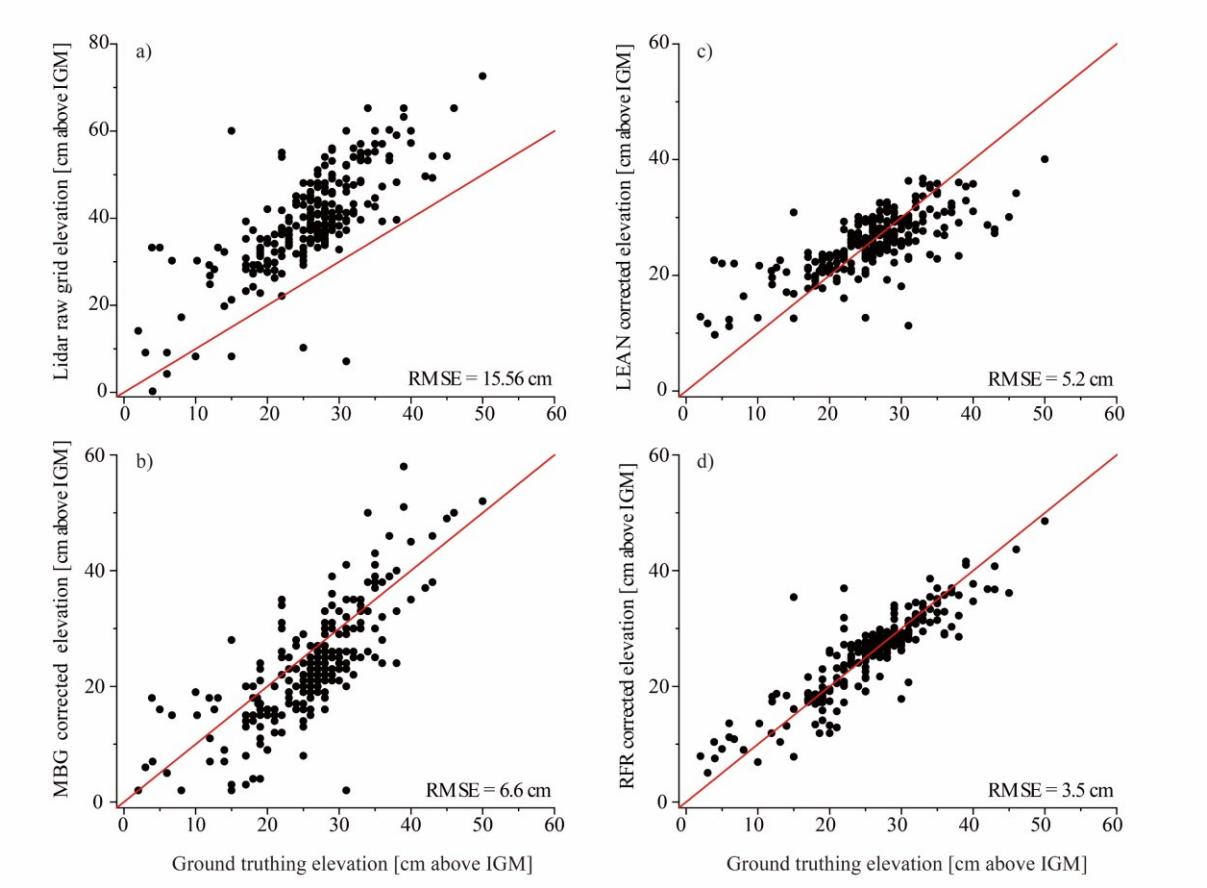

Figure 4. 12: The accuracies of lidar raw grid elevations (a), MBG corrected elevations (b), LEAN method corrected elevations (c) and RFR method corrected elevations (d). Red lines indicate y=x.

An important source of the inaccuracy of the RFR method may be related to the time gap between lidar and QB data acquisition. The lidar data were acquired in February when the vegetation can be characterized by the lowest density (Wang et al., 2009), whereas the QB data were acquired in July when the vegetation almost had the peak biomass. The vegetation changes that appeared in this period thus increase the noise in vegetation information thus affecting the accuracy of the RFR method. A better understanding of changes in the vegetation reflectance at each band or phenological parameters in different seasons or months in one year (Sun et al., 2021) would allow one to map the vegetation species at the season of lidar data acquisition, which

can be one possible step to minimize this noise.

4.5.2 Vertical distributions of halophytic vegetation and biomass production

We analyzed the vertical distribution of halophytic vegetation and the variations in AGB with higher elevation, based on a corrected DEM. However, the DEM is constructed by using FA and NDVI in 2003, thus generating an intrinsic link between elevations extracted from the DEM and the FA of each species. This suggests that the analyzed vertical variations in the dominance of each species (Fig. 4.8c and d), in the mean FA (Fig. 4.9b) and in QB-derived vegetation-state metrics in 2003 (Fig. 4.11a, b and c) are not completely objective.

However, thanks to that marsh accretion (with a rate of about 3 mm/year, Day et al., 1998) can be negligible in two years, the IKONOS data acquired in 2001 and paired field observations allow us to estimate the FA, further determining the most abundant species, and to assess the vegetation-related metrics, which are independent of the corrected DEM, thus providing the opportunity to detect the vegetation and/or AGB vertical distribution at the whole marsh scale. Indeed, the vertical distribution patterns of vegetation or related metrics (NDVI, SFA and emAGB) observed in 2001 suggest that FA of vegetation species or bare soil and AGB are strongly related to the marsh elevation. These are similar to those observed in 2003 (Figs 4.8-4.11), indicating that our analyses of the vegetation-elevation relationship based on 2003 maps are also reliable. In addition, lidar-derived LAI is also independent of the multi-spectral data and FA maps, on average displaying a similar vertical distribution pattern with other metrics (Fig. 4.11), supporting that the link between AGB and elevation observed in this study can reflect the real situations on the marsh.

The observed vegetation species sequence (Fig. 4.8) and the dependency of AGB on elevations are in line with the *in-site* observations over the same marsh (Silvestri et al., 2005, Roner et al., 2016). This is the first time to extend the vegetation-elevation relationship observed at the local scale to a whole marsh scale, indicating relevant implications to analyze marsh evolution and vulnerability by considering the marshes characterized as highly mixed vegetation species.

4.6. Conclusions

In this study, we first developed a method based on the Random Forest Regression (RFR) algorithm and applied it to lidar-point cloud data acquired over the marsh in 2003. In particular, we make full use of the information contained by the fractional abundance (FA) of each species and NDV mapped by using the multi-spectral data acquired in the same year. This method can construct the lidar-derived DEM with high accuracy (R^2=0.79 and RMSE = 3.5 cm), further suggesting that the RFR method can be an important tool to monitor marsh ecogeomorphic patterns.

Then we coupled the DEM with FA maps and the most abundant species maps (in both 2001 and 2003) to describe the vegetation-elevation relationship at the whole marsh scale. Our results suggest that each species lives within its preferable elevation ranges (i.e., the ecological niche), thus leading to the observation of the

species sequence with higher elevation.

After that, the variations in the above-ground biomass with increasing elevation were explored by using some eco-morphodynamic metrics, such as NDVI, SFA and eAGB, derived from multi-spectral data in both 2001 and 2003. We also explore changes in lidar-derived LAI (in 2003), another reliable indicator of above-ground biomass (AGB), with elevation. All these analyses conclude that higher marsh elevations can facilitate above-ground biomass production, thus providing important information to inform and test eco-geomorphic models. We also suggest these results are of importance in further analyses on marsh eco-morphic patterns within contexts populated by multiple species.

Author Contributions: Conception or design of the work, Z.Y.; Data collection, A.D., M.M., S.S., and E.B.; Data analysis and interpretation Z.Y., and X.L.; Drafting the article, Z.Y.; Critical revision of the article, Z.Y., A.D., M.M., and S.S..

Chapter 5: Long-term monitoring of halophytic vegetation and marsh ecomorphic patterns by using high spatial resolution remote sensing data

This chapter is a manuscript to be submitted to Remote Sensing of Environment. This chapter is focused on the detection of eco-morphodynamic changes through the analysis of changes in the spatial distribution of halophytic vegetation, on the basis of the application of the Random Forest Soft classification method proposed in Chapter 3 to a temporal series of remote sensing images with high spatial resolutions (O (1 m)). The spatial dynamics of halophytic vegetation is then analyzed mainly through the most abundant species (the species with the highest fractional abundance) replacement and changes in the patch-size distribution. In addition, the distribution of and changes in above-ground biomass spatial distribution are then analyzed by using a temporal series of fractional abundance maps of each species and field observed above-ground biomass. We suggest that remote sensing data with high spatial resolutions (O (1 m)) can be a useful tool to analyze eco-morphodynamics over the marsh.

PAPER

Long-term monitoring of halophytic vegetation and marsh ecomorphic patterns by using high spatial resolution remote sensing data

Zhicheng Yang[1], Enrica Belluco[2], Davide Tognin[2], Sonia Silvestri[3], Marco Marani[2], and Andrea D'Alpaos[1*]

[1] *Department of Geosciences, University of Padua, Padua, Italy*

[2] *Department ICEA, University of Padua, Padua, Italy*

[3] *Department of Biological, Geological, and Environmental Sciences, University of Bologna, Bologna, Italy*

Abstract

Salt marshes are import ecosystems, providing critical ecosystem services, but disappearing fast worldwide. Halophytic vegetation plays a key role in supporting marsh survival through complex eco-morphodynamic feedbacks. Although halophytic vegetation cover is an important indicator of marsh function, high resolution (O (1 m)) long-term monitoring studies of halophytic vegetation dynamics at the whole marsh scale are still limited. Towards the goal of improving the current understanding of marsh eco-morphodynamic processes, we analyzed a series of multi-spectral remote sensing images, acquired for a typical marsh in a micro-tidal environment (the San Felice marsh in the Venice lagoon, Italy) between 2001 and 2019, to analyze the dynamics of marsh vegetation spatial distributions and above-ground biomass production. The dynamics of marsh vegetation spatial distribution was analysed by considering changes in the most abundant species (the one with the highest fractional abundance (FA) in each pixel). The dynamics of above-ground biomass (AGB) was analyzed on the basis of using the estimated FA and field observations of above-ground biomass. Our

analyses suggest that: i) the area of the San Felice marsh decreased with a rate of about 2'345 m^2/yr, due to marsh boundary retreat, channel enlargement, and expansion of inner ponds, that we considered a signature of the erosion trend characterizing the Venice lagoon; ii) *Spartina* and *Salicornia* are more likely to be replaced by bare soil, whereas *Limonium* and *Sarcocornia* tend to encroach unvegetated areas, and the transitions among different species or between vegetated and unvegetated are widely observed over the marsh, indicating that ecogeomorphic patterns are highly dynamic and site-specific; iii) changes in the slope of the patch-size distribution can represent the changes of halophytic vegetation in response to environmental forcing; iv) although the observed dieback event of *Spartina* notably led to a relative lower AGB in 2003, the AGB reached its previous level in 2006 and then maintained a consistency until 2019; v) the distance to channels cannot be a reliable indicator of vegetation distribution and spatial dynamics, whereas the AGB generally decreases with longer distances to channels. We speculate that the increase in the AGB between 2003 and 2006 is an indicator of the biomorphodyanmic feedbacks to balance such loss, highlighting the high dynamic of marsh ecogeomorphic processes. Moreover, we suggest that remote sensing data with high spatial resolutions (O (1 m)) and suitable vegetation classification methods are useful tools to support further efforts on marsh evolution and simulations.

5.1 Introduction

Salt marshes are important wetland ecosystems located between mean sea level (MSL) and mean high water level (MHWL), representing transition zones between marine and terrestrial systems (D'Alpaos and Marani, 2016; Kirwan and Murray, 2008; Marani et al., 2004; Reents et al., 2021). Salt marshes provide important ecosystems services. They are characterized by high biodiversity and primary productivity (Janousek et al., 2016; Morris and Haskin, 1990; Scarton, 2006), protect coastal lines from waves and storms (Möller et al., 2014; Möller and Spencer, 2002; Rupprecht et al., 2017), and act as highly efficient organic carbon sinks (Kirwan and Mudd, 2012; Mueller et al., 2016, 2019). However, marshes are disappearing fast over the world (Campbell et al., 2017; Carniello et al., 2009; Marani et al., 2007; Jankowski et al., 2017; Schuerch et al., 2018; Tommasini et al., 2019; Day et al., 2000; Gedan et al., 2009), mainly due to the increase in relative sea level (Blum and Roberts, 2009; Horton et al., 2018; Kirwan et al., 2010), wave-associated lateral erosion (Marani et al., 2011) and increasing human activities (D'Alpaos, 2010; Enwright et al., 2016; Silvestri et al., 2018).

Halophytic vegetation species, the salt-tolerant plants that populate salt marshes, significantly influence marsh erosional and depositional patterns and contribute to marsh survival through complex biomorphodynamic feedbacks (D'Alpaos et al., 2007b; Fagherazzi et al., 2012; Kirwan et al., 2016a; Kirwan and Megonigal, 2013; Marani et al., 2007). Halophytic vegetation can increase flow resistance and alter the hydrodynamic field (Bouma et al., 2007; Bouteiller and Venditti, 2015; Temmerman et al., 2007), directly trap inorganic sediment (Mudd et al., 2004, 2010; D'Alpaos, 2011; Fagherazzi et al., 2012), and directly contribute to marsh accretion through organic soil production (Janousek et al., 2016; Kirwan and Guntenspergen, 2012; Morris et al., 2002; Mudd et al., 2004).

Halophytic vegetation distribution is mainly controlled by edaphic conditions (Colmer and Flowers, 2008; Herrero and Castañeda, 2013; Osland et al., 2014; Qi et al., 2018; Snedden et al., 2015; Ursino et al., 2004; Vittori Antisari et al., 2017; Watson and Byrne, 2009; Xin et al., 2013), inter-specific activities (Bertness and Ewanchuk, 2002; Engels et al., 2011; Pennings et al., 2003; Pennings and Callaway, 1996; Steven C Pennings and Callaway, 1992) and plants ability to change salt-marsh landscapes through biogeomorphic feedbacks (D'Alpaos et al., 2012; Da Lio et al., 2013; Marani et al., 2013). Halophytic vegetation is spatially organized in sharply defined patches composed of single species or of typical species associations, forming zonation patterns (Álvarez Rogel et al., 2001; Engels et al., 2011; Janousek et al., 2016; Moffett et al., 2012, 2010; Steven C. Pennings et al., 2005; Steven C. Pennings and Callaway, 1992; Silvestri and Marani, 2004). Standing on a marsh platform one can indeed observe many small patches, progressively rarer large ones, and no characteristic patch size s (Marani et al., 2006a; Taramelli et al., 2018; Weerman et al., 2012), such that the patch-size distribution displays statistical self-similarity, i.e., it can be described by a power-law, indicating that marsh vegetation is self-organized (Kéfi et al., 2007; Taramelli et al., 2018; van Belzen et al., 2017; Zhao et al., 2019).

Previous analyses have documented that halophytic vegetation displays a characteristic vertical distribution in the tidal frame(Donnelly and Bertness, 2002; Silvestri et al., 2005), i.e. each species occupies specific elevation ranges. Some authors suggest that the distance to tidal channels controls the distribution and richness of halophytic vegetation species(Sanderson et al., 2001, 2000), whereas others suggest otherwise (e.g., Silvestri et al., 2005; Marani et al., 2006). Halphytic vegetation vertical distribution has been widely documented worldwide (Janousek et al., 2019; Marani et al., 2003b; Steven C. Pennings et al., 2005; Qi et al., 2021; Schoutens et al., 2020; Silvestri et al., 2003) and accounted for in biomorphodynamic models of marsh evolution (D'Alpaos et al., 2007b; D'Alpaos and Marani, 2016; Da Lio et al., 2013; Feagin et al., 2010; Marani et al., 2013). However, observational evidence on marsh vegetation spatial distribution and dynamics at high resolution spatial and temporal scales is still limited (Zheng et al., 2016), thus calling for further efforts on field observations and monitoring.

Changes in vegetation spatial distribution are agreed to retain the signatures of changes in the environmental forcing and inter-specific cooperation or competition (Steven C. Pennings et al., 2005; Qi et al., 2021). In specific, the patch size distribution represents the physical stress (Kéfi et al., 2007; Taramelli et al., 2021) and inter-specific feedbacks (Scanlon et al., 2007). In addition, vegetation replacement is the net result of changes in edaphic conditions and species interactions, i.e., species, occupying higher marsh portions, will be replaced by those living within lower marsh areas when the marsh sites are subjected to the submergence beyond a threshold value (Steven C. Pennings et al., 2005; Qi et al., 2021; Strain et al., 2017). In particular, the disappearance of vegetation is an alarming signal for marsh survival (Ganju et al., 2017), because this would eliminate the biomorphic feedbacks that sustain marsh survival, possibly leading to the submergence and transition to tidal flats (Coleman and Kirwan, 2019; Schulze et al., 2021). As a result, the description of halophytic vegetation replacement, especially the transition from vegetated to unvegetated configurations, is of critical importance to our current understanding and capability to predict marsh dynamics and survival,

althoug the number of related analyses is still limited.

Due to the high dynamic of halophytic vegetation and difficulties to reach lower marsh portions, conducting conventional marsh-wide *in-situ* measurements and sample collections are labor-intensive and time-consuming (Elmore et al., 2000; Zheng and Moskal, 2009). Remote sensing is a useful tool for the long-term monitoring of vegetation dynamics. Many previous remote-sensing studies aiming at detecting changes in marsh vegetation spatial distribution, either used images with low spatial resolutions (O (10 m)) (Gong et al., 2021; Klemas, 2011; Mahdianpari et al., 2020; Olliver and Edmonds, 2017; Taramelli et al., 2017) or focused on multi-spectral data derived vegetation indices (Fagherazzi et al., 2019; Schwarz et al., 2014; Feng et al., 2016; Ghosh et al., 2016; Laengner et al., 2019; Moffett et al., 2015; Lalimi et al., 2017; Zinnert et al., 2016). The main disadvantage of these analyses is that difficulties arise in accurately capturing vegetation spatial dynamics and replacement due to the high heterogeneity of vegetation species at the above recalled spatial resolution (O (10 m)) (Sadro et al., 2007; Wang et al., 2007; Yang et al., 2020). Another drawback is that the above recalled analyses cannot describe the species-specific response of halophytic species to changes in the environmental conditions. In addition, some vegetation indexes are sensitive to the appearance of water (Kearney et al., 2009), leading to the increase in the noise in their delivered information on vegetation distribution and richness. A large number of classification algorithms for vegetation spatial distribution have been developed and applied to images with fine pixel-sizes (O (1 m)) (Artigas and Pechmann, 2010; Belluco et al., 2006; Berhane et al., 2019; Chai et al., 2019; Davranche et al., 2010; Juel et al., 2015; Marani et al., 2006b, 2003b; O'Neil et al., 2018; Sadro et al., 2007; Van Beijma et al., 2014; Wang et al., 2007; Yang et al., 2020; Yeo et al., 2020). Yet, the number of studies focusing on the changes in the spatial distribution of typical species and/or associations based on high spatial resolution data is still limited (Campbell et al., 2017; Campbell and Wang, 2020, 2019; Jensen et al., 2020; Sun et al., 2020). A clear gap exists that prevents the detection of vegetation spatial changes with high spatial resolutions. To fill this gap, we applied a recently developed halophytic vegetation classification method (Yang et al., 2019) to a series of remote sensing images with high spatial resolution (O (1 m)), in order to detect changes in the spatial distribution of typical species and associations.

The above-ground biomass (AGB), which is intrinsically related to the below-ground biomass (BGB) (Adam Langley et al., 2013; Curcó et al., 2002; Daleo et al., 2008; O'Connell et al., 2021; Penk et al., 2020), is an important indicator of marsh eco-morphodynamic processes and survival (D'Alpaos et al., 2011; Kirwan & Murray, 2007; Morris et al., 2002), because it strongly controls inorganic sediment settling and capture, and organic soil production (Curcó et al., 2002; Mudd et al., 2010; Kirwan and Guntenspergen, 2012; Wu et al., 2020), , The AGB of some typical marsh vegetation species has widely been documented thorugh *in-situ* field observations and related laboratory analyses (Janousek et al., 2016; Liao et al., 2008; Morris et al., 2002; Morris and Haskin, 1990; Mudd et al., 2009; Scarton, 2006; Scarton et al., 2002), whereas the spatially-extended estimation of AGB has seldomly been documented (Jensen et al., 2020; van Belzen et al., 2017). At the same time, changes in AGB in response to variations in the environmental forcing are strongly species-specific (Huckle et al., 2000; Janousek et al., 2016, 2020) and are also influenced by interspecific

interactions (Pennings et al., 2005). As a consequence, changes in AGB at the whole marsh scale have seldomly been documented (Ghosh et al., 2016). The coupling of field observations and remote sensing analyses provides the opportunity to accurately estimate the AGB at the marsh-landscape scale, where a variety of vegetation species can be observed(Jensen et al., 2020; Kulawardhana et al., 2014; Roelfsema et al., 2014; Silvestri et al., 2005). Thus, limited kwowledge on the distribution of and changes in AGB at the whole marsh scale hinders analyzing the eco-morphodynamic processes by considering changes in AGB over a whole marsh. In order to bridge this gap, this study also estimated and analyzed the variations in AGB over the marsh by using the same remote sensing dataset that was used in the analyses of vegetation distribution.

Towards the goal of improving the current understanding of key eco-morphodynamic processes at the marsh-lanscaope scale, a temporal series of multi-spectral images with a high spatial resolution (O (1 m)) acquired between 2001 and 2019 was analyzed to describe changes in the spatial distribution of halophytic vegetation species. Together with the local field observed AGB dataset (Scartion, 2006), the distribution and dynamics of related above-ground biomass were also explored. The main aims of this study are to: (1) explore the possibility to analyze changes in the spatial distribution of marsh vegetation and the above-ground biomass by using high-resolution (O (1 m)) remotely sensed images; (2) detect variations in vegetation distribution through the analysis of vegetation replacement and changes in patch-size distribution; (3) explore the changes in above-ground biomass at the marsh spatial scale.

5.2 Methods

5.2.1 Research area

Our research was carried out in the San Felice salt marsh, which is located in the northern area of the Venice lagoon (Italy, Figure 5.1a). The Venice lagoon, situated in the northeastern part of Italy, is the largest lagoon in the Mediterranean Sea with a waterbody area of about 550 km^2. It is characterized by a semi-diurnal tide with an average tidal range of about 1.0 m and a maximum spring tidal range of approximately 1.5 m. The lagoon is connected to the Adriatic Sea through three inlets: Lido, Malamocco and Chioggia. Salt marshes in the Venice lagoon have severely been eroded in the last decades (Carniello et al., 2009; Laengner et al., 2019; Tommasini et al., 2019), mainly because of drowning, wave-induced lateral erosion and human activities such as river diversion (D'Alpaos, 2010; Day et al., 1998; Marani et al., 2011; Silvestri et al., 2018; Tommasini et al., 2019).

The San Felice marsh (Figure 5.1b) is slightly affected by human activities and is thus agreed to be one of the most naturally preserved areas within the lagoon (Marani et al., 2006b; Roner et al., 2016; Yang et al., 2020). Unfortunately, this marsh is currently threatened by the increase in the relative mean sea level observed in the first two decades of the current century, because local accretion rates (ranging between 1.7 and 4.3 mm/yr, Yang et al., submitted) have been shown to be unable to balance the rate of relative sea level rise (4.4 mm/yr, Valle Levinson et al., 2021; Yang et al., submitted). As a result, it is really urgent to

quantitatively analyze local marsh vegetation dynamics and related biomorphodynamic processes. This issue is timely and relevant for many other marsh areas worldwide.

Four main halophytic vegetation species are observed on the San Felice marsh. These species are typical of the Venice lagoon and of the Mediterranean climate, including annual species (species finish their entire life cycle in a single growing season), i.e., *Salicornia veneta* (hereafter "*Salicornia*"), and perennial species (species can persist for many years), i.e., *Spartina maritima* (hereafter "*Spartina*"), *Limonium narbonense* (hereafter "*Limominum*") and *Sarcocornia fruticosa* (hereafter "*Sarcocornia*").

Each vegetation species occupies specific elevation ranges (e.g., ecological niche), leading to the observation of a typical species sequence in the vertical frame. *Salicornia* encroaches lowest marsh boundaries, *Spartina* encroaches relatively lower marsh elevations, *Limonium* is more likely to be observed on areas with higher elevations, and *Sarcocornia* prefers to occupy even higher marsh areas (Belluco et al., 2006; D'Alpaos and Marani, 2016; Da Lio et al., 2013; Marani et al., 2013, 2006a; Silvestri et al., 2005, 2003; Silvestri and Marani, 2004; Yang et al., 2020). *Limonium* and *Sarcocornia* are always highly mixed with each other (Wang et al., 2007; Yang et al., 2020), constituting a typical association encroaching the highest marsh portions.

2.2 Remote Sensing Observations

Because the main aim of this study is to analyze halophytic vegetation dynamics at the whole marsh scale with a high spatial resolution, a dataset composed of 5 multi-spectral data with fine pixel sizes (O (1 m)), acquired between 2001 and 2019, was analysed. Our remote sensing dataset includes data from the following sensors:

(1) IKONOS. The IKONOS data are composed of 4 multi-spectral bands, ranging from visible and near-infrared bands with a spatial resolution of 4 m, and a Panchromatic band (409-1048 nm) with a finer resolution of 1 m (Belluco et al., 2006).

(2) QuickBird (QB). The QB data are composed of 4 multi-spectral bands (450–520; 520–600; 630–690; 760–900 nm), having a ground resolution of about 2.88 m, and a Panchromatic band (405-1053 nm) with a spatial resolution of about 0.72 m (Belluco et al., 2006).

(3) World-View 2 (WV2). The WV2 data contain a high-resolution (0.5 m) Panchromatic band (447-808 nm) and eight lower spatial resolution (2 m) spectral bands, spanning 4 primary multispectral bands (including traditional blue, green, red and near-infrared 1 bands) and 4 application-oriented bands (coastal, yellow, red edge, and near-infrared 2 bands) (Yang et al., 2020).

General information of these images is also summarized in Table 5.1. It should be recalled that the tidal level is an important factor influencing the accuracy of vegetation classification (Kearney, 2015; Yang et al., 2020). Moreover, the season of data acquisition can also influence the vegetation distribution map because vegetation traits change in different seasons (Morris, 1990), especially as far as annual species are concerned,

because they almost finish their life cycle in winter. Thus, information on both image acquisition date and tidal level (measured at the Punta Salute station, Figure 5.1a) is also included in Table 5.1.

5.2.3 Field surveys

To provide correct ground truthing information for the vegetation species classification, the paired ancillary field surveys were carried out within 3 months before/after each data acquisition. During each field campaign, regions of interest (ROIs, i.e., ground-truthing areas used for training and validating classification model) were randomly selected over the marsh to include all local typical single species and species associations. In each ROI, the fractional abundance (FA, i.e., relative vertical projection area occupied by a given species) of each species and bare soil were estimated using the standard Braun-Blanquet visual method (i.e., records the presence of each species by 10 intervals between 0% and 100%) (Belluco et al., 2006). The boundary of each ROI was accurately delimited through differential GPS (Leica CS15 in RTK mode, minimum accuracy of ±1 cm). Finally, all ROIs were overlaid on the corresponding georeferenced multi-spectral images (as explained in Section 5.2.4) and only pixels entirely falling within an ROI were selected to build a dataset used to construct classification models.

5.2.4 Image preprocessing

Despite classification accuracy and final species maps being seldom affected by the atmospheric correction, such corrections are still carried out here to provide more reliable spectral information to possible comparisons with past or future acquisitions and analyses. In specific, IKONOS and QB images were atmospherically corrected by the usage of MODTRAN (Richter and Schläpfer, 2002) and the remaining WV2 acquisitions were atmospherically corrected using the Fast Line-of-sight Atmospheric Analysis of Spectral Hypercubes (FLAASH) algorithm (Matthew et al., 2002) in Envi 5.4 based on the "Mid-Latitude Winter" Atmospheric Model and the "Maritime" Aerosol Model and aerosol optical thickness data at the nearest AERONET station on the acquisition date (https://aeronet.gsfc.nasa.gov/). Then, all multi-spectral data were pan-sharpened using the corresponding panchromatic bands through the Gram–Schmidt Pan Sharpening algorithm (Maurer, 2013) in Envi 5.4. After that, all images were spatially corrected by using 5 stable points. To avoid problems caused by differences in spatial resolution, the georeferenced QB and WV2 data were resampled to those with a spatial resolution of 1 m to be consistent with IKONOS data by using the nearest neighbor method. Spatial correction and resample were performed in ArcGIS 10.8.

5.2.5 Detection of changes in the marsh area

The boundaries of the marsh, of the channel network, and of the inner pond (Figure 5.1) in each image were manually digitalized to estimate the area within marsh boundary, marsh area, channel area, and inner pond area (Fig. 5.1b). The manual digitalization and area determination were performed in ArcGIS 10.8. Finally, rates of change in these areas over the considered period were estimated through the linear regression method.

5.2.6 Image classification and accuracy estimation

It is generally agreed (Berhane et al., 2019; Costa et al., 2017) that the most abundant species maps generated by considering the fractional abundance (FA), which are estimated by algorithms trained and tested by heterogeneous and homogenous patches, are more reliable than the traditional hard classification maps, which are trained by only dominant (FA > 60%) patches. Moreover, the estimation of the FA of each species or bare soil also allowed us to estimate the above-ground biomass by using an empirical dataset, that is considered to be more reliable than the assumption that each pixel is entirely occupied by a single species or bare soil. Thus, in the present study, we estimated the FA of each species and bare soil by using the Random Forest soft classification method, which was shown to be reliable for halophytic vegetation classification in marsh landscapes (Yang et al., 2020).

The Random Forest (RF) is a machine learning algorithm based on the ensemble of Classification and Regression Trees (CARTs) (Breiman, 2001). In this method, pruning CARTs are trained on the basis of field observed classes (species) and sample weights (observed FA in each ROI). After this phase, when an unknown pixel value is input into the model, each CART assigns it to a specific class independently, which can be considered as the 'vote' for a class. Then, the RF records the probability value that the pixel belongs to one specific species, based on the frequency of the votes to each class (Breiman, 2001), and finally interprets this probability value as the fractional abundance of this species or bare soil. Following Yang et al. (2020), the RF algorithm is applied using the Scikit-learn package (Pedregosa et al., 2011). The number of CARTs (*ntree*) was selected as 490 and the remaining parameters were pre-decided as the default values in the Scikit-learn package. Detailed information and the advantages of the RF can be found in the literature (Breiman, 2001, 1996; Immitzer et al., 2012; Yang et al., 2020).

In this work, to accurately provide vegetation distribution information, the RF was constructed and validated independently for each image on the basis of the paired field surveys. Specifically, for the data in each year, pixels in the original ROIs of each field survey were randomly divided into two independent sub-datasets, i.e., 75% of the pixels were used for training the model and the remaining 25% pixels were used for the validation. At the end of the classification, the observed FA in the validation sub-dataset was used to test the accuracy and the error of estimated FA by RF for each species, represented by root-mean-square error (RMSE) and the coefficient of determination (R^2):

$$\mathrm{RMSE} = \sqrt{\frac{\sum_{i=1}^{n}(y_i - \hat{y}_i)^2}{n}} \tag{5.1}$$

$$R^2 = \frac{\sum_{i=1}^{n}(\hat{y}_i - \bar{y})^2}{\sum_{i=1}^{n}(y_i - \bar{y})^2} \tag{5.2}$$

where y_i, $\hat{y}_i$, and $\overline{y}$ represents the ground referential value, the predicted value, and the average of the observed values respectively, and n is the size of the validation dataset.

After estimating of FA for each species and bare soil, the most abundant species in each pixel was chosen as the one with the highest FA, indicating that pixel as dominated by, and considered as the habitat of, that

particular species (Van Beijma et al., 2014). As mentioned above, *Limonium* and *Sarcocornia* are always highly mixed with each other and represent the associations occupying higher marsh portions. Therefore we consider pixels where either one of or the sum value of their FAs are higher than other species as habitats of such a typical association, classified as *Limonium* and *Sarcocornia*.

5.2.7 Post-classification change detection

The manual digitalization of marsh area and channel network allowed us to accurately determine the distance (l) of any marsh site to the nearest channel. The distance of each marsh pixel to the channels was calculated by the Euclidean distance in MATLAB R2020a. In order to describe the relative position of each species with reference to the channel network, we used the frequency of l for each most abundant species to represent vegetation spatial distribution, and further used the temporal changes in l to describe variations in the position of each species.

We defined the patch boundaries of the most abundant species by using the von Neumann neighborhood (i.e., four neighborhood) method (Toffoli and Margolus, 1987). Then, the probability (P) distribution of the patch-size of each species was calculated and fitted by a power-law distribution through the least square method. The power law can be expressed as:

$$P(X \geq x) \propto x^{-a} \tag{5.3}$$

where x is the patch size and α is the scaling exponent of the distribution (Kéfi et al., 2011, 2007; Pascual et al., 2002; Taramelli et al., 2013; Weerman et al., 2012).

5.2.8 Empirical estimation of above-ground biomass production

Based on the RF-yielded FA map of each species and the field-observed above-ground biomass dataset (Scarton, 2006), we empirically estimated the above-ground biomass (eAGB) for each year. Scarton (2006) measured the dry weight of each species on a large number of marshes across the Venice lagoon. To minimize the error in the AGB estimation, we selected the average value that Scarton (2006) measured from different marshes to empirically represent the characteristic AGB for each species ($eAGB_i$), as if it entirely covererd an area of 1 m^2, as shown in Table 2. Thus, the eAGB in each pixel was calculated as:

$$eAGB = FA_i \cdot eAGB_i \tag{5.4}$$

where FA_i is the FA of ith species. Finally, the changing rate of eAGB (RAGB) was calculated by applying the linear fitting method to the eAGB values in the temporal series of the corresponding pixels and the frequency distribution of the RAGB was analyzed by using the Kernel Density Estimator (Bowman and Azzalini, 1997) in MATLAB 2020a.

Table 5. 1: Information on the remote sensing data

Acquisition year	**2001**	**2003**	**2006**	**2013**	**2019**
Sensor	IKONOS	QuickBird	IKONOS	World-View 2	World-View 2
Spatial resolution	P: 1 m M: 4 m	P: 0.72 m M: 2.88 m	P: 1 m M: 4 m	P: 0.5 m M: 2 m	P: 0.5 m M: 2 m
Acquisition date	26/06	25/07	31/08	03/12	07/11
Flight time (GMT)	10:00	9:45	10:37	10:24	10:23
Tidal level	−45 cm	+7 cm	+8 cm	+43 cm	+45 cm

P=panchromatic; M=multispectral

Table 5. 2: The empirical dry weight of each species (g/m^2) based on data by Scarton (2006) used to determine the estimated above-ground biomass (eAGB).

***i* (Species)**	**Dry weight** (g/m^2)
Salicornia	583
Limonium	222
Sarcocornia	887
Spartina	534

Table 5. 3: Accuracy information of the RF soft classifier. Limo = *Limonium*, Sarc = *Sarcocornia*, Spar = *Spartina*, Sali = *Salicornia*.

	2001		**2003**		**2006**		**2013**		**2019**	
	R^2	**RMSE**	R^2	**RMSE**	R^2	**RMSE**	R^2	**RMSE**	R^2	**RMSE**
Limo	0.63	19.00	0.69	12.64	0.72	16.64	0.86	12.47	0.80	16.18
Sarc	0.82	16.27	0.64	10.44	0.67	18.81	0.58	14.03	0.75	14.60
Spar	0.90	11.32	0.90	4.83	--	--	0.68	11.37	0.70	12.02
Sali	--	--	--	--	0.87	5.49	0.58	9.95	0.71	13.00
Soil	0.87	9.54	0.74	9.53	0.89	9.85	0.95	9.47	0.88	8.81

Table 5. 4: Statistics of *l* for each species in each observation year. *Limo* & *Sarc* = *Limonium* and *Sarcocornia*, *Spar* = *Spartina*, *Sali* = *Salicornia*

***l* (m)**	**2001**			**2003**			**2006**			**2013**			**2019**		
	25th	**50th**	**75th**	**25th**	**50th**	**75th**	**25th**	**50th**	**75th**	**25th**	**50th**	**75th**	**25th**	**50th**	**75th**
Limo* & *Sarc	5.0	8.9	15.6	4.0	7.3	13.9	5.4	9.2	15.8	3.2	7.0	13.3	3.6	7.1	14.0
Spar	5.0	11.2	19.2	4.0	8.5	15.0	--	--	--	5.7	9.8	15.3	6.4	10.6	15.5
Sali	--	--	--	--	--	--	2.0	6.0	13.6	5.8	10.0	16.1	3.6	7.0	13.0

25th = 25th percentile; 50th = median; 75th = 75th percentile

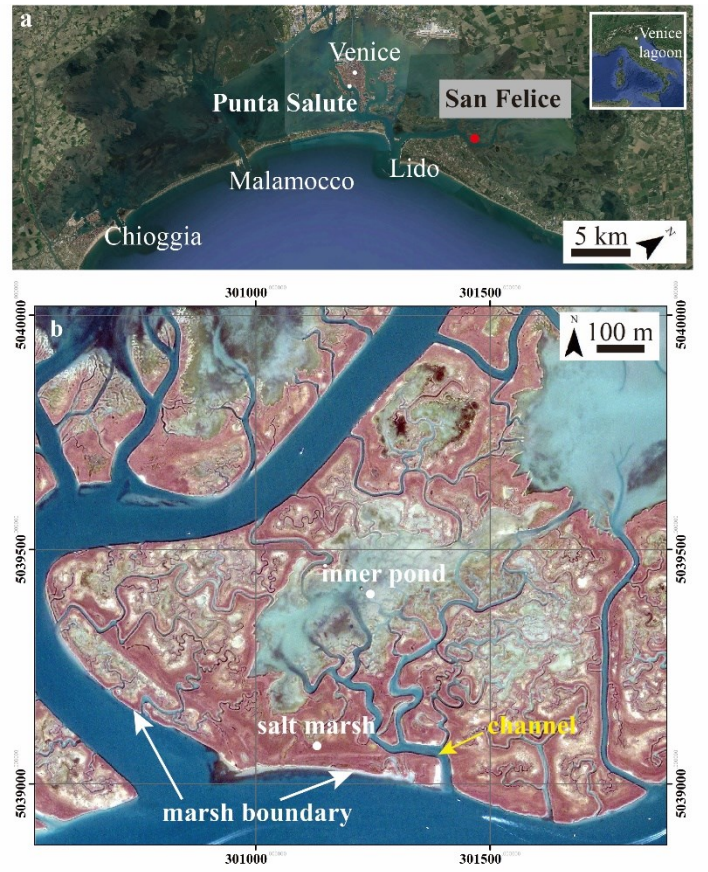

Figure 5. 1: Research area. (a) shows the position of the San Felice marsh; (b) shows the map of the San Felice marsh (RGB of IKONOS in 2001).

5.3 Results

5.3.1 Marsh area changes

We first analyzed changes in the marsh area between 2001 and 2019. Figure 5.2 shows a declining trend in marsh area with a rate of about 2345 m^2/yr (from about 52×10^4 in 2001 to about 48×10^4 m^2 in 2019). In fact, the marsh boundary retreat (inner boundary area decreased with a rate of about 1308 m^2/yr), the expansion in channel planform area (787 m^2/yr), and the slight enlargement in the inner pond area (250 m^2/yr) resulted in the shrinking of the marsh area (Figure 5.2a).

The lateral-retreat of marsh boundary and the expansion of the channel planform area possibly indicate an increase in channel crosse-ctional area, which is strongly related to the flowing tidal prism (D'Alpaos et al., 2010; Marani et al., 2006a). We suggest that this is a symptom of the erosional trend of the marshes in the Venice lagoon, because the decrease in marsh elevations and the deepening of the tidal flats (Tommasini et al., 2019), locally and at the whole system scale, lead to larger tidal prisms, which further lead to channel headward extension and increase in channel cross-sectional size (D'Alpaos et al., 2007b, 2005).

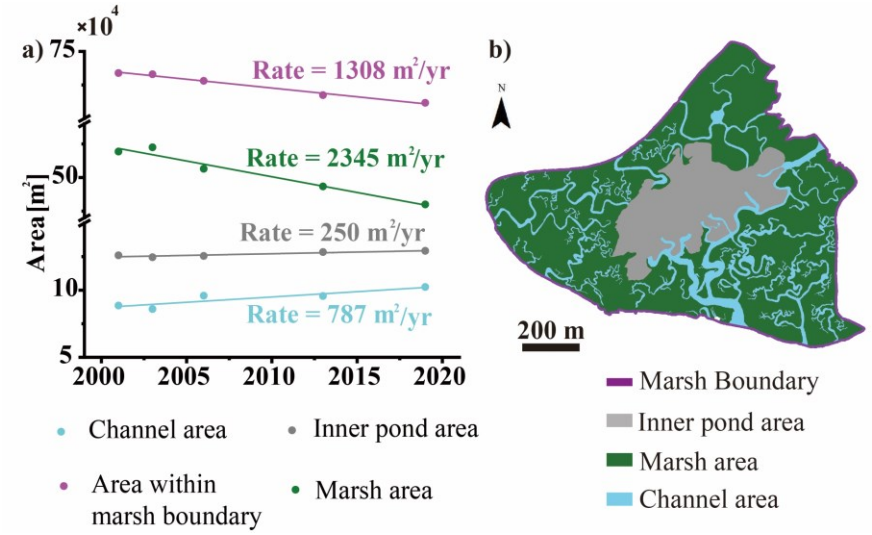

2405

Figure 5. 2: Changes in marsh area between 2001 and 2019. (a) shows the rate of change of channel area, inner pond area, marsh area, and area within marsh boundaries; (b) shows an example of the marsh area digitalization by using the WV2 image in 2019.

5.3.2 Vegetation classification

2410 Table 5.3 shows the accuracy information of the fractional abundance (FA) in each year estimated by the RF soft classifier, and highlights the high accuracy of the classification for each acquisition year ($0.58 < R^2 < 0.96$, $5.49\% < \text{RMSE} < 19.0\%$). This suggests that the most abundant species or bare soil maps (Fig. 5.3a-e) provide reliable information on halophytic vegetation distribution patterns in the considered period.

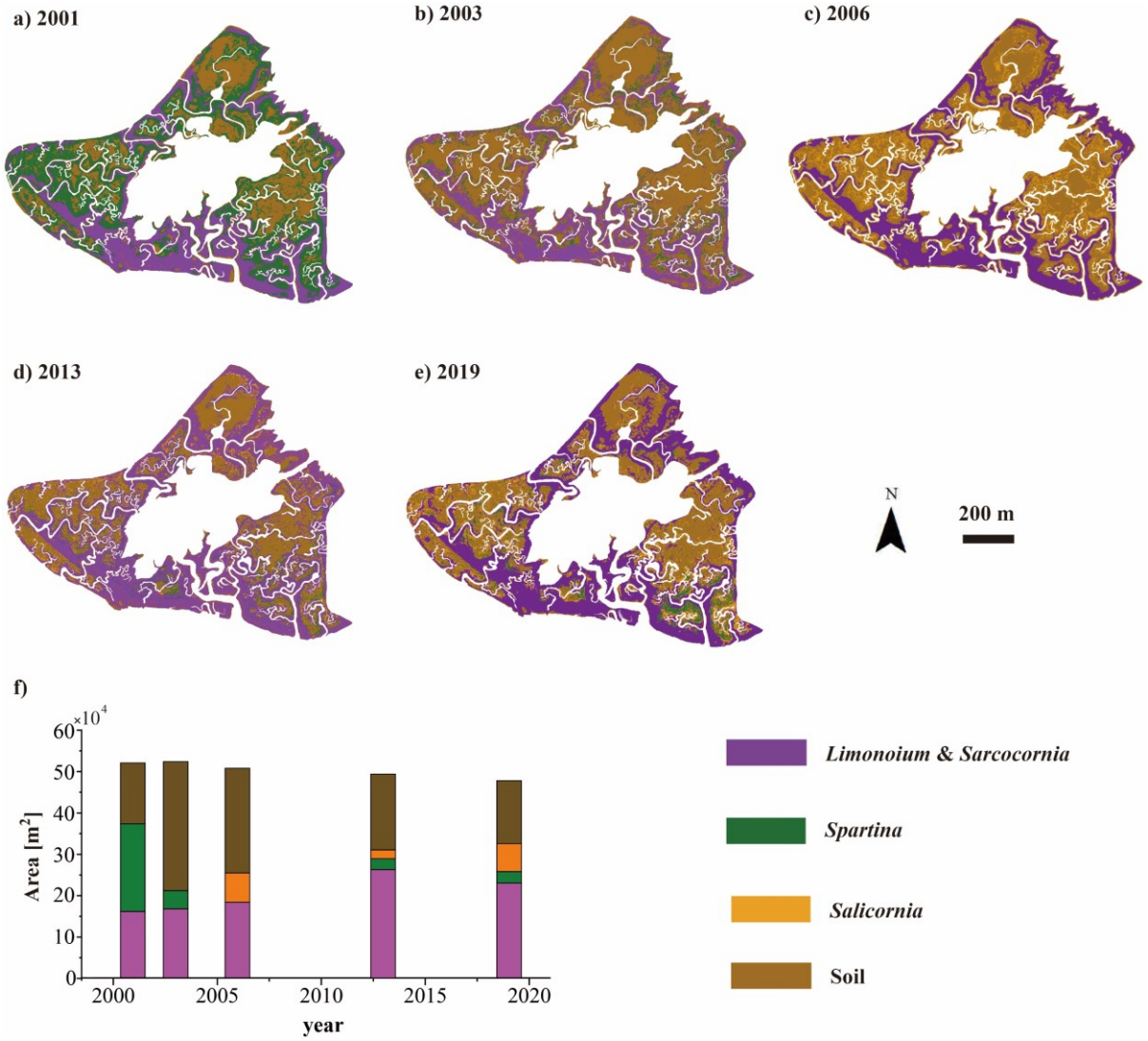

Figure 5. 3: Changes in the distribution of the most abundant species in the San Felice marsh between 2001 and 2019. (a) – (e) show the maps of the most abundant species between 2001 and 2019; (f) shows changes in the area of each most abundant species or bare soil.

5.3.3 Changes in the area of each most abundant species or bare soil

Visual observation on the most abundant species maps suggests that the area of *Spartina* habitat almost disappeared in 2006 (Fig. 5.3c and f), following a sharp decline between 2001 and 2003 (Fig. 5.3a, b and f). This indicates the possible occurrence of a *Spartina* dieback event in this period. *Salicornia* seems to be an invasive species for the San Felice marsh, because it was not observed in the San Felice marsh before 2006 (Figs. 5.3a, b and f). We also note that the areas mainly encroached by *Salicornia* in 2013 are smaller than those observed in 2006 and 2019 (Fig. 5.3c, d and f), likely due to the fact that the WV2 image used to determine vegetation distribution in 2013 was acquired in winter (Table 5.1), when *Salicornia* almost finished its life cycle and almost disappeared from the marsh. In addition, areas encroached by *Limonium* and *Sarcocornia* generally increased over these 18 years.

Fig. 5.4 provides information on the vegetation replacement in each time interval, indicating that the inter-

species replacement and transitions between vegetated and unvegetated states are commonly observed in each interval. Between 2001 and 2003 (Fig. 5.4a), the wide disappearance of the *Spartina* resulted in the enlargement of bare-soil areas. *Limonium* and *Sarcocornia* encroached some bare soil areas between 2003 and 2006, and the encroachment of *Salicornia* also resulted in a decrease in unvegetated areas (Fig. 5.4b). Fig. 5.5c shows that, between 2006 and 2013, *Limonium* and *Sarcocornia* kept encroaching bare soil areas, while *Spartina* reappeared on this marsh mainly through the colonization of unvegetated areas, of some portions that were previously occupied by *Limonium* and *Sarcocornia,* or of its previous habitats (Fig. 5.3). After 2013 (Fig. 5.5d), some species replacements were still observed, related in particular to the transitions between bare soil and vegetation configurations. In fact, the replacement of *Limonium* and *Sarcocornia* by *Salicornia* was also observed between 2013 and 2019, mainly due to the fact that a large amount of *Salicornia* almost finished its life and disappeared when data the acquisition in 2013 (December, Table 5.1). As a consequence, the remaining *Limonium* and *Sarcocornia* became the local most abundant species, while *Salicornia* was highly abundant in those portions when acquired data in 2019 (November, Table 5.1). Figs. 5.3 and 5.4 suggest that transitions among different dominant species or bare soil are widely distributed over the marsh, and adjacent sites (pixels) were not subjected to clear replacement patterns, further indicating the site-specific and high dynamic behavior of marsh ecogeomorphic patterns.

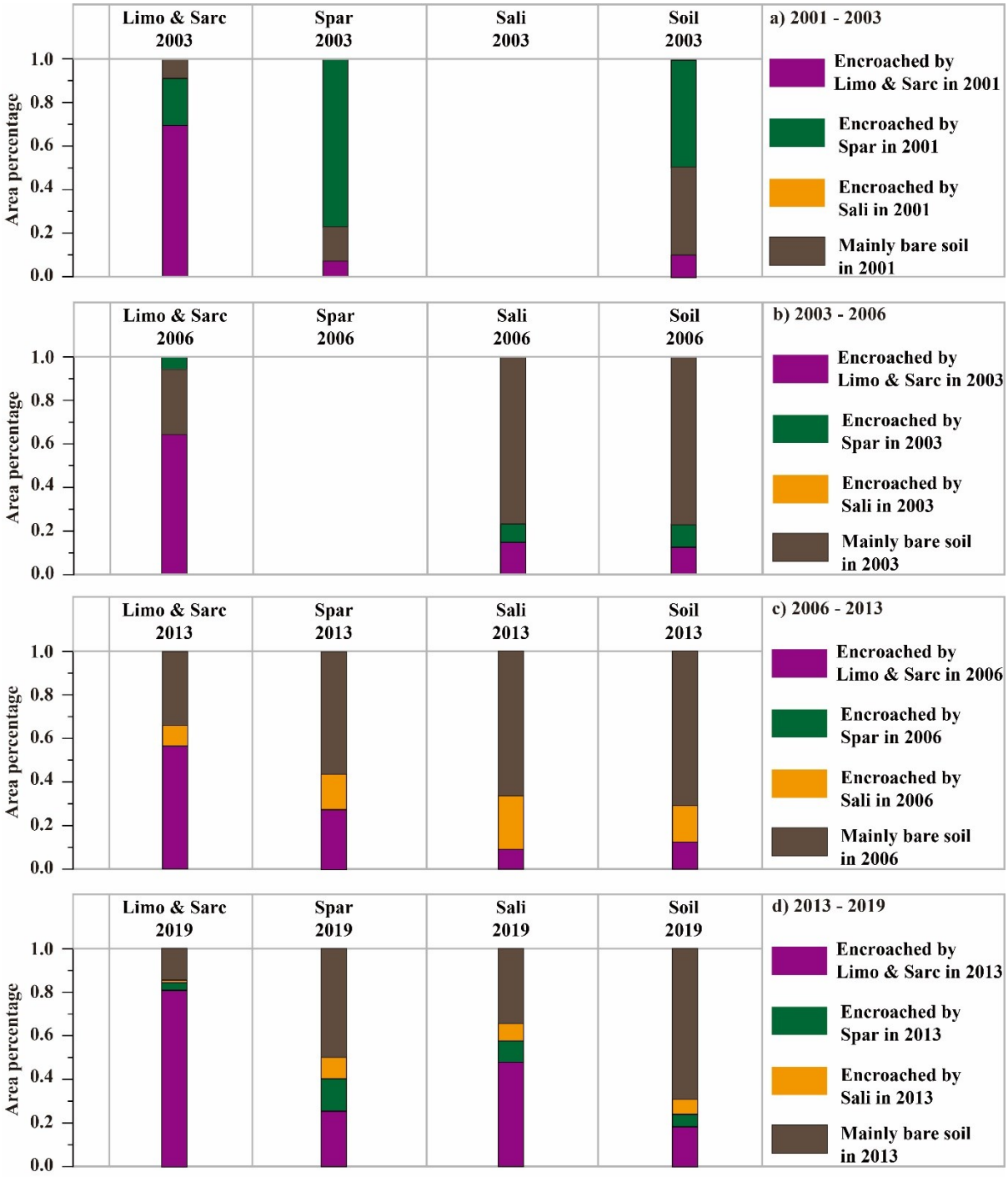

Figure 5. 4: Vegetation replacement in each observation interval. The horizontal axis shows the species observed in each year, the vertical axis shows the percentage value of the area conditioned by the appearance of the most abundant species in each observation date and occupied by each species in the last observation date. *Limo* & *Sarc* = *Limonium* and *Sarcocornia*, *Spar* = *Spartina*, *Sali* = *Salicornia.*

5.3.4 Spatial distribution of each species

We then analyzed the position of each species habitat relative to tidal channels. Table 5.4 and Fig. 5.5 provide information on the distance to the closest channel (*l*) in each year. Fig. 5.5 shows that the peaks in *l*-frequency for all species fall with a distance of about 10 m to the channels, indicating that all species prefer the encroach marsh portions close to channels, due to the fact that the marsh displays a concave-up profile with higher

portions close to the channels and that oxygen content in soil is higher along channel sides and rapidly decreases with distance from channels (Ursino et al., 2004).

Variations in the peak values of *l*- frequency for each species also suggest that the relative position of each species referred to channels networks can be horizontally shifted in different years (Fig. 5a-e). In particular, in 2001, the frequency of *Spartina* decreased from channels to inner marsh portions, indicating that *Spartina* preferred to occupy areas along channels. Indeed, it was widely distributed along minor channels (Fig. 5.3a), while *Limonium* and *Sarcocornia* tended to encroach marsh portions at a slightly longer distance (about 4.5 m) to channels, compared to *Spartina*. All species (*Limonium* & *Sarcocornia* and *Spartina*) tended to encroach marsh portions with distances of about 2.5-4.5 m from channels in 2003 (Fig. 5.5b). *Salicornia* mainly encroached borders of minor channels and creeks in 2006 (Fig. 5.3c), and the peak in its *l*-frequency was observed along channels, while the peak in the *l*-frequency of *Limonium* and *Sarcocornia* was found at 4.5 m from the channels (Fig. 5.5c). In 2013, *Limonium* and *Sarcocornia* were more likely to be observed at sites with distances of about 2.5 - 4.5 m from channels, while *Spartina* and *Salicornia* preferred to occupy areas at slightly longer distances (about 4.5 and 7.5 m) to the channel networks (Fig. 5.5d). In 2019, both the association *Limonuim* and *Sarcocornia* and the single species *Salicornia* were more likely to be observed at sites close (about 2.5 - 4.5 m) to channels while *Spartina* tended to occupy areas further from channels (Fig. 5.5e). The median and quartile values of *l* for each species (Table 5.4 and Fig. 5.5f) also suggest that the relative position of each species in the horizontal frame changed in different years. Moreover, the annual changes in median and quartile values of *l* fluctuated over the period but without any consistent trend (Table 5.4 and Fig. 5.5f), indicating that changes in vegetation cover cannot be simply represented as a function of the distance to channels.

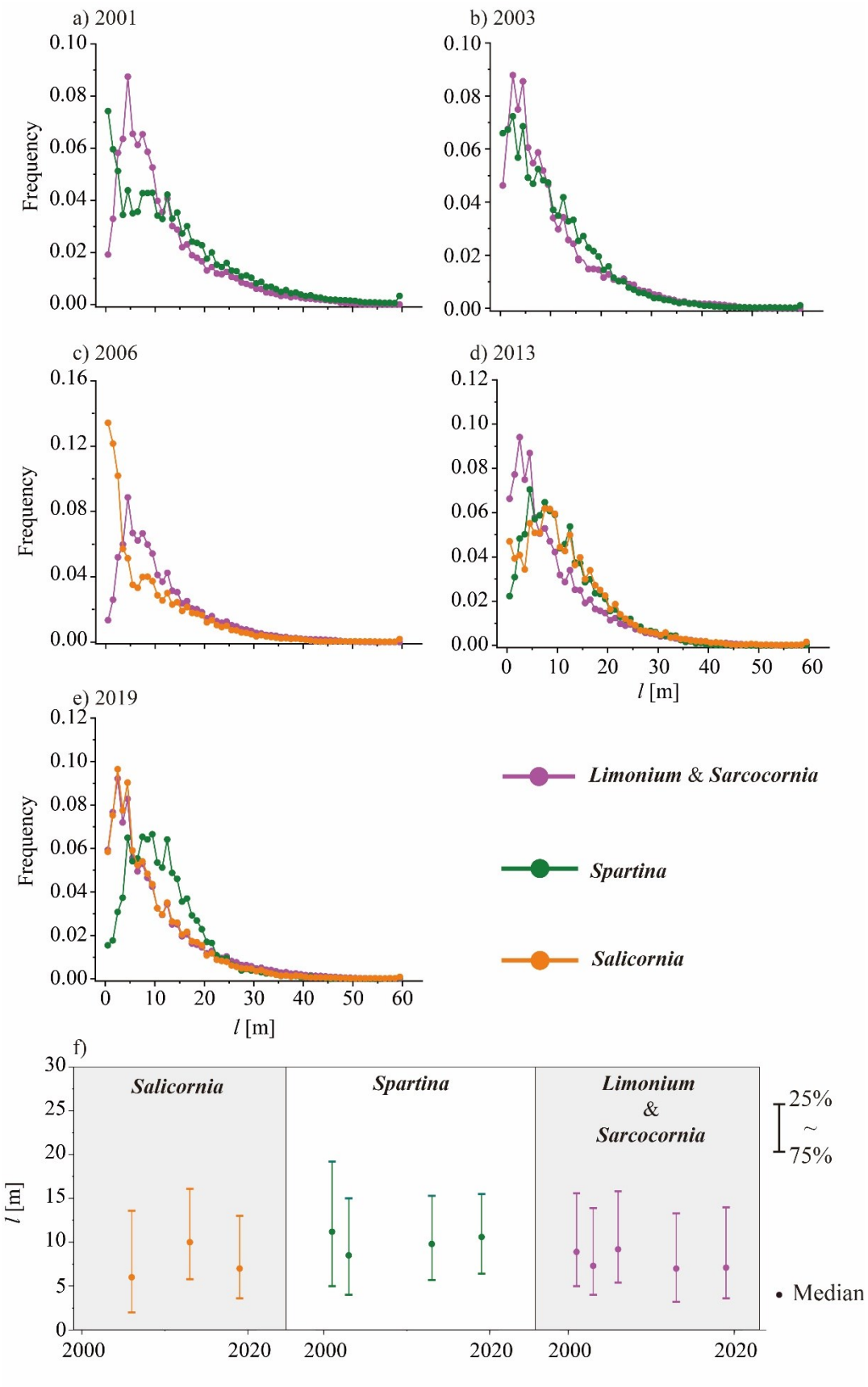

Figure 5. 5: Distance of each species to channels in each year. (a)-(e) show the frequency distribution of *l* for each species in each observation year. (f) is the whisker plot for l in each observation year.

5.3.5 Patch size distribution

The patch-size distribution of each species was then analyzed. Figure 5.6 shows that the patch-size distribution of each species is consistent with a power law (R^2 in Table 5.5) over many years, indicating that vegetation patches were present over a wide range of size scales, with many small patches, relatively fewer large ones, and without any typical patch sizes.

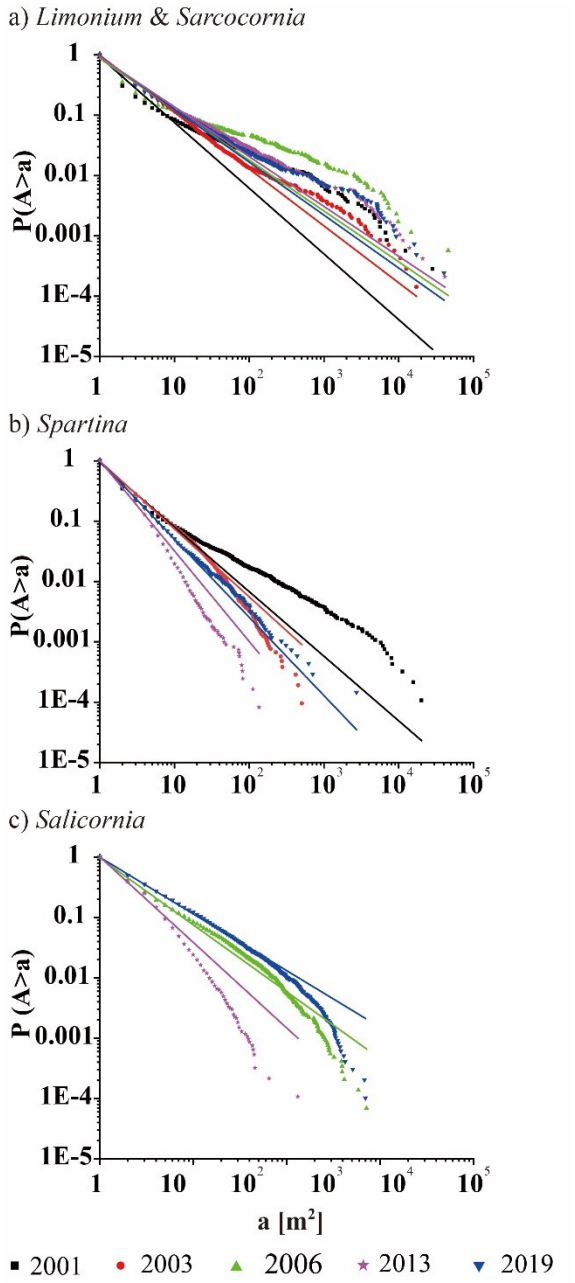

Figure 5. 6: Patch size distribution of each species

Table 5. 5: Summary of power-law (equation 5.3) features fitted to the patch-size in the San Felice marsh. *Limo & Sarc* = *Limonium* and *Sarcocornia*, *Spar* = *Spartina*, *Sali* = *Salicornia*, std = standard deviation.

Species	2001	2003	2006	2013	2019	std

	a	R^2	a	R^2	a	R^2	a	R^2	a	R^2	
Limo & Sarc	1.15	0.94	0.95	1.00	0.93	0.90	0.87	0.97	0.90	0.98	0.099
Spar	1.07	0.97	1.13	1.00	--	--	1.42	0.99	1.30	1.00	0.138
Sali	--	--	--	--	1.13	0.99	1.50	1.00	0.94	1.00	0.234

5.3.6 estimated above ground biomass

Figure 5.7a-e show the maps of the empirical above-ground biomass (eAGB) in the San Felice marsh between 2001 and 2019, which were estimated by coupling FA maps and the field-observed dataset (Table 4). Visual observation suggests that, in each year, some of the narrow marsh portions along the marsh boundaries were more likely to be characterized by higher eAGB. Fig. 5.7g confirms this trend, indicating that the eAGB generally decreases from channels to inner marsh portions, although there are a few inner sites with higher eAGB. The declining trend of eAGB with longer distances to channels can be attributed to the fact that channels are able to ameliorate soil conditions by increasing oxygen availability (Ursino et al., 2004; Xin et al., 2013) and to increase elevations on both sides (Temmerman et al., 2003a) thus decreasing waterlogging period and frequency. The appearance of a few inner marsh sites with higher eAGB can be attributed to the lower physical pressure (Pennings et al., 2005) caused by local higher elevations (Roner et al., 2016), which can be observed by coupling elevation data (Wang et al., 2009) and eAGB maps (Figure 5.7a-e).

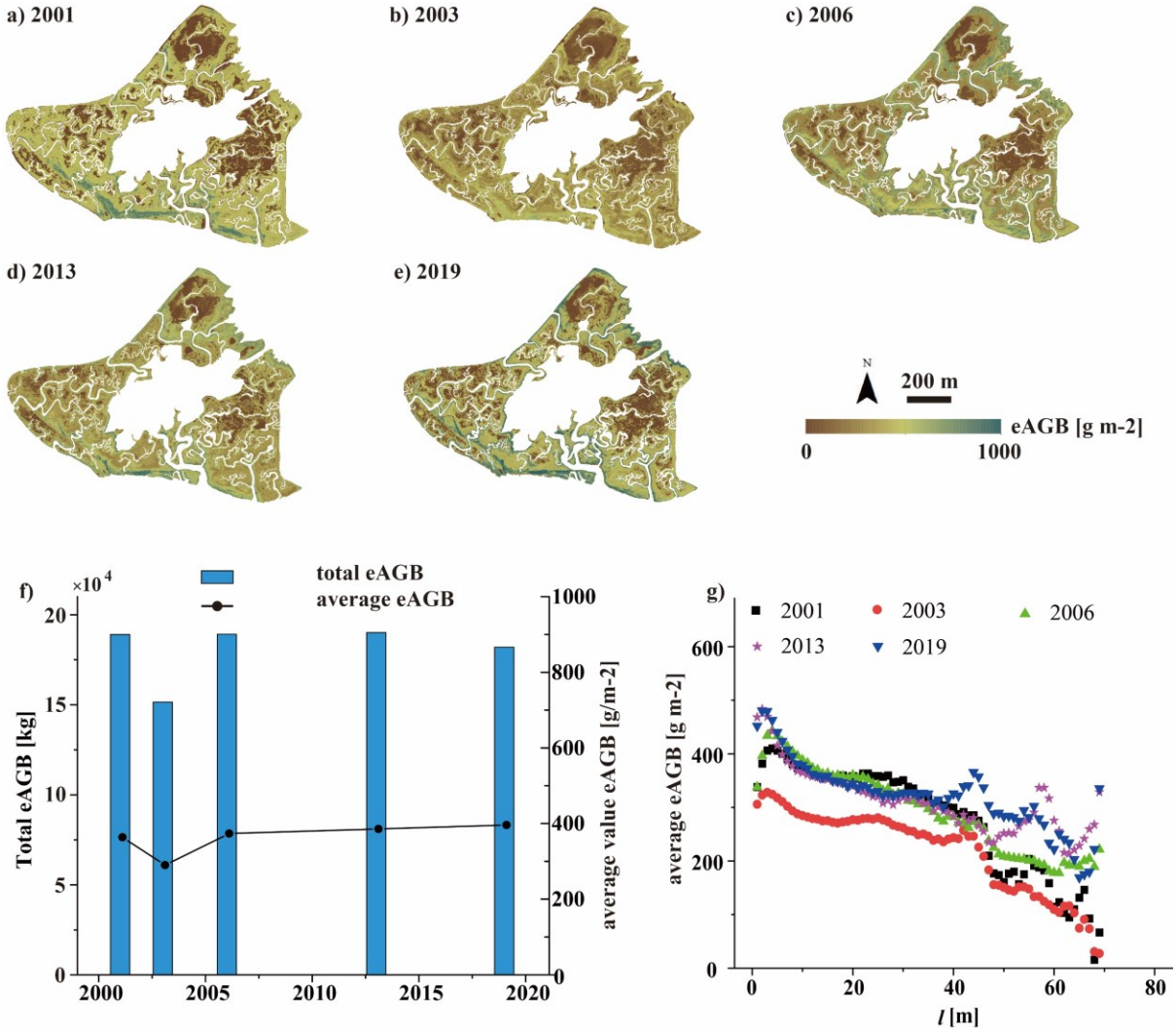

Figure 5. 7: Variations in the eAGB in the San Felice marsh; (a)-(e) show the eAGB maps of the San Felice marsh; (f) shows the changes in the total eAGB and average value of eAGB in the marsh surface with an area of 1 m^2. (g) shows the changes in the average value of eAGB with increasing distance to channels.

In general, both the total and average values of eAGB maintained almost constant over the period (Fig. 5.7f), with an exception of 2003 when we observe a dieback event of *Spartina* (Fig. 5.3). The sum value of eAGB decreased from 18.90×10^4 (2001) to 15.15×10^4 kg (2003, Fig. 5.7f). We speculate this notable decrease in AGB is associated with the dieback event, with the wide replacement of *Spartina* by bare soil (Fig. 5.3a and b). After 2003, the total and/or average values of eAGB increased until 2006 and then maintained constant. Fig. 7g shows that the average values of eAGB in most of the marsh sites referred to channels in 2003 are lower than the corresponding values in other years, confirming the general trend observed in Fig. 5.7f.

5.4 Discussion

In this study, we analyzed the spatial distribution patterns of the most abundant species with a spatial resolution of 1 m shown in Fig. 5.3. The FA estimation is based on the application of the RF soft classification method, characterized by the high accuracy (Table 3, $0.58 < R^2 < 0.96$, $5.49\% < \text{RMSE} < 19.0\%$), suggesting

that the RF soft method is reliable in the assessment of halophyte species FA and the most abundant species mapping, thus potentially to be a useful tool to facilitate the analyses of marsh eco-morphodynamic processes. In addition, based on the application of the RF soft method to a temporal series multi-spectral image, we further explored the dynamics of the most abundant species and the empirical above-ground biomass in a high spatial resolution, highlighting that the dynamics of halophytic species and the relevant above-ground biomass can be detected by using remote sensing data with a high spatial resolution (O (1 m)).

5.4.1 Vegetation die-off

The process that vegetation is replaced by bare soil is considered as the die-off in the current study. Between 2001 and 2006 (Fig. 5.8), *Spartina* is the species characterized by the highest die-off probability, mainly because of the observed dieback event, which leads to the marginal increase in the area of bare soil at the corresponding period (Figs. 5.3 and 5.8). This event has been reported in other observations over the Venice lagoon (Belluco et al., 2006; Strain et al., 2017). This dieback is possibly associated with the heatwave event starting from the spring of 2003 (Strain et al., 2017). In particular, the associated extremely high temperature and drought lead to the increase in soil temperature and the decrease in soil moisture, further resulting in the wide dead biomass of *Spartina* (Alber et al., 2008; Strain et al., 2017). After 2006, *Salicornia* became the species with the highest die-off probability (Fig. 5.8) in the San Felice marsh. In fact, *Salicornia* and *Spartina* can be characterized by species with high fragility, possibly due to i) they always encroach lowest marsh portions characterized by tough physical conditions (e.g., higher water-logging period and frequency) (Silvestri et al., 2005); ii) they are the lowest compatibility among species on the marsh (Pennings et al., 2005); iii) *Salicornia* is the annual species, which means it has to recolonize this marsh in the Spring and the seeds germination is highly vulnerable to changes in environmental forcing (Gul et al., 2013; Muñoz-Rodríguez et al., 2017; van Regteren et al., 2020); and iv) *Spartina* is very sensitive to the drought events and changes in soil chemical conditions (Alber et al., 2008).

The vegetation die-off is disastrous to the marsh, because the transition from vegetated configuration to bare soil represents the decrease in sedimentation (Coleman and Kirwan, 2019; D'Alpaos et al., 2011), thus indicating the decrease in local marsh elevation and the possibility of transit to tidal flats. Therefore, this study suggests the opportunity for coastal managers to monitor changes in *Salicornia* and *Spartina* as indicators of marsh degradation processes.

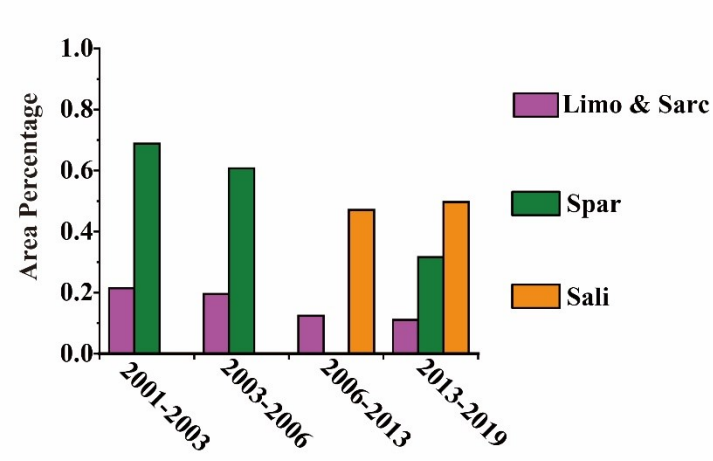

Figure 5. 8: The percentage value of the area encroached by each vegetation species which has been replaced by soil in each time interval. *Limo & Sarc* = *Limonium* and *Sarcocornia*, *Spar* = *Spartina*, *Sali* = *Salicornia.*

2550

5.4.2 Vegetation encroachment on bare soil

Besides the dieoff observed above, there is also a decrease in bare soil area between 2003 and 2019 (Fig. 5.3f), mainly due to the encroachment of vegetation. Fig. 5.9 suggests that *Limonium* and *Sarcocornia* have the highest ability to encroach on bare soil, leading to an increase in the area occupied by this association.
2555 The invasion of *Salicornia* in 2006 also notably reduced the unvegetated area. In fact, visual observation suggests that large areas, used to be colonized by *Spartina* and *Salicornia*, were subjected to the transition from an unvegetated state to a configuration dominated by *Limonium* and *Sarcocornia* in the following years (Fig. 5.3b-e). We speculate that the encroachment of *Limonium* and *Sarcocornia* on those areas is associated with the previous appearance of the *Spartina* or *Salicornia*, who ameliorated the edaphic conditions before
2560 their disappearance, being characterized by the facilitation effects (Ewanchuk and Bertness, 2003).

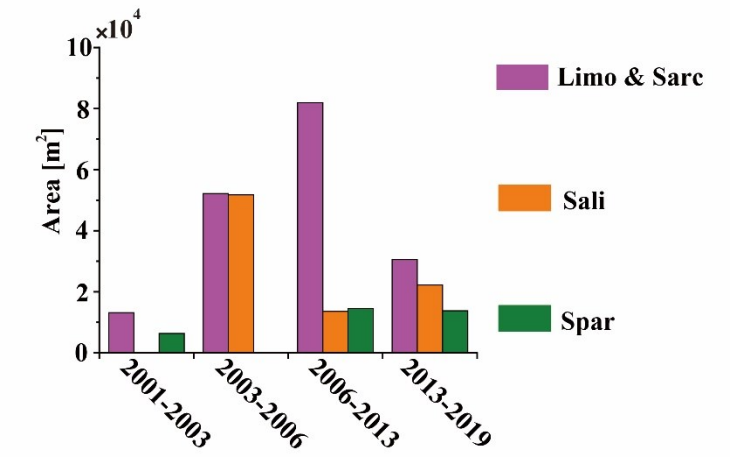

Figure 5. 9: Area of each species encroach on bare soil in each observation interval. *Limo & Sarc* = *Limonium* and *Sarcocornia*, *Spar* = *Spartina*, *Sali* = *Salicornia.*

2565 The encroachment on the bare soil of vegetation is also of high importance in coastal protection and

restoration (Brisson et al., 2014), because the reappearance of halophytic vegetation can prevent marshes submergence by increasing local sedimentation (D'Alpaos et al., 2011; Kirwan et al., 2016a). Therefore, the observed encroachment of halophytic vegetation on bare soil is speculated to be one of the symptoms that marsh vegetation tends to support marsh survival through the eco-morphodynamic feedbacks.

5.4.3 Distance to channels

If one only considers the vegetation distribution can be represented by the distance to channels (*l*), Fig. 5.5 and Table 5.4 display that all species in the marsh prefer to encroach marsh portions close to channels. Our observation suggests that there is no typical species sequence with the increasing *l* in every single year (Fig. 5.5a-e), being stable over the period and the temporal variations in the *l* of each species did not show any typical trends (Fig. 5.5f). This indicates that, in the San Felice marsh, the *l* cannot be an indicator of vegetation species distribution. This is different from the previous observations in other marshes (Sanderson et al., 2001, 2000; Zheng et al., 2016) but consistent with *in-situ* observations in the same marsh (Silvestri et al., 2005). The possible reasons for this can be explained by that the effects of channel networks on soil aeration conditions are limited in narrow areas from channels (Ursino et al., 2004).

Although Fig. 5.5 and Table 5.4 show that *l* cannot directly represent vegetation species distribution, we still realized that some boundaries of the marsh and edges of main channels (Fig. 5.3), characterized by higher marsh elevations (Roner et al., 2016) and lower physical stress (i.e., lower inundation frequency and waterlogging period), are encroached by *Limonium* and *Sarcocornia*, because they are of higher compatibility compared with *Spartina* and *Salicornia* (Pennings et al., 2005). Meanwhile, we also noticed that some *Spartina* and *Salicornia* constitute the narrow border of minor channels in inner bare soil areas (Fig. 5.3), due to the fact that minor channels improve the edaphic oxygen availability of these areas and increase local elevations to support the establishment of these two species (Ursino et al., 2004; Temmerman et al., 2003). Thus, together with previous vegetation elevation analyses in the same marsh (Silvestri et al., 2005), we suggest that the marsh elevation and inter-specific interreactions are the key controllers of vegetation distribution, which is also minorly affected by channel networks.

In terms of the distribution of eAGB, our analyses suggest that the average eAGB generally declines with longer distances to channels, indicating that channel networks control the above-ground biomass. In fact, all species prefer to encroach areas close to channels (Fig. 5.5a-e), thus increasing the local eAGB. All of these suggest that the effects of channel networks on halophytic vegetation are mainly through controlling on above-ground biomass, instead of species distribution.

5.4.4 Patch size distribution

The patch-size distribution of each species in the San Felice marsh is consistent with power-laws over a period of multiple years (Fig. 5.6), which is consistent with observations from the same marsh (Marani et al., 2004, 2006) and other marshes over the world (Taramelli et al., 2018; Koppel et al., 2005; Zhao et al.,

2019).

However, the behaviors of scaling exponent (α) of patch-size distribution over time can be characterized by highly species-specific (Fig. 5.6 and Table 5.5). More in detail, $\alpha_{Limo\&Sarc}$ decreased between 2001 and 2013, indicating that *Limonium* and *Sarcocornia* gradually colonized areas given by the dieback of *Spartina* (Fig. 5.3) to construct continuous patches. After that, $\alpha_{Limo\&Sarc}$ maintained relatively constant, representing this association approached a relatively stable state. α_{Spar} displayed an obvious increase between 2001 and 2003, indicating that *Spartina* became more fragmented, being a result of the dieback event. While the highest value of α_{Spar} appeared in 2013, implying that the initial colonization of this species is mainly in the form of small patches (Taramelli et al., 2018). Interestingly, the upper deviation of the patch size distribution of *Spartina* shifted to the downward deviation in 2003, possibly because this species is sensitive to the stress associated with the heat-wave event (Kéfi et al., 2007). In terms of the behavior of α_{Sali}, the highest value is also observed in 2013, instead of the first year to observe it (2006). This could be due to the fact that the data is acquired in winter when it almost finished the lifecycle such that there were few large patches. In addition, α_{Sali} in 2019 is lower than that in 2006, indicating that *Salicornia* gradually establishes continuous patches after its initial colonization (Schwarz et al., 2018). All these also suggest that the high dynamic behaviour of marsh ecogeomorphic pattern.

Moreover, we also realized that the scaling exponent of *Limonium* and *Sarcocornia* (std = 0.099, Table 5.5) is more stable than the other two species (std = 0.138 and 0.234 for *Spartina* and *Salicornia*, respectively, Table 5.5) over the period, highlighting that the patch-size distribution of *Limonium* and *Sarcocornia* is more stable than that of *Spartina* and *Salicornia*. This higher stability represents that this association is more likely to maintain its self-similarity, being an indicator that *Limonium* and *Sarcocornia* are minor affected by changes in external pressure (Kéfi et al., 2007), compared with *Salicornia* and *Spartina*.

For the first time we analyzed the temporal behavior of the patch-size distribution of halophytic vegetation in the Venice lagoon. Indeed, the scaling exponent (α) of patch-size distribution represents the possibility to construct continuous patches, indicating the response of vegetation to variations in environmental forcing (Kéfi et al., 2007) and vegetation local-scale interactions (Scanlon et al., 2007; Van Wesenbeeck et al., 2008; Zhao et al., 2019). On the other hand, the patch-size of each species is an indicator of fragmentation (Andren, 1994), primarily resulting from habitat loss (Llauss and Nogué, 2012) in response to external forcing (Bogaert et al., 2005), thus in turn determining the vegetation ability to colonize percentage of marsh landscapes. Thus, we speculate that the percentage of marsh areas occupied by each specific species (Fig. 5.5) is linked to its α. Fig. 5.10 displays the function of α and marsh portion of each species in the San Felice marsh and Saeftinghe salt marsh in Scheldt estuary (Taramelli et al., 2018), indicating that the a is linked to the marsh proportion encroached by each species by a log law (fitting line in Fig. 5.10). In addition, the link between a and marsh proportion is strongly site-specific characteristics, because a in Saeftinghe marsh is higher than that in San Felice with the same marsh portion encroached by every single species or typical association. This relationship is very important to inform and test landscape ecological and eco-

morphodynamic models. This implies a simple way to infer the patch-size distribution of each species. However, this link is only tested in two cases in this study and further validation is still needed by carrying out spatially-extended observations over marshes populated by more than one speices.

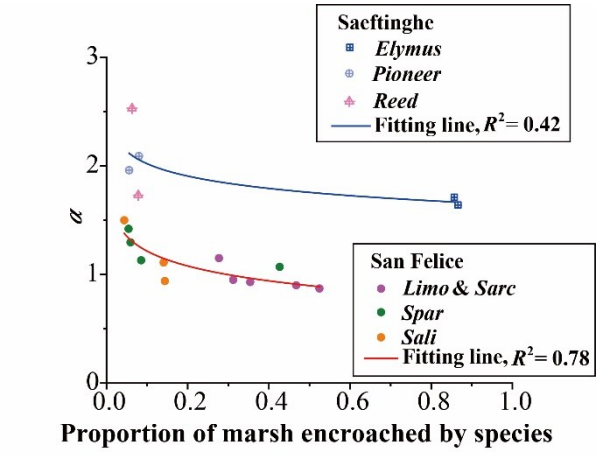

Figure 5. 10: The relationship between α and the proportion area of the marsh encroached by each species.

5.4.5 Biomass production

In this study, we also analyzed the spatial distribution of and changes in the above-ground biomass (AGB). For the first time we analyzed the spatial distribution of AGB and detect temporal changes at a whole marsh scale in the Venice lagoon. The eAGB displays a consistent behavior over time, with the exaptation of 2003. In fact, the eAGB in areas where *Spartina* (2001) was replaced by bare soil (2003) (Brown bar in the fourth column in Fig. 5.5a) decreased from 9.6×10^4 to 5.8×10^4 kg in this 2-year (Fig. 5.11), which is found to be almost equal to changes in total eAGB in the same period (Fig. 5.7f). We suggest this supports our hypothesis that the dieback event is the main reason for the relatively lower total or/and average eAGB of the marsh in 2003 compared with other years. One might wonder why the total value of eAGB in these areas in 2003 is not equal to 0 (Fig. 5.7f). This is mainly because some of these sites were still halophytic vegetation, but the FAs of these species were lower than bare soil.

After 2003, both the average and total values of eAGB in these areas gradually increased but were still lower than their values in 2001 (Fig. 5.11), indicating that the AGB in these marsh portions cannot approach its previous state immediately (Brisson et al., 2014). Moreover, some of these portions cannot transit to the vegetated configuration in the following years (Fig. 5.3), possibly resulting in the decrease in local elevations and submergence by increasing relative mean sea level. This suggests that the vegetation dieoff, especially the significant dieback event, is disastrous to marsh survival.

It should be noted that Fig. 5.11 only describes the changes in eAGB in areas that were mainly encroached by *Spartina* in 2001 but replaced by bare soil in 2003 (Brown bar in the fourth column in Fig. 5.4a). Although the changes in FA of *Spartina* in other marsh portions can trigger obvious variations in the local AGB, which is difficult to be statistically expressed mainly due to the fact that the FA of other species would be changed

simultaneously but also species-specifically, Fig. 5.11 still can represent the loss in AGB linked to the dieback event of *Spartina* to a high extent, since the decrease in the *Spartina*'s FA in these portions is more significant than other areas thus resulting in the replacement by bare soil.

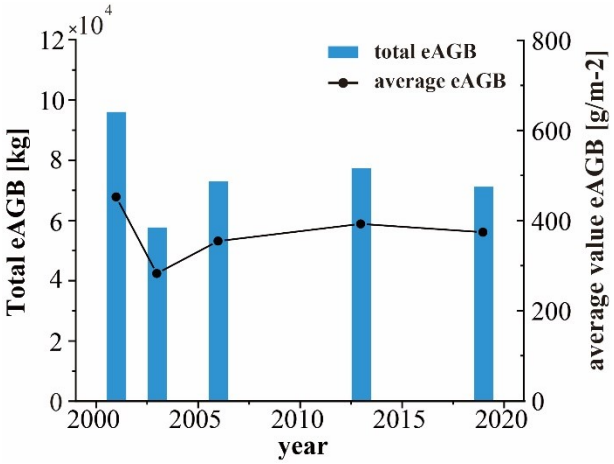

Figure 5. 11: The total and average values of the above-ground biomass in areas shifted from *Spartina* (2001) to bare soil (2003).

One might wonder why both the average and total values of eAGB of the whole marsh obviously increased between 2003 and 2006 (Fig. 5.7f) and then maintained constant until 2019, although the eAGB in the areas mainly encroached by *Spartina* before 2003 cannot approach the level before its dieback. The main reason for that could be the expansion of *Limonium* and *Sarcocornia* and the colonization of *Salicornia* also increased the AGB in other marsh portions (Figs. 5. 9 and 5.12) to balance the AGB loss caused by the dieback of *Spartina*. Indeed, Fig. 5.11 only includes 27% percent of marsh portions, while over the majority (68%, Fig 5.12) of marsh portions displayed an increase in AGB between 2003 and 2019. The general increase in RAGB after 2003 suggests that the marsh vegetation tends to increase their above-ground biomass to support marsh survival after significant climate change events. In fact, the changes in the above-ground biomass are intrinsically linked to the edaphic conditions (Curcó et al., 2002; Pennings et al., 2003), elevations (Roner et al., 2016) and interactions among different species (Steven C Pennings and Callaway, 1992), thus further efforts focused on the coupling of *in-situ* measurements and spatially-extended analyses are still needed to facilitate further analyses on marsh biomorphodynamic evolution.

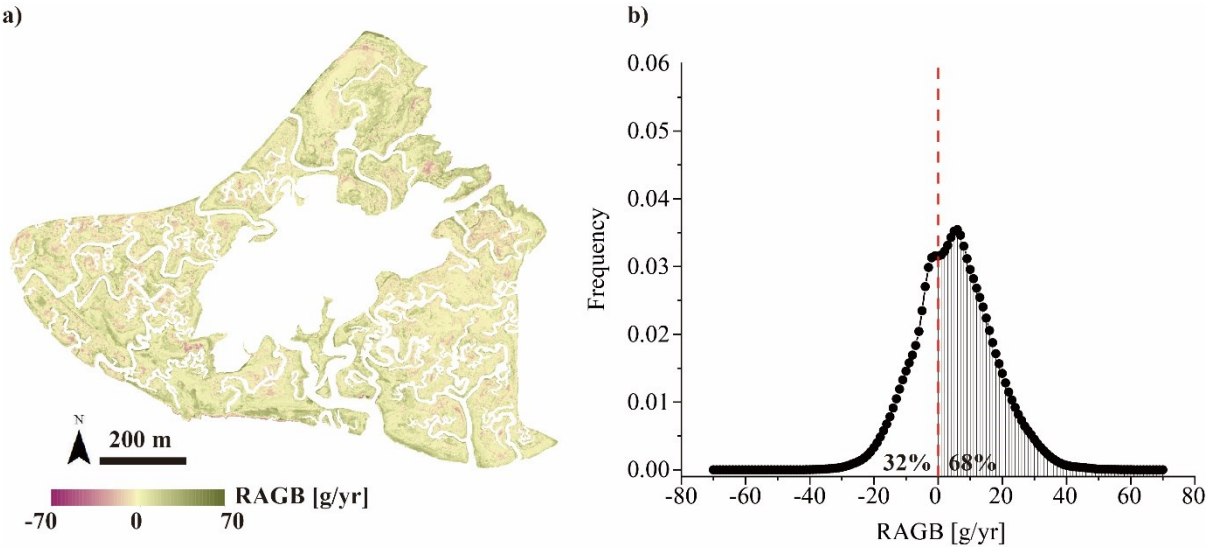

Figure 5. 12: The rate of above-ground biomass change (RAGB) between 2003 and 2019; (a) shows the distribution of RAGB over the marsh; (b) shows the frequency distribution of the RAGB.

5.4.6 Inaccuracy analyses

A major source of the inaccuracy of this study might be high tidal levels at the acquisition time (Table 5.1) of images collected in 2013 and 2019 (+43 and + 45 cm above MSL, respectively). The marsh elevation ranges from 15 – 60 cm above MSL, indicating that large portions of the marsh were flooded when the data were acquired. It has been documented that the higher tidal elevation can lead to an obvious reduction in near-infrared bands (Kearney et al., 2009), thus further reducing the accuracy of the classification and above-ground biomass estimation.

Another inaccuracy is the image in 2013 is collected in winter, which is characterized by the low FA of each species and widely disappearance of *Salicornia*, while others are acquired in summer and fall, characterized by high biomass production and FA. This would increase the noise in the analyses of changes in areas encroached by each species and patch-size distribution analyses.

5.5 Conclusions

In this study, based on remote sensing data with high spatial resolution (O (1 m)) coupled with detailed field observations, we analyzed changes in marsh area, spatial distribution of the most abundant species, and the above-ground biomass in the San Felice marsh (Venice Lagoon, Italy) over a period of about 18 years.

The RF soft classification method proves to be reliable in the estimation of FA of halophytic vegetation species and bare soil, being characterized by high accuracy (0.58 R^2 < 0.96, 5.49% < RMSE < 19.0%) when applied to multiple remote sensing data. The robustness of the RF soft classification method allowed us to analyse the distribution of each species habitat and the related changes, together with the distribution of the AGB y. We first conclude that the RF soft classification method and remote sensing images with high spatial resolutions (O (1 m)) are useful tools to analyze halophytic vegetation spatial distribution and variations

thereof, in response to climate changes.

Our analyses also reveal that the San Felice marsh area decreased with a rate of about 2345 m^2/yr, due to the marsh boundary retreat, the expansion of the channel planform area, and the enlargement of the inner pond. This suggests that marshes in the Venice lagoon are experiencing a degradation process over the same period.

In terms of dynamics of each species, our observations suggest that *Spartina* and *Salicornia* are more sensitive to changes in the environmental forcing, which is also confirmed by patch-size distribution analyses, indicating a possibility to monitor them to study eco-geomorphological dynamics. *Limonium* and *Sarcocornia* were more likely to encroach bare soil to balance the increase in the unvegetated area mainly due to the dieoff of other species. The vegetation species replacement and transitions between vegetated and unvegetated states were widely observed over the marsh, further emphasizing the highly dynamic behaviour of marsh ecogeomorphic patterns.

The patch-size distributions of each species are consistent with power laws, but with different slopes, possibly indicating the high dynamic behavior of marsh biogeomorphodynamic processes. We suggest that slope changes represent vegetation response to variations in environmental forcing, emphasizing the opportunity for coastal managers and researchers to describe vegetation dynamics. Moreover, we realized that the scaling factor (a) is linked to the total proportional marsh area encroached by each typical species or association, which can be a useful tool to inform and test further ecogeomorphic models concerning environments with high bio-diversity. However, this relationship was never documented before and was only tested in two cases, thus calling for further validations.

For the first time, we analyzed the changes in above-ground biomass (AGB) in a typical marsh in the Venice lagoon. The total and the average values of eAGB generally maintained almost constant through the considered period. In particular, although the dieback event of *Spartina* resulted in a sudden decrease in eAGB, the average/total eAGB over the whole marsh was able to recover immediately and reached its previous (2001) level in 2006. It then maintained stable in time, indicating that the expansion of *Limoninium* and *Sarcocornia* and the invasion of *Salicornia* were able to balance the loss of AGB caused by dieback of *Spartina*. These findings suggest that marsh ecogeomorphic patterns dynamically maintain the AGB, thus calling for further spatially-explicit eco-morphodynamic models.

Finally, we also noticed that distance from the channel network cannot be used as a proxy for vegetation species distribution in the San Felice marsh, because all species prefer to live within narrow areas from channels. However, we observe is a strong link between the distance from channel networks and eAGB, indicating that eAGB decreases towards inner marsh portions, consistently over the considered time period. These findings are deemed to be of high importance to future eco-morphodyanic analyses, especially in marshes encroached by multiple halophytic vegetation species.

Author Contributions: Conception or design of the work, Z.Y., A.D., M.M., and S.S.; Data collection, Z.Y., A.D., M.M., S.S., E.B., and D.T.; Data analysis and interpretation Z.Y.; Drafting the article, Z.Y.; Critical revision of the article Z.Y., A.D., M.M., S.S., and D.T..

Chapter 6: Conclusions

Salt marshes are important coastal ecosystems that provide important ecosystem services. Unfortunately, these vital coastal landscapes are disappearing fast worldwide due to natural processes exacerbated by climate changes and by increasing human interferences. These vital and at the same time fragile landscapes host halophytic vegetation species, i.e. plants adapted to live in salty environments regularly flooded by the tide. Halophytic vegetation plays a critical role in supporting marsh development and survival through complex interactions and mutual adjustments between biological and physical processes, i.e. through biogeomorphic feedbacks.

Improving our current understanding of vegetation dynamics and of the related biogeomoprhic feedbacks is therefore a key step for the protection and conservation of these delicate coastal ecosystems. The present thesis has addressed this relevant issue through the combined analysis of *in situ* field observations and remote sensing data. We have analyzed in detail the intertwined dynamics of marsh elevations and of vegetation distribution both in the vertical and horizontal frames between 2000 and 2019 for the San Felice salt marsh, in the Venice Lagoon, Italy.

The study was mainly developed through:

i) the description of the vegetation-elevation relationship over a 20 year period (between 2000 and 2019) by analyzing a unique marsh elevation – vegetation cover dataset of 2700 point data. This analysis allowed us to describe marsh surface elevation changes and the coupled vegetation dynamics in response to increasing rates of relative sea level rise (Chapter 2);

ii) the extension of the above-described analysis to the whole marsh-system scale through the coupling of vegetation classification maps and lidar-derived digital elevation model, corrected by fully using information derived from vegetation characteristics (Chapter 4). This analysis required the preliminary set-up of a new vegetation classification method based on a Random Forest algorithm (Chapter 3);

iii) changes in vegetation spatial distribution and above-ground biomass in the horizontal plane over the marsh (Chapter 5), explored by analyzing a series of remote sensing images of the San Felice marsh based on the newly developed vegetation classification algorithm (Chapter 3).

The main results that stemmed from this Doctoral thesis can be summarized as follows:

- The analysis of the coupled elevation-vegetation response to changes in relative mean sea level carried out by using accurate elevation measurements and vegetation cover information from the San Felice marsh, surveyed 7 times between 2000 and 2019, that organic and inorganic deposition over the marsh surface allowed almost all marsh points to increase their absolute elevations (relative to the fixed IGM datum). However, a more detailed scrutiny of marsh response performed by considering elevations referred to the current RMSL showed that most of the marsh sites were not able to keep pace with the current rate of RSLR, thus suggesting progressive marsh drowning. This clearly emphasizes the need to refer to local marsh elevations referenced to RMSL when monitoring marsh evolution and response to changes in the environmental forcing.

- In addition, we observe that marsh accretion rates are strongly site-specific and change at sites within distances of a few tens or hundreds of meters. At adjacent sites accretion rates range between 1.7 and 4.3 mm/year, with differences that crucially affect marsh response to the current rate of RSLR (4.4 mm/yr). Accretion rates are found to be strongly linked to marsh surface elevation and sediment availability provided by marsh edge erosion. Our findings crucially call for spatially distributed marsh monitoring and properly informed spatially-explicit biomorphodynamic models of marsh evolution.

- Finally, our analyses show that vegetation species respond to changes in the environmental forcing by modifying their preferential elevation ranges. Vegetation response is strongly species-specific. For the first time, we observe the consistency, over a period of 20 years, of the vegetation-species sequence with increasing elevations. We deem this is a signature of vegetation resilience to changes in the forcing.

- Our observations point at a strong coupling between geomorphological and ecological dynamics, with relevant implications for the further eco-morphodynamic analyses.

- We developed a new approach based on the application of Random Forest (RF) soft classification for estimating the fractional abundance of each species within vegetation associations. The main advantage of this method is making full use of the frequency of "votes" produced by individual decision trees and interpreting this frequency as the corresponding fractional abundance (FA). The method was applied to and tested to a WV-2 multispectral image, indicating that this method can estimate the FA of each species with high accuracy ($6.7\% < \text{RMSE} < 18.7\%$ and $0.65 < R^2 < 0.96$). In addition, the proposed RF soft classification method performs much better than the traditional RF regression method (Immitzer et al., 2018), and therefore it is more suitable to accurately map fractional abundance in highly-mixed halophytic associations. Moreover, the RF soft-classifier

predicted vegetation distribution is found to be in very good agreement with halophytic vegetation patterns documented by previous analyses (Belluco et al., 2006; Wang et al., 2007), thus confirming the usefulness of the method. We also show that the results obtained with the RF soft classification can be used to produce a map of the dominant species within the plant association (i.e. with percentage cover higher than 60% in our case). This map nicely agrees with a RF hard classification map produced for the same study site, thus emphasizing the RF soft-classifier robustness.

- We suggest that the RF soft classification is a useful tool to describe fractional abundance of halophytic species and bare soil on salt marshes and to provide important information about the spatial distribution of dominant species. The RF soft classification can be used to monitor the temporal evolution of halophytic vegetation, such as dieback and replacement. We, therefore, suggest that the RF soft classification method should be considered to analyze salt-marsh biogeomorphic response to sea-level changes and for the development and testing of biogeomorphic models. The high accuracy of this method allowed us to further analyze the vegetation-elevation relationship at the whole marsh scale (Chapter 4) and the temporal changes in marsh vegetation spatial distribution (Chapter 5).

- Towards the goal of analysing of the coupled elevation-vegetation response to changes in the forcing without the need to carry out time-consuming and labor-intense accurate *in situ* elevation measurements and vegetation cover observations, we first developed a new method to correct lidar-derived DEM, based on the Random Forest Regression (RFR) algorithm by fully using vegetation information contained in the fractional abundance (FA) of each species and NDVI, which are provided by multi-spectral data. This method was then applied to a lidar point cloud data acquired in 2003 over the San Felice marsh. The method was tested and proved to be able to correct lidar-derived DEM with high accuracy (R^2=0.79 and RMSE = 3.5 cm). The proposed RFR method was also found to perform better than the other two methods, i.e., LEAN method (Buffington et al., 2016), whose RMSE is equal to 5.2 cm in the San Felice marsh, and the MGB method (Wang et al., 2009), which was previously used in the San Felice site and tested to have RMSE = 6.6 cm.

- We therefore suggest that the RFR method can be a useful tool to monitor marsh eco-morphodynamic processes.

- FA maps for each species and bare soil most abundant species maps were also generated by the application of the RFSC method (Chapter 3) in 2001 and 2003. The integration of FA maps, most abundant species maps, and corrected lidar-derived DEM suggest that the vegetation-elevation relationship observed from *in-situ* measurements is consistent and reliable at the whole marsh. Moreover, the vertical distribution of vegetation-derived metrics (NDVI, SFA and LAI) suggest that the above ground biomass (AGB) generally increases with higher elevations, because higher values of these metrics are found in higher marsh portions. Our analyses suggest that integration of the passive (such as lidar) and active (such as multi-spectral) remote sensing data allows one to gain

2845 further insights on marsh eco-morphodynamic patterns at the large scale. These observations are valuable for future eco-geomorphic models concerning marshes encroached by multiple vegetation species.

- By analysing remote sensing data with high spatial resolutions (O(1 m)) through the proposed RF soft classifier (Chapter 3) coupled with detailed field observations, we analyzed changes in marsh 2850 area, spatial distribution of the most abundant species, and the above-ground biomass in the San Felice marsh (Venice Lagoon, Italy) over a period of about 18 years, between 2001 and 2019. The RF soft classification method proved to be reliable in the estimation of halophytic vegetation FA, being characterized by high accuracy (0.58 R^2 < 0.96, 5.49% < RMSE < 19.0%) when applied to multiple remote sensing data, although acquired on different dates and by different sensors. The 2855 robustness of the RF soft classification method allowed us to analyse the distribution of each species habitat and the related changes, together with the distribution of the AGB. We first conclude that the RF soft classification method and remote sensing images with high spatial resolutions (O (1 m)) are useful tools to analyze halophytic vegetation spatial distribution and variations thereof, in response to climate changes.

2860 • The San Felice marsh area decreased with a rate of about 2345 m^2/yr, due to the marsh boundary retreat, the expansion of the channel planform area, and the enlargement of the inner pond. This suggests that marshes in the Venice lagoon experienced a degradation process over the same period.

- In terms of species dynamics, we suggest that *Spartina* and *Salicornia* are more sensitive to changes in the environmental forcing, which is also confirmed by patch-size distribution analyses, 2865 suggesting to monitor them when studying eco-geomorphological dynamics. *Limonium* and *Sarcocornia* were observed to encroach bare soil to balance the increase in the unvegetated area, mainly due to the die-off of other species. Vegetation species replacement and transitions between vegetated and unvegetated states were widely observed over the marsh, further emphasizing the highly dynamic behaviour of marsh ecogeomorphic patterns.

2870 • Our analyses suggest that the slope of patch-size distribution is strongly linked to the vegetation response to changes in external forcing, highlighting the possibility to use the slope of patch-size distribution to inform and test marsh eco-geomorphic models in the future.

- We also noticed that distance from the channel network cannot be used as a proxy for vegetation species distribution in the San Felice marsh, because all species prefer to live within narrow areas 2875 from channels.

- For the first time, we analyzed the changes in above-ground biomass (AGB) in a typical marsh in the Venice lagoon. The total and the average values of eAGB generally maintained almost constant through the considered period. In particular, although the dieback event of *Spartina* resulted in a

sudden decrease in eAGB, the average/total eAGB over the whole marsh was able to recover immediately and reached its previous (2001) level in 2006. It then maintained stable in time, indicating that the expansion of *Limoninium* and *Sarcocornia* and the invasion of *Salicornia* were able to balance the loss of AGB caused by dieback of *Spartina*. These findings suggest that marsh ecogeomorphic patterns dynamically maintain the AGB, thus calling for further spatially-explicit eco-morphodynamic models.

Although our analyses were focused on the specific study case of the Venice Lagoon, we deem our results bear important consequences for a variety of marshes developed in different contexts. The unique dataset deriving from 20-year long measurements in the Venice Lagoon, allowed us to emphasize the strong relationship between elevation and vegetation dynamics, i.e. between physical and biological processes. These findings will be of help to develop and test models of marsh biomorphodynamic evolution to be applied in different systems and under different environmental forcing.

Indeed, future research will be devoted to the application of the above-described monitoring frameworks to other systems around the world to highlight similarities and differences with the considered study case and further improve current knowledge of marsh biomorphdynamic evolution. In particular, the Random Forest soft classification method can be a useful tool in dominant vegetation species map and fractional abundance estimation over the marsh, highlighting a robust algorithm to help analyses of marsh vegetation distribution and changes worldwide. In addition, the proposed Random Forest Regression method is robust in lidar-derived DEM correction over the marsh, allowing researchers to extend the local-scale topographic changes in response to different forcings and marsh biomorphodynamic processes in other tidal landscapes to large scales. In addition, we also suggest that remote sensing data with a high spatial resolution (O(1 m)) are valuable to describe the vegetation species spatial distribution and dynamics, which can be useful tools to fertilize future marsh biomorphodynamic analyses in other contexts.

Reference

Adam Langley, J., Mozdzer, T.J., Shepard, K.A., Hagerty, S.B., Patrick Megonigal, J., 2013. Tidal marsh plant responses to elevated CO2, nitrogen fertilization, and sea level rise. Glob. Chang. Biol. 19, 1495–1503. https://doi.org/10.1111/gcb.12147

Adams, J.B., Bate, G.C., 1995. Ecological implications of tolerance of salinity and inundation by Spartina maritima. Aquat. Bot. 52, 183–191. https://doi.org/10.1016/0304-3770(95)00496-3

Alber, M., Swenson, E.M., Adamowicz, S.C., Mendelssohn, I.A., 2008. Salt Marsh Dieback: An overview of recent events in the US. Estuar. Coast. Shelf Sci. 80, 1–11. https://doi.org/10.1016/j.ecss.2008.08.009

Allen, J.R.L., 2000. Morphodynamics of Holocene salt marshes: A review sketch from the Atlantic and Southern North Sea coasts of Europe. Quat. Sci. Rev. 19, 1155–1231. https://doi.org/10.1016/S0277-3791(99)00034-7

Allen, J.R.L., 1995. Salt-marsh growth and fluctuating sea level: implications of a simulation model for Flandrian coastal stratigraphy and peat-based sea-level curves. Sediment. Geol. 100, 21–45. https://doi.org/10.1016/0037-0738(95)00101-8

Allen, J.R.L., 1989. Evolution of salt-marsh cliffs in muddy and sandy systems: A qualitative comparison of British West-Coast estuaries. Earth Surf. Process. Landforms 14, 85–92. https://doi.org/10.1002/esp.3290140108

Álvarez Rogel, J., Ortiz Silla, R., Alcaraz Ariza, F., 2001. Edaphic characterization and soil ionic composition influencing plant zonation in a semiarid Mediterranean salt marsh. Geoderma 99, 81–98. https://doi.org/10.1016/S0016-7061(00)00067-7

Andren, H., 1994. Effects of Habitat Fragmentation on Birds and Mammals in Landscapes with Different Proportions of Suitable Habitat : A Review. Oikos 71, 355–366. https://doi.org/the total species diversity across habitats in a given landscape may increase when new patches of habitat are created within the continuous habitat, since new species may be found in these new habitats,

Anisfeld, S.C., Cooper, K.R., Kemp, A.C., 2017. Upslope development of a tidal marsh as a function of upland land use. Glob. Chang. Biol. 23, 755–766. https://doi.org/10.1111/gcb.13398

Archer, K.J., Kimes, R. V., 2008. Empirical characterization of random forest variable importance measures. Comput. Stat. Data Anal. 52, 2249–2260. https://doi.org/10.1016/j.csda.2007.08.015

Artigas, F., Pechmann, I.C., 2010. Balloon imagery verification of remotely sensed Phragmites australis expansion in an urban estuary of New Jersey, USA. Landsc. Urban Plan. 95, 105–112. https://doi.org/10.1016/j.landurbplan.2009.12.007

Artigas, F.J., Yang, J., 2006. Note: Spectral Discrimination of Marsh Vegetation Types In the New Jersey

Meadowlands, USA. Wetlands 26, 271–277. https://doi.org/10.1672/0277-5212(2006)26[271:SDOMVT]2.0.CO;2

Balke, T., Herman, P.M.J., Bouma, T.J., 2014. Critical transitions in disturbance-driven ecosystems: identifying Windows of Opportunity for recovery. J. Ecol. 102, 700–708. https://doi.org/10.1111/1365-2745.12241

Belgiu, M., Drăgu, L., 2016. Random forest in remote sensing: A review of applications and future directions. ISPRS J. Photogramm. Remote Sens. 114, 24–31. https://doi.org/10.1016/j.isprsjprs.2016.01.011

Belluco, E., Camuffo, M., Ferrari, S., Modenese, L., Silvestri, S., Marani, A., Marani, M., 2006. Mapping salt-marsh vegetation by multispectral and hyperspectral remote sensing. Remote Sens. Environ. 105, 54–67. https://doi.org/10.1016/j.rse.2006.06.006

Bendoni, M., Mel, R., Solari, L., Lanzoni, S., Francalanci, S., Oumeraci, H., 2016. Insights into lateral marsh retreat mechanism through localized field measurements. Water Resour. Res. 52, 1446–1464. https://doi.org/10.1002/2015WR017966

Berhane, T.M., Costa, H., Lane, C.R., Anenkhonov, O.A., Chepinoga, V. V., Autrey, B.C., 2019. The influence of region of interest heterogeneity on classification accuracy in wetland systems. Remote Sens. 11, 1–16. https://doi.org/10.3390/rs11050551

Bernhardt, J.R., Leslie, H.M., 2013. Resilience to Climate Change in Coastal Marine Ecosystems. Ann. Rev. Mar. Sci. 5, 371–392. https://doi.org/10.1146/annurev-marine-121211-172411

Bertness, M.D., Ewanchuk, P.J., 2002. Latitudinal and climate-driven variation in the strength and nature of biological interactions in New England salt marshes. Oecologia 132, 392–401. https://doi.org/10.1007/s00442-002-0972-y

Biondi, E., Blasi, C., Allegrezza, M., Anzellotti, I., Azzella, M.M., Carli, E., Casavecchia, S., Copiz, R., Del Vico, E., Facioni, L., Galdenzi, D., Gasparri, R., Lasen, C., Pesaresi, S., Poldini, L., Sburlino, G., Taffetani, F., Vagge, I., Zitti, S., Zivkovic, L., 2014. Plant communities of Italy: The Vegetation Prodrome. Plant Biosyst. 148, 728–814. https://doi.org/10.1080/11263504.2014.948527

Blum, M.D., Roberts, H.H., 2009. Drowning of the Mississippi Delta due to insufficient sediment supply and global sea-levelrise. Nat. Geosci. 2, 488–491. https://doi.org/10.1038/ngeo553

Bockelmann, A.C., Bakker, J.P., Neuhaus, R., Lage, J., 2002. The relation between vegetation zonation, elevation and inundation frequency in a Wadden Sea salt marsh. Aquat. Bot. 73, 211–221. https://doi.org/10.1016/S0304-3770(02)00022-0

Bogaert, J., Farina, A., Ceulemans, R., 2005. Entropy increase of fragmented habitats: A sign of human impact? Ecol. Indic. 5, 207–212. https://doi.org/10.1016/j.ecolind.2005.02.002

Bouma, T., De Vries, M., Herman, P., 2010. Comparing Ecosystem Engineering Efficiency of 2 Plant Species

With Contrasting Growth Strategies. Ecology 91, 100319061621033. https://doi.org/10.1890/09-0690

Bouma, T.J., De Vries, M.B., Low, E., Kusters, L., Herman, P.M.J., Tánczos, I.C., Temmerman, S., Hesselink, A., Meire, P., Van Regenmortel, S., 2005. Flow hydrodynamics on a mudflat and in salt marsh vegetation: Identifying general relationships for habitat characterisations. Hydrobiologia 540, 259–274. https://doi.org/10.1007/s10750-004-7149-0

Bouma, T.J., Friedrichs, M., Van Wesenbeeck, B.K., Temmerman, S., Graf, G., Herman, P.M.J., 2009. Density-dependent linkage of scale-dependent feedbacks: A flume study on the intertidal macrophyte Spartina anglica. Oikos 118, 260–268. https://doi.org/10.1111/j.1600-0706.2008.16892.x

Bouma, T.J., van Duren, L.A., Temmerman, S., Claverie, T., Blanco-Garcia, A., Ysebaert, T., Herman, P.M.J., 2007. Spatial flow and sedimentation patterns within patches of epibenthic structures: Combining field, flume and modelling experiments. Cont. Shelf Res. 27, 1020–1045. https://doi.org/10.1016/j.csr.2005.12.019

Boyd, B.M., Sommerfield, C.K., Elsey-Quirk, T., 2017. Hydrogeomorphic influences on salt marsh sediment accumulation and accretion in two estuaries of the U.S. Mid-Atlantic coast. Mar. Geol. 383, 132–145. https://doi.org/10.1016/j.margeo.2016.11.008

Breiman, L., 2001. Random Forests. Mach. Learn. 45, 5–32.

Breiman, L., 1996. Out-of-Bag Estimation.

Brinson, M.M., Christian, R.R., Blum, L.K., 1995. Multiple States in the Sea-Level Induced Transition from Terrestrial Forest to Estuary. Estuaries 18, 648. https://doi.org/10.2307/1352383

Brisson, C.P., Coverdale, T.C., Bertness, M.D., 2014. Salt marsh die-off and recovery reveal disparity between the recovery of ecosystem structure and service provision. Biol. Conserv. 179, 1–5. https://doi.org/10.1016/j.biocon.2014.08.013

Buffington, K.J., Dugger, B.D., Thorne, K.M., Takekawa, J.Y., 2016. Statistical correction of lidar-derived digital elevation models with multispectral airborne imagery in tidal marshes. Remote Sens. Environ. 186, 616–625. https://doi.org/10.1016/j.rse.2016.09.020

C. Schwarz, Q.H.Ye, D. van der Wal, L. Q. Zhang, T. Bouma, T. Ysebaert, and P.M.J.H., 2014. Impacts of salt marsh plants on tidal channel initiation and inheritance. J. Geophys. Res. Earth Surf. Res. 119, 385–400. https://doi.org/10.1002/2013JF002900.Received

Callaghan, D.P., Bouma, T.J., Klaassen, P., van der Wal, D., Stive, M.J.F., Herman, P.M.J., 2010. Hydrodynamic forcing on salt-marsh development: Distinguishing the relative importance of waves and tidal flows. Estuar. Coast. Shelf Sci. 89, 73–88. https://doi.org/10.1016/j.ecss.2010.05.013

Campbell, A., Wang, Y., 2020. Assessment of salt marsh change on assateague island national seashore between

1962 and 2016. Photogramm. Eng. Remote Sensing 86, 187–194. https://doi.org/10.14358/PERS.86.3.187

Campbell, A., Wang, Y., 2019. High spatial resolution remote sensing for salt marsh mapping and change analysis at fire Island national seashore. Remote Sens. 11. https://doi.org/10.3390/rs11091107

Campbell, A., Wang, Y., Christiano, M., Stevens, S., 2017. Salt Marsh Monitoring in Jamaica Bay, New York from 2003 to 2013: A decade of change from restoration to hurricane sandy. Remote Sens. 9, 1–20. https://doi.org/10.3390/rs9020131

Campbell, G.S., 1986. Extinction coefficients for radiation in plant canopies calculated using an ellipsoidal inclination angle distribution. Agric. For. Meteorol. 36, 317–321. https://doi.org/10.1016/0168-1923(86)90010-9

Carbognin, L., Teatini, P., Tosi, L., 2004. Eustacy and land subsidence in the Venice Lagoon at the beginning of the new millennium. J. Mar. Syst. 51, 345–353. https://doi.org/10.1016/j.jmarsys.2004.05.021

Carniello, L., Defina, A., D'Alpaos, L., 2009. Morphological evolution of the Venice lagoon: Evidence from the past and trend for the future. J. Geophys. Res. Earth Surf. 114, 1–10. https://doi.org/10.1029/2008JF001157

Chai, G., Wang, J., Wang, G., Kang, L., Wu, M., Wang, Z., 2019. Estimating fractional cover of non-photosynthetic vegetation in a typical grassland area of northern China based on Moderate Resolution Imaging Spectroradiometer (MODIS) image data. Int. J. Remote Sens. 40, 8793–8810. https://doi.org/10.1080/01431161.2019.1620971

Chassereau, J.E., Bell, J.M., Torres, R., 2011. A comparison of GPS and lidar salt marsh DEMs. Earth Surf. Process. Landforms 36, 1770–1775. https://doi.org/10.1002/esp.2199

Chmura, G.L., Anisfeld, S.C., Cahoon, D.R., Lynch, J.C., 2003. Global carbon sequestration in tidal, saline wetland soils. Global Biogeochem. Cycles 17, n/a-n/a. https://doi.org/10.1029/2002gb001917

Coleman, D.J., Ganju, N.K., Kirwan, M.L., 2020. Sediment Delivery to a Tidal Marsh Platform Is Minimized by Source Decoupling and Flux Convergence. J. Geophys. Res. Earth Surf. 125, 1–13. https://doi.org/10.1029/2020JF005558

Coleman, D.J., Kirwan, M.L., 2019. The effect of a small vegetation dieback event on salt marsh sediment transport. Earth Surf. Process. Landforms 44, 944–952. https://doi.org/10.1002/esp.4547

Collin, A., Long, B., Archambault, P., 2010. Salt-marsh characterization, zonation assessment and mapping through a dual-wavelength LiDAR. Remote Sens. Environ. 114, 520–530. https://doi.org/10.1016/j.rse.2009.10.011

Collins, D.B.G., 2004. Modeling the effects of vegetation-erosion coupling on landscape evolution. J. Geophys. Res. 109, F03004. https://doi.org/10.1029/2003JF000028

Colmer, T.D., Flowers, T.J., 2008. Flooding tolerance in halophytes. New Phytol. 179, 964–974. https://doi.org/10.1111/j.1469-8137.2008.02483.x

Cooley, T., Anderson, G.P., Felde, G.W., Hoke, M.L., Ratkowski, A.J., Chetwynd, J.H., Gardner, J.A., Adler-Golden, S.M., Matthew, M.W., Berk, A., Bernstein, L.S., Acharya, P.K., Miller, D., Lewis, P., 2002. FLAASH, a MODTRAN4-based atmospheric correction algorithm, its applications and validation. Int. Geosci. Remote Sens. Symp. 3, 1414–1418. https://doi.org/10.1109/igarss.2002.1026134

Costa, C.S.B., Marangoni, J.C., Azevedo, A.M.G., 2003. Plant zonation in irregularly flooded salt marshes: Relative importance of stress tolerance and biological interactions. J. Ecol. 91, 951–965. https://doi.org/10.1046/j.1365-2745.2003.00821.x

Costa, H., Foody, G.M., Boyd, D.S., 2017. Using mixed objects in the training of object-based image classifications. Remote Sens. Environ. 190, 188–197. https://doi.org/10.1016/j.rse.2016.12.017

Crain, C.M., Albertson, L.K., Bertness, M.D., 2008. Secondary succession dynamics in estuarine marshes across landscape-scale salinity gradients. Ecology 89, 2889–2899. https://doi.org/10.1890/07-1527.1

Curcó, A., Ibàñez, C., Day, J.W., Prat, N., 2002. Net primary production and decomposition of salt marshes of the Ebre delta (Catalonia, Spain). Estuaries 25, 309–324. https://doi.org/10.1007/bf02695976

Cutler, D.R., Edwards, T.C., Beard, K.H., Cutler, A., Hess, K.T., Gibson, J., Lawler, J.J., 2007. RANDOM FORESTS FOR CLASSIFICATION IN ECOLOGY. Ecology 88, 2783–2792. https://doi.org/10.1890/07-0539.1

D'Alpaos, A., Carniello, L., Rinaldo, A., 2013. Statistical mechanics of wind wave-induced erosion in shallow tidal basins: Inferences from the Venice Lagoon. Geophys. Res. Lett. 40, 3402–3407. https://doi.org/10.1002/grl.50666

D'Alpaos, A., Da Lio, C., Marani, M., 2012. Biogeomorphology of tidal landforms: Physical and biological processes shaping the tidal landscape. Ecohydrology 5, 550–562. https://doi.org/10.1002/eco.279

D'Alpaos, A., Ghinassi, M., Finotello, A., Brivio, L., Bellucci, L.G., Marani, M., 2017. Tidal meander migration and dynamics: A case study from the Venice Lagoon. Mar. Pet. Geol. 87, 80–90. https://doi.org/10.1016/j.marpetgeo.2017.04.012

D'Alpaos, A., Lanzoni, S., Marani, M., Bonometto, A., Cecconi, G., Rinaldo, A., 2007a. Spontaneous tidal network formation within a constructed salt marsh: Observations and morphodynamic modelling. Geomorphology 91, 186–197. https://doi.org/10.1016/j.geomorph.2007.04.013

D'Alpaos, A., Lanzoni, S., Marani, M., Fagherazzi, S., Rinaldo, A., 2005. Tidal network ontogeny: Channel initiation and early development. J. Geophys. Res. Earth Surf. 110, 1–14. https://doi.org/10.1029/2004JF000182

D'Alpaos, A., Lanzoni, S., Marani, M., Rinaldo, A., 2007b. Landscape evolution in tidal embayments: Modeling the interplay of erosion, sedimentation, and vegetation dynamics. J. Geophys. Res. Earth Surf. 112, 1–17. https://doi.org/10.1029/2006JF000537

D'Alpaos, A., Marani, M., 2016. Reading the signatures of biologic-geomorphic feedbacks in salt-marsh landscapes. Adv. Water Resour. 93, 265–275. https://doi.org/10.1016/j.advwatres.2015.09.004

D'Alpaos, A., Mudd, S.M., Carniello, L., 2011. Dynamic response of marshes to perturbations in suspended sediment concentrations and rates of relative sea level rise. J. Geophys. Res. Earth Surf. 116, 1–13. https://doi.org/10.1029/2011JF002093

D'Alpaos, L., 2010. `. Istituto veneto di scienze, lettere ed arti.

D'Alpaos, L., Defina, A., 2007. Mathematical modeling of tidal hydrodynamics in shallow lagoons: A review of open issues and applications to the Venice lagoon. Comput. Geosci. 33, 476–496. https://doi.org/10.1016/j.cageo.2006.07.009

Da Lio, C., D'Alpaos, A., Marani, M., 2013. The secret gardener: Vegetation and the emergence of biogeomorphic patterns in tidal environments. Philos. Trans. R. Soc. A Math. Phys. Eng. Sci. 371. https://doi.org/10.1098/rsta.2012.0367

da Lio, C., Strozzi, T., Teatini, P., Tosi, L., 2017. Computing the relative land subsidence at Venice, Italy, over the last fifty years. Proc. - 22nd Int. Congr. Model. Simulation, MODSIM 2017 999–1005. https://doi.org/10.36334/modsim.2017.h4.dalio

Da Lio, C., Teatini, P., Strozzi, T., Tosi, L., 2018. Understanding land subsidence in salt marshes of the Venice Lagoon from SAR Interferometry and ground-based investigations. Remote Sens. Environ. 205, 56–70. https://doi.org/10.1016/j.rse.2017.11.016

Daleo, P., Alberti, J., Canepuccia, A., Escapa, M., Fanjul, E., Silliman, B.R., Bertness, M.D., Iribarne, O., 2008. Mycorrhizal fungi determine salt-marsh plant zonation depending on nutrient supply. J. Ecol. 96, 431–437. https://doi.org/10.1111/j.1365-2745.2007.01349.x

Dalrymple, R.W., Choi, K., 2007. Morphologic and facies trends through the fluvial-marine transition in tide-dominated depositional systems: A schematic framework for environmental and sequence-stratigraphic interpretation. Earth-Science Rev. 81, 135–174. https://doi.org/10.1016/j.earscirev.2006.10.002

Davranche, A., Lefebvre, G., Poulin, B., 2010. Wetland monitoring using classification trees and SPOT-5 seasonal time series. Remote Sens. Environ. 114, 552–562. https://doi.org/10.1016/j.rse.2009.10.009

Day, J.W., Britsch, L.D., Hawes, S.R., Shaffer, G.P., Reed, D.J., Cahoon, D., 2000. Pattern and process of land loss in the Mississippi Delta: A spatial and temporal analysis of wetland habitat change. Estuaries 23, 425–438. https://doi.org/10.2307/1353136

Day, J.W., Rismondo, A., Scarton, F., Are, D., Cecconi, G., 1998. Relative sea level rise and Venice lagoon wetlands. J. Coast. Conserv. 4, 27–34. https://doi.org/10.1007/BF02806486

Defina, A., Carniello, L., Fagherazzi, S., D'Alpaos, L., 2007. Self-organization of shallow basins in tidal flats and salt marshes. J. Geophys. Res. Earth Surf. 112, 1–11. https://doi.org/10.1029/2006JF000550

Détriché, S., Susperregui, A.-S., Feunteun, E., Lefeuvre, J.-C., Jigorel, A., 2011. Interannual (1999–2005) morphodynamic evolution of macro-tidal salt marshes in Mont-Saint-Michel Bay (France). Cont. Shelf Res. 31, 611–630. https://doi.org/10.1016/j.csr.2010.12.015

Díaz-Uriarte, R., Alvarez de Andrés, S., 2006. Gene selection and classification of microarray data using random forest. BMC Bioinformatics 7, 1–13. https://doi.org/10.1186/1471-2105-7-3

Donatelli, C., Ganju, N.K., Fagherazzi, S., Leonardi, N., 2018. Seagrass Impact on Sediment Exchange Between Tidal Flats and Salt Marsh, and The Sediment Budget of Shallow Bays. Geophys. Res. Lett. 45, 4933–4943. https://doi.org/10.1029/2018GL078056

Donnelly, J.P., Bertness, M.D., 2002. Rapid shoreward encroachment of salt marsh cordgrass in response to accelerated sea-level rise. Proc. Natl. Acad. Sci. 98, 14218–14223. https://doi.org/10.1073/pnas.251209298

Donnelly, J.P., Cleary, P., Newby, P., Ettinger, R., 2004. Coupling instrumental and geological records of sea-level change: Evidence from southern New England of an increase in the rate of sea-level rise in the late 19th century. Geophys. Res. Lett. 31, n/a-n/a. https://doi.org/10.1029/2003gl018933

Doughty, C.L., Ambrose, R.F., Okin, G.S., Cavanaugh, K.C., 2021. Characterizing spatial variability in coastal wetland biomass across multiple scales using UAV and satellite imagery. Remote Sens. Ecol. Conserv. 1–19. https://doi.org/10.1002/rse2.198

Elmore, A.J., Mustard, J.F., Manning, S.J., Lobell, D.B., 2000. Quantifying Vegetation Change in Semiarid Environments. Remote Sens. Environ. 73, 87–102. https://doi.org/10.1016/s0034-4257(00)00100-0

Engels, J.G., Rink, F., Jensen, K., 2011. Stress tolerance and biotic interactions determine plant zonation patterns in estuarine marshes during seedling emergence and early establishment. J. Ecol. 99, 277–287. https://doi.org/10.1111/j.1365-2745.2010.01745.x

Enwright, N.M., Griffith, K.T., Osland, M.J., 2016. Barriers to and opportunities for landward migration of coastal wetlands with sea-level rise. Front. Ecol. Environ. 14, 307–316. https://doi.org/10.1002/fee.1282

Erickson, J.E., Megonigal, J.P., Peresta, G., Drake, B.G., 2007. Salinity and sea level mediate elevated CO2 effects on C3-C4 plant interactions and tissue nitrogen in a Chesapeake Bay tidal wetland. Glob. Chang. Biol. https://doi.org/10.1111/j.1365-2486.2006.01285.x

Ewanchuk, P.J., Bertness, M.D., 2003. Recovery of a northern New England salt marsh plant community from

winter icing Recovery of a Northern New England Salt Marsh Plant Community from Winter Icing. https://doi.org/10.1007/s00442-003-1303-7

Fagherazzi, S., Anisfeld, S.C., Blum, L.K., Long, E. V., Feagin, R.A., Fernandes, A., Kearney, W.S., Williams, K., 2019a. Sea Level Rise and the Dynamics of the Marsh-Upland Boundary. Front. Environ. Sci. 7, 1–18. https://doi.org/10.3389/fenvs.2019.00025

Fagherazzi, S., Carniello, L., D'Alpaos, L., Defina, A., 2006. Critical bifurcation of shallow microtidal landforms in tidal flats and salt marshes. Proc. Natl. Acad. Sci. 103, 8337–8341. https://doi.org/10.1073/pnas.0508379103

Fagherazzi, S., Kirwan, M.L., Mudd, S.M., Guntenspergen, G.R., Temmerman, S., D'Alpaos, A., van de Koppel, J., Rybczyk, J.M., Reyes, E., Craft, C., Clough, J., 2012. Numerical models of salt marsh evolution: Ecological, geomorphic, and climatic factors. Rev. Geophys. 50, RG1002. https://doi.org/10.1029/2011RG000359

Fagherazzi, S., Mariotti, G., Leonardi, N., Canestrelli, A., Nardin, W., Kearney, W.S., 2020. Salt Marsh Dynamics in a Period of Accelerated Sea Level Rise. J. Geophys. Res. Earth Surf. 125, 1–31. https://doi.org/10.1029/2019JF005200

Fagherazzi, S., Nordio, G., Munz, K., Catucci, D., Kearney, W.S., 2019b. Variations in Persistence and Regenerative Zones in Coastal Forests Triggered by Sea Level Rise and Storms. Remote Sens. 11, 2019. https://doi.org/10.3390/rs11172019

Fariña, J.M., He, Q., Silliman, B.R., Bertness, M.D., 2018. Biogeography of salt marsh plant zonation on the Pacific coast of South America. J. Biogeogr. 45, 238–247. https://doi.org/10.1111/jbi.13109

Feagin, R.A., Martinez, M.L., Mendoza-Gonzalez, G., Costanza, R., 2010. Salt marsh zonal migration and ecosystem service change in response to global sea level rise: A case study from an urban region. Ecol. Soc. 15. https://doi.org/10.5751/ES-03724-150414

Fedrigo, M., Newnham, G.J., Coops, N.C., Culvenor, D.S., Bolton, D.K., Nitschke, C.R., 2018. Predicting temperate forest stand types using only structural profiles from discrete return airborne lidar. ISPRS J. Photogramm. Remote Sens. 136, 106–119. https://doi.org/10.1016/j.isprsjprs.2017.11.018

Feng, L., Han, X., Hu, C., Chen, X., 2016. Four decades of wetland changes of the largest freshwater lake in China: Possible linkage to the Three Gorges Dam? Remote Sens. Environ. 176, 43–55. https://doi.org/10.1016/j.rse.2016.01.011

FitzGerald, D.M., Hughes, Z., 2019. Marsh Processes and Their Response to Climate Change and Sea-Level Rise. Annu. Rev. Earth Planet. Sci. 47, 481–517. https://doi.org/10.1146/annurev-earth-082517-010255

Fivash, G.S., Temmink, R.J.M., D'Angelo, M., Dalen, J., Lengkeek, W., Didderen, K., Ballio, F., Heide, T., Bouma, T.J., 2021. Restoration of biogeomorphic systems by creating windows of opportunity to support

natural establishment processes. Ecol. Appl. 31. https://doi.org/10.1002/eap.2333

Foody, G.M., 2002. Status of land cover classification accuracy assessment. Remote Sens. Environ. 80, 185–201. https://doi.org/10.1016/S0034-4257(01)00295-4

Fournier, R.A., Grenier, M., Lavoie, A., Hélie, R., 2007. Towards a strategy to implement the Canadian Wetland Inventory using satellite remote sensing. Can. J. Remote Sens. 33, S1–S16. https://doi.org/10.5589/m07-051

Ganju, N.K., D'Alpaos, A., Fagherazzi, S., Carniello, L., Defne, Z., Kirwan, M.L., 2017. Spatially integrative metrics reveal hidden vulnerability of microtidal salt marshes. Nat. Commun. 8, 14156. https://doi.org/10.1038/ncomms14156

Ganju, N.K., Kirwan, M.L., Dickhudt, P.J., Guntenspergen, G.R., Cahoon, D.R., Kroeger, K.D., 2015. Sediment transport-based metrics of wetland stability. Geophys. Res. Lett. 42, 7992–8000. https://doi.org/10.1002/2015GL065980

Ge, Z.M., Wang, H., Cao, H. Bin, Zhao, B., Zhou, X., Peltola, H., Cui, L.F., Li, X.Z., Zhang, L.Q., 2016. Responses of eastern Chinese coastal salt marshes to sea-level rise combined with vegetative and sedimentary processes. Sci. Rep. 6, 1–10. https://doi.org/10.1038/srep28466

Gedan, K.B., Silliman, B.R., Bertness, M.D., 2009. Centuries of Human-Driven Change in Salt Marsh Ecosystems. Ann. Rev. Mar. Sci. 1, 117–141. https://doi.org/10.1146/annurev.marine.010908.163930

Ghosh, A., Fassnacht, F.E., Joshi, P.K., Kochb, B., 2014. A framework for mapping tree species combining hyperspectral and LiDAR data: Role of selected classifiers and sensor across three spatial scales. Int. J. Appl. Earth Obs. Geoinf. 26, 49–63. https://doi.org/10.1016/j.jag.2013.05.017

Ghosh, S., Mishra, D.R., Gitelson, A.A., 2016. Long-term monitoring of biophysical characteristics of tidal wetlands in the northern Gulf of Mexico - A methodological approach using MODIS. Remote Sens. Environ. 173, 39–58. https://doi.org/10.1016/j.rse.2015.11.015

Gilmore, M.S., Wilson, E.H., Barrett, N., Civco, D.L., Prisloe, S., Hurd, J.D., Chadwick, C., 2008a. Integrating multi-temporal spectral and structural information to map wetland vegetation in a lower Connecticut River tidal marsh. Remote Sens. Environ. 112, 4048–4060. https://doi.org/10.1016/j.rse.2008.05.020

Gilmore, M.S., Wilson, E.H., Barrett, N., Civco, D.L., Prisloe, S., Hurd, J.D., Chadwick, C., 2008b. Integrating multi-temporal spectral and structural information to map wetland vegetation in a lower Connecticut River tidal marsh. Remote Sens. Environ. 112, 4048–4060. https://doi.org/10.1016/j.rse.2008.05.020

Givnish, T.J., Volin, J.C., Owen, V.D., Volin, V.C., Muss, J.D., Glaser, P.H., 2008. Vegetation differentiation in the patterned landscape of the central Everglades: Importance of local and landscape drivers. Glob. Ecol. Biogeogr. 17, 384–402. https://doi.org/10.1111/j.1466-8238.2007.00371.x

Gong, Z., Zhang, C., Zhang, L., Bai, J., Zhou, D., 2021. Assessing spatiotemporal characteristics of native and invasive species with multi-temporal remote sensing images in the Yellow River Delta, China. L. Degrad. Dev. 32, 1338–1352. https://doi.org/10.1002/ldr.3799

Goodin, D.G., Anibas, K.L., Bezymennyi, M., 2015. Mapping land cover and land use from object-based classification: an example from a complex agricultural landscape. Int. J. Remote Sens. 36, 4702–4723. https://doi.org/10.1080/01431161.2015.1088674

Granse, D., Suchrow, S., Jensen, K., 2021. Long-term invasion dynamics of Spartina increase vegetation diversity and geomorphological resistance of salt marshes against sea level rise. Biol. Invasions 23, 871–883. https://doi.org/10.1007/s10530-020-02408-0

Green, M.O., Coco, G., 2014. Review of wave-driven sediment resuspension and transport in estuaries. Rev. Geophys. 52, 77–117. https://doi.org/10.1002/2013RG000437

Guan, H., Li, J., Chapman, M., Deng, F., Ji, Z., Yang, X., 2013. Integration of orthoimagery and lidar data for object-based urban thematic mapping using random forests. Int. J. Remote Sens. 34, 5166–5186. https://doi.org/10.1080/01431161.2013.788261

Guerschman, J.P., Scarth, P.F., McVicar, T.R., Renzullo, L.J., Malthus, T.J., Stewart, J.B., Rickards, J.E., Trevithick, R., 2015. Assessing the effects of site heterogeneity and soil properties when unmixing photosynthetic vegetation, non-photosynthetic vegetation and bare soil fractions from Landsat and MODIS data. Remote Sens. Environ. 161, 12–26. https://doi.org/10.1016/j.rse.2015.01.021

Gul, B., Ansari, R., Flowers, T.J., Khan, M.A., 2013. Germination strategies of halophyte seeds under salinity. Environ. Exp. Bot. 92, 4–18. https://doi.org/10.1016/j.envexpbot.2012.11.006

Hemminga, M.A., Buth, G.J.C., 1991. Decomposition in salt marsh ecosystems of the S.W. Netherlands: the effects of biotic and abiotic factors. Vegetatio 92, 73–83. https://doi.org/10.1007/BF00047133

Herrero, J., Castañeda, C., 2013. Changes in soil salinity in the habitats of five halophytes after 20years. Catena 109, 58–71. https://doi.org/10.1016/j.catena.2013.05.011

Himmelstoss, E.A., Henderson, R.E., Kratzmann, M.G., Farris, A.S., 2018. Digital Shoreline Analysis System (DSAS) Version 5.0 User Guide. Open-File Rep. 2018-1179 126.

Hladik, C., Alber, M., 2012. Accuracy assessment and correction of a LIDAR-derived salt marsh digital elevation model. Remote Sens. Environ. 121, 224–235. https://doi.org/10.1016/j.rse.2012.01.018

Hladik, C., Schalles, J., Alber, M., 2013. Salt marsh elevation and habitat mapping using hyperspectral and LIDAR data. Remote Sens. Environ. 139, 318–330. https://doi.org/10.1016/j.rse.2013.08.003

Hoffbeck, J.P., Landgrebe, D.A., 1994. Effect of radiance-to-reflectance transformation and atmosphere removal on maximum likelihood classification accuracy of high-dimensional remote sensing data. Int.

Geosci. Remote Sens. Symp. 4, 2538–2540. https://doi.org/10.1109/igarss.1994.399791

Hopkinson, C.S., Morris, J.T., Fagherazzi, S., Wollheim, W.M., Raymond, P.A., 2018. Lateral Marsh Edge Erosion as a Source of Sediments for Vertical Marsh Accretion. J. Geophys. Res. Biogeosciences 123, 2444–2465. https://doi.org/10.1029/2017JG004358

Horton, B.P., Shennan, I., Bradley, S.L., Cahill, N., Kirwan, M., Kopp, R.E., Shaw, T.A., 2018. Predicting marsh vulnerability to sea-level rise using Holocene relative sea-level data. Nat. Commun. 9, 4–10. https://doi.org/10.1038/s41467-018-05080-0

Houl, C.J., Campbell, C.L., Davenport, I.J., Gurney, R.J., Holden, N., 2005. Measurement of canopy geometry characteristics using LiDAR laser altimetry: a feasibility study. IEEE Trans. Geosci. Remote Sens. 43, 2270–2282. https://doi.org/10.1109/TGRS.2005.856639

Howes, N.C., FitzGerald, D.M., Hughes, Z.J., Georgiou, I.Y., Kulp, M.A., Miner, M.D., Smith, J.M., Barras, J.A., 2010. Hurricane-induced failure of low salinity wetlands. Proc. Natl. Acad. Sci. U. S. A. 107, 14014–14019. https://doi.org/10.1073/pnas.0914582107

Huckle, J.M., Potter, J.A., Marrs, R.H., 2000. Influence of environmental factors on the growth and interactions between salt marsh plants: Effects of salinity, sediment and waterlogging. J. Ecol. 88, 492–505. https://doi.org/10.1046/j.1365-2745.2000.00464.x

Hughes, A.L.H., Wilson, A.M., Morris, J.T., 2012. Hydrologic variability in a salt marsh: Assessing the links between drought and acute marsh dieback. Estuar. Coast. Shelf Sci. 111, 95–106. https://doi.org/10.1016/j.ecss.2012.06.016

Immitzer, M., Atzberger, C., Koukal, T., 2012. Tree species classification with Random forest using very high spatial resolution 8-band worldView-2 satellite data. Remote Sens. 4, 2661–2693. https://doi.org/10.3390/rs4092661

Immitzer, M., Böck, S., Einzmann, K., Vuolo, F., Pinnel, N., Wallner, A., Atzberger, C., 2018. Fractional cover mapping of spruce and pine at 1 ha resolution combining very high and medium spatial resolution satellite imagery. Remote Sens. Environ. 204, 690–703. https://doi.org/10.1016/j.rse.2017.09.031

Immitzer, M., Vuolo, F., Atzberger, C., 2016. First experience with Sentinel-2 data for crop and tree species classifications in central Europe. Remote Sens. 8. https://doi.org/10.3390/rs8030166

Jankowski, K.L., Törnqvist, T.E., Fernandes, A.M., 2017. Vulnerability of Louisiana's coastal wetlands to present-day rates of relative sea-level rise. Nat. Commun. 8, 1–7. https://doi.org/10.1038/ncomms14792

Janousek, C., Buffington, K., Thorne, K., Guntenspergen, G., Takekawa, J., Dugger, B., 2016. Potential effects of sea-level rise on plant productivity: species-specific responses in northeast Pacific tidal marshes. Mar. Ecol. Prog. Ser. 548, 111–125. https://doi.org/10.3354/meps11683

Janousek, C.N., Dugger, B.D., Drucker, B.M., Thorne, K.M., 2020. Salinity and inundation effects on productivity of brackish tidal marsh plants in the San Francisco Bay-Delta Estuary. Hydrobiologia 847, 4311–4323. https://doi.org/10.1007/s10750-020-04419-3

Janousek, C.N., Thorne, K.M., Takekawa, J.Y., 2019. Vertical Zonation and Niche Breadth of Tidal Marsh Plants Along the Northeast Pacific Coast. Estuaries and Coasts 42, 85–98. https://doi.org/10.1007/s12237-018-0420-9

Jensen, D., Cavanaugh, K.C., Simard, M., Christensen, A., Rovai, A.S., Twilley, R.R., 2020. Accretion-driven variation in vegetation composition and biomass in Louisiana's Wax Lake Delta. Estuarine, Coast Shelf Sci. 250, 107139. https://doi.org/10.1016/j.ecss.2020.107139

Jia, G.J., Epstein, H.E., Walker, D.A., 2006. Spatial heterogeneity of tundra vegetation response to recent temperature changes. Glob. Chang. Biol. 12, 42–55. https://doi.org/10.1111/j.1365-2486.2005.01079.x

Jiang, R., Tang, W., Wu, X., Fu, W., 2009. A random forest approach to the detection of epistatic interactions in case-control studies. BMC Bioinformatics 10, 1–12. https://doi.org/10.1186/1471-2105-10-S1-S65

JK, Cronk; MS, F., 2001. Wetland Plants: Biology and Ecology Lewis Publishers Boca Raton.

Juel, A., Groom, G.B., Svenning, J.C., Ejrnæs, R., 2015. Spatial application of Random Forest models for fine-scale coastal vegetation classification using object based analysis of aerial orthophoto and DEM data. Int. J. Appl. Earth Obs. Geoinf. 42, 106–114. https://doi.org/10.1016/j.jag.2015.05.008

Kearney, M.S., 2015. Microtidal Marshes: Can These Widespread and Fragile Marshes Survive Increasing Climate–Sea Level Variability and Human Action? J. Coast. Res. 32, 686. https://doi.org/10.2112/jcoastres-d-15-00069.1

Kearney, M.S., Stutzer, D., Turpie, K., Stevenson, J.C., 2009. The Effects of Tidal Inundation on the Reflectance Characteristics of Coastal Marsh Vegetation. J. Coast. Res. 256, 1177–1186. https://doi.org/10.2112/08-1080.1

Kéfi, S., Rietkerk, M., Alados, C.L., Pueyo, Y., Papanastasis, V.P., ElAich, A., De Ruiter, P.C., 2007. Spatial vegetation patterns and imminent desertification in Mediterranean arid ecosystems. Nature 449, 213–217. https://doi.org/10.1038/nature06111

Kéfi, S., Rietkerk, M., Roy, M., Franc, A., De Ruiter, P.C., Pascual, M., 2011. Robust scaling in ecosystems and the meltdown of patch size distributions before extinction. Ecol. Lett. 14, 29–35. https://doi.org/10.1111/j.1461-0248.2010.01553.x

Kirwan, M.L., Gedan, K.B., 2019. Sea-level driven land conversion and the formation of ghost forests. Nat. Clim. Chang. 9, 450–457. https://doi.org/10.1038/s41558-019-0488-7

Kirwan, M.L., Guntenspergen, G.R., 2012. Feedbacks between inundation, root production, and shoot growth in

a rapidly submerging brackish marsh. J. Ecol. 100, 764–770. https://doi.org/10.1111/j.1365-2745.2012.01957.x

Kirwan, M.L., Guntenspergen, G.R., 2010. Influence of tidal range on the stability of coastal marshland. J. Geophys. Res. Earth Surf. 115, 1–11. https://doi.org/10.1029/2009jf001400

Kirwan, M.L., Guntenspergen, G.R., D'Alpaos, A., Morris, J.T., Mudd, S.M., Temmerman, S., 2010. Limits on the adaptability of coastal marshes to rising sea level. Geophys. Res. Lett. 37, 1–5. https://doi.org/10.1029/2010GL045489

Kirwan, M.L., Langley, J.A., Guntenspergen, G.R., Megonigal, J.P., 2013. The impact of sea-level rise on organic matter decay rates in Chesapeake Bay brackish tidal marshes. Biogeosciences 10, 1869–1876. https://doi.org/10.5194/bg-10-1869-2013

Kirwan, M.L., Megonigal, J.P., 2013. Tidal wetland stability in the face of human impacts and sea-level rise. Nature 504, 53–60. https://doi.org/10.1038/nature12856

Kirwan, M.L., Mudd, S.M., 2012. Response of salt-marsh carbon accumulation to climate change. Nature 489, 550–553. https://doi.org/10.1038/nature11440

Kirwan, M.L., Murray, A.B., 2008. Ecological and morphological response of brackish tidal marshland to the next century of sea level rise: Westham Island, British Columbia. Glob. Planet. Change 60, 471–486. https://doi.org/10.1016/j.gloplacha.2007.05.005

Kirwan, M.L., Murray, A.B., 2007. A coupled geomorphic and ecological model of tidal marsh evolution. Proc. Natl. Acad. Sci. 104, 6118–6122. https://doi.org/10.1073/pnas.0700958104

Kirwan, M.L., Temmerman, S., Skeehan, E.E., Guntenspergen, G.R., Fagherazzi, S., 2016a. Overestimation of marsh vulnerability to sea level rise. Nat. Clim. Chang. 6, 253–260. https://doi.org/10.1038/nclimate2909

Kirwan, M.L., Walters, D.C., Reay, W.G., Carr, J.A., 2016b. Model of Marsh Erosion and Migration. Geophys. Res. Lett. 43, 4366–4373. https://doi.org/10.1002/2016GL068507.Received

Klemas, V., 2011. Remote sensing of wetlands: Case studies comparing practical techniques. J. Coast. Res. 27, 418–427. https://doi.org/10.2112/JCOASTRES-D-10-00174.1

Koftis, T., Prinos, P., Stratigaki, V., 2013. Wave damping over artificial Posidonia oceanica meadow: A large-scale experimental study. Coast. Eng. 73, 71–83. https://doi.org/10.1016/j.coastaleng.2012.10.007

Koppel, J. van de, Wal, D. van der, Bakker, J.P., Herman, P.M.J., 2005. Self-Organization and Vegetation Collapse in Salt Marsh Ecosystems. Am. Nat. 165, E1–E12. https://doi.org/10.1086/426602

Korhonen, L., Korpela, I., Heiskanen, J., Maltamo, M., 2011. Airborne discrete-return LIDAR data in the estimation of vertical canopy cover, angular canopy closure and leaf area index. Remote Sens. Environ.

115, 1065–1080. https://doi.org/10.1016/j.rse.2010.12.011

Kulawardhana, R.W., Popescu, S.C., Feagin, R.A., 2014. Fusion of lidar and multispectral data to quantify salt marsh carbon stocks. Remote Sens. Environ. 154, 345–357. https://doi.org/10.1016/j.rse.2013.10.036

Kulkarni, A.D., Lowe, B., 2016. Random Forest Algorithm for Land Cover Classification. Int. J. Recent Innov. Trends Comput. Commun. 4, 58–63.

Kumar, U., Ganguly, S., Nemani, R.R., Raja, K.S., Milesi, C., Sinha, R., Michaelis, A., Votava, P., Hashimoto, H., Li, S., Wang, W., Kalia, S., Gayaka, S., 2017. Exploring subpixel learning algorithms for estimating global land cover fractions from satellite data using high performance computing. Remote Sens. 9. https://doi.org/10.3390/rs9111105

Ladd, C.J.T., Duggan-Edwards, M.F., Bouma, T.J., Pagès, J.F., Skov, M.W., 2019. Sediment Supply Explains Long-Term and Large-Scale Patterns in Salt Marsh Lateral Expansion and Erosion. Geophys. Res. Lett. 46, 11178–11187. https://doi.org/10.1029/2019GL083315

Laengner, M.L., Siteur, K., van der Wal, D., 2019. Trends in the seaward extent of saltmarshes across Europe from long-term satellite data. Remote Sens. 11, 1–25. https://doi.org/10.3390/rs11141653

Langston, A.K., Durán Vinent, O., Herbert, E.R., Kirwan, M.L., 2020. Modeling long-term salt marsh response to sea level rise in the sediment-deficient Plum Island Estuary, MA. Limnol. Oceanogr. 65, 2142–2157. https://doi.org/10.1002/lno.11444

Lantz, N.J., Wang, J., 2013. Object-based classification of Worldview-2 imagery for mapping invasive common reed, Phragmites australis. Can. J. Remote Sens. 39, 328–340. https://doi.org/10.5589/m13-041

Le Bouteiller, C., Venditti, J.G., 2015. Sediment transport and shear stress partitioning in a vegetated flow. Water Resour. Res. 51, 2901–2922. https://doi.org/10.1002/2014WR015825

Leonard, L.A., Croft, A.L., 2006. The effect of standing biomass on flow velocity and turbulence in Spartina alterniflora canopies. Estuar. Coast. Shelf Sci. 69, 325–336. https://doi.org/10.1016/j.ecss.2006.05.004

Leonard, L.A., Luther, M.E., 1995. Flow hydrodynamics in tidal marsh canopies. Limnol. Oceanogr. 40, 1474–1484. https://doi.org/10.4319/lo.1995.40.8.1474

Leonardi, N., Defne, Z., Ganju, N.K., Fagherazzi, S., 2016. Salt marsh erosion rates and boundary features in a shallow Bay. J. Geophys. Res. Earth Surf. 121, 1861–1875. https://doi.org/10.1002/2016JF003975

Leonardi, N., Fagherazzi, S., 2014. How waves shape salt marshes. Geology 42, 887–890. https://doi.org/10.1130/G35751.1

Li, W.Q., Liu, X.Z., Khan, M.A., Gul, B., 2008. Relationship between soil characteristics and halophytic vegetation in coastal region of north china. Pakistan J. Bot. 40, 1081–1090.

Liao, C.Z., Luo, Y.Q., Fang, C.M., Chen, J.K., Li, B., 2008. Litter pool sizes, decomposition, and nitrogen dynamics in Spartina alterniflora-invaded and native coastal marshlands of the Yangtze Estuary. Oecologia 156, 589–600. https://doi.org/10.1007/s00442-008-1007-0

Lightbody, A.F., Nepf, H.M., 2006. Prediction of velocity profiles and longitudinal dispersion in emergent salt marsh vegetation. Limnol. Oceanogr. 51, 218–228. https://doi.org/10.4319/lo.2006.51.1.0218

Lin, Y., Han, G., Zhao, M., Chang, S.X., 2010. Spatial vegetation patterns as early signs of desertification: A case study of a desert steppe in Inner Mongolia, China. Landsc. Ecol. 25, 1519–1527. https://doi.org/10.1007/s10980-010-9520-z

Liu, K., Shi, W., Zhang, H., 2011. A fuzzy topology-based maximum likelihood classification. ISPRS J. Photogramm. Remote Sens. 66, 103–114. https://doi.org/10.1016/j.isprsjprs.2010.09.007

Liu, M., Yang, W., Chen, J., Chen, X., 2017. An Orthogonal Fisher Transformation-Based Unmixing Method Toward Estimating Fractional Vegetation Cover in Semiarid Areas. IEEE Geosci. Remote Sens. Lett. 14, 449–453. https://doi.org/10.1109/LGRS.2017.2648863

Liu, X., Liu, H., Qiu, S., Wu, X., Tian, Y., Hao, Q., 2017. An improved estimation of regional fractional woody/herbaceous cover using combined satellite data and high-quality training samples. Remote Sens. 9. https://doi.org/10.3390/rs9010032

Llauss, A., Nogué, J., 2012. Indicators of landscape fragmentation: The case for combining ecological indices and the perceptive approach. Ecol. Indic. 15, 85–91. https://doi.org/10.1016/j.ecolind.2011.08.016

Loder, N.M., Irish, J.L., Cialone, M.A., Wamsley, T. V., 2009. Sensitivity of hurricane surge to morphological parameters of coastal wetlands. Estuar. Coast. Shelf Sci. 84, 625–636. https://doi.org/10.1016/j.ecss.2009.07.036

Lopatin, J., Dolos, K., Hernández, H.J., Galleguillos, M., Fassnacht, F.E., 2016. Comparing Generalized Linear Models and random forest to model vascular plant species richness using LiDAR data in a natural forest in central Chile. Remote Sens. Environ. 173, 200–210. https://doi.org/10.1016/j.rse.2015.11.029

Lopes, C.L., Mendes, R., Caçador, I., Dias, J.M., 2020. Assessing salt marsh extent and condition changes with 35 years of Landsat imagery: Tagus Estuary case study. Remote Sens. Environ. 247, 111939. https://doi.org/10.1016/j.rse.2020.111939

Ma, L., Li, M., Ma, X., Cheng, L., Du, P., Liu, Y., 2017. A review of supervised object-based land-cover image classification. ISPRS J. Photogramm. Remote Sens. 130, 277–293. https://doi.org/10.1016/j.isprsjprs.2017.06.001

Mahdianpari, M., Jafarzadeh, H., Granger, J.E., Mohammadimanesh, F., Brisco, B., Salehi, B., Homayouni, S., Weng, Q., 2020. A large-scale change monitoring of wetlands using time series Landsat imagery on Google Earth Engine: a case study in Newfoundland. GIScience Remote Sens. 57, 1102–1124.

https://doi.org/10.1080/15481603.2020.1846948

Marani, M., Belluco, E., D'Alpaos, A., Defina, A., Lanzoni, S., Rinaldo, A., 2003a. On the drainage density of tidal networks. Water Resour. Res. 39, 1–11. https://doi.org/10.1029/2001WR001051

Marani, M., Belluco, E., Ferrari, S., Silvestri, S., D'Alpaos, A., Lanzoni, S., Feola, A., Rinaldo, A., 2006a. Analysis, synthesis and modelling of high-resolution observations of salt-marsh eco-geomorphological patterns in the Venice lagoon. Estuar. Coast. Shelf Sci. 69, 414–426. https://doi.org/10.1016/j.ecss.2006.05.021

Marani, M., D'Alpaos, A., Lanzoni, S., Carniello, L., Rinaldo, A., 2010a. The importance of being coupled: Stable states and catastrophic shifts in tidal biomorphodynamics. J. Geophys. Res. Earth Surf. 115, 1–15. https://doi.org/10.1029/2009JF001600

Marani, M., D'Alpaos, A., Lanzoni, S., Carniello, L., Rinaldo, A., 2010b. The importance of being coupled: Stable states and catastrophic shifts in tidal biomorphodynamics. J. Geophys. Res. Earth Surf. 115, 1–15. https://doi.org/10.1029/2009JF001600

Marani, M., D'Alpaos, A., Lanzoni, S., Carniello, L., Rinaldo, A., 2007. Biologically-controlled multiple equilibria of tidal landforms and the fate of the Venice lagoon. Geophys. Res. Lett. 34, 1–5. https://doi.org/10.1029/2007GL030178

Marani, M., D'Alpaos, A., Lanzoni, S., Santalucia, M., 2011a. Understanding and predicting wave erosion of marsh edges. Geophys. Res. Lett. 38. https://doi.org/10.1029/2011GL048995

Marani, M., D'Alpaos, A., Lanzoni, S., Santalucia, M., 2011b. Understanding and predicting wave erosion of marsh edges. Geophys. Res. Lett. 38, 1–5. https://doi.org/10.1029/2011GL048995

Marani, M., Da Lio, C., D'Alpaos, A., 2013. Vegetation engineers marsh morphology through multiple competing stable states. Proc. Natl. Acad. Sci. 110, 3259–3263. https://doi.org/10.1073/pnas.1218327110

Marani, M., Lanzoni, S., Silvestri, S., Rinaldo, A., 2004. Tidal landforms, patterns of halophytic vegetation and the fate of the lagoon of Venice. J. Mar. Syst. 51, 191–210. https://doi.org/10.1016/j.jmarsys.2004.05.012

Marani, M., Silvestri, S., Belluco, E., Camuffo, M., D'Alpaos, A., Lanzoni, S., Marani, A., Rinaldo, A., 2003b. Patterns in tidal environments: Salt-marsh channel networks and vegetation. Int. Geosci. Remote Sens. Symp. 5, 3269–3271.

Marani, M., Silvestri, S., Belluco, E., Camuffo, M., D'Alpaos, A., Lanzoni, S., Marani, A., Rinaldo, A., 2003c. Patterns in tidal environments: salt-marsh channel networks and vegetation. Int. Geosci. Remote Sens. Symp. Proc. (IEEE Cat. No.03CH37477) 5, 3269–3271. https://doi.org/10.1109/IGARSS.2003.1294752

Marani, M., Silvestri, S., Belluco, E., Ursino, N., Comerlati, A., Tosatto, O., Putti, M., 2006b. Spatial organization and ecohydrological interactions in oxygen-limited vegetation ecosystems. Water Resour.

Res. 42, 1–12. https://doi.org/10.1029/2005WR004582

Marani, M., Zillio, T., Belluco, E., Silvestri, S., Maritan, A., 2006c. Non-neutral vegetation dynamics. PLoS One 1. https://doi.org/10.1371/journal.pone.0000078

Mariotti, G., Carr, J., 2014. Dual role of salt marsh retreat: long-term loss and short-term resilience 2963–2974. https://doi.org/10.1002/2013WR014676.Received

Mariotti, G., Fagherazzi, S., 2013. Critical width of tidal flats triggers marsh collapse in the absence of sea-level rise. Proc. Natl. Acad. Sci. U. S. A. 110, 5353–5356. https://doi.org/10.1073/pnas.1219600110

Matthew, M.W., Adler-Golden, S.M., Berk, A., Felde, G., Anderson, G.P., Gorodetzky, D., Paswaters, S., Shippert, M., 2002. Atmospheric correction of spectral imagery: Evaluation of the FLAASH algorithm with AVIRIS data. Proc. - Appl. Imag. Pattern Recognit. Work. 2002-Janua, 157–163. https://doi.org/10.1109/AIPR.2002.1182270

Maurer, T., 2013. HOW TO PAN-SHARPEN IMAGES USING THE GRAM-SCHMIDT PAN-SHARPEN METHOD – A RECIPE. ISPRS - Int. Arch. Photogramm. Remote Sens. Spat. Inf. Sci. XL-1/W1, 239–244. https://doi.org/10.5194/isprsarchives-XL-1-W1-239-2013

McLeod, E., Chmura, G.L., Bouillon, S., Salm, R., Björk, M., Duarte, C.M., Lovelock, C.E., Schlesinger, W.H., Silliman, B.R., 2011. A blueprint for blue carbon: Toward an improved understanding of the role of vegetated coastal habitats in sequestering CO2. Front. Ecol. Environ. 9, 552–560. https://doi.org/10.1890/110004

Mel, R., Viero, D. Pietro, Carniello, L., Defina, A., D'Alpaos, L., 2014. Simplified methods for real-time prediction of storm surge uncertainty: The city of Venice case study. Adv. Water Resour. 71, 177–185. https://doi.org/10.1016/j.advwatres.2014.06.014

Melville, B., Fisher, A., Lucieer, A., 2019. Ultra-high spatial resolution fractional vegetation cover from unmanned aerial multispectral imagery. Int. J. Appl. Earth Obs. Geoinf. 78, 14–24. https://doi.org/10.1016/j.jag.2019.01.013

Menze, B.H., Kelm, B.M., Masuch, R., Himmelreich, U., Bachert, P., Petrich, W., Hamprecht, F.A., 2009. A comparison of random forest and its Gini importance with standard chemometric methods for the feature selection and classification of spectral data. BMC Bioinformatics 10, 1–16. https://doi.org/10.1186/1471-2105-10-213

Mitsch, W.J., Gossilink, J.G., 2000. The value of wetlands: Importance of scale and landscape setting. Ecol. Econ. 35, 25–33. https://doi.org/10.1016/S0921-8009(00)00165-8

Moffett, K.B., Gorelick, S.M., 2016. Alternative stable states of tidal marsh vegetation patterns and channel complexity. Ecohydrology 9, 1639–1662. https://doi.org/10.1002/eco.1755

Moffett, K.B., Gorelick, S.M., 2013. Distinguishing wetland vegetation and channel features with object-based image segmentation. Int. J. Remote Sens. 34, 1332–1354. https://doi.org/10.1080/01431161.2012.718463

Moffett, K.B., Gorelick, S.M., McLaren, R.G., Sudicky, E.A., 2012. Salt marsh ecohydrological zonation due to heterogeneous vegetation-groundwater-surface water interactions. Water Resour. Res. 48. https://doi.org/10.1029/2011WR010874

Moffett, K.B., Nardin, W., Silvestri, S., Wang, C., Temmerman, S., 2015. Multiple stable states and catastrophic shifts in coastal wetlands: Progress, challenges, and opportunities in validating theory using remote sensing and other methods. Remote Sens. 7, 10184–10226. https://doi.org/10.3390/rs70810184

Moffett, K.B., Robinson, D.A., Gorelick, S.M., 2010. Relationship of Salt Marsh Vegetation Zonation to Spatial Patterns in Soil Moisture, Salinity, and Topography. Ecosystems 13, 1287–1302. https://doi.org/10.1007/s10021-010-9385-7

Möller, I., Kudella, M., Rupprecht, F., Spencer, T., Paul, M., Van Wesenbeeck, B.K., Wolters, G., Jensen, K., Bouma, T.J., Miranda-Lange, M., Schimmels, S., 2014. Wave attenuation over coastal salt marshes under storm surge conditions. Nat. Geosci. 7, 727–731. https://doi.org/10.1038/NGEO2251

Möller, I., Spencer, T., 2002. Wave dissipation over macro-tidal saltmarshes: Effects of marsh edge typology and vegetation change. J. Coast. Res. 36, 506–521. https://doi.org/10.2112/1551-5036-36.sp1.506

Möller, I., Spencer, T., French, J.R., Leggett, D.J., Dixon, M., 1999. Wave transformation over salt marshes: A field and numerical modelling study from north Norfolk, England. Estuar. Coast. Shelf Sci. 49, 411–426. https://doi.org/10.1006/ecss.1999.0509

Morris, J.T., 2006. Competition among marsh macrophytes by means of geomorphological displacement in the intertidal zone. Estuar. Coast. Shelf Sci. 69, 395–402. https://doi.org/10.1016/j.ecss.2006.05.025

Morris, J.T., 1990. A 5-yr Record of Aerial Primary Production and Stand Characteristics of Spartina Alterniflora Author (s): James T . Morris and Betsy Haskin Published by : Ecological Society of America A 5-YR RECORD OF AERIAL PRIMARY PRODUCTION OF AND STAND CHARACTERIST. Ecol. Soc. Am. 71, 2209–2217.

Morris, J.T., Haskin, B., 1990. A 5-yr Record of Aerial Primary Production and Stand Characteristics of Spartina Alterniflora. Ecology 71, 2209–2217. https://doi.org/10.2307/1938633

Morris, J.T., Sundareshwar, P.V., Nietch, C.T., Kjerfve, B., Cahoon, D.R., 2002. Sea Level of Coastal Wetlands To Ristng Responses 83, 2869–2877. https://doi.org/10.1890/0012-9658%282002%29083%5B2869%3AROCWTR%5D2.0.CO%3B2

Mudd, S.M., D'Alpaos, A., Morris, J.T., 2010. How does vegetation affect sedimentation on tidal marshes? Investigating particle capture and hydrodynamic controls on biologically mediated sedimentation. J. Geophys. Res. Earth Surf. 115, 1–14. https://doi.org/10.1029/2009JF001566

Mudd, S.M., Fagherazzi, S., Morris, J.T., Furbish, D.J., 2004. Flow, Sedimentation, and Biomass Production on a Vegetated Salt Marsh in South Carolina: Toward a Predictive Model of Marsh Morphologic and Ecologic Evolution. pp. 165–188. https://doi.org/10.1029/CE059p0165

Mudd, S.M., Howell, S.M., Morris, J.T., 2009. Impact of dynamic feedbacks between sedimentation, sea-level rise, and biomass production on near-surface marsh stratigraphy and carbon accumulation. Estuar. Coast. Shelf Sci. 82, 377–389. https://doi.org/10.1016/j.ecss.2009.01.028

Mueller, P., Do, H.T., Jensen, K., Nolte, S., 2019a. Origin of organic carbon in the topsoil of Wadden Sea salt marshes. Mar. Ecol. Prog. Ser. 624, 39–50. https://doi.org/10.3354/meps13009

Mueller, P., Jensen, K., Megonigal, J.P., 2016. Plants mediate soil organic matter decomposition in response to sea level rise. Glob. Chang. Biol. 22, 404–414. https://doi.org/10.1111/gcb.13082

Mueller, P., Ladiges, N., Jack, A., Schmiedl, G., Kutzbach, L., Jensen, K., Nolte, S., 2019b. Assessing the long-term carbon-sequestration potential of the semi-natural salt marshes in the European Wadden Sea. Ecosphere 10. https://doi.org/10.1002/ecs2.2556

Muñoz-Rodríguez, A.F., Sanjosé, I., Márquez-García, B., Infante-Izquierdo, M.D., Polo-Ávila, A., Nieva, F.J.J., Castillo, J.M., 2017. Germination syndromes in response to salinity of Chenopodiaceae halophytes along the intertidal gradient. Aquat. Bot. 139, 48–56. https://doi.org/10.1016/j.aquabot.2017.02.003

Murray, A.B., Knaapen, M.A.F., Tal, M., Kirwan, M.L., 2008. Biomorphodynamics: Physical-biological feedbacks that shape landscapes. Water Resour. Res. 44, 1–18. https://doi.org/10.1029/2007WR006410

Negrin, V.L., Pratolongo, P.D., Villalobos, A.E. De, Botté, S.E., Marcovecchio, J.E., 2015. Biomass , decomposition and nutrient cycling in a SW Atlantic Sarcocornia perennis marsh. J. Sea Res. 97, 50–55. https://doi.org/10.1016/j.seares.2014.12.001

Nicholls, R.J., Cazenave, A., 2010. Sea-level rise and its impact on coastal zones. Science (80-.). 328, 1517–1520. https://doi.org/10.1126/science.1185782

O'Connell, J.L., Mishra, D.R., Alber, M., Byrd, K.B., 2021. BERM: a Belowground Ecosystem Resiliency Model for estimating Spartina alterniflora belowground biomass. New Phytol. 232, 425–439. https://doi.org/10.1111/nph.17607

O'Neil, G.L., Goodall, J.L., Watson, L.T., 2018. Evaluating the potential for site-specific modification of LiDAR DEM derivatives to improve environmental planning-scale wetland identification using Random Forest classification. J. Hydrol. 559, 192–208. https://doi.org/10.1016/j.jhydrol.2018.02.009

Olliver, E.A., Edmonds, D.A., 2017. Defining the ecogeomorphic succession of land building for freshwater, intertidal wetlands in Wax Lake Delta, Louisiana. Estuar. Coast. Shelf Sci. 196, 45–57. https://doi.org/10.1016/j.ecss.2017.06.009

Osland, M.J., Enwright, N., Stagg, C.L., 2014. Freshwater availability and coastal wetland foundation species: Ecological transitions along a rainfall gradient. Ecology 95, 2778–2788. https://doi.org/10.1890/13-1269.1

Pal, M., 2005. Random forest classifier for remote sensing classification. Int. J. Remote Sens. 26, 217–222. https://doi.org/10.1080/01431160412331269698

Palubinskas, G., 2013. Fast, simple, and good pan-sharpening method. J. Appl. Remote Sens. 7, 073526. https://doi.org/10.1117/1.jrs.7.073526

Pan, F., Xie, J., Lin, J., Zhao, T., Ji, Y., Hu, Q., Pan, X., Wang, C., Xi, X., 2018. Evaluation of climate change impacts on wetland vegetation in the Dunhuang Yangguan National Nature Reserve in northwest China using landsat derived NDVI. Remote Sens. 10. https://doi.org/10.3390/rs10050735

Pascual, M., Roy, M., Guichard, F., Flierl, G., 2002. Cluster size distributions: Signatures of self-organization in spatial ecologies. Philos. Trans. R. Soc. B Biol. Sci. 357, 657–666. https://doi.org/10.1098/rstb.2001.0983

Passalacqua, P., Belmont, P., Staley, D.M., Simley, J.D., Arrowsmith, J.R., Bode, C.A., Crosby, C., DeLong, S.B., Glenn, N.F., Kelly, S.A., Lague, D., Sangireddy, H., Schaffrath, K., Tarboton, D.G., Wasklewicz, T., Wheaton, J.M., 2015. Analyzing high resolution topography for advancing the understanding of mass and energy transfer through landscapes: A review. Earth-Science Rev. 148, 174–193. https://doi.org/10.1016/j.earscirev.2015.05.012

Patil, V., Singh, A., Naik, N., Unnikrishnan, S., 2015. Estimation of Mangrove Carbon Stocks by Applying Remote Sensing and GIS Techniques. Wetlands 35, 695–707. https://doi.org/10.1007/s13157-015-0660-4

Pedregosa, F., Varoquaux, G., Gramfort, A., Michel, V., Thirion, B., Grisel, O., Blondel, M., Prettenhofer, P., Weiss, R., Dubourg, V., Vanderplas, J., Passos, A., Cournapeau, D., Brucher, M., Perrot, M., E, D., 2011. Scikit-learn: Machine Learning in Python. J. Mach. Learn. Res. 12, 2825–2830. https://doi.org/10.1145/2786984.2786995

Pellegrini, E., Boscutti, F., De Nobili, M., Casolo, V., 2018a. Plant traits shape the effects of tidal flooding on soil and plant communities in saltmarshes. Plant Ecol. 219, 823–835. https://doi.org/10.1007/s11258-018-0837-z

Pellegrini, E., Boscutti, F., De Nobili, M., Casolo, V., 2018b. Plant traits shape the effects of tidal flooding on soil and plant communities in saltmarshes. Plant Ecol. 219, 823–835. https://doi.org/10.1007/s11258-018-0837-z

Pellegrini, E., Forlani, G., Boscutti, F., Casolo, V., 2020a. Evidence of non-structural carbohydrates-mediated response to flooding and salinity in Limonium narbonense and Salicornia fruticosa. Aquat. Bot. 166, 103265. https://doi.org/10.1016/j.aquabot.2020.103265

Pellegrini, E., Forlani, G., Boscutti, F., Casolo, V., 2020b. Evidence of non-structural carbohydrates-mediated response to flooding and salinity in Limonium narbonense and Salicornia fruticosa. Aquat. Bot. 166,

103265. https://doi.org/10.1016/j.aquabot.2020.103265

Pellegrini, E., Konnerup, D., Winkel, A., Casolo, V., Pedersen, O., 2017. Contrasting oxygen dynamics in Limonium narbonense and Sarcocornia fruticosa during partial and complete submergence. Funct. Plant Biol. 44, 867. https://doi.org/10.1071/fp16369

Penk, M.R., Perrin, P.M., Waldren, S., 2020. Above- to Belowground Vegetation Biomass Ratio in Temperate North- East Atlantic Saltmarshes Increases Strongly with Soil Nitrogen Gradient. Ecosystems 23, 648–661. https://doi.org/10.1007/s10021-019-00428-z

Pennings, S.C., Callaway, R.M., 1996. Impact of a parasitic plant on the structure and dynamics of salt marsh vegetation. Ecology 77, 1410–1419. https://doi.org/10.2307/2265538

Pennings, Steven C, Callaway, R.M., 1992. Salt Marsh Plant Zonation: The Relative Importance of Competition and Physical Factors. Ecology 73, 681–690. https://doi.org/10.2307/1940774

Pennings, Steven C., Callaway, R.M., 1992. Salt Marsh Plant Zonation: The Relative Importance of Competition and Physical Factors. Ecology 73, 681–690. https://doi.org/10.2307/1940774

Pennings, Steven C, Grant, M., Bertness, M.D., 2005. Plant zonation in low-latitude salt marshes : disentangling the roles of flooding , salinity and competition 159–167. https://doi.org/10.1111/j.1365-2745.2004.00959.x

Pennings, Steven C., Grant, M.B., Bertness, M.D., 2005. Plant zonation in low-latitude salt marshes: Disentangling the roles of flooding, salinity and competition. J. Ecol. 93, 159–167. https://doi.org/10.1111/j.1365-2745.2004.00959.x

Pennings, S.C., Ho, C.K., Salgado, C.S., Wieski, K., Dav??, N., Kunza, A.E., Wason, E.L., 2009. Latitudinal variation in herbivore pressure in Atlantic Coast salt marshes. Ecology 90, 183–195. https://doi.org/10.1890/08-0222.1

Pennings, S.C., Moore, D.J., 2001. Zonation of shrubs in western Atlantic salt marshes. Oecologia 126, 587–594. https://doi.org/10.1007/s004420000548

Pennings, S.C., Selig, E.R., Houser, L.T., Bertness, M.D., 2003. Geographic variation in positive and negative interactions among salt marsh plants. Ecology 84, 1527–1538. https://doi.org/10.1890/0012-9658(2003)084[1527:GVIPAN]2.0.CO;2

Pinton, D., Canestrelli, A., Wilkinson, B., Ifju, P., Ortega, A., 2020. A new algorithm for estimating ground elevation and vegetation characteristics in coastal salt marshes from high-resolution UAV-based LiDAR point clouds. Earth Surf. Process. Landforms 45, 3687–3701. https://doi.org/10.1002/esp.4992

Pozo, J., Colino, R., 1992. Decomposition processes of Spartina maritima in a salt marsh of the Basque Country. Hydrobiologia 231, 165–175. https://doi.org/10.1007/BF00018200

Priestas, A.M., Mariotti, G., Leonardi, N., Fagherazzi, S., 2015. Coupled wave energy and erosion dynamics along a salt marsh boundary, hog island bay, Virginia, USA. J. Mar. Sci. Eng. 3, 1041–1065. https://doi.org/10.3390/jmse3031041

Pueyo, S., 2011. Desertification and power laws. Landsc. Ecol. 26, 305–309. https://doi.org/10.1007/s10980-010-9569-8

Qi, M., MacGregor, J., Gedan, K., 2021. Biogeomorphic patterns emerge with pond expansion in deteriorating marshes affected by relative sea level rise. Limnol. Oceanogr. 66, 1036–1049. https://doi.org/10.1002/lno.11661

Qi, M., Sun, T., Xue, S.F., Yang, W., Shao, D.D., Martínez-López, J., 2018. Competitive ability, stress tolerance and plant interactions along stress gradients. Ecology 99, 848–857. https://doi.org/10.1002/ecy.2147

Raabe, E.A., Stumpf, R.P., 2016. Expansion of Tidal Marsh in Response to Sea-Level Rise: Gulf Coast of Florida, USA. Estuaries and Coasts 39, 145–157. https://doi.org/10.1007/s12237-015-9974-y

Raposa, K.B., Weber, R.L.J., Ekberg, M.C., Ferguson, W., 2017. Vegetation Dynamics in Rhode Island Salt Marshes During a Period of Accelerating Sea Level Rise and Extreme Sea Level Events. Estuaries and Coasts 40, 640–650. https://doi.org/10.1007/s12237-015-0018-4

Ratliff, K.M., Braswell, A.E., Marani, M., 2015. Spatial response of coastal marshes to increased atmospheric CO2. Proc. Natl. Acad. Sci. U. S. A. 112, 15580–15584. https://doi.org/10.1073/pnas.1516286112

Reents, S., Mueller, P., Tang, H., Jensen, K., Nolte, S., 2021. Plant genotype determines biomass response to flooding frequency in tidal wetlands. Biogeosciences 18, 403–411. https://doi.org/10.5194/bg-18-403-2021

Reschke, J., Hüttich, C., 2014. Continuous field mapping of Mediterranean wetlands using sub-pixel spectral signatures and multi-temporal Landsat data. Int. J. Appl. Earth Obs. Geoinf. 28, 220–229. https://doi.org/10.1016/j.jag.2013.12.014

Richardson, J.J., Moskal, L.M., Kim, S.H., 2009. Modeling approaches to estimate effective leaf area index from aerial discrete-return LIDAR. Agric. For. Meteorol. 149, 1152–1160. https://doi.org/10.1016/j.agrformet.2009.02.007

Richter, R., Schläpfer, D., 2002. Geo-atmospheric processing of airborne imaging spectrometry data. Part 2: Atmospheric/topographic correction. Int. J. Remote Sens. 23, 2631–2649. https://doi.org/10.1080/01431160110115834

Roelfsema, C.M., Lyons, M., Kovacs, E.M., Maxwell, P., Saunders, M.I., Samper-Villarreal, J., Phinn, S.R., 2014. Multi-temporal mapping of seagrass cover, species and biomass: A semi-automated object based image analysis approach. Remote Sens. Environ. 150, 172–187. https://doi.org/10.1016/j.rse.2014.05.001

Rogers, J.N., Parrish, C.E., Ward, L.G., Burdick, D.M., 2018. Improving salt marsh digital elevation model accuracy with full-waveform lidar and nonparametric predictive modeling. Estuar. Coast. Shelf Sci. 202, 193–211. https://doi.org/10.1016/j.ecss.2017.11.034

Roner, M, D'Alpaos, A., Ghinassi, M., Marani, M., Silvestri, S., Franceschinis, E., Realdon, N., 2016. Spatial variation of salt-marsh organic and inorganic deposition and organic carbon accumulation: Inferences from the Venice lagoon, Italy. Adv. Water Resour. 93, 276–287. https://doi.org/10.1016/j.advwatres.2015.11.011

Roner, M., D'Alpaos, A., Ghinassi, M., Marani, M., Silvestri, S., Franceschinis, E., Realdon, N., 2016. Spatial variation of salt-marsh organic and inorganic deposition and organic carbon accumulation: Inferences from the Venice lagoon, Italy. Adv. Water Resour. 93, 276–287. https://doi.org/10.1016/j.advwatres.2015.11.011

Rosenfield, G.H.F.-L.K., 1986. A coefficient of agreement as a measure of thematic classification accuracy. Photogramm. Eng. Remote Sensing 52, 223–227.

Rouse, J., Haas, R., Schell, J., Deering, D., 1974. Monitoring vegetation systems in the Great Plains with ERTS, in: NASA Special Publication. pp. 309–317.

Rupprecht, F., Möller, I., Paul, M., Kudella, M., Spencer, T., van Wesenbeeck, B.K., Wolters, G., Jensen, K., Bouma, T.J., Miranda-Lange, M., Schimmels, S., 2017. Vegetation-wave interactions in salt marshes under storm surge conditions. Ecol. Eng. 100, 301–315. https://doi.org/10.1016/j.ecoleng.2016.12.030

Sadro, S., Gastil-Buhl, M., Melack, J., 2007. Characterizing patterns of plant distribution in a southern California salt marsh using remotely sensed topographic and hyperspectral data and local tidal fluctuations. Remote Sens. Environ. 110, 226–239. https://doi.org/10.1016/j.rse.2007.02.024

Sanderson, E.W., Foin, T.C., Ustin, S.L., 2001. A simple empirical model of salt marsh plant spatial distributions with respect to a tidal channel network. Ecol. Modell. 139, 293–307. https://doi.org/10.1016/S0304-3800(01)00253-8

Sanderson, E.W., Ustin, S.L., Foin, T.C., 2000. The influence of tidal channels on the distribution of salt marsh plant species in Petaluma Marsh , CA , USA 29–41.

Sanderson, E.W., Zhang, M., Ustin, S.L., Rejmankova, E., 1998. Geostatistical scaling of canopy water content in a California salt marsh. Landsc. Ecol. 13, 79–92. https://doi.org/10.1023/A:1007961516096

Sanpayao, M., Kasetkasem, T., Rakwatin, P., Isshiki, T., Chanwimaluang, T., 2017. A Subpixel Classification Algorithm Based on a Random Forest Approach 182–187.

Scanlon, T.M., Caylor, K.K., Levin, S.A., Rodriguez-Iturbe, I., 2007. Positive feedbacks promote power-law clustering of Kalahari vegetation. Nature 449, 209–212. https://doi.org/10.1038/nature06060

Scarton, F., 2006. Produttività primaria epigea di sette alofite in laguna di Venezia. Boll. Mus. Civ. St. Nat. Venezia 57, 53–71.

Scarton, F., Day, J.W., Rismondo, A., 2002. Primary production and decomposition of Sarcocornia fruticosa (L.) Scott and Phragmites australis Trin. Ex Steudel in the Po Delta, Italy. Estuaries 25, 325–336. https://doi.org/10.1007/BF02695977

Schalles, J.F., Hladik, C.M., Lynes, A.A., Pennings, S.C., 2013. Landscape estimates of habitat types, plant biomass, and invertebrate densities in a Georgia salt marsh. Oceanography 26, 88–97. https://doi.org/10.5670/oceanog.2013.50

Schepers, L., Kirwan, M., Guntenspergen, G., Temmerman, S., 2017. Spatio-temporal development of vegetation die-off in a submerging coastal marsh. Limnol. Oceanogr. 62, 137–150. https://doi.org/10.1002/lno.10381

Schieder, N.W., Walters, D.C., Kirwan, M.L., 2018. Massive Upland to Wetland Conversion Compensated for Historical Marsh Loss in Chesapeake Bay, USA. Estuaries and Coasts 41, 940–951. https://doi.org/10.1007/s12237-017-0336-9

Schile, L.M., Callaway, J.C., Parker, V.T., Vasey, M.C., 2011. Salinity and inundation influence productivity of the halophytic plant sarcocornia pacifica. Wetlands 31, 1165–1174. https://doi.org/10.1007/s13157-011-0227-y

Schmid, K.A., Hadley, B.C., Wijekoon, N., 2011. Vertical accuracy and use of topographic LIDAR data in coastal marshes. J. Coast. Res. 27, 116–132. https://doi.org/10.2112/JCOASTRES-D-10-00188.1

Schoutens, K., Heuner, M., Fuchs, E., Minden, V., Schulte-Ostermann, T., Belliard, J., Bouma, T.J., Temmerman, S., 2020. Nature-based shoreline protection by tidal marsh plants depends on trade-offs between avoidance and attenuation of hydrodynamic forces. Estuar. Coast. Shelf Sci. 236, 106645. https://doi.org/10.1016/j.ecss.2020.106645

Schuerch, M., Spencer, T., Evans, B., 2019. Coupling between tidal mudflats and salt marshes affects marsh morphology. Mar. Geol. 412, 95–106. https://doi.org/10.1016/j.margeo.2019.03.008

Schuerch, M., Spencer, T., Temmerman, S., Kirwan, M.L., Wolff, C., Lincke, D., McOwen, C.J., Pickering, M.D., Reef, R., Vafeidis, A.T., Hinkel, J., Nicholls, R.J., Brown, S., 2018. Future response of global coastal wetlands to sea-level rise. Nature 561, 231–234. https://doi.org/10.1038/s41586-018-0476-5

Schulze, D., Jensen, K., Nolte, S., 2021. Livestock grazing reduces sediment deposition and accretion rates on a highly anthropogenically altered marsh island in the Wadden Sea. Estuar. Coast. Shelf Sci. 251, 107191. https://doi.org/10.1016/j.ecss.2021.107191

Schwarz, C., Gourgue, O., van Belzen, J., Zhu, Z., Bouma, T.J., van de Koppel, J., Ruessink, G., Claude, N., Temmerman, S., 2018. Self-organization of a biogeomorphic landscape controlled by plant life-history

traits. Nat. Geosci. 11, 672–677. https://doi.org/10.1038/s41561-018-0180-y

Schwieder, M., Leitão, P.J., Suess, S., Senf, C., Hostert, P., 2014. Estimating fractional shrub cover using simulated enmap data: A comparison of three machine learning regression techniques. Remote Sens. 6, 3427–3445. https://doi.org/10.3390/rs6043427

Shi, B.W., Yang, S.L., Wang, Y.P., Bouma, T.J., Zhu, Q., 2012. Relating accretion and erosion at an exposed tidal wetland to the bottom shear stress of combined current-wave action. Geomorphology 138, 380–389. https://doi.org/10.1016/j.geomorph.2011.10.004

Silinski, A., Fransen, E., Bouma, T.J., Meire, P., Temmerman, S., 2016. Unravelling the controls of lateral expansion and elevation change of pioneer tidal marshes. Geomorphology 274, 106–115. https://doi.org/10.1016/j.geomorph.2016.09.006

Silvestri, S., D'Alpaos, A., Nordio, G., Carniello, L., 2018. Anthropogenic Modifications Can Significantly Influence the Local Mean Sea Level and Affect the Survival of Salt Marshes in Shallow Tidal Systems. J. Geophys. Res. Earth Surf. 123, 996–1012. https://doi.org/10.1029/2017JF004503

Silvestri, S., Defina, A., Marani, M., 2005. Tidal regime, salinity and salt marsh plant zonation. Estuar. Coast. Shelf Sci. 62, 119–130. https://doi.org/10.1016/j.ecss.2004.08.010

Silvestri, S., Marani, M., 2004. Salt-Marsh Vegetation and Morphology: Basic Physiology, Modelling and Remote Sensing Observations, Ecogeomorphology of Tidal Marshes. https://doi.org/10.1029/CE059p0005

Silvestri, S., Marani, M., Marani, A., 2003. Hyperspectral remote sensing of salt marsh vegetation, morphology and soil topography. Phys. Chem. Earth 28, 15–25. https://doi.org/10.1016/S1474-7065(03)00004-4

Silvestri, S., Marani, M., Settle, J., Benvenuto, F., Marani, A., 2002. Salt marsh vegetation radiometry: Data analysis and scaling. Remote Sens. Environ. 80, 473–482. https://doi.org/10.1016/S0034-4257(01)00325-X

Snedden, G.A., Cretini, K., Patton, B., 2015. Inundation and salinity impacts to above- and belowground productivity in Spartina patens and Spartina alterniflora in the Mississippi River deltaic plain: Implications for using river diversions as restoration tools. Ecol. Eng. 81, 133–139. https://doi.org/10.1016/j.ecoleng.2015.04.035

Snow, A.A., Vince, S.W., 1984. Plant Zonation in an Alaskan Salt Marsh: II. An Experimental Study of the Role of Edaphic Conditions. J. Ecol. 72, 669. https://doi.org/10.2307/2260075

Spivak, A.C., Sanderman, J., Bowen, J.L., Canuel, E.A., Hopkinson, C.S., 2019. Global-change controls on soil-carbon accumulation and loss in coastal vegetated ecosystems. Nat. Geosci. 12, 685–692. https://doi.org/10.1038/s41561-019-0435-2

Stefanon, L., Carniello, L., D'Alpaos, A., Rinaldo, A., 2012. Signatures of sea level changes on tidal geomorphology: Experiments on network incision and retreat. Geophys. Res. Lett. 39, 1–6. https://doi.org/10.1029/2012GL051953

Strain, E.M.A., van Belzen, J., Comandini, P., Wong, J., Bouma, T.J., Airoldi, L., 2017. The role of changing climate in driving the shift from perennial grasses to annual succulents in a Mediterranean saltmarsh. J. Ecol. 105, 1374–1385. https://doi.org/10.1111/1365-2745.12799

Stralberg, D., Brennan, M., Callaway, J.C., Wood, J.K., Schile, L.M., Jongsomjit, D., Kelly, M., Parker, V.T., Crooks, S., 2011. Evaluating Tidal Marsh Sustainability in the Face of Sea-Level Rise: A Hybrid Modeling Approach Applied to San Francisco Bay. PLoS One 6. https://doi.org/10.1371/journal.pone.0027388

Sun, C., Fagherazzi, S., Liu, Y., 2018. Classification mapping of salt marsh vegetation by flexible monthly NDVI time-series using Landsat imagery. Estuar. Coast. Shelf Sci. 213, 61–80. https://doi.org/10.1016/j.ecss.2018.08.007

Sun, C., Li, J., Liu, Yongxue, Liu, Yongchao, Liu, R., 2021. Plant species classification in salt marshes using phenological parameters derived from Sentinel-2 pixel-differential time-series. Remote Sens. Environ. 256, 112320. https://doi.org/10.1016/j.rse.2021.112320

Sun, L., Shao, D., Xie, T., Gao, W., Ma, X., Ning, Z., Cui, B., 2020. How does Spartina alterniflora invade in salt marsh in relation to tidal channel networks? Patterns and processes. Remote Sens. 12, 1–18. https://doi.org/10.3390/RS12182983

Tang, H., Xin, P., Ge, Z., Gong, Z., Yang, Y., Zhang, Y., Qi, W., 2020. Response of a salt marsh plant to sediment deposition disturbance. Estuar. Coast. Shelf Sci. 237, 106695. https://doi.org/10.1016/j.ecss.2020.106695

Taramelli, A., Cornacchia, L., Valentini, E., Bozzeda, F., 2013. Non-linear power law approach for spatial and temporal pattern analysis of salt marsh evolution. Earth Surf. Dyn. Discuss. 1, 1061–1095. https://doi.org/10.5194/esurfd-1-1061-2013

Taramelli, A., Valentini, E., Cornacchia, L., Bozzeda, F., 2017. A Hybrid Power Law Approach for Spatial and Temporal Pattern Analysis of Salt Marsh Evolution. J. Coast. Res. 2017-Sprin, 62–72. https://doi.org/10.2112/SI77-007.1

Taramelli, A., Valentini, E., Cornacchia, L., Monbaliu, J., Sabbe, K., 2018. Indications of Dynamic Effects on Scaling Relationships Between Channel Sinuosity and Vegetation Patch Size Across a Salt Marsh Platform. J. Geophys. Res. Earth Surf. 123, 2714–2731. https://doi.org/10.1029/2017JF004540

Taramelli, A., Valentini, E., Piedelobo, L., Righini, M., Cappucci, S., 2021. Assessment of state transition dynamics of coastal wetlands in Northern venice lagoon, Italy. Sustain. 13, 1–24.

https://doi.org/10.3390/su13084102

Temmerman, S., Bouma, T.J., Govers, G., Wang, Z.B., De Vries, M.B., Herman, P.M.J., 2005. Impact of vegetation on flow routing and sedimentation patterns: Three-dimensional modeling for a tidal marsh. J. Geophys. Res. Earth Surf. 110, n/a-n/a. https://doi.org/10.1029/2005JF000301

Temmerman, S., Bouma, T.J., Van de Koppel, J., Van der Wal, D., De Vries, M.B., Herman, P.M.J., 2007. Vegetation causes channel erosion in a tidal landscape. Geology 35, 631–634. https://doi.org/10.1130/G23502A.1

Temmerman, S., Govers, G., Meire, P., Wartel, S., 2003a. Modelling long-term tidal marsh growth under changing tidal conditions and suspended sediment concentrations, Scheldt estuary, Belgium. Mar. Geol. 193, 151–169. https://doi.org/10.1016/S0025-3227(02)00642-4

Temmerman, S., Govers, G., Wartel, S., Meire, P., 2003b. Spatial and temporal factors controlling short-term sedimentation in a salt and freshwater tidal marsh, scheldt estuary, Belgium, SW Netherlands. Earth Surf. Process. Landforms 28, 739–755. https://doi.org/10.1002/esp.495

Thenkabail, P.S., Enclona, E.A., Ashton, M.S., Van Der Meer, B., 2004. Accuracy assessments of hyperspectral waveband performance for vegetation analysis applications. Remote Sens. Environ. 91, 354–376. https://doi.org/10.1016/j.rse.2004.03.013

Thorne, K., MacDonald, G., Guntenspergen, G., Ambrose, R., Buffington, K., Dugger, B., Freeman, C., Janousek, C., Brown, L., Rosencranz, J., Holmquist, J., Smol, J., Hargan, K., Takekawa, J., 2018. U.S. Pacific coastal wetland resilience and vulnerability to sea-level rise. Sci. Adv. 4. https://doi.org/10.1126/sciadv.aao3270

Thorsten Balke, Martin Stock, Kai Jensen, Tjeerd J. Bouma, M.K., 2016. A global analysis of the seaward salt marsh extent: The importance of tidal range Thorsten. Water Resour. Res. 52, 3775– 3786. https://doi.org/10.1002/2014WR016259

Timm, B.C., McGarigal, K., 2012. Fine-scale remotely-sensed cover mapping of coastal dune and salt marsh ecosystems at Cape Cod National Seashore using Random Forests. Remote Sens. Environ. 127, 106–117. https://doi.org/10.1016/j.rse.2012.08.033

Tinkham, W.T., Smith, A.M.S., Marshall, H.P., Link, T.E., Falkowski, M.J., Winstral, A.H., 2014. Quantifying spatial distribution of snow depth errors from LiDAR using Random Forest. Remote Sens. Environ. 141, 105–115. https://doi.org/10.1016/j.rse.2013.10.021

Todd, J.M., Muneepeerakul, R., Pumo, D., Azaele, S., Miralles-Wilhelm, F., Rinaldo, A., Rodriguez-Iturbe, I., 2010. Hydrological drivers of wetland vegetation community distribution within Everglades National Park, Florida. Adv. Water Resour. 33, 1279–1289. https://doi.org/10.1016/j.advwatres.2010.04.003

Toffoli, T., Margolus, N., 1987. Cellular Automata Machines. The MIT Press.

https://doi.org/10.7551/mitpress/1763.001.0001

Tommasini, L., Carniello, L., Ghinassi, M., Roner, M., D'Alpaos, A., 2019. Changes in the wind-wave field and related salt-marsh lateral erosion: inferences from the evolution of the Venice Lagoon in the last four centuries. Earth Surf. Process. Landforms 44, 1633–1646. https://doi.org/10.1002/esp.4599

Törnqvist, T.E., Jankowski, K.L., Jankowski, K.L., Li, Y.X., Li, Y.X., González, J.L., González, J.L., 2020. Tipping points of Mississippi Delta marshes due to accelerated sea-level rise. Sci. Adv. 6. https://doi.org/10.1126/sciadv.aaz5512

Tosi, L., Da Lio, C., Teatini, P., Strozzi, T., 2018. Land subsidence in coastal environments: Knowledge advance in the Venice coastland by TerraSAR-X PSI. Remote Sens. 10. https://doi.org/10.3390/rs10081191

Tosi, L., Teatini, P., Strozzi, T., 2013. Natural versus anthropogenic subsidence of Venice. Sci. Rep. 3, 1–9. https://doi.org/10.1038/srep02710

Trincardi, F., Barbanti, A., Bastianini, M., Benetazzo, A., Cavaleri, L., Chiggiato, J., Papa, A., Pomaro, A., Sclavo, M., Tosi, L., Umgiesser, G., 2016. The 1966 flooding of Venice: What time taught us for the future. Oceanography 29, 178–186. https://doi.org/10.5670/oceanog.2016.87

Tucker, C.J., 1979. Red and photographic infrared linear combinations for monitoring vegetation. Remote Sens. Environ. 8, 127–150. https://doi.org/10.1016/0034-4257(79)90013-0

Ursino, N., Silvestri, S., Marani, M., 2004. Subsurface flow and vegetation patterns in tidal environments. Water Resour. Res. 40, 1–11. https://doi.org/10.1029/2003WR002702

Valle-Levinson, A., Marani, M., Carniello, L., D'Alpaos, A., Lanzoni, S., 2021. Astronomic link to anomalously high mean sea level in the northern Adriatic Sea. Estuar. Coast. Shelf Sci. 257, 107418. https://doi.org/10.1016/j.ecss.2021.107418

Van Beijma, S., Comber, A., Lamb, A., 2014. Random forest classification of salt marsh vegetation habitats using quad-polarimetric airborne SAR, elevation and optical RS data. Remote Sens. Environ. 149, 118–129. https://doi.org/10.1016/j.rse.2014.04.010

van Belzen, J., van de Koppel, J., Kirwan, M.L., van der Wal, D., Herman, P.M.J., Dakos, V., Kéfi, S., Scheffer, M., Guntenspergen, G.R., Bouma, T.J., 2017. Vegetation recovery in tidal marshes reveals critical slowing down under increased inundation. Nat. Commun. 8, 15811. https://doi.org/10.1038/ncomms15811

Van der Wal, D., Wielemaker-Van den Dool, A., Herman, P.M.J., 2008. Spatial patterns, rates and mechanisms of saltmarsh cycles (Westerschelde, The Netherlands). Estuar. Coast. Shelf Sci. 76, 357–368. https://doi.org/10.1016/j.ecss.2007.07.017

van Dobben, H.F., de Groot, A. V., Bakker, J.P., 2022. Salt Marsh Accretion With and Without Deep Soil

Subsidence as a Proxy for Sea-Level Rise. Estuaries and Coasts. https://doi.org/10.1007/s12237-021-01034-w

van Regteren, M., Meesters, E.H., Baptist, M.J., de Groot, A. V., Bouma, T.J., Elschot, K., 2020. Multiple Environmental Variables Affect Germination and Mortality of an Annual Salt Marsh Pioneer: Salicornia procumbens. Estuaries and Coasts 43, 1489–1501. https://doi.org/10.1007/s12237-020-00735-y

van Veelen, T.J., Fairchild, T.P., Reeve, D.E., Karunarathna, H., 2020. Experimental study on vegetation flexibility as control parameter for wave damping and velocity structure. Coast. Eng. 157, 103648. https://doi.org/10.1016/j.coastaleng.2020.103648

Van Wesenbeeck, B.K., Van De Koppel, J., Herman, P.M.J., Bouma, T.J., 2008. Does scale-dependent feedback explain spatial complexity in salt-marsh ecosystems? Oikos 117, 152–159. https://doi.org/10.1111/j.2007.0030-1299.16245.x

Venier, C., D'Alpaos, A., Marani, M., 2014. Evaluation of sediment properties using wind and turbidity observations in the shallow tidal areas of the Venice Lagoon. J. Geophys. Res. Earth Surf. 119, 1604–1616. https://doi.org/10.1002/2013JF003019

Vermote, E.F., Tanre, D., Deuze, J.L., Herman, M., Morcette, J.-J., 1997. Second Simulation of the Satellite Signal in the Solar Spectrum, 6S: an overview. IEEE Trans. Geosci. Remote Sens. 35, 675–686. https://doi.org/10.1109/36.581987

Verrelst, J., Camps-Valls, G., Muñoz-Marí, J., Rivera, J.P., Veroustraete, F., Clevers, J.G.P.W., Moreno, J., 2015. Optical remote sensing and the retrieval of terrestrial vegetation bio-geophysical properties - A review. ISPRS J. Photogramm. Remote Sens. 108, 273–290. https://doi.org/10.1016/j.isprsjprs.2015.05.005

Visser, E.J.W., Voesenek, L.A.C.J., Vartapetian, B.B., Jackson, M.B., 2003. Flooding and plant growth. Ann. Bot. 91, 107–109. https://doi.org/10.1093/aob/mcg014

Visual Information Solutions, I., 2009. ENVI User's Guide Restricted Rights Notice.

Vittori Antisari, L., Ferronato, C., Pellegrini, E., Boscutti, F., Casolo, V., de Nobili, M., Vianello, G., 2017. Soil properties and plant community relationship in a saltmarsh of the Grado and Marano lagoon (northern Italy). J. Soils Sediments 17, 1862–1873. https://doi.org/10.1007/s11368-016-1510-6

Volpe, V., Silvestri, S., Marani, M., 2011a. Remote sensing retrieval of suspended sediment concentration in shallow waters. Remote Sens. Environ. 115, 44–54. https://doi.org/10.1016/j.rse.2010.07.013

Volpe, V., Silvestri, S., Marani, M., 2011b. Remote sensing retrieval of suspended sediment concentration in shallow waters. Remote Sens. Environ. 115, 44–54. https://doi.org/10.1016/j.rse.2010.07.013

W. Bowman, A., Azzalini, A., 1997. Applied Smoothing Techniques for Data Analysis. Oxford Clarendon

Press.

Wang, C., Menenti, M., Stoll, M.P., Belluco, E., Marani, M., 2007. Mapping mixed vegetation communities in salt marshes using airborne spectral data. Remote Sens. Environ. 107, 559–570. https://doi.org/10.1016/j.rse.2006.10.007

Wang, C., Menenti, M., Stoll, M.P., Feola, A., Belluco, E., Marani, M., 2009. Separation of ground and low vegetation signatures in LiDAR measurements of salt-marsh environments. IEEE Trans. Geosci. Remote Sens. 47, 2014–2023. https://doi.org/10.1109/TGRS.2008.2010490

Wang, J., Liu, Z., Yu, H., Li, F., 2017. Mapping Spartina alterniflora biomass using LiDAR and hyperspectral data. Remote Sens. 9, 1–14. https://doi.org/10.3390/rs9060589

Wasson, K., Woolfolk, A., Fresquez, C., 2013. Ecotones as Indicators of Changing Environmental Conditions: Rapid Migration of Salt Marsh-Upland Boundaries. Estuaries and Coasts 36, 654–664. https://doi.org/10.1007/s12237-013-9601-8

Watson, E.B., Byrne, R., 2009. Abundance and diversity of tidal marsh plants along the salinity gradient of the San Francisco Estuary: Implications for global change ecology. Plant Ecol. 205, 113–128. https://doi.org/10.1007/s11258-009-9602-7

Weerman, E.J., Van Belzen, J., Rietkerk, M., Temmerman, S., Kéfi, S., Herman, P.M.J., Van De Koppel, J., 2012. Changes in diatom patch-size distribution and degradation in a spatially self-organized intertidal mudflat ecosystem. Ecology 93, 608–618. https://doi.org/10.1890/11-0625.1

Wei, X., Wang, S., Wang, Y., 2018. Spatial and temporal change of fractional vegetation cover in North-western China from 2000 to 2010. Geol. J. 53, 427–434. https://doi.org/10.1002/gj.3030

Wijnen, A.H.J. Van, Bakker, J.P., Vries, Y. De, Journal, S., Wijnen, V., 1997. Twenty Years of Salt Marsh Succession on a Dutch Coastal Barrier Island. J. Coast. Conserv. 3, 9–18.

Wu, S., Gao, X., Lei, J., Zhou, N., Wang, Y., 2020. Spatial and temporal changes in the normalized difference vegetation index and their driving factors in the desert/grassland biome transition zone of the Sahel region of Africa. Remote Sens. 12, 1–27. https://doi.org/10.3390/rs12244119

Wu, W., Biber, P., Mishra, D.R., Ghosh, S., 2020. Sea-level rise thresholds for stability of salt marshes in a riverine versus a marine dominated estuary. Sci. Total Environ. 718, 137181. https://doi.org/10.1016/j.scitotenv.2020.137181

Wulder, M.A., White, J.C., Nelson, R.F., Næsset, E., Ørka, H.O., Coops, N.C., Hilker, T., Bater, C.W., Gobakken, T., 2012. Lidar sampling for large-area forest characterization: A review. Remote Sens. Environ. 121, 196–209. https://doi.org/10.1016/j.rse.2012.02.001

Xin, P., Kong, J., Li, L., Barry, D.A., 2013. Modelling of groundwater-vegetation interactions in a tidal marsh.

Adv. Water Resour. 57, 52–68. https://doi.org/10.1016/j.advwatres.2013.04.005

Xu, M., Watanachaturaporn, P., Varshney, P.K., Arora, M.K., 2005. Decision tree regression for soft classification of remote sensing data. Remote Sens. Environ. 97, 322–336. https://doi.org/10.1016/j.rse.2005.05.008

Yan, W.Y., Shaker, A., El-Ashmawy, N., 2015. Urban land cover classification using airborne LiDAR data: A review. Remote Sens. Environ. 158, 295–310. https://doi.org/10.1016/j.rse.2014.11.001

Yang, J.Q., Nepf, H.M., 2019. Impact of Vegetation on Bed Load Transport Rate and Bedform Characteristics. Water Resour. Res. 55, 6109–6124. https://doi.org/10.1029/2018wr024404

Yang, Z., D'Alpaos, A., Marani, M., Silvestri, S., 2020. Assessing the Fractional Abundance of Highly Mixed Salt-Marsh Vegetation Using Random Forest Soft Classification. Remote Sens. 12, 3224. https://doi.org/10.3390/rs12193224

Yeo, S., Lafon, V., Alard, D., Curti, C., Dehouck, A., Benot, M.L., 2020. Classification and mapping of saltmarsh vegetation combining multispectral images with field data. Estuar. Coast. Shelf Sci. 236. https://doi.org/10.1016/j.ecss.2020.106643

Yousefi Lalimi, F., Marani, M., Heffernan, J.B., D'Alpaos, A., Murray, A.B., 2020. Watershed and ocean controls of salt marsh extent and resilience. Earth Surf. Process. Landforms 45, 1456–1468. https://doi.org/10.1002/esp.4817

Yousefi Lalimi, F., Silvestri, S., Moore, L.J., Marani, M., 2017. Coupled topographic and vegetation patterns in coastal dunes: Remote sensing observations and ecomorphodynamic implications. J. Geophys. Res. Biogeosciences 122, 119–130. https://doi.org/10.1002/2016JG003540

Zedler, J.B., Kercher, S., 2005. WETLAND RESOURCES: Status, Trends, Ecosystem Services, and Restorability. Annu. Rev. Environ. Resour. 30, 39–74. https://doi.org/10.1146/annurev.energy.30.050504.144248

Zhang, C., 2015. Applying data fusion techniques for benthic habitat mapping and monitoring in a coral reef ecosystem. ISPRS J. Photogramm. Remote Sens. 104, 213–223. https://doi.org/10.1016/j.isprsjprs.2014.06.005

Zhao, L.X., Xu, C., Ge, Z.M., Van De Koppel, J., Liu, Q.X., 2019. The shaping role of self-organization: Linking vegetation patterning, plant traits and ecosystem functioning. Proc. R. Soc. B Biol. Sci. 286. https://doi.org/10.1098/rspb.2018.2859

Zheng, G., Moskal, L.M., 2009. Retrieving Leaf Area Index (LAI) Using Remote Sensing: Theories, Methods and Sensors. Sensors 9, 2719–2745. https://doi.org/10.3390/s90402719

Zheng, Z., Zhou, Y., Tian, B., Ding, X., 2016. The spatial relationship between salt marsh vegetation patterns,

soil elevation and tidal channels using remote sensing at Chongming Dongtan Nature Reserve, China. Acta Oceanol. Sin. 35, 26–34. https://doi.org/10.1007/s13131-016-0831-z

Zhu, Z., van Belzen, J., Zhu, Q., van de Koppel, J., Bouma, T.J., 2020. Vegetation recovery on neighboring tidal flats forms an Achilles' heel of saltmarsh resilience to sea level rise. Limnol. Oceanogr. 65, 51–62. https://doi.org/10.1002/lno.11249

Zhu, Z., Zhang, L., Wang, N., Schwarz, C., Ysebaert, T., 2012. Interactions between the range expansion of saltmarsh vegetation and hydrodynamic regimes in the Yangtze Estuary, China. Estuar. Coast. Shelf Sci. 96, 273–279. https://doi.org/10.1016/j.ecss.2011.11.027

Zinnert, J.C., Shiflett, S.A., Via, S., Bissett, S., Dows, B., Manley, P., Young, D.R., 2016. Spatial–Temporal Dynamics in Barrier Island Upland Vegetation: The Overlooked Coastal Landscape. Ecosystems 19, 685–697. https://doi.org/10.1007/s10021-016-9961-6

Zong, L., Nepf, H., 2010. Flow and deposition in and around a finite patch of vegetation. Geomorphology 116, 363–372. https://doi.org/10.1016/j.geomorph.2009.11.020

ACKNOWLEDGEMENTS

After a 3-year study and research, I am almost approaching the end of my Ph.D. At first, I want to thank my principal supervisor Andrea D'Alpaos for allowing me to be a Ph.D. in the Department of Geosciences, University of Padova. Thanks to his forgiving and gentle supervision, he is always patient to teach me and discuss the research with me. Also thanks to his understanding of my situation and trying his best to help me, encourage me and develop my network for my future career. He never dislikes me because my background is not overlapped with his research and I am not a master in remote sensing, but patiently helps me to develop relevant skills. I would say that maybe I am not his best student, but he is, not one of, the best supervisor I have seen. And I am really lucky to spend more than 3 years working with him.

I am also want to greatly thank my co-supervisors Marco Marani and Sonia Silvestri. They patiently and never hesitate to help me to develop my research ideas and methods and provide suggestions. One of the most impressive things in my mind is that Sonia showed me how to use ArcGIS, ENVI and SAGA step by step. And Marco always provides critical but very important suggestions for my work. Thank them again for their help in the last 3 years.

I am truly grateful to the Cariparo Foundation, which with this scholarship has given me the opportunity to deepen my knowledge and enter the world of scientific research. I also wish to thank the Venezia2021 Research Program, coordinated by CORILA, with the contribution of the Superintendency for Public Works of Veneto, Trentino Alto Adige and Friuli Venezia Giulia for supporting data acquisition and travel during my research activity.

I would also say thanks to my colleagues Enrica Belluco, Alvise Finotello, Guillaume Goodwin, Alice Puppin, Wei Shi, Liang Geng, Bellizia Elena and Davide Tognin for their help in my work. I also appreciate the help from Prof. Massimiliano Ghinassi, Prof. Paolo Tarolli, Prof. Claudia Agnini, Prof. Nicola Surian, Prof. Dongdong Shao, Prof. Zeng Zhou, Prof. Liqiang Kang, Prof. Chunping Chang and Prof. Xin Gao. In addition, many thanks to many Chinese friends (Wenfang Cao, Yu Wang, Yikai Liu, Xue Chen, Qingliu Luo, Zihao Zheng, Yanzhang Chen, Lingzi Mo, Chaoqun Yang, Jianfeng Yang and Yixing Du and others) help and taking care of my life. My Chinese colleagues from Beijing Normal University (Dr. Qian Li, Dr. Honglei Jiang and Dr. Weilun Gao), Chinese Academy of Science (Dr. Naizheng Wang and Dr. Xiaxiang Li) also should be highly appreciated.

Zhicheng Yang
2021/12/31 Padova